Dissertation
submitted to the
Combined Faculty of Natural Sciences and Mathematics
of the Ruperto Carola University Heidelberg, Germany
for the degree of
Doctor of Natural Sciences

Presented by
M.Sc. Thomas Schackel
born in Gardelegen, Germany
Oral Examination: 14.09.2020

Biomaterial implants combined with cell therapy improve axonal regeneration after spinal cord injury

Referees: Prof. Dr. G. Elisabeth Pollerberg

Dr. Radhika Puttagunta

Dedication

Dedicated to my family and Christina

Abstract

Injury to the adult spinal cord damages ascending and descending spinal fiber tracts thereby disrupting proper information transmission between the brain, spinal cord and periphery of the body. Restoring neural connectivity beyond the site of injury is the prerequisite for functional recovery to occur. Without intervention, central nervous system (CNS) axons fail to regenerate, resulting in tremendous impairment of sensorimotor function as well as autonomic dysfunction and, consequently, a significant reduction of the patients' quality of life. Hence, putative repair strategies for spinal cord injury (SCI) were developed including cell transplantation and biomaterial implantation. However, functional axonal growth past the lesion site remains insufficient due to inappropriate implant integration, detrimental fibroglial scarring and failure of spinal axons to grow beyond the site of injury. Recently, astrocytes were identified as essential key players for neuroregeneration due to their neuroprotective and supportive functions after CNS injury. Further, immature astrocytes not only fulfil scaffolding functions during development, but might also adapt to the harsh lesion environment without adopting detrimental phenotypes. Thus, astrocyte are prime candidates to provide structural as well as trophic support for growing axons in combination with biomaterial implants at SCI lesion sites.

In the present study, novel alginate-based hydrogel implants with a defined channel microstructure were combined with cellular grafts of immature astrocytes derived either from the cortex or the spinal cord of neonatal Fischer-344 rats to: (1) provide a physical guidance structure for regrowing axons at the site of injury; and (2) establish a permissive cellular growth substrate within and beyond the hydrogel implant supporting axonal crossing of the lesion cavity of a cervical unilateral hemisection of the spinal cord in adult rats.

First, alginate-based hydrogel implants were modified with polypetides to improve their biocompatibility and cell viability *in vitro* and *in vivo*. Afterwards, immature astrocytes from neonatal rat cortex were cultivated and enriched *in vitro*. Seeding of alginate-based hydrogel implants with immature cortex-derived astrocytes improved axonal regrowth compared to non-seeded hydrogel implants following SCI. The grafted astrocytes interacted with the host astrocytic network and aligned into tissue bridges structurally guiding axons across the host-graft interface. To elucidate whether astrocytes with a spinal cord identity would elicit superior pro-regenerative effects after SCI, immature astrocytes were isolated from the spinal cord of neonatal rats and compared with cortex-derived astrocytes. Phenotypic characterization revealed minor molecular and morphological differences between both astrocyte populations *in vitro* and *in vivo.* Particularly, cortex-derived astrocytes were found to have a more mature phenotype compared to spinal cord-derived astrocytes *in vitro*, however, both cell populations adopted a differentiated morphology and expressed functional molecular astrocytic markers *in vivo* after transplantation into the intact spinal cord. After SCI, seeded hydrogel implants together with additional caudal grafts of either immature astrocyte population further enhanced axonal growth through the implantation site and promoted revascularization. The grafted cells connected with the host spinal parenchyma facilitating tissue bridging between implant and host. Finally, seeded hydrogel implants in combination with rostral and caudal immature astrocyte grafts were shown to additionally increase axonal growth through the hydrogel implants after SCI by 70% compared to the previous transplantation paradigms.

Thus, the combination of biomaterial implantation with cell transplantation superiorly promotes axonal growth through sites of acute SCI compared to treatment paradigms based only upon biomaterial implants. Moreover, additional grafts of immature astrocytes into the surrounding host tissue improve host-graft interactions by formation of a continuous cellular substrate spanning the SCI lesion site. Nonetheless, axonal re-entry into the distal host spinal cord may require additional trophic attraction.

Zusammenfassung

Die Wiederherstellung zerstörter neuronaler Verbindung über eine Läsionsstelle hinweg stellt die Grundvoraussetzung für eine funktionelle Erholung nach Rückenmarksverletzungen dar. Durch die limitierte inhärente Regenerationskapazität adulter Neurone des zentralen Nervensystems (ZNS) führen Rückenmarksverletzungen zu temporären aber meist permanenten Beeinträchtigungen der sensomotorischen sowie autonomen Funktionen des Körpers und somit zu einer signifikanten Reduktion der Lebensqualität der Betroffenen. Folglich wurden im Laufe der letzten Jahrzehnte eine Vielfalt an experimentellen Behandlungsstrategien für Rückenmarksläsionen entwickelt unter denen Zelltransplantationsansätze sowie die Implantation eines Biomaterials in die Läsionsstelle bereits vielversprechende Erfolge erzielen konnten. Nichtsdestotrotz stellt funktionell relevantes axonales Wachstum über die Rückenmarksläsionsstelle hinaus, bedingt durch die unzureichende Integration des Biomaterials, geringe Wachstumsfähigkeit adulter Rückenmarksneurone, sowie gliale Narbenbildung um die Läsionsstelle, weiterhin ein fundamentales Problem aller potentiellen Regenerationstherapien dar. In der vorliegenden Studie wurde daher untersucht, ob die Integration eines Biomaterials in das verletzte Rückenmark durch Verbesserung der inhärenten Biokompatibilität des Biomaterials an sich, sowie durch die Verbindung des Biomaterials mit Zelltransplantationen verbessert werden kann. Hierzu wurde die Oberfläche von Alginat-basierten anisotropen Kapillarhydrogelen zunächst mit dem synthetischen Polypeptid Poly-L-Ornithin und dem extrazellulären Matrix-Protein Laminin beschichtet. Die Zellvitalität in den Alginat-basierten Hydrogelen konnte hierdurch sowohl *in vitro* wie auch *in vivo* verbessert werden. Nach Implantation in die Läsionskavität einer unilateralen Hemisektionsverletzung der zervikalen (C5/6) Rückenmarks im Tiermodell der Ratte führte die Oberflächenbeschichtung zu einer dichten Zellfüllung und signifikant gesteigertem Axonwachstum innerhalb des Biomaterials, jedoch nicht darüber hinaus. Aufgrund der unzähligen unterstützenden und neuroprotektiven Funktionen von Astrozyten im adulten ZNS sowie der Tatsache, dass unreife Astrozyten während der Embryonalentwicklung als leitendes strukturelles Zellgerüst sowie als Quelle neurotropher Faktoren für wachsende Axone fungieren, wurde weiterhin untersucht, ob durch die Verbindung des Biomaterials mit Transplantation von neonatalen Astrozyten die Integration des Biomaterials in das umliegende Rückenmark weiter verbessert und axonale Regeneration über das Alginat-Hydrogel hinaus erreicht werden kann. Durch Besiedelung der Hydrogele mit Astrozyten aus dem Kortex neonataler Ratten konnte eine strukturelle Kontinuität sowie Zell-Zell-Interaktionen zwischen dem Implantat und dem umliegenden Rückenmarksgewebe hergestellt werden. Obwohl das axonale Wachstum innerhalb des Implantats weiter gefördert werden konnte, wurde axonaler Wiedereintritt in das kaudale Rückenmarksparenchym jedoch erneut nicht erreicht. Um zu untersuchen, ob Astrozyten aus dem Rückenmark einen stärkeren pro-regenerativen Effekt in Verbindung mit den Alginat-Hydrogelen besitzen, wurden neonatale Astrozyten aus dem Rü-

ckenmark isoliert und *in vitro* und *in vivo* im Vergleich zu neonatalen Astrozyten aus dem Kortex charakterisiert. Hierbei konnte ein reiferer und differenzierter Phenotyp in Kortex-Astrozyten nachgewiesen werden. Nach Transplantation in das intakte Rückenmark zeigten jedoch beide Astrozyten-Populationen ein ähnliches Verhalten, integrierten in das umgebene Wirtsgewebe und zeigten ein Markerexpressionsprofil vergleichbar zu differenzierten und funktionellen Astrozyten. Durch Besiedelung des Alginat-Hydrogels mit Kortex- sowie Rückenmarks-Astrozyten in Kombination mit zusätzlicher Zelltransplantation in das umliegende Rückenmarksparenchym konnten die Vaskularisation sowie das axonale Wachstum absteigender Rückenmarksbahnen innerhalb der Implantate nach Rückenmarksverletzung maximiert werden. Zudem generierten die Astrozyten-Populationen gleichermaßen ein kontinuierliches zelluläres Substrat über die Läsionsstelle hinweg, indem longitudinale Gewebebrücken mit Wirts-Astrozyten ausgebildet wurden, welche als Leitstrukturen für wachsende Axone dienten. Nichtsdestotrotz konnte axonale Reinnervation des kaudalen Rückenmarks nicht beobachtet werden.
Folglich konnte im Zuge der vorliegenden Arbeit nachgewiesen werden, dass die Integration eines Alginat-Hydrogels mit Hilfe von Oberflächenbeschichtung sowie zusätzlicher Zelltransplantation von neonatalen Astrozyten signifikant verbessert werden kann. Durch strukturelle Kontinuität zwischen Implantat und umgebenen Wirtsgewebe werden sowohl Axonwachstum als auch Vaskularisation in die Läsionsstelle erhöht. Um substanzielles Axonswachstum über die Läsionsstelle hinweg in das kaudale Rückenmark hinein zu erreichen, sind jedoch zusätzliche Interventionen, z.B. Chemoattraktion von wachsenden Axonen sowie Freisetzung von neurotrophischen Faktoren zur Unterstützung des regenerativen axonalen Wachstums, notwendig.

Acknowledgement

Hereby, I would like to express my deepest gratitude to everyone who supported me during my dissertation. I am very thankful that I was given the opportunity to work with many inspiring scientists, clinicians and persons throughout my time at the Laboratory for Neuroregeneration of the Spinal Cord Injury Center of the Heidelberg University Hospital.

Firstly, I would like to thank Prof. Dr. Armin Blesch. He gave me the chance to join the lab as a Masters' student and later on as a PhD student and arouse my interest in neuroregeneration and SCI research. Prof. Dr. Blesch is a very inspiring scientist and a great mentor, who always gave me trust and encouraged me to bring in my own ideas and helped me to develop as a person and as a scientist. He was always open for questions, discussions and his excellent support continued even after he left the laboratory in 2016.
Secondly, I am very grateful to Dr. Radhika Puttagunta, who safely lead the lab through troubling times after Prof. Dr. Blesch had left. She established her own leadership style and gave me absolute trust and support from the beginning on. Dr. Puttagunta is a passionate scientist, a great teacher and strongly influenced my development as a scientist within a short time. She always encouraged me to find innovative solutions for scientific problems and to constantly broaden my horizon. Moreover, she always has an open ear for all kinds of problems and selflessly supported me during all phases of my dissertation. I really enjoyed being her PhD student and highly appreciate everything she has done for me. Without her mentorship, I would not have been able to accomplish my PhD degree.
I would like to thank Prof. Dr. Norbert Weidner. As the director of the Spinal Cord Injury Center, he uniquely synergizes clinical as well as basic research expertise and tremendously influenced my scientific development. Moreover, he always had an open ear for problems and discussions. With broad experience in both fields, Prof. Dr. Weidner crucially helped to develop and push my project forward, but also taught me to always keep the clinical aspect of basic research and the patients' desires in mind. I am really grateful for his constant support and mentorship.
I feel deeply honored that I had the unique opportunity to be mentored by these three inspiring scientists. All of them sustainably influenced my scientific but also personal development.

Furthermore, I would like to thank Prof. Dr. G. Elisabeth Pollerberg for being the first examiner of my PhD thesis. In 2012, I took my first steps as a scientist under her supervision as a Bachelors' student. During that time, she taught me all the basics of scientific work and allowed me to work independently. Without her mentorship during this early period of my scientific career, I would not have been able to successfully pursue my scientific career. Moreover, Prof. Pollerberg continued to support me during my dissertation and always gave meaningful input to my project.

I would also like to thank Prof. Dr. Stephan Frings and Prof. Dr. Thomas Kuner for their agreement to join my PhD examination committee.

I would like to thank Apl. Prof. Dr. Rainer Müller for our fertile collaboration. I also want to thank his students, Manuel Brunner and Maximilian Nützl, who fabricated the alginate-based hydrogels used in this project. Additionally, I would like to thank Dr. Carmen Ruiz de Almodovar, who helped us setting up the CD31 immunostaining and tissue clearing procedures.

I am deeply grateful for all the support and help that I got from all present and past members of the Laboratory for Neuroregeneration. I would like to thank my former supervisors, Dr. Manuel Günther and Dr. Ina K. Simeonova, who helped me a lot to settle in into the field of biomaterials and SCI research. I want to thank Melanie Motsch for being a great technician and lab manager, for her support during surgeries as well as dealing with all kinds of clinic bureaucracy; Paul Ruf for being a great animal caretaker. I would like to thank Dr. Beatrice Sandner for teaching me various surgery techniques, for her help during surgeries as well as all the socializing events inside and outside the lab. I am deeply thankful to Dr. Christopher Sliwinski for being a great friend, companion and colleague. Without his support, advice and -most importantly- humorously craziness, I would have lost my mind multiple times over the last years. Furthermore, I want to thank Vasileios Kampanis for being a good friend, colleague and for bringing some Greek sunshine into the PhD tristesse. Moreover, I want to thank Dr. Shengwen Liu and Naëmi Kühn, who started as a Lab rotation student and continued as a Masters' student under my supervision and is now a PhD student in our lab. Both greatly supported me during my dissertation.

I want to express my deepest gratefulness to my parents for always giving me all the opportunities to pursue my plans and dreams. They selflessly supported me in every situation, taught me everything essential in life and helped me to become the person that I am today.

With every fiber of my heart I would like to thank Christina for being the most affectionate and kindest person I have ever met, for being my anchor and haven in every situation of my life. She always encourages me to vouch for my beliefs and dreams, she keeps me on track and brings me back to earth. Without her love, constant support and advice I would be entirely lost. On each single day of my life, I am grateful to have her at my side.

Abbreviations

ACH	Anisotropic capillary hydrogel
ab	Antibody
AFM	Atomic force microscopy
Aldh1L1	Aldehyde dehydrogenase 1 family member L1
AMP	Ampicillin
ANOVA	Analysis of variance
Ara-C	Cytosine-β-D-arabinofuranoside
ASIA	American spinal injury Association
APC	Astrocyte precursor cell
AQP4	Aquaporin-4
ATP	Adenosine triphosphate
BBB	Blood-brain-barrier
BBB motor score	Basso, Beattie and Bresnahan motor score
BDA	Biotinylated dextran amine
BDNF	Brain-derived neurotrophic factor
BMP	Bone morphogenetic protein
BMSC	Bone marrow stromal cell
BSA	Bovine serum albumin
BSCB	Blood-spinal cord-barrier
cAMP	Cyclic adenosine monophosphate
CD31	Cluster of differentiation 31
CNS	Central nervous system
CNTF	Ciliary growth factor
CO_2	Carbondioxide
CSF	Cerebrospinal fluid
CSPG	Chrondoitin sulfate proteoglycans
CST	Corticospinal tract
CTB	Cholera-toxin subunit B
Cx43	Connexin-43
DAPI	4’6-Diamidino-2-phenylindole
DCL	Dorsal column lesion
DNA	Desoxyribonucleinacid
ddH_2O	double-destilled water
Dk	Donkey serum
DMEM	Dulbecco’s modified Eagle medium
DMSO	Dimethyl sulfoxide

DPBS	Dulbecco’s phosphate buffered salt solution
dpi	days post-injury
DRG	Dorsal root ganglion
EAAT1/GLAST	Excitatory amino acid transporter-1/Glutamate aspartate transporter
EAAT2/GLT-1	Excitatory amino acid transporter-2/Glutamate transporter-1
ECM	Extracellular matrix
EDTA	Ethylendiamine tetraacetic acid
EGF	Epidermal growth factor
eGFP	Enhanced green fluorescent protein
ESC	Embryonic stem cell
EtOH	Ethanol
F-12	F-12 Nutrient Mixture (Ham)
FBS	Fetal bovine serum
FES	Functional electrical stimulation
FGF	Fibroblast growth factor
fMRI	Functional magnetic resonance imaging
FN	Fibronectin
GAP43	Growth-associated protein-43
GDNF	Glial-derived growth factor
GEN	Gentamycin
GFAP	Glial fibrillary acidic protein
GFP	Green fluorescent protein
GM	Grey matter
HBSS	Hank’s buffered salt solution
HCl	Hydrochloric acid
HDI	Hexamethylene diisocyanate
hESC	Human embryonic stem cell
h	Hour
IbaI	Ionized calcium-binding adaptor molecule 1
i.m.	Intramuscular
i.p.	Intraperitoneal
ISNCSCI	International standards for neurological classification of spinal cord injury
i.v.	Intravenous
ICC	Immunocytochemistry
IFN	Interferon
IgG	Immunoglobulin G

IHC	Immunohistochemistry
IL	Interleukin
iPSC	Induced pluripotent stem cell
JAK/STAT3	Janus kinase/Signal transducers and activators of transcription
kDA	Kilo-Dalton
kg	Kilogram
lam	Laminin
LDM	Laser dissection microscopy
M	Molar
MAPK	Mitogen-activated protein kinase
MeOH	Methanol
mg	Milligram
min	Minute
ml	Milliliter
mM	Millimolar
mm	Millimeter
mRNA	Messenger-ribonucleic acid
ms	Mouse
µl	Microliter
µm	Micrometer
µM	Micromolar
NaCl	Sodium chloride
NaOH	Sodium hydroxide
NEAA	Non-essential amino acids
NF	Neurofilament
NFIA/B	Nuclear factor-1A/B
ng	Nanogram
NGF	Nerve growth factor
nl	Nanoliter
nm	Nanometer
nM	Nanomolar
NPC	Neural precursor cell
ns	Not significant
NSC	Neural stem cell
NT-3	Neurotrophin-3
NT-4	Neurotrophin-4
O_2	Oxygen

OEC	Olfactory ensheathing cell
P	Postnatal day
Pa	Pascal
PB	Phosphate buffer
PBS	Phosphate buffered salt solution
PEG	Poly-ethylene glycol
PEN/STREP	Penicillin/Streptomycin
PFA	Paraformaldehyde
PGA	Poly-glycolic acid
pHEMA	Poly-2-hydroxyethyle methacrylate
pHEMA-MMA	Poly-2-hydroxyethyle methacrylate-co-methyl methacrylate
PI3K	Phosphoinositide-3 kinase
PLGA	Poly-lactic-co-glycolic acid
PLO	Poly-L-ornithine
PNS	Peripheral nervous system
PNN	Perineural network
PTEN	Phosphatase and tensin homolog
rb	Rabbit
RNA	Ribonucleic acid
RNAseq	RNA sequencing
RT	Room temperature
rt	Rat
ROI	Region of interest
ROS	Reactive oxygen species
rpm	Rotations per minute
s.c.	Subcutaneous
SC	Schwann cell
SCI	Spinal cord injury
SEM	Standard error of the mean
SNI	Spared nerve injury
SNL	Spinal nerve ligation injury
Shh	Sonic hedgehog
Sox2	Sex-determining region Y-box 2
Sox9	Sex-determining region Y-box 9
SVZ	Subventricular zone
S100β	S100 calcium binding protein β
TBS	TRIS-buffered salt solution
TBI	Traumatic brain injury

TF	Transcription factor
TNF	Tumor necrosis factor
TRIS	Tris(hydroxymethyl)aminomethane
TrypLE™Express	Stable trypsin replacement enzyme
U/ml	Units per ml
VEGF	Vascular endothelial growth factor
Vim	Vimentin
vWF	von Willebrand factor
WM	White matter
WMT	White matter tract
w/o	without
w/v	weight per volume
2D	Two-dimensional
3D	Three-dimensional
5-HT	5-Hydroxytryptamine

Table of contents

List of figures

List of tables

Table 25: List of software used for imaging, data processing and analysis, statistical analysis and data illustration

List of supplementary tables

1 Introduction

The adult mammalian central nervous system (CNS) is characterized by a high degree of cellular, morphological and functional complexity. Over the past century, our understanding of its anatomy and function expanded continuously but is still far from being complete. Consequently, traumatic injuries and degenerative states of the brain and spinal cord represent major obstacles of both medical science and modern society.

The spinal cord anatomically and functionally connects the instructive and regulatory control centers of the brain (sensorimotor cortex) via descending axonal tracts with effector compartments in the body, namely muscles and tendons of torso and limbs. On the other side, ascending axonal tracts convey sensory information from the periphery back to the cortex, where they contribute to regulatory feedback loops, constantly modulating the brains' output signals. Hence, spinal cord injury (SCI) damages ascending and descending axonal tracts, thereby disrupting proper information transmission between the brain, the spinal cord, and the body periphery. Re-establishing neural connectivity beyond the site of injury is an essential prerequisite for functional recovery to occur. Without intervention, CNS axons fail to regenerate, leading to a mostly permanent impairment of sensorimotor function, sexual function, and autonomic dysfunction, tremendously reducing the patients' quality of life.

Constant progress in neuroscience, surgical procedures, clinical management and rehabilitative paradigms significantly improve functional outcomes and decrease morbidity in SCI patients. Thus, nowadays, affected individuals reach a lifespan comparable to healthy individuals but face years and decades of permanent paralysis, sensory and motor disabilities as well as neuropathic pain, dependent upon the location and severity of the injury (Rowland, Hawryluk et al. 2008, Blesch and Tuszynski 2009, Weidner, Rupp et al. 2017). Although a considerable effort has been spent over the last decades to develop new effective treatment paradigms, no randomized clinical trial has yet shown significant functional improvement after SCI (Fehlings, Tetreault et al. 2017, Blight, Hsieh et al. 2019, Courtine and Sofroniew 2019, Silvestro, Bramanti et al. 2020). A putative repair strategy must tackle several aspects of the multi-facetted pathophysiology of SCI to achieve clinical efficacy. Amongst the plethora of different experimental approaches, biomaterial-supported transplantation of axonal growth-permissive cells holds great promise in facilitating axonal regeneration across SCI lesion site to restore neural connectivity and eventually improve functional outcomes (Liu, Schackel et al. 2017).

1.1 Spinal cord injury

Spinal cord injury is clinically defined as either traumatic or non-traumatic induced damage to the neural tissue of the spinal cord that results in neurological deficits below the level of injury (Weidner, Rupp et al. 2017). Globally, SCI has a total incidence of 10.5 cases per 100,000 individuals with ~ 250,000 to 500,000 new cases every year. Based on worldwide region-dependent differences, in Europe, the mean incidence is 3.4 cases per 100,000 individuals and 5.1 cases per 100,000 individuals in the USA/Canada (WHO 2013, Singh, Tetreault et al. 2014, Kumar, Lim et al. 2018).

Traumatic SCI results from a mechanical impact onto the spinal column causing contusion, compression, extension, flexion, laceration or (partial) transection of the spinal tissue. According to the National Spinal Cord Injury Statistical Center, traumatic SCI is most frequently caused by traffic accidents (38.6%), bodily violence (14.0%), sport accidents (7.8%), and falls (32.2%) (National Spinal Cord Injury Statistical Center 2020). Epidemiological analysis of the age distribution revealed 2 peaks within the SCI populations, the first peak was identified for young adults at 15 – 29 years of age and the second peak for the elderly people with an age above 65 years. The sex ratio tends to show a predominance of males among cases (van den Berg, Castellote et al. 2010, Kumar, Lim et al. 2018). Along with the global demographic change in age, also the fraction of elderly SCI patients is constantly increasing. Hence, the prevalence of falls of elderly and SCI pathologies as consequences of non-traumatic conditions such as cancer, chronic neurodegenerative diseases, infection, (neuro-)inflammatory events and other etiologies are dramatically increasing (McKinley, Jackson et al. 1999, van den Berg, Castellote et al. 2010, Silvestro, Bramanti et al. 2020). Statistical analysis regarding the level of injury showed 54% of all human SCI occur in the cervical, 24% in the thoracic, 19% in the lumbar and ~1% in the sacral spinal cord and, interestingly, a greater fraction of cervical SCI was found in the elderly (> 60 years, 94% cervical SCI) compared to younger individuals (< 60 years, 70% cervical SCI) (Pickett, Campos-Benitez et al. 2006). Hence, SCI was recognized as an important global health priority representing a significant burden for the affected individuals and their social environment as well as for modern medicine and society (Global Burden of Disease Study 2016: Traumatic Brain Injury and Spinal Cord Injury Collaborators 2019).

1.1.1 Pathophysiology of spinal cord injury in humans

The clinical picture of SCI can be classified as sensory and/or motor complete or incomplete reflecting varying degrees of sensorimotor and autonomic impairment below the level of injury. Dependent upon the level of SCI, motor impairments can affect only the hindlimbs (paraplegic)

or affect all extremities (tetraplegic). A commonly used clinical classification system for SCI is the American Spinal Cord Injury Impairment scale according to standardized neurological examination protocols testing sensory and motor functions below the neurological level of injury (Roberts, Leonard et al. 2017).

The pathophysiology of SCI is a sequence of a myriad of different molecular, cellular and systemic processes triggered by the initial damage to the spinal tissue. It can be subcategorized into primary and secondary injury phase followed by the persisting chronic phase (**FIG 1**).

Initially, a mechanical force impacts the spinal column what directly induces neural tissue destruction, disruption of axonal tracts, intraspinal bleeding and subsequently spinal swelling and eventually cell death by compression and/or (partial) transection of the spinal cord (Norenberg, Smith et al. 2004, Rowland, Hawryluk et al. 2008). Additionally, bone and tissue fragments of the initial impact can penetrate the spinal tissue and thereby exacerbate neural damage. Subsequently, the secondary injury phase follows which is characterized by a breakdown of the blood-spinal cord-barrier (BSCB) and a delayed period of extensive hemorrhaging in the grey and white matter (GM/WM), (neuro-)inflammation, hypoxia, and ischemia leading to progressing additional necrotic tissue loss (Rowland, Hawryluk et al. 2008, Ahuja, Nori et al. 2017). As a consequence of vasculature destruction and progressing BSCB leakage, blood vessels at the lesion penumbra become hyperpermeable, enabling the infiltration of inflammatory cells into the lesion site and the surrounding spinal parenchyma (Haggerty, Maldonado-Lasuncion et al. 2018). Signals released from damaged and apoptotic cells recruit and orchestrate the initial acute immune response at the lesion site, which is composed of mainly activated macrophages/microglia as well as other blood-derived immune cells such as lymphocytes and neutrophils (Zhang and Mosser 2008, Zhang, Raoof et al. 2010). Within the first 12 hours post-injury, infiltrated inflammatory cells secrete immunomodulatory factors like tumor necrosis factor α (TNFα), interleukin-1α (IL-1α), IL-1β, and IL-6 (Nakamura, Houghtling et al. 2003, Donnelly and Popovich 2008, Kim, Ha et al. 2017). Additionally, deteriorated tissue homeostasis causes ionic dysregulation, excitotoxicity, accumulation of reactive oxygen species (ROS) and nitric oxide (NO), and intracellular hypercalcemia further contributes to neuronal and glial cell loss (Li and Stys 2000, Park, Velumian et al. 2004, Rowland, Hawryluk et al. 2008, Ahuja, Nori et al. 2017). Onset of oligodendrocyte apoptosis leads to chronic demyelination, anterograde axonal dieback and ongoing Wallerian degeneration (Norenberg, Smith et al. 2004). Together, all these processes participate in the propagation of necrosis and tissue loss aggravating lesion extent and finally exacerbating neurological deficits early after SCI (0 – 48 hours post-injury) (Liu, Wu et al. 2015).

A few days after SCI, cell and myelin debris clearance reaches its maximum and the inflammatory spread is chemically and physically restricted by narrow astrocytic scars separating the

necrotic lesion core from the healthy adjacent spinal parenchyma (Sofroniew 2014, Sofroniew 2015). Further, cells associated with tissue repair and replacement -including endothelial progenitors, fibroblast-lineage cells and neural precursors- become locally activated and migrate towards the lesion core (Burda and Sofroniew 2014). Intact spinal tissue directly adjacent to the SCI becomes partially activated and undergoes substantial tissue reorganization, local circuit remodeling, and collateral axonal sprouting (Rowland, Hawryluk et al. 2008, O'Shea, Burda et al. 2017). Spontaneous functional recovery may occur during the subacute and later on in the chronic phase due to spared axonal tracts, but this remains very limited (Rowland, Hawryluk et al. 2008).

In the subchronic and chronic phase after SCI (> 6 months post-injury), a cystic cavitation has formed in most cases at the lesion epicenter surrounded by a cellular compartment comprised mainly of non-neural stromal cells and the surrounding astrocytic and fibroglial scars have fully matured (O'Shea, Burda et al. 2017). More than a year after the initial injury, neurological deficits in sensory and motor function have clinically manifested and stabilized in most cases (Rowland, Hawryluk et al. 2008). Neurological deficits range from partial or complete paralysis of the lower and upper extremities (paraplegia and tetraplegia) to sensory (mechanosensation, thermal sensation) and proprioceptive impairments as well as pathologic neuropathic pain, and autonomic dysfunction including respiratory, cardiovascular and thermoregulatory, bowel and bladder function as well sexual function can be affected in a location and severity-dependent fashion (Winslow and Rozovsky 2003, Finnerup, Sorensen et al. 2007, Felix and Widerstrom-Noga 2009, Finnerup 2013, Hou and Rabchevsky 2014, Weidner, Rupp et al. 2017). Further, several secondary complications might develop in the chronic phase like, for instance, pressure ulcers, impaired immunity, spasticity, muscular atrophy, and osteoporosis as well as psychological symptoms such as (severe) depression and distress (McKinley, Jackson et al. 1999, Craig, Tran et al. 2009, Sezer, Akkus et al. 2015).

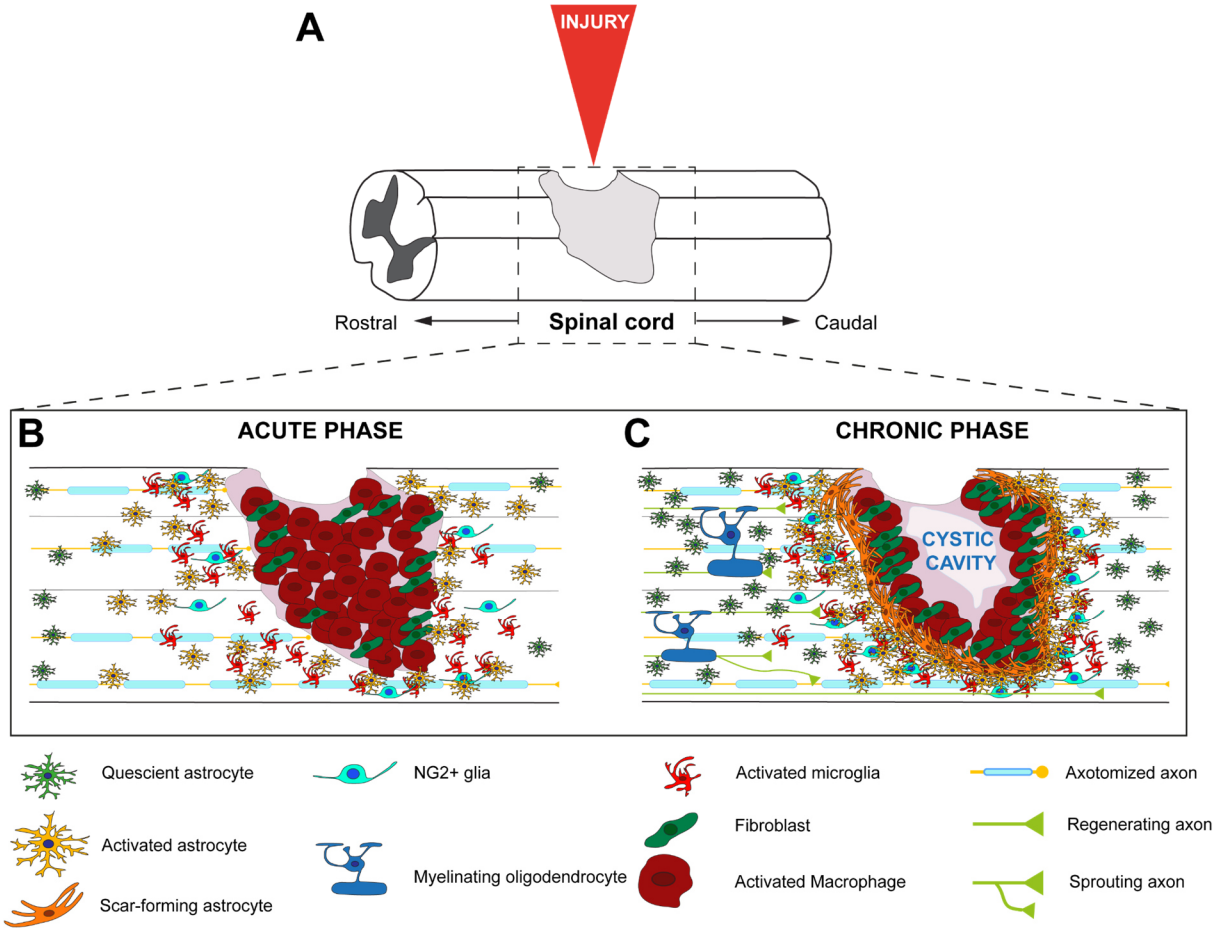

Figure 1: Pathophysiology of traumatic SCI. (**A**) An initial trauma to the spinal column leads to the destruction of spinal tissue. Ascending and descending axonal tracts become disrupted accompanied by BSCB breakdown and vasculature collapse. (**B**) Consequently, the lesion site is filled with blood, cellular and myelin debris and, subsequentially, infiltrated by activated resident microglia/macrophages and blood-derived immune cells initiating a neuroinflammatory cascade that results in the recruitment of further immune cells, activated resident astrocytes as well as NG2⁺ glia precursors and meningeal fibroblasts. Ongoing neuroinflammation causes an expansion of the necrotic lesion into the adjacent intact spinal cord. Moreover, neural cell loss proceeds, and more activated astrocytes are recruited to the lesion site. Activated astrocytes start to seal the disrupted blood-spinal cord-barrier. In contrast, activated scar-forming astrocytes, in parallel with fibroblasts and other stromal cells, form a fibrotic scar at the lesion core. Activated scar-forming astrocytes finally form a dense network of elongated astrocytic processes to seal the necrotic lesion core and prevent further expansion of the damaged area. Damaged spinal axons retract and degenerate. (**C**) In the chronic phase, the astroglial scar is fully matured and surrounds the lesion. A cystic cavity has been established at the lesion core, surrounded by stromal cells and meningeal fibroblasts. Local neuronal circuit reorganization and other neuroplastic changes occur in the spinal tissue adjacent to the lesion site leading and contributing to a minimal amount of natural recovery. Freshly differentiated oligodendrocytes start to myelinate the newly organized circuitries and re-myelinate spared spinal axons.

1.1.2 Hurdles for spinal cord regeneration

In addition to destructive primary and secondary injury mechanisms, there are various intrinsic and extrinsic hurdles for CNS axon regeneration (Blesch and Tuszynski 2009, Cregg, DePaul et al. 2014, Ahuja, Nori et al. 2017, Sofroniew 2018).

For decades, astroglial scarring around CNS injury sites was proposed to be a major cause for CNS axonal regenerative failure (Cajal 1928). Reactive, scar-forming astrocytes were considered as an impermeable physical barrier for growing axons and, more importantly, as the primary source of growth-repulsive molecules (diffuse and contact-depending axonal growth inhibitors) such as chondroitin sulfate proteoglycans (CSPGs) at the lesion site (Davies, Goucher et al. 1999, Jones, Margolis et al. 2003, Tang, Davies et al. 2003, Tom, Doller et al. 2004, Tom, Steinmetz et al. 2004, Buss, Pech et al. 2009, Wanner, Anderson et al. 2013, Cregg, DePaul et al. 2014). However, over the last years, compelling evidence arose that challenged this view of the astroglial scar as the major hurdle for axonal regeneration in the CNS (Sofroniew 2018). Mature scars at CNS lesions are built up in a structurally layered manner. After an injury, perivascular/meningeal fibroblasts and stromal cells accumulate at the lesion epicenter, forming a non-neural lesion core considerably contributing to the inhibitory character of the scar (Pasterkamp, Giger et al. 1999, Bundesen, Scheel et al. 2003, Goritz, Dias et al. 2011, Soderblom, Luo et al. 2013).

More intriguing, the extracellular milieu and molecular environment in the intact as well as damaged adult mammalian CNS does not allow for extensive long-distance axonal growth but only local axonal sprouting and plasticity (Ahuja, Nori et al. 2017, Fuhrmann, Anandakumaran et al. 2017, Curcio and Bradke 2018, Fawcett and Verhaagen 2018, Fuhrmann, Anandakumaran et al. 2018). As a consequence of myelin sheath destruction during CNS injury, potent axon growth-inhibitors including neurite outgrowth inhibitor-A (Nogo-A), myelin-associated glycoprotein (MAG), oligodendrocyte-myelin glycoprotein (OMgp), semaphorins, and ephrins are released (McKerracher, David et al. 1994, Chen, Huber et al. 2000, GrandPre, Nakamura et al. 2000, Kottis, Thibault et al. 2002, Moreau-Fauvarque, Kumanogoh et al. 2003, Benson, Romero et al. 2005) Although structurally distinct, Nogo-A, MAG and OMgp bind to the same receptor, Nogo receptor 1 (NgR1), comprised with other complex members p75-NTR and LINGO-1 (Atwal, Pinkston-Gosse et al. 2008). Receptor binding, hence, activates Rho A/ROCK (Rho-associated protein kinase) signaling resulting in actin cytoskeleton destabilization, growth cone collapse and finally inhibition of neurite outgrowth (Winton, Dubreuil et al. 2002, Filbin 2003, Yiu and He 2006). Experimental blocking of ligand binding to NgR or genetic depletion of myelin-associated inhibitors lead to promising results in rodent models, but the extent of its benefits in human SCI patients is still under investigation (Bregman, Kunkel-Bagden et al. 1995, Huang, McKerracher et al. 1999, Zheng, Atwal et al. 2005, Lee, Chow et

al. 2010, Lee, Geoffroy et al. 2010) also by a phase II clinical trial in our department ("NISCI – Nogo Inhibition in Spinal Cord Injury", NCT identifier: NCT03935321).

Furthermore, CSPG expression at and around adult CNS lesion sites has long been considered as purely inhibitory to axonal regeneration (Davies, Fitch et al. 1997, Davies, Goucher et al. 1999). At acute SCI lesions, several cell types, including astrocytes, activated microglia and macrophages, pericytes, and meningeal/perivascular fibroblasts express different subtypes of CSPGs like aggrecan, brevican, neurocan, and versican (Volpato, Fuhrmann et al. 2013, Anderson, Burda et al. 2016, van Niekerk, Tuszynski et al. 2016). CSPGs mediate their axonal growth inhibition via activation of the Rho/ROCK pathway, phosphorylation of epidermal growth factor receptor (EGFR), Akt inhibition, and Erk1/2 phosphorylation through binding to their receptors, leukocyte common antigen-related phosphatase (LAR), protein tyrosine phosphatase σ (PTPσ) as well as the Nogo receptors NgR1 and NgR3 (Koprivica, Cho et al. 2005, Cregg, DePaul et al. 2014, Dyck, Alizadeh et al. 2015). Recent studies implicated CSPG expression of neurons and astrocytes as an essential part of the perineuronal net (PNN) that limits and restricts synapse remodeling and neuroplasticity during development and adulthood but also after CNS insults and disease (Wang and Fawcett 2012, Mironova and Giger 2013, Dyck, Alizadeh et al. 2015). Interestingly, also myelin-associated inhibitors were implicated in regulating synapse remodeling during health and disease (Schwab and Strittmatter 2014). Experimental removal of CSPGs at acute and chronic lesion sites by genetic depletion, enzymatic digestion or receptor blockade failed to induce long-distance axonal growth but rather lead to local circuit reorganization, especially in models of incomplete SCI (Bradbury, Moon et al. 2002, Massey, Hubscher et al. 2006, Garcia-Alias, Barkhuysen et al. 2009, Wang, Ichiyama et al. 2011, Shinozaki, Iwanami et al. 2016). Hence, axonal growth inhibition through myelin-associated inhibitors and CSPGs might be rather relative than absolute as shown *in vitro* and *in vivo*. For example, a permissive laminin substrate can induce neurite outgrowth *in vitro* even in the presence of growth inhibitors (Tom, Steinmetz et al. 2004). *In vivo*, not only repulsive molecules such as myelin-associated inhibitors and CSPGs but also growth permissive substrates like laminin are present at SCI lesion sites (Anderson, Burda et al. 2016). Moreover, appropriately stimulated and chemoattracted axons grow robustly through regions of increased CSPG expression and astrocytic scars in a laminin-integrin-dependent manner (Jones, Sajed et al. 2003, Lu, Jones et al. 2007, Anderson, Burda et al. 2016).

Finally, since adult CNS neurons have downregulated their developmental axonal growth capacity, they essentially lack the capacity to initiate developmental genetic growth programs thereby fail to regrow after injury during adulthood (Goldberg, Klassen et al. 2002, Sun and He 2010, Puttagunta, Tedeschi et al. 2014, He and Jin 2016). In contrast, neurons of the peripheral

nervous system (PNS) harbor the ability to regenerate in adulthood (Plunet, Kwon et al. 2002, Raivich, Bohatschek et al. 2004, Seijffers, Allchorne et al. 2006).

1.1.3 Endogenous repair mechanisms

Since the adult CNS harbors only a very limited intrinsic regenerative capacity, insults such as spinal cord injury are especially devastating for the affected individuals and their social communities. Adult CNS neurons fail to regenerate across extended SCI lesion sites due to (1) lack of intrinsic genetic programs to initiate and maintain axonal growth, (2) growth-inhibitory microenvironment at CNS lesion sites, (3) lack of (neuro-)trophic support, and (4) lack of structural support and guidance for regenerating axons at lesion sites (Blesch and Tuszynski 2009, Silver, Schwab et al. 2014, Fawcett and Verhaagen 2018, Sofroniew 2018). Nonetheless, the notion that the adult mammalian CNS is entirely static is incorrect, although long-distance axonal regeneration does not naturally occur, local axonal sprouting and circuit reorganization do allow for a limited degree of functional recovery (Onifer, Smith et al. 2011). In particular, electromyographic (EMG) recordings revealed recovery of hindlimb function after contusion or transection injuries in rodents (Basso, Beattie et al. 1996, Loy, Magnuson et al. 2002, Basso, Fisher et al. 2006). Likewise, EMG analysis found reoccurring muscle activity in SCI patients after complete cervical or thoracic SCI (Calancie, Molano et al. 2002, Dietz, Grillner et al. 2009).
Intriguingly, the formation of an astroglial scar has to be considered as an essential endogenous repair mechanism early after SCI. Scar-forming astrocytes align into a distinct limitans border that separates the necrotic and apoptotic lesion core from the healthy surrounding spinal parenchyma, thereby, restricting the spread of neuroinflammation, necrosis and neural tissue loss (Sofroniew 2015). Notably, neither experimental ablation of astrocyte scar formation nor the removal of chronic astrocytic scars leads to enhanced spontaneous axonal regeneration after SCI but significantly enhanced axonal dieback (Anderson, Burda et al. 2016).
Further, the recruitment of inflammatory and blood-derived immune cells to the lesion site immediately after the initial impact to the spinal cord primarily serve to clear the lesion site from pathogens, foreign bodies as well as cellular and myelin debris (Okada 2016). Upon resolution of the acute immune response, tissue-resident activated macrophages phenotypically transform from a cytotoxic inflammatory state (M1 macrophages) into a regulatory pro-regenerative state (M2 macrophages) (Kigerl, Gensel et al. 2009). Although pro-inflammatory, M1 macrophages secrete pro-angiogenic factors that initiate revascularization of the lesion site and the later M2 macrophages promote stabilization and maturation of the newly formed vasculature (Nucera, Biziato et al. 2011, Spiller, Nassiri et al. 2015). Additionally, M2 macrophages were shown to be involved in the regulation of oligodendrocyte differentiation, remyelination, and

neuroprotection (Kigerl, Gensel et al. 2009, Miron, Boyd et al. 2013). Moreover, activated macrophages can functionally adapt their phenotype in a context-dependent manner in response to new stimuli (Stout and Suttles 2004, Martinez and Gordon 2014, Gensel and Zhang 2015). Initially after SCI (~24 h post-injury), local $NG2^+$ glia precursors become activated and differentiate into scar-forming astrocytes (Zai and Wrathall 2005, Hackett, Yahn et al. 2018). Later, platelet-derived growth factor-receptor α^+ ($PDGFR\alpha^+$) glia precursors give rise to oligodendrocyte precursor cells (OPCs) and finally myelinating Schwann cells (SC) and mature oligodendrocytes (Assinck, Duncan et al. 2017). Moreover, SC remyelination occurs shortly after SCI (within 7 - 14 days post-injury) compared to oligodendrocytic remyelination (Duncan, Radcliff et al. 2018). Hence, there is substantial and progressing remyelination of spared axons after SCI (Powers, Lasiene et al. 2012, Assinck, Duncan et al. 2017).

More importantly, the adult spinal cord is characterized by a certain degree of neuronal plasticity after injury. Although many synapses are lost at the site of injury and in the spinal areas below the injury, local spontaneous axonal sprouting and neuronal circuit remodeling occur (Weidner, Ner et al. 2001, Bareyre, Kerschensteiner et al. 2004, Rosenzweig, Courtine et al. 2010). In particular, after incomplete SCI, axonal sprouting of descending spinal tracts (e.g., corticospinal tract (CST), raphespinal tract, reticulospinal tract) and local supraspinal axons possibly could account for spontaneous functional recovery (Courtine, Song et al. 2008, Takeoka, Vollenweider et al. 2014).

1.1.4 Current treatment regimens and preclinical approaches

The complex and highly variable pathophysiology of SCI makes clinical management extraordinarily challenging. Most current SCI treatment regimens aim at ameliorating secondary injury mechanisms to prevent lesion expansion and limit neural tissue loss. Mostly, immediate securing of respiratory function, circulation stabilization and prevention of acute hypotension followed by surgical decompression of the lesioned spinal area represents the first clinical interventions established to improve the patients' functional outcome (Batchelor, Wills et al. 2013, Ahuja, Nori et al. 2017, AOSPINE 2017). To date, immediate administration (< 8 h post-injury) of high doses of the glucocorticoid steroid methylprednisolone (MP) for 24 h represents the only pharmacologic intervention shown to elicit neurological benefits for the affected individuals. Mechanistically, MP treatment reduces oxidative stress and ameliorates the acute inflammatory response, thereby enhancing neuroprotection and neural cell survival (Ahuja, Nori et al. 2017, AOSPINE 2017). However, its use in acute SCI patients remains controversial (Hurlbert, Hadley et al. 2013). Additionally, blood pressure augmentation was shown to improve tissue preservation and neurological outcome measures by enhancing perfusion

(Wilson, Forgione et al. 2013, Ahuja, Nori et al. 2017). After clinical handling of acute injury-related pathologies, rehabilitative training is widely used to induce neuronal circuit reorganization and neuroplasticity in affected individuals (Field-Fote, Lindley et al. 2005, Morawietz and Moffat 2013).

Since clinical interventions for acute SCI patients remain limited in number and success, various experimental approaches to improve neuroprotection and support endogenous neuroregeneration were developed and partially tested in clinical trials. Putative pharmacological agents for SCI treatment include mainly anti-inflammatory and neuroprotective drugs. For example, Riluzole, a benzothiazole sodium channel blocker, restricts presynaptic glutamate release and blocks sodium influx into neurons, thereby preventing excitotoxic cell death (Nogradi, Szabo et al. 2007). Studies in animal models demonstrated its efficacy after SCI and a randomized control phase II/III clinical trial was launched in 2017/2018 (Schwartz and Fehlings 2001, Simard, Tsymbalyuk et al. 2012, Ahuja, Nori et al. 2017). Riluzole is approved by the US Food and Drug Administration (FDA) and European as well as Canadian health authorities for amyotrophic lateral sclerosis (ALS) treatment (Bhatt and Gordon 2007).

Minocycline, a bacteriostatic tetracycline antibiotic, was shown to elicit neuroprotection and anti-inflammatory behavior by inhibition of microglial activation and downregulation of pro-inflammatory cytokines in preclinical models of CNS disease and animal SCI models (Giuliani, Fu et al. 2005, Festoff, Ameenuddin et al. 2006, Seabrook, Jiang et al. 2006). In patients with incomplete cervical SCI, a completed phase II clinical trial demonstrated elevated neurological outcomes and lead to a placebo-controlled phase III trial (Casha, Zygun et al. 2012).

Besides synthetic drugs, growth factors were enrolled in experimental treatment paradigms. For example, granulocyte colony-stimulating factor (G-CSF) has been demonstrated to have anti-inflammatory and anti-apoptotic effects in the CNS and was tested for safety in a non-randomized phase I/IIa clinical trial that also showed improvements in American Spinal Injury Association Impairment Scale (AIS) outcomes (Takahashi, Yamazaki et al. 2012, Wallner, Peters et al. 2015). Additionally, fibroblast growth factor (FGF) and hepatocyte growth factor (HGF) showed promising neuroprotective and anti-inflammatory effects with respective improved functional outcomes in animal models and early phase I/II clinical trials (Teng, Mocchetti et al. 1999, Kitamura, Fujiyoshi et al. 2011). Furthermore, pharmacological agents that interfere with the axonal degeneration and support neuroregeneration were tested experimentally but also in clinical trials. For instance, Cethrin/VX-210 is a specific Rho inhibitor that was tested in phase I/II clinical trials, where it showed no adverse side effects and improved motor recovery (Fehlings, Tetreault et al. 2017). A phase III trial in acute cervical SCI subjects was recently initiated (Fehlings, Kim et al. 2018). Similarly, monoclonal antibodies against Nogo-A (anti-

Nogo) showed promising results in terms of animal studies by neutralizing the inhibitory environment at SCI sites. Anti-Nogo antibodies were successfully tested in phase I (Bregman, Kunkel-Bagden et al. 1995, Kucher, Johns et al. 2018) and recently, a European-wide multicenter phase II clinical trial was launched, including our own department (NISCI – Nogo Inhibition in Spinal Cord injury, NCT identifier: NCT03935321).
Alternatively, various neurotechnology approaches including brain-computer-interface (BCI)-driven neuroprostheses, functional electrostimulation (FES) of the spinal cord alone or in combination with (weight-supported) locomotion training as well as gait-supporting exoskeletons are currently under investigation in SCI patients (Rupp 2014, Courtine and Sofroniew 2019).

1.2 Astrocytes as key players in the healthy and injured central nervous system

The adult mammalian CNS is characterized by a high degree of morphological and functional complexity. Based upon this complexity, injuries to the adult CNS, such as SCI, have a multifactorial character with various molecular and cellular components, and their intricate interactome leading to disastrous consequences for injury affected individuals. Over the last decades, resident CNS glia cells, namely astrocytes and microglia, came into focus in the neuroregeneration field as potential key players for both regenerative success and failure after CNS injury or disease.
Neuroglia, in particular astrocytes, were first described by Rudolf Virchow in the middle of the 19th century as a homogenous cell population that supports neuronal (Virchow 1858). Since then, astrocytes have been characterized as the most abundant cell type in the adult mammalian CNS, outnumbering neurons by nearly eightfold (Freeman 2010, Sofroniew and Vinters 2010). On average, each astrocyte extends processes and interacts with 8 neuronal cell bodies, 5 blood vessels, and more than 100,000 synapses (Bushong, Martone et al. 2002). Hence, astrocytic loss of function or abnormal gain of function is often associated with severe CNS disorders and disabilities (Sofroniew and Vinters 2010).

1.2.1 Astrocyte development, specification and heterogeneity

Neurogenesis developmentally precedes gliogenesis with neural stem cells (NSCs) and radial glia cells as the cellular origin for both neurons and glia cells, respectively. Gliogenesis is initiated by inhibition of neurogenesis in NSCs through acetylation and tri-methylation of the proneuronal genes *neurogenin-1 (ngn-1)* and *neurogenin-2 (ngn-2)* inducing the transition from

NSCs to glia-restricted precursor cells (GRPs) (Hirabayashi, Itoh et al. 2004, Hirabayashi, Suzki et al. 2009). This so-called gliogenic switch occurs at embryonic day 12.5 (E12.5) in the developing spinal cord and in the cortex at E16-18 in rodents (Deneen, Ho et al. 2006, Ge, Miyawaki et al. 2012, Kang, Lee et al. 2012). Additionally, positive Notch signaling activates cardiotrophin-1 (CT-1)/Janus kinase-signal transducers and activators of transcription (JAK-STAT) axis in GRPs inducing the expression of pro-glionic and eventually pro-astrocytic genes such as Nuclear factors-1A and B (NFIA/B) and Sex-determining region Y-box 9 (Sox9) (Namihira, Kohyama et al. 2009). The transcription factor Sox9 is expressed by NSCs from E10.5 on in the ventricular zone (VZ) of the developing mammalian spinal cord and triggers NFIA/B expression at E11.5 (Stolt, Lommes et al. 2003, Kang, Lee et al. 2012). Both factors form a transcriptional complex that acts as an inducer of GFAP (Glial fibrillary acidic protein) expression either directly or indirectly via enhanced STAT3 signaling in GRPs in a Sonic hedgehog (Shh)- and Notch-dependent way (Namihira, Kohyama et al. 2009). From E17.5 on, GFAP is expressed in mice and represents a key regulator of the astrocytic lineage driving astrocyte precursor cell (APC) migration and terminal specification. However, GFAP itself is finely regulated by other signaling cascades, including Notch and Bone morphogenetic protein (BMP) signaling (Barnabe-Heider, Wasylnka et al. 2005, Miller and Gauthier 2007, Namihira, Kohyama et al. 2009). Extrinsically, astrocyte differentiation can be influenced by IL-6, CT-1, JAK/STAT, and Ciliary neurotrophic factor (CNTF)/Leukemia inhibitory factor (LIF) cascades (Barnabe-Heider, Wasylnka et al. 2005, Miller and Gauthier 2007). Finally, APCs start to migrate along radial glia processes in the late embryonic stage towards their final destinations throughout the CNS. Importantly, evidence from lineage-tracing studies in rodents suggests a second wave of APC migration in the postnatal stage along white matter tracts and radially into grey matter regions as well as limited migration from their ventricular zone origin (Hatton, Nguyen et al. 1993, Jacobsen and Miller 2003).

During migration, terminal astrocyte specification and functional maturation are initiated in APCs. The exact mechanism of how APCs adopt their final molecular and functional phenotype still remains elusive. However, lineage-tracing studies clearly support an instructive role of developmental patterning to be essential in astrocyte subtype specification (Molofsky, Krencik et al. 2012). Tight spatial and temporal expression profiles of morphogenic genes and transcription factors result in domain patterning along the dorsoventral axis of the developing spinal cord where distinct domains give rise to specific neuronal and astrocytic subtypes representing their original patterning domain (Muroyama, Fujiwara et al. 2005, Molofsky, Krencik et al. 2012). For example, three subclasses of white matter astrocytes (VA1, VA2, VA3) arise from the postnatal ventral spinal cord (Hochstim, Deneen et al. 2008). In adulthood, a plethora of plastic specialized astrocyte subtypes develop depending on their location and overall CNS

physiology. From a classical anatomical perspective, the adult CNS contains two different astrocyte subtypes, namely protoplasmic astrocytes in the GM and fibrous astrocytes in the WM (Freeman 2010). Recently, multiple astrocyte subtypes were identified by astrocyte-specific reporter mouse lines, sophisticated single cell-RNA sequencing and transcriptional profiling approaches (Emsley and Macklis 2006, Molofsky, Kelley et al. 2014, Lanjakornsiripan, Pior et al. 2018). Zeisel and colleagues applied single cell-transcriptional profiling in combination with data-driven taxonomy clustering to ~500,000 cells of the adult mouse CNS. They were able to classify seven regionally distinct astrocytic subtypes within the brain. The spatial distribution of these astrocytic subtypes correlated with different anatomical brain compartments with little to no overlap. Moreover, the spatial distribution was associated with potential functional implications; for example, the separation between telencephalic and non-telencephalic astrocytes was evident at the anatomical level, and also when the expression of neurotransmitter transporters were present. In particular, vesicular glutamate transporter 1 (VGLUT1) was expressed by telencephalic astrocytes, whereas glycine transporter (GLYT1) was exclusively expressed in non-telencephalic astrocytes (Zeisel, Hochgerner et al. 2018). Likewise, Batiuk et al. performed single cell-transcriptional profiling and *in situ*-hybridization (RNAscope) on cortex- and hippocampus-derived astrocytes and found five molecularly distinct astrocyte subtypes. Interestingly, from all analyzed genes, only 30% were commonly expressed across the majority of astrocytes, with > 70% of all genes differentially expressed. Commonly expressed genes were mainly associated with energy metabolism (e.g., *Ldha* involved in glycolysis/lactate synthesis) and astrocyte specification (e.g., *Sox9*). Furthermore, two identified subtypes were linked to neurogenesis (expression of stem cell genes *Ascl1, Dab1* and *Slc1a3*) and adult astrocyte precursor niches (expression of cell cycle control genes *Sirt2, Sept2, Emp2*) (Batiuk, Martirosyan et al. 2020). Within the neocortex, layer-specific astrocyte populations with distinct morphologies were recently identified using a combination of Aldh1L1- and GLT-1/EAAT2-reporter mouse lines together with fluorescence activated cell sorting (FACS) and RNAseq (Morel, Chiang et al. 2017, Morel, Men et al. 2019). In adulthood, molecular differences between outer cortex layer (I + II) and deeper layer (III, IV) astrocytes might reflect layer-specific neuron-astrocyte interactions and originate from developmental cortex layering, since Layer I astrocytes are born around E12 in mouse and retain a rather immature and precursor-like transcriptome, whereas later-born astrocytes of cortical layer III and IV predominantly express perisynaptic astroglial proteins. Furthermore, Layer I astrocytes developmentally originate from ventricular zone-precursors at the basal lamina and deeper layer astrocytes from subventricular zone-derived radial glia and immature astrocyte precursors in the late embryonic and early postnatal stage, which may also contribute to layer-specific differences (Ge, Miyawaki et al.

2012, Tabata 2015). Additionally, astrocytes from different cortex layers display distinct morphological patterns and structural interactions with synapses. For instance, Layer I astrocytes occupy a smaller territorial domain than deeper layer astrocytes (Layer II – IV). Cell orientation clustering analysis revealed a radial orientation in Layer I astrocytes and a tangential orientation in astrocytes from Layer II and III (Lanjakornsiripan, Pior et al. 2018).

Proliferation of APCs and maturing astrocytes adds another level of heterogeneity. During development, APC proliferation in the cortex bimodally peaks at E14.5 in the VZ and E16.5 in the surrounding parenchyma, whereas in the spinal cord, APC proliferation maximizes at E14.5 and P2/3 (Ge, Miyawaki et al. 2012, Tien, Tsai et al. 2012). The first wave of proliferation occurs most likely before APC migration at the precursor niches, where radial glia-like cells give rise to early APCs by asymmetric cell divisions (Tien, Tsai et al. 2012). The second wave is done by APCs after migration to their final destinations with symmetric cell divisions (Masahira, Takebayashi et al. 2006, Rowitch and Kriegstein 2010). Importantly, APC proliferation and maturation are molecularly linked through Mitogen-activated protein kinase (MAPK) - Extracellular signal-regulated kinase (ERK) pathway-dependent cytokine expression (Li, Newbern et al. 2012). Additionally, CNS disease and insult tremendously increase astrocyte heterogeneity in a spatial-, temporal- and context-dependent fashion (Anderson, Ao et al. 2014). Liddelow et al. introduced a classification scheme for reactive astrocytes based on a panel of 10 – 13 differentially expressed genes in reactive astrocytes in response to activating stimuli such as IL-1α compared to native quiescent astrocytes. In particular, A1 astrocytes were considered as detrimental and potentially neurotoxic, whereas A2 astrocytes resemble pro-regenerative characteristics (Liddelow, Guttenplan et al. 2017). However, a strict classification of reactive astrocytes into distinct subtypes might not be appropriate, since reactive astrocyte phenotypes were shown to be highly plastic, reversible and -most importantly- dependent on the molecular environment of the individual astrocytes rather than on an intrinsic reactivity program (Hara, Kobayakawa et al. 2017). Given the plastic and heterogeneous nature of APCs as well as terminally differentiated astrocytes during health and disease, the astrocytic transcriptome and marker expression profile remains complex and highly dynamic (Hamby, Coppola et al. 2012, Zamanian, Xu et al. 2012, Rodriguez, Yeh et al. 2014). Thus, astrocyte heterogeneity is determined by differential developmental origins and mainly spatial and cellular context-dependent intrinsic diversity. Astrocyte heterogeneity during reactivity, hence, is stimulus-dependent and additionally added on top of an intrinsically morphological and functionally diverse cell population.

1.2.2 Astrocytes in the healthy central nervous system

During early postnatal CNS development, astrocyte-secreted proteins -including thrombospondins, glypicans, ephrins, and integrins- actively participate in the formation, modulation and elimination of synapses as well as scaffolding and support of migrating neuroblasts and NPCs (Pfrieger and Barres 1997, Christopherson, Ullian et al. 2005, Reichenbach, Derouiche et al. 2010, Kucukdereli, Allen et al. 2011, Allen, Bennett et al. 2012).

In adulthood, one central astrocyte function is the tissue and extracellular homeostasis of ions, metabolites, pH, water, and neurotransmitters (Barres 2008, Obara, Szeliga et al. 2008, Allaman, Belanger et al. 2011, Papadopoulos and Verkman 2013). Especially the regulation of ions and transmitter substances at synaptic clefts underlines their involvement in neuronal network activity and modulation of synaptic transmission and plasticity that leads to the development of the concept of the “tripartite synapse” (Araque and Navarrete 2010). Here, the pre- and post-synaptic compartments are ensheathed by astrocytes enabling them to actively participate in the signal transmission process. For example, buffering of extracellular potassium levels through the inward-rectified potassium channel Kir4.1 was found to be predominantly done by astrocytes in close spatial association to motor neurons in the ventral horn of the spinal cord and in cortical layers II/III and V (Olsen, Campbell et al. 2007, Kelley, Ben Haim et al. 2018). Alternatively, astrocytes can modulate the signal transmission process via secretion of gliotransmitters (e.g., glutamate, D-serine, ATP, adenosine) in a Ca^{2+}-dependent manner (Volterra and Meldolesi 2005, Durkee and Araque 2019). Importantly, astrocytes were shown to mediate activity-dependent stabilization and/or elimination of synapses (Luo and O'Leary 2005, Stevens, Allen et al. 2007, Halassa and Haydon 2010). Astrocytes may additionally support oligodendrocyte-mediated myelination as well as axonal sprouting (Ishibashi, Dakin et al. 2006, Liauw, Hoang et al. 2008, Watkins, Emery et al. 2008). Furthermore, astrocytes form and maintain the blood-brain-barrier (BBB) and the blood-spinal cord-barrier thereby regulating blood flow and molecule transfer between blood and neurons (Takano, Tian et al. 2006, Attwell, Buchan et al. 2010).

Another main feature of astrocytes is their metabolic coupling to neurons. In particular, astrocytes were identified as the primary energy suppliers for neurons in the CNS. Astrocytes take up glucose from nearby blood capillaries, store it intracellularly as glycogen and transmit it as lactate via monocarboxylate transporter 1 or 4 (MCT-1/-4) and MCT-2 to neurons, where lactate is finally converted to pyruvate and serves for ATP synthesis associated with long-term memory formation (Suzuki, Stern et al. 2011). Another implication of the metabolic coupling is uptake, clearance and recycling of neurotransmitters at the synaptic cleft. Since the overstimulation of neuronal glutamate receptors is highly toxic to neurons, excessive glutamate is taken

up by nearby astrocytes via glutamate transporter-1 (GLT-1) and glutamate aspartate transporter (GLAST) and re-distributed to neurons (Bak, Schousboe et al. 2006, McKenna 2007, Sarafian, Montes et al. 2010). Additionally, due to their high expression of antioxidants and ROS-detoxifying enzymes, astrocytes are critical in handling oxidative stress in the CNS (Shih, Johnson et al. 2003, Belanger and Magistretti 2009). Thus, astrocytes are involved in basically all physiological processes of the developing and adult mammalian CNS and are, therefore, key to normal neuronal function.

1.2.3 Astrocytes in the injured central nervous system

The astrocytic response to CNS insults is classically termed reactive astrogliosis and is hallmarked by a broad, finely tuned spectrum of molecular, morphological and functional changes of astrocytes reflecting the type, severity and context of the insult. Most importantly, astrocytes do not respond alone but rather in a coordinated fashion together with other cells including resident microglia and precursor populations as well as non-neural cells to CNS damage. Hence, the CNS response is a plastic cascade of multifactorial and multi-cellular events in a temporal and spatial context-dependent fashion (Sofroniew 2014).

Immediately after injury, reactive astrogliosis is initiated by a myriad of extracellular signaling molecules released and secreted by the damaged neural tissue itself, such as neurotransmitters, purines, ROS, NH_4^+, extracellular glucose and ATP, and infiltrating activated macrophages/microglia as well as blood-derived immune cells (e.g., IL-1, IL-1β, IL-6, interferon γ (INFγ), TNFα) (Sofroniew 2009, Burda and Sofroniew 2014, Sofroniew 2014, Liddelow, Guttenplan et al. 2017). Following BBB/BSCB breakdown, the lesion environment becomes hypoxic contributing to astrocyte activation. Additionally, damaged endothelial cells and blood-derived macrophages secrete endothelin-1 (ET-1) or CT-1 that specifically activate the resident astrocytes and promote injury-related astrocyte proliferation (Barnabe-Heider, Wasylnka et al. 2005, Gadea, Schinelli et al. 2008). As a key event during activation, astrocytes upregulate GFAP in a context- and severity-dependent fashion triggering intracellular cascades including Notch, JAK/STAT, and BMP signaling (Miller and Gauthier 2007, Gallo and Deneen 2014, Hammond, Gadea et al. 2014). Thus, changes in the astrocyte transcriptome are highly selective and linked to specific trigger factors or combinations of different factors enabling the activated astrocytes to react to any alteration of the molecular and cellular environment (Cahoy, Emery et al. 2008, Zamanian, Xu et al. 2012, Anderson, Ao et al. 2014, Orre, Kamphuis et al. 2014, Liddelow, Guttenplan et al. 2017). However, the specific molecular interactions and mechanisms of astrocyte activation remain far from being fully understood.

Another pathological hallmark of injury-activated astrocytes is cellular hypertrophy accompanied by strongly enhanced GFAP expression and increased interdigitation between neighboring astrocytes dependent upon the severity and proximity of the individual astrocyte to the lesion (Sofroniew and Vinters 2010, Anderson, Ao et al. 2014, Sofroniew 2015). Under normal conditions, individual astrocytes occupy spatially distinct and non-overlapping domains in the CNS parenchyma, but during severe astrogliosis, those domains start to overlap since interdigitation between individual astrocyte processes increases (Wilhelmsson, Bushong et al. 2006, Wanner, Anderson et al. 2013). Besides cellular hypertrophy, astrocytes start to proliferate upon injury-related activation. Molecular triggers as well as the origin of the newly proliferated astrocytes at CNS lesion sites, remain elusive and incompletely characterized. However, it has been shown that factors like EGF, FGF, ET-1, Shh and extracellular ATP and the serum proteins albumin and thrombin are experimentally linked to astrocyte proliferation *in vivo* (Gadea, Schinelli et al. 2008, Neary and Zimmermann 2009, Sirko, Behrendt et al. 2013). There is evidence that adult astrocytes can re-enter the cell cycle upon injury-related activation (Buffo, Rite et al. 2008, Gadea, Schinelli et al. 2008). Moreover, $NG2^+$ glia precursors as well as several other precursor cell pools in the adult CNS are considered as potential sources for proliferating astrocytes (Magnus, Carmen et al. 2008, Meletis, Barnabe-Heider et al. 2008, Carlen, Meletis et al. 2009).

Hypertrophic reactive astrocytes start to migrate away from the lesion epicenter towards the lesion margins (penumbra) and blend with newly proliferated astrocytes at the lesion margins (Faulkner, Herrmann et al. 2004). The reactive astrocytes arrange into a thin layer and form a dense mesh-like barrier of entangled filamentous processes at the penumbra that entirely encapsulates the lesion site. Hence, scar-forming reactive astrocytes form a chemical and physical barrier separating the lesion core from the surrounding intact neural networks prohibiting extensive tissue loss and spread of inflammation and necrosis (Wanner, Anderson et al. 2013, Cregg, DePaul et al. 2014, Sofroniew 2015, Anderson, Burda et al. 2016). Finally, maturing astroglial scars start to express and deposit high concentrations of CSPGs (Tang, Davies et al. 2003, Cregg, DePaul et al. 2014).

Thus, for decades, reactive astrocytes and astroglial scars were seen as the primary cause of regenerative failure after CNS damage but this view has been revised over the last years. In fact, reactive astrocytes fulfill a plethora of mainly neuroprotective and immunomodulatory functions, and thereby represent an integral part of the naturally occurring CNS response to damage. For example, CSPG deposition from reactive hypertrophic astrocytes was recently proven to be an essential component for the reorganization of the spared, intact neural tissue adjacent to the lesion site (Wang and Fawcett 2012, Mironova and Giger 2013, Khakh and Sofroniew 2015). Moreover, putative inhibitory CSPGs were mainly secreted by non-neural

stromal cells at the mature lesion core (Anderson, Burda et al. 2016). For instance, aggrecan is absent from acute and mature astroglial scars but present in considerable quantities in the PNN of the adjacent intact tissue (Andrews, Richards et al. 2012, Lang, Cregg et al. 2015, Anderson, Burda et al. 2016). In contrast, scar-forming astrocytes express growth-promoting laminin, and the antibody-blockade of laminin-integrin binding prohibits axonal growth after injury (Anderson, Burda et al. 2016). Moreover, upon appropriate stimulation, regrowing CNS axons extend in direct contact to reactive astrocytes and astroglial scars (Kawaja and Gage 1991, Lee, Geoffroy et al. 2010, Zukor, Belin et al. 2013, Anderson, Burda et al. 2016). Since reactive astrocytes partially originate from adult precursor populations, they share many characteristics of immature astrocytes. Indeed, axons were shown to grow along aligned radial glia cells and astrocyte precursors during development and through cellular grafts containing immature astrocytes (Mason, Edmondson et al. 1988, Davies, Huang et al. 2006, Raper and Mason 2010, Wanner, Anderson et al. 2013, Shih, Lacagnina et al. 2014, Zhang, Burda et al. 2015, Rigby, Gomez et al. 2020). Further, formation of aligned astrocytic bridges at the lesion penumbra was identified by numerous studies as an anatomical predictor for axonal regeneration through SCI lesions (Joosten, Bar et al. 1995, Xu, Guenard et al. 1995, Guest, Hesse et al. 1997, Spilker, Yannas et al. 2001, Iseda, Nishio et al. 2004, Ma, Wei et al. 2004, Liu, Lu et al. 2010, Hurtado, Cregg et al. 2011, Zukor, Belin et al. 2013).

Most intriguingly, genetic ablation or pharmacological depletion of astroglial scarring leads to greatly expanded CNS lesion sites, massive infiltration of inflammatory cells, and worse functional outcomes (Faulkner, Herrmann et al. 2004, Okada, Nakamura et al. 2006, Herrmann, Imura et al. 2008, Wanner, Anderson et al. 2013, Anderson, Burda et al. 2016). In line with this, also genetic ablation of single molecules expressed by reactive astrocytes did not result in significantly improved recovery but appeared to be rather detrimental. For example, although KO of GFAP and vimentin decreased astrogliosis and promoted axonal regrowth, lesion size and immune response were exacerbated which in turn worsens the outcome (Liedtke, Edelmann et al. 1998, Wilhelmsson, Li et al. 2004). In contrast, the combination of administration of chondroitinase ABC (ChABC) and FGF1 was shown to interfere with astrocyte scar formation in such a way to facilitate long-distance axonal regeneration and functional recovery of urinary tract function in a SCI transection model in rats (Tsai, Shen et al. 2008, Lee, Lin et al. 2013). Specifically, FGF1 treatment induced a morphological shift in a subpopulation of reactive astrocytes towards a bipolar/elongated cell shape that formed aligned astrocyte bridges between uninjured host tissue and the lesion site.

As astrocytes make up the BBB/BSCB, they serve as gatekeepers for immune cell invasion into the CNS as well as contact-/diffusion-mediated trafficking of immunomodulatory cytokines. Hence, astrocytes actively take part in the recruitment, instruction and restriction of leukocyte

invasion into the CNS (Bush, Puvanachandra et al. 1999, Voskuhl, Peterson et al. 2009). Dependent upon the type, severity and context of the insult, the transcriptome and secretome of reactive astrocytes adopt pro- and anti-inflammatory capacities (Sofroniew 2014). After exposure to immune-activating molecules (e.g., lipopolysaccharide (LPS), TNFα), reactive astrocytes upregulate signaling pathways such as nuclear factor-κB (NFκB) or suppressor of cytokine signaling 3 (SOCS3) cascades and pro-inflammatory mediators like CC-chemokine ligand 2 (CCL2) and CXC-chemokine ligand 10 (CXCL10) (Okada, Nakamura et al. 2006, Brambilla, Persaud et al. 2009, Kim, Hoffman et al. 2014, Mills Ko, Ma et al. 2014). In contrast, reactive astrocytes can act anti-inflammatory, especially at the lesion penumbra, where astroglial scarring spatially restricts the inflammatory reaction, thereby enhancing tissue sparing (Faulkner, Herrmann et al. 2004, Voskuhl, Peterson et al. 2009, Toft-Hansen, Fuchtbauer et al. 2011). The gp130-STAT3 signaling pathway was identified as crucial for astrocyte-mediated anti-inflammatory processes (Okada, Nakamura et al. 2006, Herrmann, Imura et al. 2008, Wanner, Anderson et al. 2013). Additional secretion of transforming growth factor β (TGFβ), IL-10, IL-11, IL-19, and IL-27 and other signaling molecules by reactive astrocytes attenuates activated macrophages/microglia and supports the resolution of inflammation (Meeuwsen, Persoon-Deen et al. 2003, Min, Yang et al. 2006, Hamby, Coppola et al. 2012, Zamanian, Xu et al. 2012, Norden, Fenn et al. 2014). Importantly, along with their immunomodulatory properties, reactive astrocytes regulate BBB/BSCB integrity, breakdown and repair after CNS insults via secretion of various factors including Shh, retinoic acid, and apolipoprotein E (APOE) (Alvarez, Dodelet-Devillers et al. 2011, Argaw, Asp et al. 2012, Bell, Winkler et al. 2012, Chapouly, Tadesse Argaw et al. 2015).

Finally, non-scar-forming reactive astrocytes in the adjacent intact tissue additionally contribute to neuroprotection via re-establishing and maintenance of the extracellular homeostasis as well as neutralization of free radicals and excitotoxic neurotransmitters (Bush, Puvanachandra et al. 1999, Chen, Vartiainen et al. 2001, Shih, Johnson et al. 2003, Lin, Lou et al. 2008, Zador, Stiver et al. 2009).

1.3 Experimental approaches for spinal cord repair

Unfortunately, although an enormous effort has been spent over the last decades to find new effective treatment paradigms for SCI patients, no randomized clinical trial has shown efficacy in restoring significant function after SCI (Fehlings, Tetreault et al. 2017, Blight, Hsieh et al. 2019, Courtine and Sofroniew 2019). Due to the multi-facetted pathophysiology of SCI, a putative effective repair strategy has to tackle several aspects at once including (1) initiation and maintenance of the intrinsic regenerative capacity of adult CNS neurons, (2) neutralization or

modification of the growth-inhibitory (micro-)environment at lesion sites, as well as (3) structural guidance and trophic support of regrowing axons. Hence, various experimental strategies were developed and tested in preclinical animal models of SCI that addressed individual or multiple of the targets mentioned here.

1.3.1 Modification of central nervous system lesion sites

While the adult PNS is able to regenerate over long distances, the adult CNS fails to regenerate even over short distances. Therefore, the PNS environment seems to be more permissive for axonal growth than the environment at the CNS lesion. As a consequence of this observation, numerous experimental approaches aimed at the modification of the microenvironment at the CNS lesion site to create a milieu allowing for robust axonal growth (Fawcett 2020).

Neutralization of the inhibitory molecules at CNS lesion sites was achieved by the delivery of either ChABC or antibodies blocking myelin-associated inhibitors such as MAG, OMgp or Nogo-A. In particular, administration of ChABC alone or in combination with cells and/or biomaterials resulted in reduction of CSPG levels at lesion sites, fibroglial scarring and partially led to functional recovery (Bradbury, Moon et al. 2002, Massey, Hubscher et al. 2006, Shinozaki, Iwanami et al. 2016, Burnside, De Winter et al. 2018, Fuhrmann, Anandakumaran et al. 2018, Nori, Khazaei et al. 2018, Rosenzweig, Salegio et al. 2019). Blockage of PTPσ receptor binding similarly promoted axonal regeneration and improved functional outcomes (Lang, Cregg et al. 2015). However, the observed functional recovery may have be due to axonal plasticity and reorganization of the PNN rather than restoration of original axonal connections beyond the lesion site (Garcia-Alias, Barkhuysen et al. 2009, Sorg, Berretta et al. 2016). In line with these findings, experimental manipulation of Nogo and its receptors led to long-distance axonal growth and functional recovery in the injured spinal cord, but the underlying anatomical changes in the spinal cord are still unclear (Bregman, Kunkel-Bagden et al. 1995, Huang, McKerracher et al. 1999, Zheng, Ho et al. 2003, Zheng, Atwal et al. 2005, Liu, Lu et al. 2010). Again, positive outcomes after Nogo treatment might be attributed to synapse remodeling and circuit reorganization in the adjacent spinal tissue (Schwab and Strittmatter 2014).

Furthermore, axonal growth could be supported by the reduction of fibroglial scarring around SCI lesions. For example, the microtubule-stabilizing drugs Paclitaxel, Epothilone B and D were used to interfere with fibroblast migration/polarization attenuating scarring and stabilizing regrowing axons at SCI lesion site, thereby, contribute to the recovery of hindlimb locomotor function (Hellal, Hurtado et al. 2011, Ruschel, Hellal et al. 2015, Ruschel and Bradke 2018, Sandner, Puttagunta et al. 2018).

1.3.2 Trophic factor delivery

During development, growing axons are extrinsically guided and attracted by various soluble trophic factors secreted by other CNS cells, however, after damage in the adult CNS, regrowing axons lack this trophic support (Blesch and Tuszynski 2009). Hence, delivery of growth factors and neurotrophins alone or in combination with biomaterials and/or cells into the injured CNS has been extensively investigated over the last decades. Among those trophic factors, neurotrophin-3 (NT-3) and brain-derived neurotrophic factor (BDNF) delivery via various systems for administration promoted regrowth of different spinal tracts after SCI (Bamber, Li et al. 2001, Shumsky, Tobias et al. 2003, Zhou and Shine 2003, Oudega, Hao et al. 2019). However, growth factor delivery also elicited controversial outcomes (Bradbury, King et al. 1998, Griffin and Bradke 2020). Although BDNF delivery in combination with cell transplantation (e.g., BMSCs, SCs) was associated with axonal regeneration after SCI (Sasaki, Radtke et al. 2009, Gunther, Weidner et al. 2015, Ritfeld, Patel et al. 2015, Liu, Sandner et al. 2017), continuous overexpression of BDNF was also linked to abnormal spasticity (Fouad, Bennett et al. 2013). Likewise, ectopic overexpression of NGF was linked to severe hyperalgesia in rats (Tang, Tanelian et al. 2004, Lu, Blesch et al. 2012). The combination of growth factors with stem cell-derived NPCs was found to facilitate long-distance axonal growth within the injured spinal cord, but may harbor the risk of tumor formation (Hofstetter, Holmstrom et al. 2005, Mitsui, Fischer et al. 2005, Johnson, Tatara et al. 2010, Lu, Wang et al. 2012, Lu, Kadoya et al. 2014).

1.3.3 Reawakening of the intrinsic growth capacity of central nervous system neurons

Early transplantation studies of embryonic grafts into CNS lesion sites revealed that graft-derived and, therefore, embryonic axons could grow even over longer distances within the adult CNS (Reier, Bregman et al. 1986, Wictorin, Brundin et al. 1990). Additionally, axons originating from fetal NSC-grafts showed long-distance growth and synapse formation with mature host neurons (Lu, Wang et al. 2012, Lu, Kadoya et al. 2014). Therefore, the inhibitory environment of the adult CNS does not affect embryonic axons, while mature CNS neurons have lost their ability to regrow (Fawcett 2020). Thus, reawakening of this embryonic growth state in adult CNS neurons may have the capacity to induce robust long-distance axonal growth. Moreover, PNS neurons initiate an intrinsic pro-regenerative genetic program after injury leading to the upregulation of regeneration-associated genes (RAGs) thought to be encoding for instructive and regulatory axonal growth-associated genes that finally enables them to regenerate, while, in contrast, damaged CNS axons harbor only a very limited capacity to upregulate RAGs,

therefore, fail to regenerate (Schmitt, Breuer et al. 2003, Palmisano, Danzi et al. 2019). This is particularly striking in sensory axons of the dorsal root ganglia (DRG). Here, the peripheral branch regenerates after axotomy, while the central branch does not. Moreover, after lesioning the peripheral DRG branch, the regenerative capacity of the central branch is significantly improved (Oblinger and Lasek 1984, Erturk, Hellal et al. 2007). This phenomenon was termed a "conditioning effect" and initiates the upregulation of RAGs in the central and peripheral branch of the DRG neuron (Blesch, Lu et al. 2012). Early attempts to mimic the pro-regenerative program of peripheral neurons in the CNS used intraganglionic injection of cyclic adenosine monophosphate (cAMP) *in vitro* and *in vivo* after dorsal column lesion (DCL), however, this did not entirely recapitulate the conditioning effect (Neumann, Bradke et al. 2002, Blesch, Lu et al. 2012).

Transcriptional analysis of conditioned DRG neurons revealed that injury-induced RAGs do not entirely reflect the developmental axonal growth program (Enes, Langwieser et al. 2010). Numerous studies focused on the manipulation of these developmental signaling pathways in injured adult CNS neurons. Most of these pathways are involved in developmental regulation of cytoskeleton dynamics of cellular growth and size as well as axon growth and pathfinding but become inactive in mature CNS neurons. For example, the GTPase RhoA and its downstream effectors are essential mediators of cytoskeleton dynamics of axonal growth and pathfinding during development. However, after injury the adult CNS, RhoA levels are increased at the lesion site and were associated with axonal degeneration and p75-NTR-dependent cell death (Wu and Xu 2016, Kalpachidou, Spiecker et al. 2019). After SCI, inhibition of RhoA can block the detrimental character of myelin-associated inhibitors in rodents and humans (Monnier, Sierra et al. 2003, Joset, Dodd et al. 2010, Fehlings, Theodore et al. 2011). Likewise, Phosphatase and tensin homolog (PTEN) is a negative regulator of the phosphatidylinositol-3-kinase (PI3K)/mammalian target of rapamycin (mTOR) signaling cascade, which controls cell size and growth during development. Thus, genetic depletion of PTEN activated PI3K/AKT pathway eliciting robust axonal regeneration of retinal ganglion cells and corticospinal tract (CST) axons after injury (Park, Liu et al. 2008, Liu, Lu et al. 2010, Zukor, Belin et al. 2013). Similarly, extrinsic inhibition of Glycogen synthase kinase 3 (GSK3), which is involved in microtubule dynamics in axons and gene transcription at the neuronal soma, leads to activation of PI3K pathway and subsequently SMAD1, a transcription factor associated with sensory axon regeneration (Saijilafu, Hur et al. 2013). Alternatively, overexpression of axon growth-stimulating mediators increased axonal regeneration after injury. For example, several studies overexpressed JAK/STAT3 cascade components to successfully boost axon elongation (Miao, Wu et al. 2006, Bareyre, Garzorz et al. 2011, Mehta, Luo et al. 2016). Accordingly, depletion of SOCS3, a negative regulator of the JAK/STAT3 downstream cascade, induced collateral

sprouting of the CST and improved forelimb function after pyramidotomy in mice (Jin, Liu et al. 2015). Additionally, external regulation of JAK/STAT3-dependent transcription factors of the Krüppel-like family (KLF) showed some promise in enhancing axon elongation of mature CNS neurons. KLF7, for instance, is expressed by CNS neurons during developmental periods of axon growth but becomes downregulated in mature CNS neurons. Hence, extrinsic overexpression of KLF7 promoted sprouting as well as long-distance growth of damaged CST axons in adult mice (Moore, Blackmore et al. 2009, Blackmore, Wang et al. 2012).
Alternatively, interfering with the epigenetic regulation of RAGs was extensively tested to promote axonal regeneration. For instance, manipulation of DNA histone modifiers such as histone acetyltransferases (HATs) and histone deacetylases (HDACs) to induce transcription of RAGs was shown to promote axonal regeneration after SCI (Gaub, Joshi et al. 2011, Puttagunta, Tedeschi et al. 2014, Hervera, Zhou et al. 2019).

1.3.4 Transplantation approaches

In the scope of putative treatment strategies for the complex SCI pathology, transplantation approaches that aim at filling the SCI lesion cavity with (1) a cellular graft, (2) a biomaterial-based delivery matrix for trophic factors or pharmacological compounds, (3) a biomaterial-based delivery matrix for cellular grafts, (4) a physical scaffold that provides structural guidance for regrowing spinal axons, and/or (5) various combinations of the aforementioned strategies, were developed and extensively tested in numerous SCI animal models and -partially- in human SCI patients (Fuhrmann, Anandakumaran et al. 2017, Katoh, Yokota et al. 2019, Griffin and Bradke 2020).

1.3.4.1 Cell transplantation

Historically, transplanting cells into the areas of tissue loss is one of the oldest treatment strategies after CNS injury going back to pioneer experiments performed in Ramon y Cajal's laboratory in the late 19th century (Cajal, DeFelipe et al. 1991). The primary goal of cell transplantation after SCI is to compensate for tissue loss and disrupted axonal connections with (1) neurons to either directly replace the lost connections or to form a neuronal relay across the lesion site, (2) neural cells to create a growth-permissive environment and to support the endogenous axonal regeneration, or (3) stem and precursor cells that differentiate into neurons and glia. Further, the grafted cells can be genetically modified to express trophic factors to attract and promote axonal growth additionally. Hence, a plethora of different cell types that

have been used for cell transplantation approaches following SCI, a selection of which will be discussed below.

1.3.4.1.1 Schwann cells

Schwann cells (SCs) are the myelinating cells of the PNS and were found to be essential for peripheral nerve regeneration. Early studies showed axon regeneration after spinal cord transection where peripheral nerve grafts (PNGs) containing surviving adults SCs were implanted into the lesion cavity (Richardson, McGuinness et al. 1980). Important for clinical translation, SCs can be obtained in appropriate quantities from peripheral nerve biopsies of human subjects and expanded *in vitro*. Furthermore, SCs do not form tumors after transplantation (Bunge 2016). Thus, the transplantation of autologous adult SCs was extensively tested in animal models of SCI. For example, purified SCs in PAN/PVC channel implants formed tissue bridges spanning complete spinal cord transection injuries, thereby promoted robust axonal regeneration and remyelination (Xu, Guenard et al. 1995, Xu, Chen et al. 1997, Xu, Zhang et al. 1999, Williams, Henao et al. 2015). Similar results were found after thoracic contusion injuries in adult rats, when SCs were grafted directly into the lesion epicenter 1 week post-injury (Takami, Oudega et al. 2002, Pearse, Sanchez et al. 2007). Notably, SCs secrete several trophic factors after transplantation including NGF, NT-3, GDNF and CNTF (Golden, Pearse et al. 2007, Zhang, Huang et al. 2013). The combination of SC transplantation with additional treatments such as growth factor secretion, ChABC and transgenic overexpression of neurotrophins was shown to be even more effective (Weidner, Blesch et al. 1999, Fouad, Schnell et al. 2005, Golden, Pearse et al. 2007, Enomoto, Bunge et al. 2013, Flora, Joseph et al. 2013, Kanno, Pressman et al. 2014). Consequently, autologous SC transplantation was tested in clinical trials in human patients with acute SCI (< 1 month post-injury) and determined to be safe. Hence, a second phase I clinical trial (NCT identifier: NCT02354625) was initiated to test autologous SC transplantation in chronic SCI patients (Guest, Santamaria et al. 2013, Bunge 2016). The study was completed in August 2019, but results are not yet available.

1.3.4.1.2 Olfactory ensheathing cells

Olfactory ensheathing cells (OECs) represent a unique, terminally differentiated glia cell type located in the peripheral olfactory nerve and the central olfactory nerve layer. OECs wrap the olfactory receptor neurons, enabling them to regenerate throughout their entire life (Schwob, Jang et al. 2017, Gomez, Sanchez et al. 2018). Hence, it was thought that OECs have the

capacity to facilitate CNS axonal regeneration and were therefore studied as potential candidates for cell transplantation after SCI. OECs showed some promise in promoting axonal regeneration in acute and chronic SCI. For example, OECs can act neuroprotective via secretion of trophic factors and ECM metalloproteinases dampening astrocyte reactivity and scar-associated CSPG deposition (Garcia-Alias, Lopez-Vales et al. 2004, Pastrana, Moreno-Flores et al. 2006, Sasaki, Hains et al. 2006, O'Toole, West et al. 2007). Adult OECs can serve as a cellular substrate for growing axons and were shown to remyelinate damaged axons after SCI *in vivo* (Radtke, Akiyama et al. 2004). Further, OEC transplantation into full transection injuries of the rodent spinal cord led to functional recovery of sensory and motor function (Ramon-Cueto, Cordero et al. 2000, Ruitenberg, Plant et al. 2003, Li, Li et al. 2011). Based upon this promising experimental data, OEC transplantation alone or in combination with SC transplantation was investigated in several human clinical trials, but only modest or partially controversial results were reported so far (Mackay-Sim, Feron et al. 2008, Chen, Huang et al. 2014, Guest and Dietrich 2015).

1.3.4.1.3 Bone marrow stromal cells and other mesenchymal stem cells

Bone marrow stromal cells (also known as bone marrow-derived mesenchymal stem cells, BMSCs) are pluripotent, non-hematopoietic stem cells. Since BMSCs can be obtained from the bone marrow of patients via biopsies, expanded and easily genetically manipulated *in vitro*, they have been extensively tested in various disease conditions (Forostyak, Jendelova et al. 2013, Yang, Zhu et al. 2014, Hernigou, Flouzat-Lachaniette et al. 2015, Kim, Shapiro et al. 2015). They secrete a myriad of different trophic factors and ECM components, and act in an immunomodulatory manner (Meirelles Lda, Fontes et al. 2009, Ren, Jin et al. 2011). After SCI, BMSCs elicited tissue sparing and functional recovery (Ohta, Suzuki et al. 2004, Nandoe Tewarie, Hurtado et al. 2009, Ritfeld, Nandoe Tewarie et al. 2012). Other studies have shown that BMSCs improved axonal regrowth and suppressed astroglial scarring in a contusive SCI model (Urdzikova, Jendelova et al. 2006, Ide, Nakai et al. 2010, Okuda, Horii-Hayashi et al. 2017). In contrast, subacute intraparenchymal grafting of BMSCs did not improve tissue sparing and had only minimal impact on functional recovery after thoracic contusion injury in adult rats (Sandner, Ciatipis et al. 2016). However, multiple phase I and phase I/II clinical trials were initiated recently to test autologous BMSC transplantation in human SCI patients showing safety and efficacy after chronic SCI and partially clinical improvement (El-Kheir, Gabr et al. 2014, Mendonca, Larocca et al. 2014, Satti, Waheed et al. 2016, Silvestro, Bramanti et al. 2020).

However, BMSCs grafts often lack integration and/or survival into the injured spinal cord, which significantly reduces their impact on axonal regeneration. Dependent upon the transplantation technique, either grafted BMSCs infiltrated and colonized the SCI lesion site or were not detectable even short-time after transplantation (Ohta, Suzuki et al. 2004, Okuda, Horii-Hayashi et al. 2017, Romero-Ramirez, Wu et al. 2020).

1.3.4.1.4 Astrocytes

Astrocytes play a myriad of different essential functions both under physiological and pathophysiological conditions in the CNS. Over 30 years ago, the idea of taking advantage of the astrocytic supportive character for neurons during development, but also after SCI had developed. Hence, early transplantation studies grafted neonatal cortex-derived astrocytes into acute SCI lesions in adult rats. After crush injury of the L5 dorsal root entry zone (DREZ), immature astrocytes were seeded into a Millipore pennant and implanted directly into the lesion site. The grafted cells integrated into the lesion site, migrated along WM tracts and partially reduced inflammation and glial scarring around the implantation site. Moreover, regrowth of sensory axons through the implantation site was strikingly enhanced compared with lesion and pennant controls. Some sensory axons re-entered the spinal cord and extended rostrally along the dorsal columns (Kliot, Smith et al. 1990). Likewise, immature cortex-derived astrocytes filled the lesion cavity of a unilateral L3 hemisection injury in adult Sprague-Dawley rats and significantly reduced the surrounding scar volume 4 and 8 weeks post-injury. Grafted astrocytes spread out into the surrounding uninjured host tissue and were intermingled with fibrous host-derived astrocytes and promoted the regrowth of Neurofilament (NF)-labeled axons into and partially through the transection site (Wang, Chuah et al. 1995). Later studies showed that phenotypical and morphological differences in the graft astrocyte populations strikingly affected their impact on axonal regeneration (Williams, Henao et al. 2015). In particular, $A2B5^-/GFAP^+$ cortex-derived astrocytes formed dense clusters encapsulated with fibroglial scar tissue, while $A2B5^+/GFAP^+$ cortex-derived astrocytes formed an aligned network at the lesion site (Blakemore and Crang 1989, Franklin, Crang et al. 1992, Wang, Chuah et al. 1995, Joosten, Veldhuis et al. 2004). The latter astrocyte grafts were closely associated with the adjacent host tissue and penetrated by newly formed microvasculature (Olby and Blakemore 1996).
Besides phenotypical differences, also developmental differences might affect the functional outcome of astrocyte transplantation as mature astrocytes -although plastic- become reactive and potentially scar forming after SCI (Sofroniew 2014, Hara, Kobayakawa et al. 2017). In contrast, immature astrocytes retain some of their developmental characteristics and consequently harbor scaffolding functions for growing neurons (Joosten and Gribnau 1989,

McDermott, Barry et al. 2005, Nomura, Kim et al. 2010). Hence, various studies using different kinds of immature astrocytes alone or with additional treatments showing a positive effect on acute SCI lesion sites. For example, immature cortex-derived astrocytes ($A2B5^-/GFAP^+$) were seeded into a collagen type I matrix and implanted into a dorsal hemisection injury of the thoracic spinal cord (Th7 – 9) of adult Wistar rats. After 4 weeks, the grafted astrocytes remained at the injury site. They were closely associated with regrowing NF-positive axons and BDA-traced CST axons at the implantation site, whereas animals that only received the collagen matrix only contained sparse individual axons. Furthermore, animals with astrocyte grafts showed subtle functional improvements of hindlimb locomotion as assessed by the Basso, Beattie and Bresnahan (BBB) motor score, BBB subscores and CatWalk™ gait analysis (Joosten, Veldhuis et al. 2004). Importantly, immature cortex-derived astrocytes were shown to be more axon growth-permissive than their mature counterparts *in vitro* and *in vivo* which might be attributed to a higher expression of matrix metalloproteinase-2 (MMP-2) (Filous, Miller et al. 2010). Hence, immature astrocytes have the ability to modulate the ECM at CNS lesion sites.

Moreover, grafted immature astrocytes formed tissue bridges to structurally guide growing axons past corpus callosum microlesions in combination with ChABC (Filous, Miller et al. 2010). Similarly, transplantation of APCs derived from *in vitro* pre-differentiated glia-restricted precursors (GRPs) obtained from E13.5 rat spinal cords was shown to positively affect axonal regeneration after a unilateral DCL at cervical level C1/2 in adult rats. The grafted APCs integrated into the lesion cavity, suppressed neurocan and NG2 expression, and aligned with host-derived astrocytes to serve as a tissue bridge for regrowing rubrospinal axons. Moreover, animals with immature astrocyte grafts performed significantly better in the Grid-walk test compared with lesion controls or animals that received non-differentiated GRPs (Davies, Huang et al. 2006). Another study confirmed these promising findings with immature astrocytes derived from human GRPs (Walczak, All et al. 2011). Unfortunately, a follow-up study that used CNTF and BMP to pre-differentiate GRPs *in vitro* was not able to reproduce the previously observed findings, since APCs pre-differentiated with CNTF and undifferentiated GRPs induced mechanical allodynia and thermal hyperalgesia after unilateral DCL (Davies, Proschel et al. 2008). Consequently, pre-differentiation of GRPs to APC as well as tissue origin of the GRPs were identified as crucial determinants for the properties of the resulting astrocyte populations (Davies, Huang et al. 2006, Strathmann, Wang et al. 2007, Davies, Proschel et al. 2008, Davies, Shih et al. 2011, Noble, Davies et al. 2011). For example, spinal cord-derived GRPs pre-differentiated with BMP4 mediated neuroprotection, promoted axonal regeneration of ascending dorsal column axons and functional recovery, whereas telencephalic GRPs pre-differentiated with CNTF induced sensory abnormalities associated with enhanced calcitonin-gene-

related peptide-positive ($CGRP^+$) fiber sprouting in the spinal dorsal horn (Hofstetter, Holmstrom et al. 2005, Macias, Syring et al. 2006, Davies, Proschel et al. 2008, Davies, Shih et al. 2011). In line with these findings, different *in vitro* pre-differentiation protocols generated different astrocyte subpopulations with varying properties *in vitro* and *in vivo* (Bonaguidi, McGuire et al. 2005, Krencik, Weick et al. 2011, Haas, Neuhuber et al. 2012, Haas and Fischer 2013). Nevertheless, APCs generated via BMP exposure most likely resemble immature spinal cord astrocytes and showed striking neuroprotective effects without adverse side effects *in vivo* (Davies, Huang et al. 2006, Davies, Proschel et al. 2008, Jin, Neuhuber et al. 2011, Fan, Zheng et al. 2013, Haas and Fischer 2013).

1.3.4.1.5 Oligodendrocyte precursor cells

Oligodendrocyte precursor cells (OPCs) represent a bipotent glia precursor population capable of generating myelinating oligodendrocytes and quiescent $NG2^+$ glia precursors. As a consequence of SCI, myelin loss and oligodendrocyte apoptosis are prominent pathologies that contribute to functional impairment due to axonal signal conduction disruption (Norenberg, Smith et al. 2004). Therefore, compensating oligodendrocyte cell loss and enhancing remyelination might be a powerful way to support functional strategy to restore function after SCI (Myers, Bankston et al. 2016, Assinck, Duncan et al. 2017). For example, human iPSC-derived OPCs were delayed (7 dpi) transplanted into the host spinal cord rostrally and caudally to the epicenter of a Th10 contusion SCI in adult rats. After 8 weeks, grafted OPCs were terminally differentiated into mature oligodendrocytes and myelinated NF-labeled host axons which induced moderate locomotion recovery of the hindlimbs as assessed via increased BBB motor score and improved hindlimb kinematics (e.g., paw rotation, toe spread) (Keirstead, Nistor et al. 2005). Likewise, human iPSC-derived OPCs remyelinated $NF200^+$ axons after clip compression injury of the thoracic spinal cord (Th7), leading to increased BBB motor scores as well as reduced footfalls during the Grid walk test and improved interlimb coordination 2 months post-injury (Karimi-Abdolrezaee, Eftekharpour et al. 2006). Interestingly, both studies showed that functional recovery is only observed when cells are grafted subacutely in comparison to cell transplantation in the chronic phase after SCI (> 10 months). Another study grafted iPSC-OPCs only 1 day after injury directly into the lesion epicenter and was able to show reduced lesion size and improved remyelination of spared host axons correlated with an improvement in BBB motor scores (All, Gharibani et al. 2015). Moreover, Wu et al. isolated OPCs from neonatal rats and transplanted them delayed (1 week post-injury) into the lesion cavity of a Th10 contusion injury in adult Sprague-Dawley rats. Treated rats showed increased BBB motor scores and improved motor evoked potentials (MEPs) as well as somatosensory evoked potentials

(SSEP) during electrophysiological evaluation 8 weeks after SCI (Wu, Sun et al. 2012). However, recent work demonstrates that a certain threshold of remyelination has to be reached until functional improvements can occur and, most intriguingly, that functional recovery of stepping after contusive SCI does not require oligodendrocyte-mediated remyelination (Plemel, Chojnacki et al. 2011, Duncan, Manesh et al. 2018). Hence, it still remains unclear if and how efficient endogenous remyelination helps after SCI since most studies report effects on spared axons rather than improved axonal regeneration.

1.3.4.1.6 Neural stem and precursor cells

Neural stem cells (NSCs) and neural precursor cells (NPCs) are multipotent cell populations that can differentiate into both neurons and glia, capable of replacing the lost neural tissue after SCI. Furthermore, NSC/NPC grafts were shown to extend axons into the surrounding spinal parenchyma and form synapses with host-derived neurons. Hence, NPCs/NSCs harbor the potential to not only compensate for lost tissue but also restore lost axonal connections via neuronal relay formation but might require additional trophic support (Lu, Wang et al. 2012, Lu, Kadoya et al. 2014). Recently, it was shown that fetal NPCs without additional trophic factor supply arrange into functional domains and that damaged spinal ascending and descending axons regrow into appropriate interneuronal layers of the domains (Dulin, Adler et al. 2018, Kumamaru, Lu et al. 2019). In most studies, rodent or human NSCs/NPCs were obtained from fetal tissue resulting in post-transplantation differentiation into neurons and glia, whereas adult-derived NSCs/NPCs predominantly differentiated into astrocytes and oligodendrocytes (Wictorin, Brundin et al. 1990, Cao, Zhang et al. 2001, Pfeifer, Vroemen et al. 2004, Karimi-Abdolrezaee, Eftekharpour et al. 2010). Besides relay formation, NSC/NPC grafts secrete various trophic and immunomodulatory factors that promote and attract axonal growth towards and into the grafts (Lu, Jones et al. 2003, Kokaia, Martino et al. 2012). Moreover, E12 spinal cord-derived NPCs transplanted with a fibrin matrix into a C5 dorsal column lesion (DCL) in adult mice induced a sustained embryonic transcriptional state in injured CST axons (Poplawski, Kawaguchi et al. 2020). Nonetheless, the use of human embryonic or fetal tissue as the source for NSCs/NPCs makes their use in regenerative medicine controversial or at least more difficult for clinical translation.

1.3.4.1.7 Induced pluripotent stem cells

Induced pluripotent stem cells (iPSCs) are multipotent stem cells that were artificially generated by reprogramming adult somatic cells via re-expression of embryonic stem cell (ESC)

transcription factors (Takahashi and Yamanaka 2006, Nagoshi and Okano 2018). They share characteristics of ESCs and can give rise to all three germ layers and circumvent many problems associated with transplantation of ectopic cells, e.g., adverse immune responses, as they can be obtained in a patient-specific manner from skin biopsies. Nonetheless, iPSCs harbor the potential risk of tumorigenicity, however, modification of the induction protocols and pretreatment of the cells with a γ-secretase inhibitor significantly reduces tumor formation after iPSC-NPC transplantation (Okano, Nakamura et al. 2013, Okubo, Iwanami et al. 2016, Okubo, Nagoshi et al. 2018). After contusive Th 10 SCI in mice, grafted iPSCs predominantly differentiated into myelinating oligodendrocytes that enhanced remyelination of spared host axons and induced regrowth of serotonergic axons around the lesion site finally facilitating hindlimb locomotion recovery as assessed by increased Basso Mouse Scale (BMS) motor scores (Tsuji, Miura et al. 2010, Salewski, Mitchell et al. 2015). Besides remyelination, iPSCs were shown to differentiate into neurons forming synapses with choline acetyltransferase (ChAT)-labeled host axons, promoted revascularization and axonal regeneration of serotonergic raphespinal axons which finally lead to improved electrophysiological (e.g., MEPs) and motor outcomes of the hindlimbs in mice (Nori, Okada et al. 2011) and primates (Kobayashi, Okada et al. 2012). Numerous studies used iPSCs for transplantation into different SCI animal models with variable success (Fujimoto, Abematsu et al. 2012, Lu, Woodruff et al. 2014, Oh, Lee et al. 2015, Pomeshchik, Puttonen et al. 2015, Romanyuk, Amemori et al. 2015, Ruzicka, Machova-Urdzikova et al. 2017). Consequently, a pioneer clinical trial using human iPSCs for the treatment of subacute SCI patients (cervical/thoracic SCI, ASIA-A classification, 2 – 4 weeks post-injury) was recently started in Japan (Tsuji, Sugai et al. 2019). However, significant concerns regarding undifferentiated proliferation and tumorigenesis as well as detrimental long-term effects of the grafted iPSCs due to the virally induced pluripotency or reprogramming techniques remain.

1.3.4.2 Biomaterial implantation

Since cavitation at the lesion epicenter is a prominent characteristic of SCI, experimental approaches were developed to implant biomaterial constructs into the lesion cavity to fill the physical gap and provide neural cells as well as regrowing axons with a growth substrate. Additionally, the topographical structure of the implant can be combined with cells and/or bioactive compounds like drugs and growth factors. Nonetheless, some fundamental issues need to be considered in biomaterial-based approaches, namely (1) biocompatibility, (2) cytocompatibility, (3) physicochemical properties, (4) topography, and (5) biodegradability/biotransformability of the biomaterial implant. Thus, the structure of biomaterial implants reaches from

hollow conduits and tubes to solid and semi-solid hydrogels, self-assembling peptides as well as electrospun (nano-)fibers and gelfoams (Fuhrmann, Anandakumaran et al. 2017). In the following sections hydrogel-based approaches will be the focus.

1.3.4.2.1 Hydrogels as biocompatible implants

Among potential biomaterial formulations, hydrogels fabricated from synthetic and natural polymers represent a promising candidate since their mechanical (e.g., stiffness, elasticity, micro-architecture) as well as chemical properties (e.g., surface modification, biodegradability, binding of additional factors) can easily be modified to match those of the intact spinal cord tissue. Further, due to their high water content, they mimic the hydrophilic 3D network of the ECM of the surrounding spinal cord tissue.

Chemically, hydrogels are elastic coherent colloid-dispersed systems with at least one chemical component and high amounts of water (≥ 60% v/w) as the dispersion medium. On the structural level, the dispersed component(s) forms polymer chains that arrange (Liu, Sandner et al. 2017, Grijalvo, Nieto-Diaz et al. 2019) into a 3D network whose interspaces are filled with aqueous solution and additional hydrogel components (e.g., cross-linking agents, peptides, etc.). Other macrostructural features like pore size, flexibility, elasticity and -to a lesser degree- biodegradability are determined by the physicochemical and electrostatic properties of the gel-forming polymers. Finally, based upon their hydrophilic state and usually high flexibility/elasticity, classical hydrogels exhibit low interfacial tensions and tension/shear forces at tissue interfaces and allow for molecule and gas diffusion, cell migration and penetration (Nisbet, Pattanawong et al. 2007, Khaing, Ehsanipour et al. 2016, Fuhrmann, Anandakumaran et al. 2017).

1.3.4.2.2 Synthetic hydrogels

Hydrogels fabricated from synthetic polymers such as poly-2-hydroxyethyl methacrylate (pHEMA), and other polyacrylamides, polyethylene glycol (PEG) as well as poly-lactic acid (PLA) and poly-lactic-co-glycolic acid (PLGA) were extensively studied over the last decades for biomedical applications (Atala, Lanza et al. 2018). pHEMA hydrogel implants were tested individually or in combination with cells and/or trophic factors in numerous preclinical SCI studies. For example, animals that received a pHEMA hydrogel implant after a full transection of the thoracic spinal cord at Th7 showed greater regrowth of NF-labeled axons originating from the reticular, vestibular and raphe brain nuclei as identified via retrograde axonal tracing compared with non-treated control animals (Tsai, Dalton et al. 2004). In another study, pHEMA

implants significantly reduced GFAP upregulation at the lesion margins of a Th7 DCL in adult Wistar rats (Li, Fuhrmann et al. 2013). Furthermore, Bakshi et al. implanted pHEMA hydrogels either non-functionalized or functionalized with BDNF into the lesion cavity of a lateral DCL at cervical level C3 – 4 in adult Sprague-Dawley rats. After 4 weeks, only the BNDF-pHEMA implants facilitated a reduction in scar volume, CSPG expression as well as ingrowth of microvessels and NF-labeled axons, although pure pHEMA did not affect axonal regrowth nor scarring (Bakshi, Fisher et al. 2004). A similar study used pHEMA implants functionalized with serotonin in combination with spinal cord-derived NPCs and implanted them into a 2 mm-wide unilateral hemisection lesion of the Th8 spinal cord in adult Wistar rats. After 3 months, significantly more blood vessels and axons were found in the pHEMA + NPC group compared with animals that received either pHEMA hydrogels or NPCs alone (Ruzicka, Romanyuk et al. 2013). However, no study reported significant functional improvements so far.

Additionally, several studies used PLGA- or PLG-based hydrogel implants in various experimental SCI models in rodents and primates. Implantation of a PLG multichannel hydrogel implant into the lesion cavity of a unilateral C4-5 hemisection lesion leads to growth of CST axons through the hydrogel implant back into the caudal host parenchyma in adult GFP-transgenic C57Bl6 mice. This associated with fewer errors of the ipsilateral forelimb in the horizontal ladder test 10 weeks post-injury, whereas no effect was observed in the cylinder test. However, a causal relationship between the observed axonal growth within the implant and the behavioral results was not examined (Pawar, Cummings et al. 2015). PLGA-based multichannel hydrogels in combination with SC transplantation (suspended in Matrigel) promoted growth of NF-labeled axons after thoracic (Th7) full transection in adult Sprague-Dawley rats. The implants were filled with the seeded SCs and infiltrated macrophages, whereas control groups (no treatment, PLGA hydrogel + Matrigel) showed less cell infiltration and no axonal growth within the implant channels (Moore, Friedman et al. 2006). Alternatively, PLGA nanoparticles can be used to release BDNF and NT-3 (Pakulska, Elliott Donaghue et al. 2016). After clip compression of the thoracic spinal cord in adult rats, PLGA nanoparticles were used to intraspinally deliver Neuregulin-1 immediately after injury. After 4 weeks, treated animals showed greater tissue sparing and reduced neuroinflammation/scarring around the lesion site accompanied by axonal sparing (Santhosh, Alizadeh et al. 2017). Biodegradable PLGA hydrogels seeded with human NSCs were implanted into African green monkeys after hemisection of the thoracic spinal cord at Th9 – 10. Although axonal regrowth through the implant was not investigated, decreased axonal dieback of the CST as well as improved locomotion parameters of the affected hindlimb were observed 12 weeks after implantation (Pritchard, Slotkin et al. 2010) Noteworthy, a phase I clinical trial was launched in 2014 which aimed to assess the safety and feasibility of the implantation of a biodegradable PLGA implants after thoracic SCI in a total of

20 human patients (“The INSPIRE Study: Probable Benefit of the Neuro-Spinal Scaffold for Treatment of ASIA A Thoracic Acute Spinal Cord Injury, Identifier: NCT02138110). The first participant (25 years, male) underwent spinal cord decompression and fixation followed by implantation immediately after the initial spinal cord trauma (within the first 12 hours post-injury). A 1 cm-long PLGA implant was placed directly into the lesion cavity of a multivertebra-trauma, thoracic compression SCI (ASIA A, injury level Th11). After 3 months, the patient improved to an L1 ASIA C grade with hints of sacral spinal cord sparing, intact voluntary anal contraction and deep anal sensation as well as voluntary bladder function. Moreover, the patient showed normal dermatome sensation above spinal level L1 and improved muscle strength in hip extensors and knee flexors. Within a 6 months long post-implantation follow-up timespan, no adverse side effects, complications or apparent safety issues were reported (Theodore, Hlubek et al. 2016). Nonetheless, although encouraging, the outcomes of this pioneer trial have to be critically reviewed for several reasons including, firstly, the lack of control groups; and, secondly, due to the immediate implantation of the PLGA hydrogel within hours after SCI, it is impossible to dissect a putative therapeutic effect of the implant from spontaneous recovery.

Finally, PEG-based hydrogels were used alone or for the functionalization of other solid hydrogel implants. For example, a composite implant containing an outer PLGA tube and an inner PEG core was seeded with NPCs and implanted into the cavity of a unilateral hemisection injury at Th9 – 10 in adult Sprague-Dawley rats. After 8 weeks, NPC-seeded implants were vascularized and NF200-positive as well as GAP-43-labeled axons extended into the implants. Notably, non-seeded implants remained structurally separated from the surrounding host tissue and only minimally penetrated by blood vessels (Rauch, Hynes et al. 2009). Similarly, a NT-3 – and PEG-functionalized PLA hydrogel was placed into a Th8 unilateral hemisection injury in adult male Sprague-Dawley rats. Animals that received implants releasing NT-3 performed better on the gridwalk test and showed significantly improved BBB motor scores compared with animals that only received the co-polymer implant. The observed functional recovery was associated with increased axonal growth of the CST and raphespinal tract through the implant and back into the distal spinal cord (Piantino, Burdick et al. 2006). Other studies focused on a PEG-functionalized poly-N-isopropyl-acrylamide hydrogel modified to release BDNF and tested it in a cervical DCL SCI model in adult Sprague-Dawley rats. The BDNF-releasing implant did not negatively affect the host immune response and contained more $NF200^{+}$ axons compared with non-BDNF-releasing implants. Moreover, individual rubrospinal axons completely crossed the implants, however, axonal re-entry into the distal spinal cord was not observed. BDNF delivery may have caused local sprouting of the RST which led to improved performance of the rats during the cylinder test and in reach-grasp-paradigms

(Conova, Vernengo et al. 2011, Grous, Vernengo et al. 2013). Recently, Koffler and colleagues facilitated 3D bioprinting to fabricate a PEG-based hydrogel mimicking the tract-specific anatomy of the Th3 rat spinal cord and seeded the scaffold with NPCs prior to implantation. The scaffolds remained structurally intact up to 6 months post-injury and mediated axonal regrowth of CST and serotonergic axons, which may have led to the recovery of electrophysiological signal transmission through the implantation site as measured by MEP recordings at the hindlimbs after transcranial stimulation as well as locomotor function as indicated by elevated BBB motor scores. Notably, complete crossing of host-derived serotonergic axons was only found, when the implant was seeded with NPCs. Non-seeded implants contained host-derived serotonergic axons, but these axons did not completely cross the implants (Koffler, Zhu et al. 2019).

Although synthetic hydrogels showed some promise in experimental SCI models and were already tested in humans, several limitations remain, namely the high potential for long-term toxicity due to the instability of bound chemical additives, or toxic degradation products or the low biocompatibility of the synthetic implants *per se*. In particular, most studies only revealed pre-regenerative properties of the implants when they were combined with either growth factors or cellular grafts (Moore, Friedman et al. 2006, Ruzicka, Romanyuk et al. 2013, Koffler, Zhu et al. 2019). Moreover, in some studies, the synthetic implants lead to expansion of the lesion or elevated macrophage activation (Moore, Friedman et al. 2006, Pritchard, Slotkin et al. 2010).

1.3.4.2.3 Natural hydrogels

Although synthetic hydrogels were partially shown to be promising in experimental SCI models, natural hydrogels may be more suitable to the injured spinal cord by providing a *per se* biocompatible matrix, native biological surfaces and inherent bioactivity. Importantly, natural hydrogels undergoing biodegradation most likely do not release (cyto-)toxic byproducts or other toxic additives in comparison with synthetic fabricates (Fuhrmann, Anandakumaran et al. 2017).

Among the natural polymers that can be used to form hydrogel implants, collagen and hyaluronic acid are the main components of the mammalian ECM and, therefore, endogenous to the CNS. Hence, *in situ*-polymerizing or structural collagen hydrogels have been utilized as carrier matrices for cells and trophic factors and promoted axonal regrowth. For example, adult Schwann cells were suspended with a collagen:laminin carrier matrix and transplanted into the

lesion cavity of a Th9 contusion injury in adult Fischer rats. Although the implantation site contained neurofilament-positive axons and blood vessels, no functional recovery was observed. Surprisingly in the same study, animals that received an SC graft (suspended in BD Matrigel™) did show elevated BBB motor scores 4 weeks post-injury (Patel, Joseph et al. 2010). Similarly, NF-labeled axons entered a multichannel collagen implant biofunctionalized with NT-3 after a 2 mm-wide full transection of the thoracic spinal cord at Th9 in Sprague-Dawley rats, but did not show any significant recovery compared with non-functionalized collagen implants (Yao, Daly et al. 2013). However, linear type I collagen fibers bound to a sponge-like implant facilitated regrowth of rubrospinal axons after Th9 full transection in Fischer rats. Furthermore, some of the regrown axons were re-myelinated and signal transduction was partially restored through the implantation site as assessed via MEP recordings (Suzuki, Kanchiku et al. 2015). Another study found similar results after a 6 mm-wide transection injury of the thoracic spinal cord (Th8 – 9) in adult rats, when a linearly organized collagen fiber implant releasing myelin-neutralizing antibodies and BDNF was implanted immediately after lesioning. After 8 weeks, the implant contained NF^+ axons and spinal somatosensory evoked responses (SSERs) could be recorded rostral to the injury after stimulation of the tibial nerve. However, non-functionalized implants nor implants that just released BDNF or the myelin inhibitors showed any functional recovery (Han, Jin et al. 2010).

Hyaluronic acid is a glycosaminoglycan and, in most cases, used in combination with either methylcellulose (HAMC) or PLGA nanoparticles for trophic factor or cell delivery after SCI. In combination with adult brain-derived NSCs/NPCs and delivery of PDGFA, a HAMC implant was implanted delayed and shown to enhance survival and oligodendrocytic differentiation of the co-grafted precursor cells and reduced lesion size as well as microglial activation around a Th2 clip compression injury in adult Wistar rats. Although rats did not improve their BBB motor scores, HAMC-treated animals performed better on the horizontal ladder test and showed fewer footfalls compared to animals that only received an NPC graft (Mothe, Tam et al. 2013). Similar results were obtained when the HAMC implant released NT-3 (Elliott Donaghue, Tator et al. 2015). After a dorsal Th9 hemisection SCI in Sprague-Dawley rats, a hyaluronic acid-based multichannel hydrogel modified with BDNF-, VEGF- and Anti-Nogo-releasing PLGA nanoparticles improved vascularization and regrowth of NF-labeled axons 4 and 8 weeks after injury. Furthermore, animals exhibited higher BBB motor scores and less prominent weight distribution on the forelimbs as assessed by CatWalk™ gait analysis (Wen, Yu et al. 2016). However, in none of the studies, did the HAMC itself directly affect axonal growth, since axon numbers as well as functional improvements were only observed when the HAMC implant was combined with either cells or growth factors.

Alternatively, ECM-derived hydrogels can be generated based on fibrin. In particular, fibrin and fibrin glue (a mixture of fibrinogen and thrombin) have been extensively studied in wound healing and peripheral nerve regeneration (Cote, Amin et al. 2011). After SCI, fibrin matrices were often used as a carrier matrix for NPC transplantation (Lu, Wang et al. 2012, Lu, Kadoya et al. 2014) but were also shown to impact axonal regeneration alone or in combination with NT-3. In particular, a fibrin matrix releasing NT-3 was implanted into a Th 9 full transection injury in adult Long Evans rats and lead to a higher density of locally sprouting CGRP-, ChAT, and 5-HT-labeled axons throughout the implant, but did not affect motor outcomes as BBB motor scores were not different from non-treated controls (Taylor, Rosenzweig et al. 2006). Similarly, a 2 week-delayed implantation of pre-polymerized fibrin hydrogels into the cavity of a dorsal hemisection injury at Th9 in adult Long Evans rats resulted in increased axonal density, whereas animals that received injections of an *in situ*-polymerizing fibrin hydrogel did only show minimal axonal growth at the lesion site. Moreover, the *in situ*-polymerizing implants were already degraded after 1 week post-implantation. Nonetheless, functional improvements were not found in both groups (Johnson, Parker et al. 2010). In another study, a hydrogel based on collagen, fibronectin, fibrin or a mixture of fibrin and fibronectin was placed into a lateral DCL injury at Th7 – 9 in adult Wistar rats. Histological analysis of the implant 1 or 4 weeks post-SCI revealed substantial axonal ingrowth only into the fibrin + fibronectin group along with SC infiltration and vascularization, whereas all other groups did only showed minor axonal growth (King, Alovskaya et al. 2010). Thus, functional improvements were not observed in any of the studies, most likely due to the instability and lack of physical guidance provided by the fibrin-based implants. However, an open-label, prospective, non-controlled phase I clinical trial was initiated recently in which chronic cervical and thoracic SCI patients (> 24 months post-SCI) received a fibrin glue matrix releasing FGF1 and additional bolus injections of FGF1 3 and 6 months after the initial treatment. In a 24 months follow-up, safety and feasibility were proven along with modest recovery in a subcohort of participants as indicated by improved ASIA motor and sensor scores (e.g., light touch, pinprick) (Wu, Huang et al. 2008, Wu, Huang et al. 2011). In contrast to the above-mentioned hydrogels, BD Matrigel™ is a heterogenous extract of basal membrane proteins derived from mouse sarcoma cell lines containing a plethora of different ECM components, for instance, laminin, type IV collagen as well as EGF and FGF (Hughes, Postovit et al. 2010). Although no experimental study was able to show a pro-regenerative effect of BD Matrigel™ itself, it is used in numerous studies to improve graft cell survival or integration of other biomaterial scaffolds (Xu, Zhang et al. 1999, Park, Lee et al. 2012, Williams, Henao et al. 2015, Han, Lee et al. 2018).

Another type of natural hydrogels is fabricated based on polysaccharides. For example, chitosan is a linear deacetylated polysaccharide obtained from crustaceans and insects. It has

been shown to act anti-oxidatively and anti-apoptotic in various biomedical approaches (Khor and Lim 2003, Zou, Yang et al. 2016) and neuroprotectively on neurons in an *in vitro* assay of amyloid β deposition (Khodagholi, Eftekharzadeh et al. 2010). Within the spinal cord, chitosan sheets showed no signs of degradation or mass loss as well as no chronic immune response even 12 months after implantation into the intact spinal cord (Kim, Tator et al. 2011). Several studies tested chitosan hydrogels with a channel structure in spinal transection injuries where the implants served as physical guidance structures and/or carrier matrix for cells. For example, chitosan channels seeded with adult spinal cord-derived NPCs implanted 3 weeks after a clip compression injury at Th8 in Sprague-Dawley rats facilitated the robust survival of the seeded NPCs. Although NF200-labeled axons entered the channels and no excessive immune response at the implantation site occurred, also no functional recovery in BBB motor scores was observed 9 weeks post-injury (Bozkurt, Mothe et al. 2010). In contrast, empty chitosan channels were implanted into a Th8 full transection injury and facilitated the formation of a continuous cellular bridge between the rostral and caudal spinal cord stumps within 14 weeks after SCI. The tissue bridge was mainly formed by host-derived radial glia-like cells and some $NF200^+$ axons were found to grow along the processes of these cells. However, no complete axonal crossing of the implantation site, nor any functional improvement was observed (Nomura, Baladie et al. 2008). In line with these findings, additional release of dibutyryl-cAMP from PLGA microspheres filled into a chitosan tube additionally seeded with adult spinal cord-derived NPCs lead to minimal improvements in BBB motor scores after a Th8 full transection but complete axonal crossing of the implantation site was again not observed (Kim, Zahir et al. 2011). Another complex approach used chitosan tubes seeded with adult brain-derived NPCs and placed them into the lesion cavity of a Th8 transection in adult rats. Additionally, a Nogo-66 receptor fusion protein and growth factors cocktail (EGF, FGF2, PDGF-AA) were intrathecally delivered via osmotic pumps, which induced a predominantly oligodendrocytic cell fate in the grafted NPCs and promoted the growth of NF200-labeled axons throughout the chitosan channel. BDA-traced CST axons entered the rostral extent of the chitosan channel but did not extend further caudally. Retrogradely traced descending rubro-, reticulo- and vestibulospinal axons did not enter the lesion site at all. Thus, no functional improvements were detected 12 weeks post-injury (Guo, Zahir et al. 2012). Moreover, Li and colleagues achieved hindlimb locomotion recovery mediated by axonal growth of the damaged CST beyond a type I collagen-filled chitosan channel implant 12 months after partial spinal cord transection at Th9 in adult Wistar rats (Li, Yang et al. 2009). A recent study showed functional restoration of electrophysiological signal transduction through a NT-3-releasing chitosan channel in primates after thoracic hemisection (Rao, Zhao et al. 2018).

Agarose and alginate are both polysaccharide polymers originally isolated from seaweed and widely used in the food industry and biomedicine. In more detail, agarose in aqueous solution can form a solid hydrogel in a temperature-dependent manner, whose mechanical properties can easily be altered by variation of the fabrication processes (Dillon, Yu et al. 1998, Balgude, Yu et al. 2001). Freeze-dried agarose hydrogels with a channel/honeycomb structure were shown in combination with BDNF either released from a collagen matrix within the agarose channels or directly incorporated into the agarose hydrogel to promote and physically guide regrowing NF-labeled axons through an acute cervical (C3) dorsal hemisection SCI lesion site in adult Fischer rats. In both groups, no fibrous encapsulation of the implants was found, but the implantation site remained separated from the surrounding spinal tissue (Stokols and Tuszynski 2006). In a combinatorial approach, multichannel agarose hydrogels were seeded with NT-3-releasing BMSCs and combined with a rostral lentiviral-delivery of NT-3 and implanted into a C4 DCL in adult Fischer rats. The intrinsic growth potential of the sensory axons was additionally initiated with a conditioning lesion of the sciatic nerve. Although ascending sensory axons completely crossed the hydrogel, axonal re-entry into the rostral spinal cord of regrown axons was not achieved (Gros, Sakamoto et al. 2010). Similarly, an agarose hydrogel seeded with BDNF-BMSCs facilitated regrowth of rubrospinal and serotonergic axons through the lesion, but axons failed to re-enter host tissue beyond the implantation site after a full transection of the thoracic spinal cord at Th3 in adult Fischer rats (Gao, Lu et al. 2013). Nonetheless, functional recovery of sensorimotor function was not reported, even when the hydrogel implantation was combined with cell transplantation and growth factor delivery.
Others used agarose to deliver bioactive peptides such as ChABC to SCI sites. Lee et al. performed a dorsal hemisection injury at Th10 in adult Sprague-Dawley rats and implanted agarose-microtubes releasing thermostabilized ChABC into the lesion cavity. The intervention reduced astrocyte reactivity and CSPG expression at the lesion site and induced sprouting of serotonergic axons rostral to the lesion. Moreover, ascending sensory axons completely traversed the lesion site, which was correlated with improved locomotion parameters in the CatWalk™ gait analysis (e.g., wider stride length) but did not affect thermal hypersensitivity 6 weeks after injury (Lee, McKeon et al. 2010).

Alginate is a hydrophilic, chain-forming polysaccharide composed of β-D-mannuronic acid and α-L-guluronic acid organized in homopolymeric blocks or alternating polysaccharide sheaths. A solid hydrogel matrix is formed between the different homopolymeric blocks upon ionotropic crosslinking initiated by divalent cations (Draget, Skjak-Braek et al. 1997, Braccini and Perez 2001). Similar to agarose, the mechanical properties of the alginate-based hydrogels can be

modified by alteration of the alginate concentration and/or interfering with the chemical crosslinking after hydrogel polymerization (Lee, Rowley et al. 2000, Kong, Lee et al. 2002, Lee and Mooney 2012). After chemical crosslinking, alginate-based hydrogels are not biodegradable, but non-crosslinked alginate-based hydrogels rapidly dissolve in physiological solution by replacing the ionotopically crosslinked divalent cations with monovalent cations (Shoichet, Li et al. 1996).

Due to its high biocompatibility, versatility and low immunogenicity, alginate-based hydrogels are widely used as a food additive and for various biomedical applications including dental applications and specialized wound dressings (Sweeney, Miraftab et al. 2012, Dumville, Keogh et al. 2015). Further, alginate or alginate-based additives are currently tested for several medical conditions in phase I/II clinical trials, including novel dental restoration class II composites (Torres, Mailart et al. 2020), alginate-antacid add-on medication in patients with gastro-oesophageal reflux disease (Coyle, Crawford et al. 2017), or as mucosa-sealing agent in patients with neoplastic lesions in the esophageal or gastric mucosa (Uemura, Oda et al. 2019).

Early studies implanted alginate-based sponge-like hydrogels after thoracic full transection injuries in neonatal (Kataoka, Suzuki et al. 2001) and young adult rats (Suzuki, Suzuki et al. 1999, Kataoka, Suzuki et al. 2004) proving complete crossing of ascending and descending axons which was accompanied with MEP and SEP recording across the lesion. Recently, a homogenous soft alginate-based hydrogel implant facilitated hindlimb motor function recovery as assessed via BBB and Louisville swim score (LSS) after Th9 – 10 hemisection injury in Wistar rats (Sitoci-Ficici, Matyash et al. 2018).

Alternatively, alginate-based hydrogels can also be designed as *in situ*-polymerizing implants. Here, gel formation is initiated after injection into the damaged area by parallel co-injection of divalent cation-containing aqueous solution (e.g., $CaCl_2$), resulting in a homogenous gel matrix that is able to fill even irregularly shape lesion cavities (Grulova, Slovinska et al. 2015). Moreover, *in situ*-polymerizing alginate-based hydrogels are widely used in bone, cartilage, cardiac and intervertebral disk regeneration (Bidarra, Barrias et al. 2014). Notably, due to very recent progress in 3D bioprinting techniques, alginate-based hydrogels can be fabricated into highly complex 3D structures with precisely defined mechanical properties (Giuseppe, Law et al. 2018, Joung, Truong et al. 2018). To further enhance biocompatibility and overcome the biologically inert surface charge of alginate polymers, surface modifications with synthetic peptides, RGD peptides as well as integrin ligands and ECM components were developed (Ning, Xu et al. 2016, Wen, Xiao et al. 2019).

Alginate-based hydrogels and microcapsules were used individually or in combination with other biomaterial matrices to deliver cells and bioactive compounds, e.g., BDNF, VEGF and ChABC, to sites of acute SCI. For example, BDNF-expressing fibroblasts were encapsulated

into alginate capsules and injected into a dorsolateral funiculotomy at C4 in adult Sprague-Dawley rats. Eight weeks after injury, treated rats performed significantly better in the cylinder and horizontal rope test compared with non-treated control animals or animals that only received a fibroblast graft. Although BBB motor scores were equal across groups and rubrospinal axons failed to enter the lesion site (Tobias, Han et al. 2005). In another study, alginate was used to generate a permeable membrane to enwrap the PLLA microfibers and to constantly release Rolipram after implantation into a cervical C5 hemisection cavity in adult Athymic rats. Two months after lesioning, partially myelinated axons were present in the implants and animals showed improved locomotion of the affected forepaw as assessed via the Martinez open-field score (Downing, Wang et al. 2012). Likewise, adult rats showed improved BBB motor scores after Th9 full transection when a synthetic electrospun fiber mesh mixed with alginate beads releasing NGF and ChABC was implanted into the lesion epicenter (Colello, Chow et al. 2016). Moreover, Long Evans rats showed improved base of support values of their hind paws during CatWalk™ gait analysis after a *in situ*-polymerizing alginate hydrogel containing fibrinogen and GDNF-releasing PLGA microspheres was implanted into a unilateral hemisection of the thoracic spinal cord (Th9). Neurofilament-positive as well as GAP43-labeled axons extended through the lesion site but did not re-enter the caudal host spinal cord (Ansorena, De Berdt et al. 2013). In contrast, in a later study, no functional improvement was observed after implantation of a similar alginate implant releasing VEGF (des Rieux, De Berdt et al. 2014).

Alternatively, different types of solid anisotropic capillary alginate-based hydrogels were used by our laboratory and others to provide orientated physical guidance for regrowing axons in *ex vivo* slice culture models and *in vivo* both after DCL and cervical unilateral hemisection injuries in adult Fischer rats (Prang, Muller et al. 2006, Pawar, Mueller et al. 2011, Gunther, Gunther et al. 2015, Pawar, Prang et al. 2015).

To summarize, natural hydrogel implants were used in various preclinical SCI models, however, their impact on regenerative success after traumatic SCI remains limited. Most studies used the hydrogel implants as a delivery matrix; hence, the implant only indirectly affected axonal growth and tissue regeneration as it served mainly as a physical protection of the co-transplanted cells from the hostile SCI environment or as a deposit for bioactive compounds such as growth factors of ChABC at acute lesion sites. Moreover, many studies reported insufficient integration of the implant into the lesion site since fibrotic tissue or cystic cavities often surrounded the hydrogels, which was only improved when the biomaterial implant was combined with trophic factors and/or cell transplantation. This is further supported by the fact that animals that only received the individual hydrogel implant showed minimal axonal growth

even into the implant as well as a lower degree of vascularization, but a greater immune cell response (e.g., higher density of activated macrophages or reactive astrocytes at the implantation site). Although axonal regrowth was detected in most studies within the hydrogel implants, axons typically failed to traverse the host-graft interface and re-entry into the distal spinal cord was only occasionally observed.

1.3.4.3 Biomaterial-supported cell transplantation

Numerous synthetic and natural hydrogel biomaterials were developed and tested in various experimental SCI and other injury/disease models. Although some biomaterial applications were already enrolled in phase I/II clinical trials, e.g., PLGA, fibrin glue or alginate, the potential of a biomaterial implant alone to significantly impact regeneration is very limited. In particular, regrowing axons extended into the hydrogel implants but failed to grow beyond the site of injury in most studies. The same holds true for cell transplantation approaches, since axonal growth rarely goes beyond the cellular grafts, thereby limiting their therapeutic potential and functional outcomes.

Hence, treatment paradigms that combine different approaches might represent a powerful strategy to overcome the diverse limitations of the individual approaches. For example, Anderson and colleagues elegantly tackled multiple hurdles of CNS regeneration by combining the implantation of a growth permissive substrate (di-block co-polypeptide $K_{180}L_{20}$ hydrogel) at the SCI lesion epicenter with endogenous induction of CNS axonal regeneration (AAV-mediated PTEN knock-down and osteopontin, IGF1 and CNTF expression) and trophic support as well as chemoattraction (sustained release of EGF, FGF2, GDNF) to facilitate functional relevant regrowth of descending propriospinal axons across a complete spinal cord crush injury at Th10 (Anderson, O'Shea et al. 2018). Alternatively, biomaterial implants can be combined with cell transplantation to overcome some limitations of cell transplantation alone, such as low survival rates at acute lesion sites, irregular lesion filling, lack of a 3D physical adherence matrix as well as lack of directed axonal guidance. On the other hand, cellular grafts can compensate for some drawbacks associated with the implantation of biomaterial scaffolds, including inappropriate implant integration, adverse immune reactions, enhanced astroglial/fibroglial scarring around the implantation site as well as lack of long-distance axonal growth. Consequently, biomaterial-supported cell transplantation represents a strategy to reconstruct the lost spinal tissue physically, cellularly and chemically (Liu, Schackel et al. 2017).

1.3.4.3.1 Biomaterials and NSCs/NPCs

Transplantation of NSCs/NPCs after SCI has shown promising results in terms of replacement of lost spinal tissue, neuroprotection as well as trophic support and neuronal differentiation. However, NSC/NPC-containing cellular grafts often show low survival rates after transplantation into the damaged spinal cord. Thus, co-delivery of growth factors and/or the use of a biomaterial matrix were facilitated to improve the survival of the grafted cells. However, additional growth factors might not only affect the survival but also the differentiation potential of the NSCs/NPCs; hence, the risk for uncontrolled post-transplantation differentiation and tumor formation rises. In contrast, a biomaterial matrix provides structural support as well as physical protection from the harsh lesion environment, thereby improving graft cell survival without influencing their differentiation potential. For example, fetal spinal cord E14.5 NSCs or adult SCs were seeded into macrocapillary PLGA hydrogels and implanted into a Th8 – 9 full transection injury which promoted excessive growth of neurofilament-positive axons throughout the implant, but did not affect motor recovery since no differences in BBB motor scores were seen 4 weeks post-implantation (Olson, Rooney et al. 2009). Similarly, early neonatal NSCs were seeded onto a surface- and PEG-functionalized PLGA scaffold, which facilitated proper implant integration, neuronal differentiation of the grafted cells and regrowth of host-derived NF-positive as well as regenerating $GAP43^+$ spinal axons after implantation into a thoracic hemisection lesion (Rauch, Hynes et al. 2009). Further, seeding of adult NSCs into HAMC hydrogels releasing PDGFα led to improved bladder function after delayed implantation (9 dpi) into a thoracic full compression injury (Mothe, Tam et al. 2013). Adult brain- or spinal cord-derived NSCs/NPCs in combination with a chitosan channel implant predominantly differentiated along the glial lineage and mediated tissue sparing and tissue bridge formation across a 10 mm-wide transection cavity (Nomura, Zahir et al. 2008). Moreover, cell line-derived NSCs were seeded into a macroporous PLGA and implanted into a thoracic hemisection lesion at Th9 – 10. Four months post-implantation, superior WM sparing as well as axonal growth of BDA-traced CST axons across the lesion site were observed and linked to improved motor function. Behavioral testing at 10 weeks post-injury revealed significant improvement of BBB motor scores and a better performance of the animals on the incline plane test, whereas control groups (PLGA implant only, cell graft only) exhibited only limited axonal regrowth and worse behavioral outcomes (Teng, Lavik et al. 2002).

Additional delivery of bioactive compounds did even further boost the pro-regenerative effects of biomaterial-supported stem cell transplantation after SCI. For instance, neonatal brain-derived NSCs were transfected to overexpress NT-3 and TrkC and seeded into a PLGA hydrogel. Ten weeks after implantation into a Th10 full transection injury in adult Sprague-Dawley rats, animals that received the NSC-seeded implants showed elevated BBB motor scores and a

continuous tissue bridge had formed across the implantation site. The transplanted NSCs differentiated into MAP2-positive neurons and appeared to form synaptic connections with host-derived axons. However, although NF200-positive axons penetrated the implant from the rostral and caudal spinal cord, no CST axons were present within the tissue bridge (Du, Xiong et al. 2011). In a later study, NSCs expressing TrkC were cocultured with adult SCs expressing NT-3, seeded together into a gelfoam matrix and placed into the lesion cavity of a thoracic transection at Th10 in Sprague-Dawley rats. Similarly, the grafted NSCs differentiated into $MAP2^+$ neurons and formed synapses with host-derived axons. Although a continuous tissue bridge had formed, no long-distance growth of either CST nor RST axons was found but rather local sprouts of serotonergic and adrenergic axons at the lesion site. However, minor improvements in BBB motor scores and signal transduction across the lesion was electrophysiologically measured (Wang, Zeng et al. 2011). Studies that used biomaterial-supported transplantation of NSCs in combination with interventions aiming at neutralization of the growth-inhibitory environment around SCI lesion reported similar results (Hwang, Kim et al. 2011, Li, Tang et al. 2011, Li, Xiao et al. 2013). In a pilot primate study, Pritchard and colleagues implanted NSC-seeded PLGA scaffolds into a 10-mm long unilateral Th9 hemisection lesion. Upon transgenic NT-3 expression in NSCs, they reported ameliorated CST axonal dieback and minimal hindlimb motor recovery as assessed by video-taped gait analysis. However, results were highly variable between animals (Pritchard, Slotkin et al. 2010). Recently, fetal spinal cord-derived NSCs/NPCs in combination with a 3D bioprinted PEG-based hydrogel formed electrophysiologically active neuronal relays spanning a 2-mm long full transection lesion of the thoracic Th3 spinal cord (Koffler, Zhu et al. 2019).

1.3.4.3.2 Biomaterials and Schwann cells

Although transplantation of SCs alone after SCI led to a certain degree of axonal growth, the combination of SCs with biomaterial implants might still be superior. Here, the axon growth-promoting effect of the SCs can be combined with the structural guidance properties of a biomaterial implant. In numerous studies it has been shown that SC seeding into synthetic PAN/PVC channel implants could elicit axonal growth of proprio- and supraspinal axons either alone (Xu, Chen et al. 1997) or in combination with BDNF and NT-3 delivery (Xu, Guenard et al. 1995) after thoracic full transection injuries in adult Fischer rats. However, complete axonal crossing was only achieved in a less severe thoracic hemisection injury (Xu, Zhang et al. 1999). Locomotor recovery in terms of improved BBB motor scores occurred when the PAN/PVC channel was seeded with SCs, OECs grafted into the surrounding spinal parenchyma and

ChABC delivered additionally (Fouad, Schnell et al. 2005). In all of the above-mentioned studies, SCs were delivered with a Matrigel matrix to the PAN/PVC channels. When SCs were grafted in a fluid Matrigel matrix, tissue bridging between the implant and surrounding spinal tissue was improved, which helped descending spinal axons to re-enter the caudal host spinal cord facilitating gross motor recovery of the hindlimbs after Th8 full transection injury in adult Fischer rats (Williams, Henao et al. 2015). Furthermore, Novikova et al. combined SCs with a tubular poly-β-hydroxybutyrate implant and observed regrowth of CST and raphespinal axons after implantation into a cervical (C3/4) hemisection model in adult Sprague-Dawley rats (Novikova, Pettersson et al. 2008). Our own group was recently able to show that solid alginate-based hydrogel implants with an anisotropic channel structure can be seeded with adult syngeneic SCs into the lesion cavity of a unilateral C5 hemisection. This promote daxonal crossing and caudal re-entry of descending axons upon additional caudal SC grafts and BDNF expression in adult Fischer rats (Liu, Sandner et al. 2017).

1.3.4.3.3 Biomaterials and astrocytes

Cells of the astrocytic lineage were among the first cell types that were grafted in combination with biomaterial implants. Kliot et al. seeded fetal astrocytes into a Millipore pennant and implanted the construct into the injured L5 dorsal root entry zone and found regrowth of sensory axons from the dorsal root through the lesion site back into the spinal cord and a decreased inflammatory response at the lesion site (Kliot, Smith et al. 1990). Similarly, neonatal cortex-derived astrocytes soaked into a gelfoam matrix lead to reduced scarring at an acute L3 hemisection lesion in adult Sprague-Dawley rats. Importantly, graft- as well as host-derived astrocytes intermingled and associated with neurofilament-positive axons that partially traversed the lesion cavity (Wang, Chuah et al. 1995). Moreover, neonatal cortex-derived astrocytes delivered via a collagen matrix formed aligned bridges associated with regrowing CST axons at the lesion margins after implantation into a 2-mm long thoracic hemisection lesion, leading to subtle functional recovery of hindlimb locomotion (BBB and CatWalk™ gait analysis) (Joosten, Veldhuis et al. 2004). Another study from Deumens et al. demonstrated that astrocytes could align longitudinally onto PLA matrices. The astrocyte-seeded matrices were implanted into a dorsal hemisection injury at Th 11/12 in adult Lewis rats and together with additional astrocyte grafting into the surrounding host spinal cord, enhanced regrowth of the CST towards the implant but, unfortunately, no axonal growth into the biomaterial bridge was observed (Deumens, Koopmans et al. 2006). Likewise, transplantation of immature astrocyte populations alone can contribute to robust axonal regeneration and partial locomotor recovery after cervical SCI, as

described in the previous section (Davies, Huang et al. 2006, Davies, Proschel et al. 2008, Davies, Shih et al. 2011).

A prominent observation in these studies was the bridging function of the grafted astrocytes in combination with the different biomaterial implants, which is further supported by additional *in vitro* work showing alignment of astrocytes with each other or with structured biomaterial substrates (East, de Oliveira et al. 2010, Pawar, Prang et al. 2015, Zuidema, Desmond et al. 2015). However, today, studies examining the combination of astrocyte grafting and solid structurally defined biomaterial implants within acute SCI lesions sites are limited.

1.4 Rationale and hypothesis

Various experimental strategies have been developed over the years to tackle the individual or multiple hurdles of CNS regeneration. However, none of these approaches alone showed reliable efficacy in restoring meaningful sensorimotor function in either experimental animal models or clinical trials (Ahuja, Nori et al. 2017, Sofroniew 2018, Courtine and Sofroniew 2019). Putative effective treatment strategies should therefore combine different approaches to address multiple CNS regeneration hurdles at once. Although still in the preclinical stage, biomaterial-supported cell transplantation alone or in combination with additional therapeutic interventions such as growth factor delivery and chemoattraction represent a powerful tool and promising way to achieve meaningful functional recovery after SCI.

Thus far, we were able to show that alginate-based hydrogel implants with an anisotropic channel structure physically guide regrowing spinal axons in rostrocaudal orientation through acute sites of SCI (Pawar, Mueller et al. 2011, Gunther, Gunther et al. 2015). Moreover, additional transplantation of genetically modified BMSCs overexpressing the neurotrophin BDNF significantly enhances axonal growth into the alginate-based hydrogel implants (Gunther, Weidner et al. 2015). The combination of SC transplantation into and caudal to the hydrogel implant together with regulated viral BDNF delivery in the distal host spinal cord facilitate complete axonal crossing of the lesion site and caudal axonal re-entry (Liu, Sandner et al. 2017). However, implant integration as well as the survival of co-transplanted cells crucially rely on the biocompatibility of the biomaterial implant, since a biologically non-accessible implant might lead to a foreign body reaction of the host (Badylak 2015). Consequently, a strong immune response will negatively affect graft cell survival at acute SCI lesion sites even within biomaterial implants. Hence, graft cell survival has to be assured by either an additional supportive transplantation matrix (e.g., collagen or Matrigel) within the biomaterial implant or by modification of the biomaterial implants itself to improve its biocompatibility to reduce the hosts' reaction to the implant, thereby support the survival of co-transplanted cells and axonal growth at the implantation site.

Nonetheless, although axonal crossing of various synthetic or natural hydrogel implants was achieved, axonal re-entry into the distal host spinal cord and functional recovery was only occasionally observed (Li, Yang et al. 2009, Lee, McKeon et al. 2010). Furthermore, hydrogel implants often remain spatially separated from the surrounding host spinal parenchyma by possibly the formation of glia limitans, whereas tissue continuity across the implantation site as well as tissue alignment at the lesion margins were identified as essential contributors to successful axonal crossing of the host-graft interface (Xu, Guenard et al. 1995, Guest, Hesse

et al. 1997, Xu, Chen et al. 1997, Xu, Zhang et al. 1999, Hurtado, Cregg et al. 2011, Zukor, Belin et al. 2013, Williams, Henao et al. 2015, Lee, Wu et al. 2017). Immature astrocytes were shown in this regard to be capable of mediating alignment of host and graft tissue (Joosten, Veldhuis et al. 2004, Davies, Huang et al. 2006, Davies, Proschel et al. 2008, Davies, Shih et al. 2011) as well as to be essential for axonal growth after SCI (Kliot, Smith et al. 1990, Wang, Chuah et al. 1995, Anderson, Burda et al. 2016, Anderson, O'Shea et al. 2018). However, the combination of astrocytes with a defined hydrogel guidance structure has yet to be investigated.

The overall aim of this study was to examine whether the combination of biocompatible alginate-based hydrogel implants with an anisotropic channel structure along with transplantation of immature astrocytes into the hydrogel implant and into the surrounding host spinal cord allows for integration into the injured host spinal cord as well as axonal growth across an extended 2 mm-long SCI lesion sites in a unilateral cervical level C5 hemisection model in adult Fischer-344 rats.

Hypothesis

Immature astrocytes obtained from the cortex or spinal cord facilitate the integration of the alginate-based hydrogel implants into the injured host spinal cord and promote regeneration of damaged spinal axons. Additional transplantation of immature astrocytes into the surrounding spinal parenchyma facilitates axonal crossing of the host-graft interface and re-entry into the caudal host spinal cord.

Aims

1. Analyze whether surface coating of alginate-based hydrogels improves cell attachment and cell survival as well as axonal growth *in vitro* and *in vivo*.

2. Determine whether the transplantation of immature cortex-derived astrocytes into alginate-based hydrogels improves implant integration and axonal regrowth after SCI.

3. Characterize phenotypic differences between immature spinal cord- and cortex-derived astrocytes.

4. Examine whether the transplantation of immature spinal cord- and cortex-derived astrocytes into alginate-based hydrogels and the surrounding host spinal cord improves implant integration and axonal regrowth after SCI.

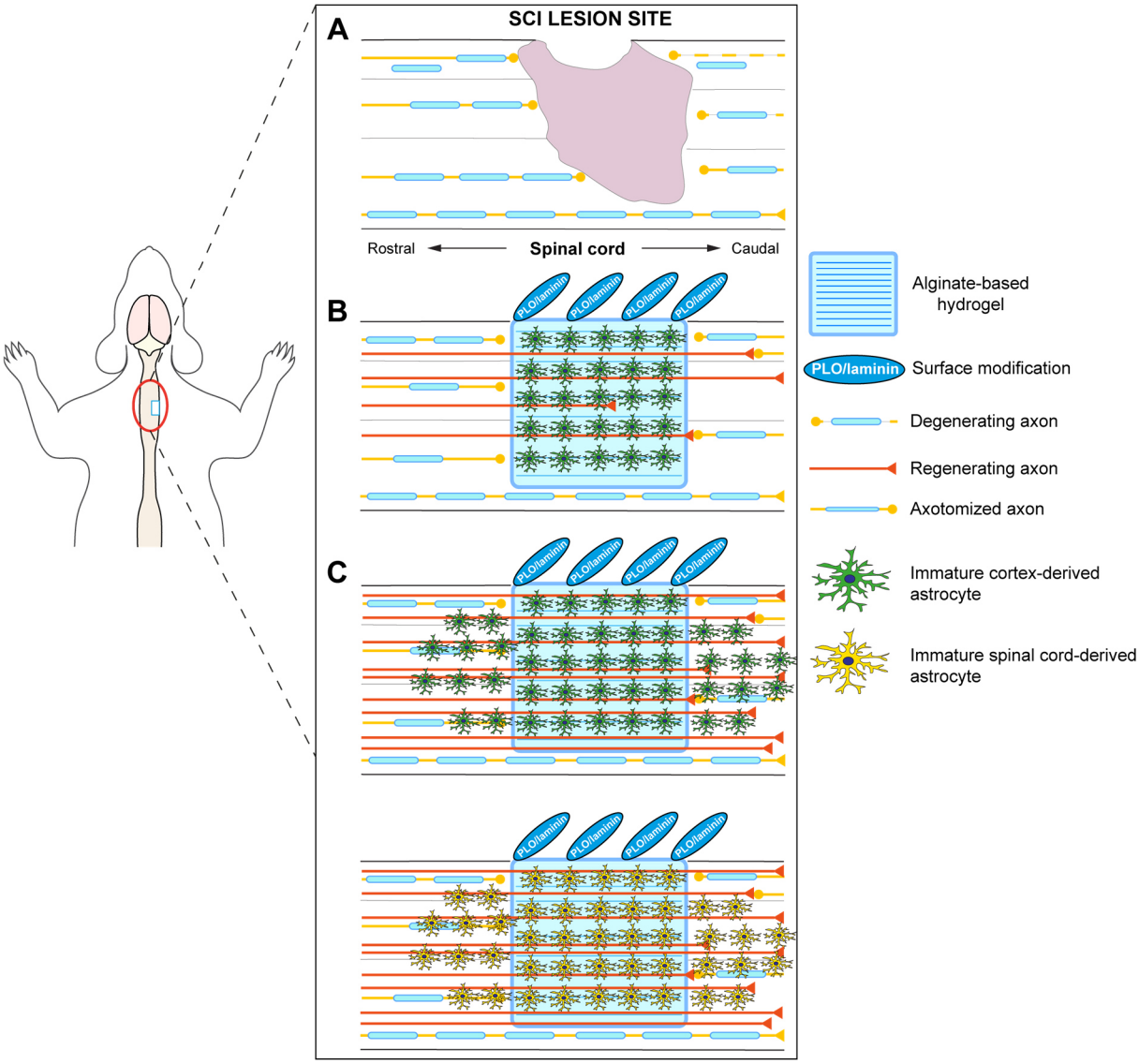

Figure 2: Hypothesis. (**A**) After SCI, spinal axons are damaged and neural tissue at the lesion epicenter is lost. (**B**) Regrowing spinal axons are physically guided in rostrocaudal direction through the SCI site by the implantation of an alginate-based hydrogel implant with anisotropic channel structure. The polypeptide PLO and ECM component laminin are bound to the surface of the hydrogel implant to enhance biocompatibility and viability within the implants. Additional seeding of the hydrogel with immature astrocytes further enhances axonal growth into and through the hydrogel implant. (**C**) Complete axonal crossing of the SCI site can be achieved by co-transplantation of either immature cortex- or spinal cord-derived astrocytes into the hydrogel implant and additionally into the adjacent host spinal cord. The grafted immature astrocytes create a continuous growth-permissive substrate for regrowing spinal axons.

2 Material and methods

2.1 Materials

2.1.1 Animals

All experiments were conducted in accordance with national guidelines for animal care in accordance with the European Union Directive (2010/63/EU) and approved by the local governing body (Regierungspräsidium Karlsruhe). All *in vitro*- and *in vivo*-experiments were carried out with adult female Fischer-344 rats obtained from Charles River (Strain: F344-Tg(UBC-EGFP)F455Rrrc) or Janvier labs (Strain: F344/HanZtmRj). *In vivo*-studies were exclusively performed with wildtype animals (> 150 g, 10 – 12 weeks old; >150 g); cells and tissues were dissected from either wildtype or stable GFP-transgenic Fischer-344 rats of both sexes. All rats were housed in groups of 4 – 5 animals/cage on a 12/12-hour light/dark cycle with free access to food and water (*ad libitum)* in the animal facility at the Spinal Cord Injury Center of the Heidelberg University Hospital. Animal well-being as well as temperature (20 ± 1°C) and humidity (45 - 65%) were checked daily by trained staff of the animal facility.
For *in vivo*-experiments, animals were randomly subdivided into different experimental groups and data from different cohorts combined for statistical analysis.

2.1.2 Animal care

Drug	Agent	Dose	Company
Ampicillin-ratiopharm®	Ampicillin	50 mg/kg	Ratiopharm
Ampi-Dry®	Ampicillin	50mg/kg	Veryx-Pharma GmbH
Bepanthen®	Dexpanthenol	-	Bayer Vital GmbH
Burpenovet®	Burprenophine	0.03 mg/kg	Bayer Vital GmbH
Ketamine 10%	Ketamine	62.5 mg/kg	HFW Bremer Pharma GmbH
NaCl 0.9%	-	-	Braun
Rimadyl®	Carprofen	5 mg/kg	Pfizer
Ringer electrolyte solution	-	-	Braun
Temgesic®	Burprenophine	0.03 mg/kg	Reckitt Benckiser
Ventraquil® 1%	Acepromacine	0.625 mg/kg	Ceva
Xylariem®	Xylacine	3.175 mg/kg	Ecuphar®

Table 1: List of animal medication.

Drug	Final concentration	For 20 ml
Acepromacine	0.625 mg/kg	0.75 ml
Ketamine	62.5 mg/kg	7.50 ml
Xylacine	3.175 mg/kg	1.90 ml
NaCl 0.9%	-	9.85 ml

Table 2: Anesthesia mixture.

2.1.3 Antibodies

2.1.3.1 Primary antibodies

Antibody	Species	Isotype	Type	Dilution	Company
AQP4	ms	IgG1	monoclonal	1:1000	Sigma Aldrich
GLT-1	rb	IgG1κ	monoclonal	1:200	Merck Millipore
GFAP	ms	IgG1	monoclonal	1:1000	Merck Millipore
GFAP	rb	IgG	polyclonal	1:1000	Dako
Nestin	ms	IgG1	monoclonal	1:1000	Merck Millipore
NFIA	rb	IgG	polyclonal	1:200	Abcam
S100 β	ms	IgG1	monoclonal	1:1000	Sigma Aldrich
Sox 2	gt	IgG	polyclonal	1:200	Santa Cruz Biotechnology
Sox 9	rb	IgG	monoclonal	1:500	Abcam
Vimentin	ms	IgG1	monoclonal	1:1000	Merck Millipore
Vimentin	rb	IgG	monoclonal	1:1000	Abcam

Table 3: List of primary antibodies used for characterization of neonatal astrocytes *in vitro*.

Antibody	Species	Isotype	Type	Dilution	Company
AQP4	ms	IgG1	monoclonal	1:1000	Sigma Aldrich
A2B5	ms	IgM	monoclonal	1:500	Abcam
CX43	rb	IgG	polyclonal	1:500	Invitrogen
GFAP	ms	IgG1	monoclonal	1:1000	Merck Millipore
GFAP	rb	IgG	polyclonal	1:1000	Dako
GFP	gt	IgG	polyclonal	1:1000	Rockland Inc.
GFP	rb	IgG	polyclonal	1:1000	Merck Millipore
GLT-1	gp	-	polyclonal	1:500	Merck Millipore
Ki67	rb	IgG	monoclonal	1:1000	Abcam
Nestin	ms	IgG1	monoclonal	1:1000	Merck Millipore
Sox 2	gt	IgG	polyclonal	1:200	Santa Cruz Biotechnology
Sox 9	rb	IgG	monoclonal	1:500	Abcam
S100 β	ms	IgG1	monoclonal	1:1000	Sigma Aldrich
Vimentin	ms	IgG1	monoclonal	1:1000	Merck Millipore

Table 4: List of primary antibodies used for characterization of neonatal astrocytes *in vivo*.

Antibody	Species	Isotype	Type	Dilution	Company
CD31	gt	IgG	polyclonal	1:300	Biocompare
GFAP	ms	IgG1	monoclonal	1:1000	Merck Millipore
GFAP	rb	IgG	polyclonal	1:1000	Dako
GFP	gt	IgG	polyclonal	1:1000	Rockland Inc.
GFP	rb	IgG	polyclonal	1:1000	Invitrogen
Iba-1	rb	IgG	polyclonal	1:500	Wako
βIII-tubulin	ms	IgG	monoclonal	1:1000	Promega
5-HT	rb	IgG	polyclonal	1:2000	Immunostar
von Willebrand factor	rb	IgG	polyclonal	1:1000	Sigma Aldrich

Table 5: List of primary antibodies used for analysis of alginate-based hydrogels after implantation into the injured spinal cord.

2.1.3.2 Secondary antibodies

Antibody	Species	Isotype	Target species	Dilution	Company
Alexa Fluor®-488	dk	IgG (H+L)	ms	1:300	Invitrogen
Alexa Fluor®-488	dk	IgG (H+L)	rb	1:300	Invitrogen
Alexa Fluor®-488	dk	IgG (H+L)	gt	1:300	Invitrogen
Alexa Fluor®-594	dk	IgG (H+L)	ms	1:300	Invitrogen.
Alexa Fluor®-594	dk	IgG (H+L)	rb	1:300	Invitrogen
Alexa Fluor®-594	dk	IgG (H+L)	gt	1:300	Invitrogen
Alexa Fluor®-594-conjugated Streptavidin	dk	IgG (H+L)	-	1:500	Jackson
Cy5®	dk	IgG (H+L)	ms	1:500	Jackson
Cy5®	dk	IgG (H+L)	rb	1:500	Jackson

Table 6: List of secondary antibodies used to detect immunolabeling.

2.1.4 Cells and cell culture

2.1.4.1 Primary cell cultures

Cell type	Origin	Donor species	Developmental stage	Genetic background
Neonatal astrocytes	Cortex	Fischer-344 rat	P1, 3	eGFP$^+$
	Cortex	Fischer-344 rat	P1, 3	WT
	Spinal cord	Fischer-344 rat	P1, 3	eGFP$^+$
	Spinal cord	Fischer-344 rat	P1, 3	WT
DRG-derived neurons	L4-L6 DRG	Fischer-344 rat	adult (8 -12 weeks)	eGFP$^+$

Table 7: List of primary cells.

2.1.5 Cell culture reagents, supplements and equipment

Reagents/supplements	Company
1x Alpha medium	Life Technologies
B-27 supplement (50x)	Life Technologies
bidest. water	Life Technologies
destilled water	-
DMSO	NeoLab
DMEM (1x; high glucose, + NEAA, no pyruvate, no L-glutamine)	Life Technologies
DMEM/F12 (1x; 1:1)	Life Technologies
DPBS	Life Technologies
Gentamycin (10 mg/ml)	Life Technologies
L-glutamine (100x)	Life Technologies
Laminin (1 mg/ml)	Sigma Aldrich
PAA Gold FBS	Biochrome
Paraformaldehyde	Carl Roth
Penicillin (10,000 Units/ml)	Life Technologies
Poly-L-ornithine (10 mg/l)	Sigma Aldrich
Streptomycin (10,000 Units/ml)	Life Technologies
Cytosine-β-D-arabinofuranoside (10 mg/ml)	Sigma Aldrich

Table 8: List of cell culture reagents and supplements.

Enzyme/reagent	Company
Collagenase XI (10 mg/ml)	Sigma Aldrich
Dispase I (10 mg/ml)	Worthington
DNAse I (1 mg/ml)	Worthington
Fibrinogen (100 mg/ml)	Sigma Aldrich
Thrombin (100 Units/ml)	Sigma Aldrich
TrypLE Express™ (1x)	Life Technologies

Table 9: List of enzymes.

Equipment	Company
AQUAline AL25 water bath	Lauda
“Blaudeckel” glass bottles	NeoLab
Cell strainer, 70 µm, Nylon	Sigma Aldrich
6-well cell culture plates	Greiner Bio-One
12-well cell culture plates	Greiner Bio-One
24-well cell culture plates	Greiner Bio-One
Glass coverslips (12 mm, 15 mm)	Menzel GmbH
Disposable pipette tips (1000 µl, 200 µl, 20 µl,)	VWR
DOS-20S orbital shaker	NeoLab
Eppendorf tubes (0.5 ml, 1.5 ml, 2 ml)	Eppendorf
Falcon tubes (15 ml, 50 ml)	Greiner Bio-One
HERAcell 240i CO_2 incubator	Thermo Scientific
MSC-Advantage 1.2 Class II Microbiological safety cabinet	Thermo Scientific
Neubauers’ hemacytometer, 0.00025 mm^2	Paul Marienfeld
Pasteur glass capillary pipettes	WU Mainz
PIPETBOY acu2	INTEGRA Bioscience
PIPETMAN® pipettes (1000 µl, 200 µl, 100 µl, 20µl, 10 µl, 2µl)	Gilson, Inc.
Rotina 380R cell culture centrifuge	Hettich Zentrifugen
Cell culture flasks (T25, T75. T175)	Greiner Bio-One
Vortex mixer	NeoLab

Table 10: List of cell culture equipment.

2.1.6 Cell culture medium

2.1.6.1 DRG neurons

Reagent/supplement	Stock concentration	Final concentration
DMEM/F12 (1x)	-	-
B-27 supplement	50x	
L-Glutamine	200 mM	2 mM
Penicillin/Streptomycin	10,000 Units/ml each	100 Units/ml each

Table 11: Cell culture medium for DRG neurons.

2.1.6.2 Neonatal astrocytes

Reagent/supplement	Stock concentration	Final concentration
DMEM (1x)	-	-
L-Glutamine	200 mM	2 mM
PAA Gold FBS	-	5%
Gentamycin	10,000 Units/ml	100 Units/ml
Penicillin/Streptomycin	10,000 Units/ml each	100 Units/ml each

Table 12: Cell culture medium for neonatal astrocytes.

2.1.7 Alginate-based hydrogels

All alginate-based hydrogels were fabricated and kindly provided by Apl. Prof. Dr. Rainer Müller from the Department of Physical and Theoretical Chemistry of the University of Regensburg, Germany. All experiments of this study were performed using alginate-based anisotropic hydrogels fabricated with either Sr^{2+} or Zn^{2+} ions.

2.1.8 Chemicals, solutions, buffers and equipment

2.1.8.1 General chemicals

Chemical	Company
Aceton	Carl Roth
Agar-agar, danish	Carl Roth
D(+)-Saccharose (Sucrose)	Carl Roth
Ethanol 99.8% (denatured)	Carl Roth
Gelatine	Carl Roth
D(+)-Glucose	Carl Roth
HCl (1 N)	NeoLab
Isopropanol	Carl Roth
HDI	Sigma Aldrich
Methanol	Carl Roth
Na_2HPO_4	Carl Roth
NaH_2PO_4	Carl Roth
Na_3PO_4	Carl Roth
NaCl	VWR
40% NaOH (10 N)	Carl Roth
Paraformaldehyde	Carl Roth
Sodium alginate (2% w/w)	FMC Biopolymer AS d/b/a Novamatrix
Sodium azide	Carl Roth
$Sr(NO_3)_2$	Carl Roth
Tissue-Tek O.C.T.™ compound	Sakura
Trizma (TRIS) base	NeoLab
Trizma (TRIS) hydrochloride	Carl Roth
Triton X-100	NeoLab
Ultrapure™ agarose	Invitrogen
$Zn(NO_3)_2$	Carl Roth

Table 13: List of general chemicals.

2.1.8.2 Chemicals and kits used for immunolabeling

Reagent	Company
Cytoseal™ 60	Thermo Scientific
DAB peroxidase substrate kit	Vector Stain
4',6-diamidino-2-phenylindole (DAPI)	Sigma Aldrich
Dk serum	Biochrome
Fluoromount-G	Southern Biotechnology Associates
VECTASTAIN® ABC Elite kit	Vector Stain

Table 14: List of chemicals and kits used for immunolabeling.

2.1.8.3 Equipment and instruments for surgical procedures

Equipment/Instrument	Company
Braunol®	Braun Melsungen AG
Disposable scalpel #11, #15	FEATHER Safety Razor
Friedman-Pearson Rongeurs	Fine Science Tools
Forceps Dumont #2	Fine Science Tools
Forceps Dumont #5	Fine Science Tools
Forceps Dumont #55	Fine Science Tools
Halsey Needle Holder	Fine Science Tools
Octagon forceps	Fine Science Tools
4/0 suture silk, braided, coated, non-adsorbable	Braun Melsungen AG
Steel wound clips, stainless, 9 mm	MikRon Precision, Inc.
PICOSPRITZER® III Microinjector	General Valve
Fisherbrand™ FB70155 pump	Fisher Scientific
Steri 250, dry bead sterilizator	LAT Scientific Instruments

Table 15: List of equipment used for surgical procedures.

2.1.9 Solutions and buffers

Reagent	For 1 liter
Trizma (TRIS) base	1.94 g
Trizma (TRIS) hydrochloride	13.22 g
NaCl	9.00 g
dH_2O	1.00 l
Adjust pH to 7.4 using 10 N NaOH or 1 N HCl, respectively	

Table 16: 1x TRIS-buffered saline, pH 7.4.

Reagent	Concentration	For 1 liter
NaH_2PO_4	0.25 M	230 ml
Na_2HPO_4	0.2 M	770 ml
Adjust pH to 7.3 using 10 N NaOH or 1 N HCl, respectively		

Table 17: 0.2 M phosphate buffer, pH 7.3.

Solutions of mono- and dibasic sodium phosphate are prepared separately in dH_2O and blended afterwards.

2.1.10 Buffers and solutions for transcardial perfusion

Reagent	Final concentration	For 1 liter
NaCl	-	9.00 g
0.2 M phosphate buffer, pH 7.3	0.1 M	500.00 ml
dH_2O	-	500.00 ml

Table 18: 0.9% perfusion saline, pH 7.4.

Reagent	Final concentration	For 1 liter
Paraformaldehyde	-	40.00 g
0.2 M phosphate buffer, pH 7.3	0.1 M	500.00 ml
dH_2O	-	500.00 ml
NaOH	10 N	4 drops

Table 19: 4% paraformaldehyde fixative.

Reagent	Final concentration	For 1 liter
D(+)-Sucrose	-	300.00 g
0.2 M phosphate buffer, pH 7.3	0.1 M	350.00 ml
dH_2O	-	350.00 ml

Table 20: 30% sucrose solution.

2.1.11 Buffers for immunolabeling

Reagent	Final concentration	For 100 ml
Dk serum	1% (v/v)	1 ml
10% Triton X-100	0.1% (v/v)	1 ml
1x TBS	-	98.00 ml

Table 21: Blocking buffer for immunocytochemistry.

Reagent	Final concentration	For 100 ml
Dk serum	5% (v/v)	5 ml
10% Triton X-100	0.25% (v/v)	2.5 ml
1x TBS	-	92.5 ml

Table 22: Blocking buffer for immunohistochemistry.

2.1.12 Equipment and software

Equipment	Company
AL 5 water bath	Lauda
Anodized aluminum molds	Schuett-Biotech
Centrifuge Type 5418	Eppendorf
HM 550 microtome	Zeiss
ISMATE® REGLO Digital MS-4/8	IDEX Health & Science Oak Harbor
Microscope glass slides (75 x 25 mm)	Carl Roth
PB-11 pH meter	Satorius
PAP PEN liquid blocker	Kisker Biotech
Razorblades	Apollo Solingen
RS basic 2 heating plates	IKA
Single stage microelectrode puller PP-830	Narishige Scientific Instrument Lab
SUPERFROST® PLUS microscope glass slides (25 x 75 mm)	Menzel GmbH
ThermoMixer C	Eppendorf
TissueCut® Type #42 microtome blades	MEDITE
Vibratome VT 1000S	Leica

Table 23: List of laboratory equipment.

Microscope/Imaging equipment	Company
BX53 upright epifluorescence microscope	Olympus Life Sciences
BX61 confocal laser-scanning microscope	Olympus Life Sciences
CKX41 inverted epifluorescence microscope	Olympus Life Sciences
IX81 motorized epifluorescence microscope	Olympus Life Sciences
SZ51 stereo zoom microscope	Olympus Life Sciences
XC30 CCD digital camera	Olympus Life Sciences

Table 24: List of microscopes and imaging equipment.

Software	Company	Application
Adobe Illustrator CS6	Adobe, Inc.	Data illustration
Adobe Photoshop CS6	Adobe, Inc.	Image processing, data illustration
Cell^{F}	Olympus Life Sciences	Fluorescence microscopic imaging
Cell^{P}	Olympus Life Sciences	Fluorescence microscopic imaging
FluoView 2.1.c	Olympus Life Sciences	Confocal laser-scanning fluorescence imaging, image processing
ImageJ	NIH	Image processing, data analysis
MatLab™	TheMathWorks, Inc.	Data processing and analysis, statistical analysis
Microsoft Excel 2016	Microsoft Corporation	Data processing and analysis
Prism 8 Graphpad	Graphpad Software, Inc.	Statistical analysis and data illustration

Table 25: List of software used for imaging, data processing and analysis, statistical analysis and data illustration.

2.2 Methods

2.2.1 Alginate-based hydrogels

2.2.1.1 Fabrication of alginate-based hydrogels with anisotropic channels structure

Alginate-based hydrogels were manufactured with minor modifications as previously described (Gunther, Gunther et al. 2015, Gunther, Weidner et al. 2015, Liu, Sandner et al. 2017) in the laboratory of Apl. Prof. Dr. Rainer Müller from the Department of Physical and Theoretical Chemistry of the University of Regensburg, Germany. Hydrogels were produced with sodium alginate (Pronova UP MVG, FMC Biopolymer AS d/b/a Novamatrix) with a guluronic acid content of > 70% and a dynamic viscosity of 211 mPa*s (10 g/l, 20 °C). Hydrogel polymerization and channel formation were performed using divalent Sr^{2+} (channel diameter: 40 – 60 µm) or Zn^{2+} ions (channel diameter: 70 – 90 µm); the type of the hydrogel used will be stated later on for each experiment.
In brief, 65 g sodium alginate were dissolved in purified dH_2O (final concentration: 20 g/l) under constant stirring until a homogeneous alginate solution was formed and transferred into anodized cylindrical aluminum molds (dimensions: 5.5 cm diameter, 4 cm height, Schuett-Biotech). For polymerization, the aqueous alginate solution was carefully overlayed with 20 ml of either a 1M $Sr(NO_3)_2$ or 1M $Zn(NO_3)_2$ solution. Gel formation was performed at 10°C for at least 36 h until polymerization was completed. Afterwards, hydrogels were rinsed with dH_2O (4x, 4h each) and chemically stabilized for 4 h at room temperature by an interpenetrating polymer network of hexamethylene-di-isocyanat (100 mM in dry acetone; HDI, Sigma Aldrich). Excessive HDI was removed by repeated washing steps in dry acetone (5 mins each; Carl Roth). Hydrogel blocks were rinsed in dH_2O at 70°C and constant stirring until CO_2 emission stopped. Non-complexed divalent cations were removed from the hydrogel matrix by repeated washes in 0.1 M HCl (5x, 2 h each, Carl Roth) and finally neutralized in purified dH_2O.

For *in vitro*-experiments, capillary-free alginate hydrogels blocks were cut into slices (300 µm thick, 1 cm x 1 cm) using a vibratome (Leica VT1000S, Leica Biosystems GmbH).
For *in vivo*-experiments, cuboid alginate-based hydrogel implants (2 mm length x 2 mm height x 1.3 mm width) with anisotropic capillaries parallelly orientated to the 2 mm long edge were cut on a vibratome.
Hydrogel matrix homogeneity, channel structure and orientation were inspected under a light microscope (Olympus BX53; Olympus Life Sciences). Hydrogels were stored in 70% EtOH at 4°C until further use.

2.2.1.2 Surface coating of alginate-based hydrogels

All hydrogels used for cell culture experiments and *in vivo*-studies were beforehand surface coated with poly-L-ornithine (PLO) and the extracellular matrix component laminin.
First, hydrogel implants and slices were coated with PLO (0.5 mg/ml in ice-cold dH_2O; Sigma Aldrich) overnight at 37°C, 5% CO_2 followed by 2 washing steps in sterile 1x DPBS (30 mins each) on an orbital shaker (60 rpm, NeoLab). Subsequently, laminin (10 µg/ml in 1x DPBS; Sigma Aldrich) was added for 2 h at 37°C, 5% CO_2 and the PLO-coated hydrogel slices afterwards rinsed 3x 30 mins in 1x DPBS (Life Technologies) and stored in sterile 1x DPBS at 4°C until further use.

2.2.2 Cell culture

2.2.2.1 Surface coating of cell culture dishes and glass coverslips

All cell culture dishes used for the cultivation of primary neonatal astrocytes were beforehand surface coated with PLO and laminin under sterile conditions.
First, stock solutions of PLO (10 mg/ml) and laminin (1 mg/ml) were diluted in dH_2O. The PLO solution (20 µg/ml) was added to the cell culture dishes and incubated for 1 h at 37°C, 5% CO_2. Afterwards, the dishes were washed once with ice-cold dH_2O and the laminin solution (10 µg/ml) was added and incubated for 2 h at 37°C, 5% CO_2 followed by a final washing step with ice-cold dH_2O. PLO/laminin-coated cell culture dishes were immediately used for cell culture experiments.
To coat glass coverslips (12 mm or 15 mm in diameter, Menzel GmbH), stock solutions of PLO and laminin were prepared in ice-cold dH_2O. First, glass coverslips were washed 3x in dH_2O and subsequentially incubated for 16 h at room temperature in PLO (10 µg/ml) followed by a washing step with ice-cold dH_2O. Laminin (5 µg/ml) was added to the PLO-coated coverslips for 2 h at 37°C, 5% CO_2. Finally, the coated glass coverslips were rinsed once with ice-cold dH_2O and immediately used.

2.2.2.2 Isolation and cultivation of astrocytes from neonatal Fischer-344 rats

2.2.2.2.1 Cortex-derived astrocytes

Cortex-derived astrocytes were isolated from neonatal (postnatal day 1 (P1) and postnatal day 3 (P3)) wildtype and GFP-transgenic Fischer-344 rat pups of both sexes. Briefly, animals were killed by decapitation and their brains dissected. Brain hemispheres were separated and transferred into a 30 mm-cell culture dish (Greiner Bio One) containing 1 ml ice-cold 1x DMEM (Life Technologies). Excessive non-cortical tissues, meninges and blood vessel were carefully removed under a dissection microscope (Olympus SZ51; Olympus Life Sciences) using microscissors and forceps (Fine Science Tools). Afterwards, cortices were transferred into 12-well cell culture plates (Greiner Bio One) and mechanically dissociated using forceps and enzymatically digested by adding 500 µl of a 1:1 mixture of Collagenase XI (1,200 U/mg in HBBS, Sigma Aldrich) and Dispase I (4 U/mg in HBBS, Worthington). Enzymatic digestion was done for 45 min at 37°C, 5% CO_2 under permanent mechanical agitation (125 rpm) on an orbital shaker (NeoLab). Each individual cortex was used to generate a separate primary astrocyte culture; these unique cultures were not pooled later on. Following enzymatic digestion, 1 ml pre-warmed astrocyte cell culture medium containing 1x DMEM (Life Technologies) +5% FBS (Merck) +1% L-glutamine (200 mM, Life Technologies) + 0.5% Pen/Strep (10,000 U/ml each; Life Technologies), +0.5% Gentamycin (10,000 U/ml each; Life Technologies) was added and the tissue was further dissociated by gentle mechanical trituration (10x) with a sterile fire-polished Pasteur glass pipette (WU Mainz). The cell solution was afterwards filtered through a sterile cell strainer (70 µm pore size, Nylon; Sigma Aldrich) into 50 ml falcon tubes (Greiner Bio One). The filter was washed twice with 10 ml ice-cold 1x DMEM and the cell solution spun down at 9°C for 8 mins at 1,300 rpm. The cell pellet was resuspended in 1 ml pre-warmed astrocyte culture medium and cells seeded into T75 cell culture flasks (Greiner Bio One) containing 15 ml pre-warmed cell culture medium. Cell culture medium was changed every two days.

2.2.2.2.2 Spinal cord-derived astrocytes

Spinal cord-derived astrocytes were isolated from neonatal Fischer-344 rat pups of both sexes at postnatal day 1 and 3. Briefly, neonatal rat pups were killed by decapitation, their torsos were fixed on a dissection plate and opened ventrally via a skin incision using angled surgical scissors (Fine Science Tools). The chest was opened and all intestines removed with blunt forceps (Fine Science Tools) and microscissors (Fine Sciences Tools). The paravertebral mus-

cles were carefully removed, the spinal column opened ventrally using thin forceps and microscissors under a dissection microscope (Olympus SZ51; Olympus Life Sciences) and the spinal cord exposed. Ventral and dorsal roots were cut, the spinal cord dissected and transferred into a 30-mm cell culture dish coated with a thin 5% agarose gel. The spinal cord was cleared from dura mater and blood vessels and finally transferred into a 2-ml Eppendorf tube (Eppendorf) containing 1 ml ice-cold 1x DMEM. Each individual spinal cord was used to generate an individual primary astrocyte culture; unique cultures were not pooled later on. Spinal cords were mechanically and enzymatically digested as described above. After dissociation, the spinal cell solution was filtered through a 70-µm cell strainer and centrifuged for 8 mins at 1,300 rpm. The resulting cell pellet was dissolved in 1 ml pre-warmed astrocyte cell culture medium and cells plated into PLO/laminin-coated T75 cell culture flasks. Cell culture medium was changed every 2 days.

2.2.2.2.3 Enrichment of primary neonatal astrocytes

To obtain enriched astrocytic cultures, non-astrocytic and neuronal cells were reduced from primary cultures of cortex-derived and spinal cord-derived astrocytes. 150 µl of cytosine-β-D-arabinofuranoside (Ara-C, 1 mg/ml in 1x DMEM; Sigma Aldrich) were added to each T75 cell culture flask and incubated for 6 h under permanent mechanical agitation (225 rpm) on an orbital shaker at 37°C, 5% CO_2. Afterwards, cells were washed once with 20 ml pre-warmed 1x DPBS and enzymatically detached by adding 3 ml of the trypsin-analogon TrypleExpress™ (1x, Life Technologies) and incubated at 37°C, 5% CO_2. After 8 minutes, the cell solution was spun down for 8 min at 1,300 rpm at 9°C. The cell pellets were resuspended in 1 ml pre-warmed astrocyte cell culture medium and finally plated into new T75 cell culture flasks at a density of 0.5 x 10^6 cells, into 24-well cell culture plates at a density of 10,000 cells/well or onto glass coverslips (diameter 15 mm) at a density of 10,000 cells/coverslip. Cell culture medium was changed every 2 days.

2.2.2.2.4 Purity control of enriched neonatal astrocytes

All experiments were carried out with neonatal astrocytes of passage 2. To assure astrocyte enrichment, probes of each Ara-C-treated astrocyte culture were immunolabeled with antibodies specific for the astrocyte marker GFAP (1:1,000; Dako), the neuronal marker βIII-tubulin (1:1,000; Promega), and IbaI to detect macrophages/microglia (1:500; Wako Chemicals). Immunolabeling was visualized using Alexa-fluorophore-conjugated secondary antibodies (1:300; Life Technologies) and detected under an epifluorescence microscope (Olympus IX81;

Olympus Life Sciences). For all *in vitro*- and *in vivo*-experiments, cortex-derived astrocyte cultures with > 95% of total cells expressing GFAP and spinal cord-derived astrocyte cultures with > 65% of total cells expressing GFAP were used.

2.2.2.2.5 Isolation of DRG neurons from adult Fischer-344 rats

Adult Fischer-344 rats (10 – 12 weeks, > 150 g) were deeply anesthetized with an intraperitoneal (i.p.) injection of a mixture of ketamine (62.5 mg/kg), xylazine (3.175 mg/kg), and acepromazine (0.625 mg/kg) (final conc. 5 ml/kg). Animals were killed by decapitation and the spinal column was exposed. The spinal cord was removed and the dorsal root ganglia were carefully dissected and collected in ice-cold Hibernate A medium (Life Technologies). Samples were washed once with ice-cold HBSS and enzymatically digested by incubation in a 1:1 mixture of Collagenase XI (1,200 U/ml in HBSS; Sigma Aldrich) and Dispase I (4 U/ml in HBSS; Worthington) for 30 mins at 37°C, 5% CO_2 with constant mechanical agitation (125 rpm) on an orbital shaker (NeoLab). DRG were washed once with 1x DMEM/F12 (Life Technologies) +10% FBS (Merck) and allowed to settle down before the supernatant was discarded. Afterwards, DRG were resuspended in DRG cell culture medium (1X DMEM/F12 +2% B-27 supplement (Life Technologies) +1% L-glutamine (200 mM, Life Technologies) +1% Penicillin/Streptomycin (10,000 U/ml each, Life Technologies) and immediately plated onto alginate-based hydrogel slices.
To fix primary cells, all cell culture medium was removed and the cells were washed once with pre-warmed 1x DPBS. Afterwards, 4% PFA/0.1 M PB was added for 30 mins at room temperature followed by 3 washing steps with 1x TBS (10 mins each). For storage, 0.05% sodium azide/0.1 M PB was added and cells were stored at 4°C until further use.

2.2.3 Immunocytochemistry

Immunocytochemical labeling was performed on primary astrocytes isolated from the cortex or the spinal cord of neonatal Fischer-344 rats (P1 or P3) or on DRG neurons isolated from adult Fischer-344 rats.
After fixation, cells were washed 3 times with 1x TBS. Blocking and permeabilization was performed by incubation in 1x TBS +0.1% Triton-X 100 +1% donkey serum for 1 h at room temperature. All primary antibodies were diluted in blocking buffer and added overnight at 4°C. Excessive primary antibodies were removed by 3 washing steps in 1x TBS +1% donkey serum for 10 mins each at RT. All secondary antibodies and 4', 6-diamidino-2-phenylindole (1:2,000, DAPI) were diluted in 1x TBS +1% donkey serum and added to the samples for 2 h at RT in

the dark. Finally, cells were rinsed 3x in 1x TBS (10 mins each). Cells in cell culture plates were stored in 0.05% sodium azide/0.1 M PB at 4°C in the dark; cells on glass coverslips or hydrogel slices were mounted with Fluoromount G (Southern Biotechnology Associates) onto glass objective slides (Carl Roth) and stored in the dark.

To phenotypically characterize neonatal astrocytes derived from cortices and spinal cord of postnatal day 1 and 3 Fischer-344 rats *in vitro*, varying combinations of the following markers have been used. Mouse anti-Nestin (1:1,000; Merck Millipore) and anti-Vimentin (mouse, 1:1,000; rabbit, 1:2,000; both Merck Millipore) to identify stem cells/astrocyte precursors and astrocyte reactivity, and goat anti-Sox2 (sex-determining region Y-box 2, 1:200; Santa Cruz Biotechnology) to identify proliferating precursors. The transcription factors rabbit anti-NFIA (Nuclear factor 1A, 1:500; Abcam) and rabbit anti- Sox9 (sex determining region Y-box 9, 1:500; Abcam) were used to label early astroglial precursors. Mature astrocytes were immunolabeled with anti-GFAP (Glial fibrillary acidic protein, mouse, 1:1,000; Merck Millipore and rabbit, 1:1,000; Dako), anti-Aldh1L1 (Aldehyde dehydrogenase 1 family member L1, mouse, 1:2,000; Merck Millipore), anti-AQP4 (Aquaporin 4, mouse, 1:500; Sigma Aldrich), anti-A2B5 (mouse, 1:500; Abcam), anti-GLAST (Glutamate/aspartate transporter 1, rabbit, 1:200; Abcam), anti-GLT1 (Glial glutamate transporter 1, rabbit, 1:200; Merck Millipore), and anti-S100β (S100 calcium binding protein β, mouse, 1:2,000; Sigma Aldrich).

The following secondary antibodies were used: donkey anti-mouse/anti-rabbit Alexa Fluor®-594 (1:300, Life Technologies) for GFAP; donkey anti-goat/anti-mouse/anti-rabbit Alexa Fluor®-488 (1:300, Life Technologies) for Nestin, Vimentin, Sox2, Sox9, Aldh1L1, AQP4, A2B5, GLAST, GLT1, and S100β.

To measure neurite growth in response to surface coating of alginate-based hydrogels *in vitro*, DRG neurons were plated onto non-coated or coated hydrogel slices and immunolabeled with mouse anti-βIII-tubulin (1:1,000; Promega). The primary antibody was detected with donkey anti-mouse Alexa Fluor® 488 (1:300; Life Technologies).

2.2.3.1 Characterization of neonatal astrocytes in vitro

To examine the molecular phenotype, probes of neonatal astrocytes cultures isolated from P1 and P3 cortices and spinal cords were plated into PLO/laminin-coated 24-well cell culture plates (BioOne Greiner) after Ara-C treatment and were allowed to recover for 2 days before cells were fixed as described previously. All analysis was performed with cells of passage 2.

Immunolabeling was visualized using epifluorescence illumination with a fluorescence microscope (Olympus BX53; Olympus) with attached camera (Olympus XC30; Olympus). Images

of all cultures were taken at 20x magnification with the same exposure time per marker, resolution, optical aperture, and filter cube settings. Per astrocyte culture and marker, 5 individual wells were analyzed and averaged. The total number of cells in a randomly selected field of 1 mm^2 was determined (number of $DAPI^+$ nuclei) and the number of positive cells for the different markers counted using the CellCounter plug-in for ImageJ and expressed as percentage of total cells or percentage of $GFAP^+$ cells. Cell counts of at least 5 individual cultures were averaged to obtain an expression profile of the cell isolation cycle (n represents a biological sample). Finally, data of 5 independent biological replicates were used (total n = 5).

2.2.3.2 Quantification of cell morphology of neonatal astrocytes in vitro

To analyze the cell morphology of neonatal astrocytes, samples of individual GFP-positive astrocyte cultures were plated onto PLO/laminin-coated glass coverslips (diameter: 15 mm; Menzel GmbH) after Ara-C treatment (passage 2) and allowed to recover for 2 days. Afterwards cells were fixed, immunocytochemically stained with goat anti-GFP (1:1,000; Rockland) and rabbit anti-GFAP (1:1,000; Dako) and mounted onto microscopic glass slides with Fluoromount-G.

Immunolabeling was visualized using epifluorescence illumination with a confocal laser scanning microscope (Olympus FluoView1000 BX61; Olympus). Images were taken at 20x magnification, constant laser/ detector settings, and identical digital resolution (1024 x 1024 pixel). Cell morphology was only examined from $GFAP^+$ cells as these cells were considered to be part of the astroglial lineage. Since GFAP is not expressed in the entire soma of astrocytes, whereas the cytosolic GFP is expressed in the soma and in all processes, GFP immunolabeling was used to analyze the cell morphology of $GFAP^+$ cells.

Prior to analysis, 4 cell morphology categories were defined (**FIG 3**): GFAP-expressing cells with a longitudinal or triangle cell shape were defined as **(1) bi-/tripolar**, roundish $GFAP^+$ cells with no or only a few short processes and a cell area < 100 μm^2 were defined as **(2) small fibrous,** roundish $GFAP^+$ cells with no or only a few short processes and a cell area > 100 μm^2 were defined as **(3) large fibrous**, and star-shaped process-bearing $GFAP^+$ cells were defined as **(4) stellate**. The number of cells per category were counted and expressed as a percentage of $GFAP^+$ cells. Data of at least 5 individual cultures were averaged to obtain a morphological profile of each cell isolation cycle (n represents a biological sample). Finally, data of 5 independent biological replicates were averaged (total n = 5).

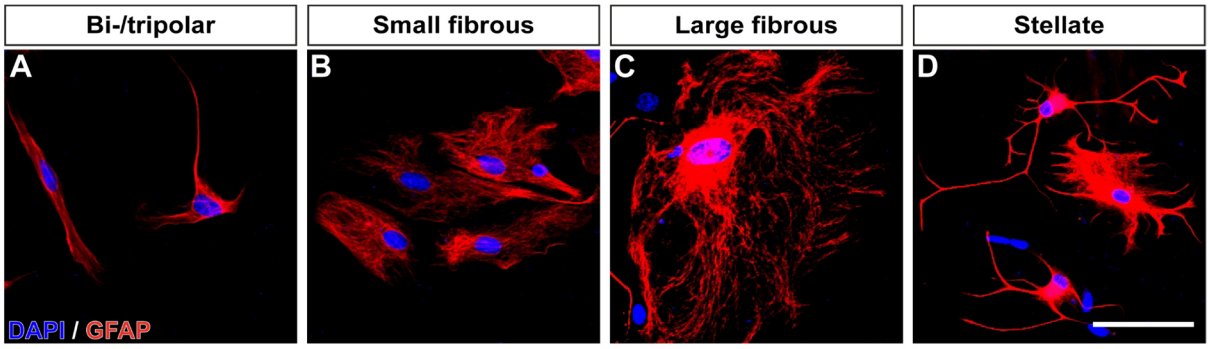

Figure 3: Astrocyte morphology categories *in vitro*. Immature astrocytes were isolated either from the cortex or spinal cord of neonatal Fischer-344 rats and their cell morphology categorized as bi-/tripolar (**A**), small fibrous (**B**), large fibrous (**C**), or stellate (**D**). Scale bar in **D**: 25 µm.

2.2.3.3 Quantification of neurite outgrowth on surface-coated alginate-based hydrogels in vitro

After isolation, DRG neurons were plated onto non-coated, PLO or PLO/laminin-coated slices of alginate-based hydrogels. Neurons were allowed to grow for 48 h before fixation with 4% PFA/0.1 M PB. Immunolabeling was visualized using epifluorescent illumination with a fluorescent microscope (Olympus BX53; Olympus). Images of each hydrogel slice were taken at 10x magnification with a digital camera (Olympus XC30; Olympus) attached to the microscope in a randomly selected field of 1 mm^2. Neurite growth was assessed by measuring the longest neurite from each βIII-tubulin-labeled DRG neuron using the NeuronJ plug-in for ImageJ.

2.2.4 Animal experiments

All *in vivo*-studies were performed in accordance with the European Union Directive (EU/2010/63) as well as National and Institutional guidelines and approved by the local authorities (Regierungspräsidium Karlsruhe). A total of 92 adult female *Fischer-344* rats (wildtype or stable GFP-transgenic,10 -12 weeks, > 150 g) was used in this study. A detailed summary of all animal experiments is depicted in **Suppl. Tab. 1**. All animal experiments were carried out by experienced staff of the Laboratory for Neuroregeneration of the Spinal Cord Injury Center of the Heidelberg University Hospital.

2.2.4.1 Spinal cord injury

A total of 80 animals underwent a unilateral spinal cord hemisection lesion at cervical level C5/6 combined with immediate implantation of a alginate-based anisotropic capillary hydrogel (2 mm in length, 2 mm in height, 1.3 mm in width) directly into the lesion cavity as previously described (Gunther, Gunther et al. 2015, Gunther, Weidner et al. 2015, Liu, Sandner et al. 2017).

Animals were deeply anesthetized via an i.p. injection with a mixture of ketamine (62.5 mg/kg), xylazine (3.175 mg/kg), and acepromazine (0.625 mg/kg) in sterile 0.9% saline (final conc. 2.5 ml/kg). For surgery, the surgical area shaved and sterilized with Braunol®. Following a skin incision, the spinal column was exposed and a laminectomy was performed at cervical level C5/6 using a micro-rongeur (Fine Science Tools). A rostrocaudal incision along the spinal midline was made into the dura with a scalpel and the spinal cord was exposed. For lesioning, the dura incision was spread and a block of spinal cord tissue (approx. 2 mm in length) was carefully removed unilaterally using bent microscissors (Fine Science Tools) and microaspiration under a surgical microscope (Olympus SZ51; Olympus Life Sciences). The resulting lesion cavity was washed once with sterile Ringer solution to remove blood and tissue debris. Hydrogels were directly implanted into the lesion cavity with their channels in rostrocaudal direction using thin blunt forceps (Fine Science Tools). Implant integrity and channel orientation were immediately checked with a surgical microscope (Olympus SZ51; Olympus Life Sciences).

After hydrogel implantation, the dura was covered with a thin dried agarose film (1% UltraPure™ agarose in sterile dH_2O; Life Technologies) and sealed with tissue glue (2 µl fibrinogen (100 mg/ml) + 2 µl thrombin (400 U/ml); both Sigma Aldrich). Paravertebral muscle layers were readapted, sutured and the skin stapled. Each animal received a subcutaneous injection of 1 ml Ringer solution to compensate for surgery-related dehydration. After surgery, animals were placed back into their home cages with free access to water and food.

Postoperatively, all rats were subcutaneously injected with burphrenophin (0.03 mg/kg in sterile 0.9% saline; Reckitt Benckiser) to ameliorate acute pain and with ampicillin (50 mg/kg in sterile 0.9% saline; Ratiopharm) to prevent wound infection for the first 2 days after surgery. If animals still showed signs of acute pain, Carprofen (5 mg/kg in sterile 0.9% saline; Pfizer) was given once per day as needed. Skin staples were removed after 7 days when the wound was completely closed. To support recovery, animals were fed with a high caloric drink (Fresubin; Fresenius Kabi) up to 3x daily until their body weight stabilized.

2.2.4.1.1 Implantation of surface-coated alginate-based hydrogels

To examine the impact of surface coating of alginate-based hydrogels with peptides on implant integration and axonal growth, a total of 24 wildtype adult female Fischer-344 rats was used received a unilateral C5/6 hemisection lesion as described previously. In this study, alginate-based hydrogel implants fabricated with Sr^{2+} ions and had a corresponding channel diameter of 39.0 $\pm$ 1.6 µm. The implanted alginate-based hydrogels have dimensions of 2 mm in length, 2 mm in height and 1.3 mm in width and therefore entirely fill out the cavity of the hemisection lesion. One group of animals was implanted with alginate-based hydrogels surface coated prior to surgery with PLO and laminin (n = 10), uncoated hydrogels served as controls (n = 9). Animals were allowed to recover for 4 weeks and were euthanized afterwards by transcardial perfusion with 4% PFA/0.1 M PB (3 animals died immediately after SCI.

2.2.4.1.2 Implantation of astrocyte-seeded alginate-based hydrogels

A total of 18 adult female Fischer-344 rats underwent a unilateral spinal cord hemisection at cervical level C5/6. 10 animals received PLO/lam-coated alginate-based hydrogel implants (Sr^{2+}, channel diameter: 50.2 $\pm$ 2.1 µm) that were seeded with GFP-expressing astrocytes derived from cortices of P1 Fischer-344 rats, whereas 8 animals received non-seeded PLO/lam-coated hydrogels and served as controls. Briefly, a total of 200,000 cells (diluted in 1% glucose/0.1 M PB, 2 µl total volume) was soaked into the channels of the hydrogels immediately before implantation. Channels were inspected for dense cellular filling and the absence of air bubble under a surgical microscope (Olympus SZ51; Olympus Life Sciences). If the hydrogel channels were not densely filled with cells and/or contained air bubbles, the seeding procedure was repeated. Astrocyte-seeded hydrogels were then implanted into the SCI lesion cavity as described above with their channels oriented in the rostrocaudal direction (1 animal died immediately after SCI). Animals survived for 4 weeks and were afterwards euthanized via transcardial perfusion.

2.2.4.1.3 Implantation of astrocyte-seeded alginate-based hydrogels combined with caudal astrocyte co-transplantation

A total of 18 adult female Fischer-344 rats underwent a unilateral spinal cord hemisection at cervical level C5/6 and were implanted with PLO/lam-coated alginate-based hydrogels. In this study, alginate-based hydrogel implants fabricated with Zn^{2+} were used resulting in a channel diameter of 78.2 $\pm$ 1.7 µm. A total of 12 rats received hydrogel implants that were pre-seeded

with 200,000 GFP-expressing neonatal astrocytes whether derived from P1 cortices (n = 6) or P3 spinal cords (n = 6) of Fischer-344 rats; non-seeded PLO/lam-coated implants served as controls (n = 6; 1 died after surgery).

Animals that were implanted with astrocyte-seeded hydrogels additionally received an injection of GFP-expressing neonatal astrocytes from the same origin caudal to the hydrogel implant. After hydrogel implantation, animals were fixed in a stereotaxic frame (Kopf instruments) using ear fixation bars. The astrocytes were again diluted in 1% glucose/0.1 M PB (final concentration: 100,000 cells/µl) and injected into the spinal cord with the PicoSpritzer® II microinjector (General Valve) and pulled glass capillaries (inner diameter: 100 µm). A total of 1 µl cell solution (100,000 cells total) was slowly injected ipsilateral to the hemisection lesion (coordinates: 1 mm caudal to hydrogel implant, 0.5 mm lateral to spinal midline, 1.5 mm deep) into the uninjured caudal spinal cord parenchyma. The capillary was held in place for 2 minutes to prevent reflux out of the injection site. After cell injection, the rats were removed from the stereotaxic frame and their wound sutured and stapled. Animals were euthanized via transcardial perfusion 4 weeks after SCI.

2.2.4.1.4 Implantation of astrocyte-seeded alginate-based hydrogels combined with rostral and caudal astrocyte co-transplantation

A total of 22 adult female Fischer-344 rats was used and all animals received a unilateral hemisection injury at cervical level C5/6 followed by immediate implantation of non-seeded PLO/lam-coated hydrogel implants (Zn^{2+}, channel diameter: 88.6 $\pm$ 2.9 µm; controls; n = 6, 1 died after surgery) or hydrogel implants seeded with GFP-expressing neonatal astrocytes (200,000 cells total,2 µl in 1% glucose/0.1 M PB) derived either from P1 cortices (n = 8, 2 died after surgery) or P3 spinal cords (n = 8, 2 died after surgery) of *Fischer-344* rat pups. Again, animals that received astrocyte-seeded hydrogels were stereotaxically injected with GFP-expressing neonatal astrocytes from the same origin 1 mm caudal (coordinates: 1 mm caudal to hydrogel implant, 0.5 mm lateral to spinal midline, 1.5 mm deep) to the implantation site (100,000 cells total diluted in 1 µl 1% glucose/0.1 M PB) and additionally received a second cell injection of astrocytes rostral to the implantation site (100,000 cells total diluted in 1 µl 1% glucose/0.1 M PB; coordinates: 1 mm rostral to hydrogel implant, 0.5 mm lateral to spinal midline, 1.5 mm deep). All animals were sacrificed 8 weeks after SCI by transcardial perfusion.

2.2.4.2 Axonal tracing

Axonal tract tracing studies were performed on all SCI animals. Animals were deeply anesthetized (**see 2.2.4.1**) 7 days before transcardial perfusion. The rats were fixed in a stereotactical frame and a laminectomy was performed at cervical level C2 using micro-scissors and micro-rongeurs (Fine Science Tools). A total volume of 1 µl of 10 kDa biotinylated dextran-amine (BDA, 10% in sterile 0.9% saline; Sigma Aldrich) was injected ipsilateral to the SCI lesion (coordinates: 0.3 mm lateral to spinal midline, 1 mm deep) using the PICOSPRITZER® II microinjector. After tracer injection, the paravertebral muscle layers were sutured and the skin was stapled, the rats subsequentially received 1 ml Ringer solution (s.c.) to compensate for dehydration during surgery. Postoperatively, injections (s.c.) of burprenorphine (0.03 mg/kg, twice for 2 days) for pain relief and ampicillin (50 mg/kg) as an antibiotic were given.

2.2.4.3 Transplantation of neonatal astrocytes into the intact spinal cord

To phenotypically characterize isolated astrocytes derived from the cortex or the spinal cord of neonatal Fischer-344 rat pups (P1 and P3) *in vivo*, a total of 12 adult female Fischer-344 rats underwent a laminectomy at cervical level C5/6. Each animal received bilateral injections of astrocytes derived from P1 cortices or P3 spinal cords of neonatal Fischer-344 rats into the white matter of the C5 spinal cord (coordinates: 0.5 mm lateral of spinal midline, 1.5 mm deep). A total of 200,000 GFP-positive astrocytes was injected (100,000 cells per injection on each side, 1 µl per side) using a PICOSPRITZER®. After cell injections, muscle layers were readapted, skin stapled and the animals received s.c. injections of 1 ml Ringer solution. Pain medication and antibiotics were administered as described above. Animals were transcardially perfused after 2 or 4 weeks.

2.2.5 Tissue processing

All animals used in this study were euthanized at 2, 4 or 8 weeks after surgery depending upon the experiment. Animals received a lethal dose of a mixture of ketamine (62.5 mg/kg), xylazine (3.175 mg/kg) and acepromazine (0.625 mg/kg) diluted in sterile 0.9% saline intraperitoneally and were transcardially perfused with 0.9% saline and 4% PFA/0.1 M PB. The spinal cords and brains were carefully dissected in post-fixed for 1 h at RT in 4% PFA/0.1 M PB and subsequently cryoprotected for 2 days in 30% sucrose/0.1 M PB at 4°C. Afterwards, the cervical spinal cord was embedded in Tissue-Tek O.C.T.™ compound (Sakura) and serially cut into 30 µm thick horizontal sections using a Cryostat (Leica Biosystems). Tissue sections were directly

mounted onto glass slides (Menzel GmbH) with every 14th section on the same slide and stored at -80°C until further use.

2.2.6 Immunohistochemistry

Serial sections of the cervical spinal cord were used for immunohistochemical analysis. Tissue sections were thawed and dried for 30 mins at RT and encircled with liquid blocker. Samples were washed 3x for 20 mins each in 1x TBS and incubated for 2.5 h in 1x TBS +0.25% Triton-X 100 +5% dk serum at RT to permeabilize the tissue and to block unspecific antibody binding. All primary antibodies were diluted in 1x TBS +0.25% Triton-X 100 +5% dk serum incubated overnight at 4°C under humid conditions. Afterwards, tissue sections were rinsed 3 times in 1x TBS +1% dk serum for 20 mins each at RT. All secondary antibodies and DAPI were diluted in 1x TBS +1% dk serum and samples were incubated for 2.5 h at RT in the dark. Finally, samples were washed 3x in 1x TBS for 20 mins each, dried for 10 min at RT and sealed with Fluoromount-G.

To visualize the axonal tracer BDA, tissue sections were permeabilized blocked as described above. BDA was detected with Alexa Fluor® 594-conjugated Streptavidin (Jackson Immuno Research). Primary antibodies including Alexa Fluor®-594-conjugated Streptavidin were diluted in 1x TBS +0.25% Triton-X 100 +5% dk serum and samples were incubated for 48 h at 4°C in the dark. After 3 washing steps in 1x TBS +1% dk serum (20 min each), tissue sections were incubated with secondary antibodies, rinsed and cover-slipped as described above.

Vascularization of the SCI lesion site and the hydrogel implant was immunodetected using an antibody specific for the endothelial cell marker CD31/PECAM-1 (Cluster of Differentiation 31; R&D Systems). Tissue sections were thawed and briefly dried at RT, encircled with liquid blocker and blocked and permeabilized in 1x TBS +0.5% Triton-X 100 +5% dk serum overnight at 4°C under humid conditions. After blocking, samples were incubated with primary antibodies (in 1x TBS +0.5% Triton-X 100 +1% dk serum) overnight at 4°C under humid conditions followed by 3 washing steps in 1x TBS +1% dk serum for 30 mins each. Secondary antibodies were diluted in 1x TBS +1% dk serum overnight at 4°C under humid conditions in the dark. Finally, tissue sections were rinsed 3x in 1x TBS (20 mins each), briefly dried and cover-slipped with Fluoromount-G.

For tissue analysis, tissue sections of the cervical spinal cord including the lesion/implantation site (2 sections per animal, intersectional distance between individual sections was 200 µm) were used.

To characterize host cell infiltration, immunolabeling with mouse anti-GFAP (1:1,000; Merck Millipore) to identify astrocytes, rabbit anti-IbaI (Ionized calcium-binding adapter molecule 1, 1:500; Wako) to identify macrophages/microglia, mouse anti-p75-NTR (p75 neurotrophin receptor, 1:500; generated from 192 MB Hybridoma supernatant) to identify Schwann cells were performed in animals that received non-coated or PLO/lam-coated alginate-based hydrogel implants on serial horizontal section of the cervical spinal cord including the SCI lesion/implantation site.
The following secondary antibodies has been used: donkey anti-mouse Alexa Fluor®-488 for GFAP and p75-NTR, and donkey anti-rabbit Alexa Fluor®-594 for Iba I, respectively.

To visualize grafted GFP-transgenic neonatal astrocytes, tissue sections of animals that received astrocyte-seeded hydrogel implants whether in combination with or without cell injections into the surrounding spinal cord were labeled with anti-GFP (Green fluorescent protein, goat, 1:1,000; Rockland and rabbit, 1:1,000; Invitrogen) and anti-GFAP (mouse P, 1:1,000; Merck Millipore and rabbit, 1:1,000, Dako).
To phenotypically characterize the grafted astrocytes, immunolabeling with varying combinations of the following markers have been used: mouse anti-Vimentin (1:1,000, Merck Millipore) and mouse anti-Nestin (1:1,000,Merck Millipore) for stem cells/astrocyte precursors and astrocyte reactivity, goat anti-Sox2 (1:200; Santa Cruz Biotechnology) for proliferating stem cells and progenitors, rabbit anti-Sox9 (1:500, Abcam) for astrocyte progenitors, rabbit anti-Ki67 (1:500, Abcam) for proliferating cells as well as mouse anti-AQP4 (1:500, Sigma Aldrich), mouse anti-A2B5 (1:500, Abcam), rabbit anti-CX43 (Connexin 43, 1:500, Invitrogen), guinea pig anti-GLT1 (1:500, Merck Millipore), and mouse anti-S100ß (1:1,000; Sigma Aldrich) to label mature astrocyte subtypes.
To visualize immunolabeling the following secondary antibodies were used: donkey anti-goat Alexa Fluor®-488, donkey anti-rabbit Alexa Fluor®-488 (1:300, Life Technologies) for GFP, and donkey anti-goat/anti-mouse/anti-rabbit Alexa Fluor®-594 (1:300, Life Technologies) for GFAP, Nestin, Sox2, Sox9, Ki-67, AQP4, Aldh1L1, A2B5, CX43, GLT1 and S100ß. Donkey anti-mouse and donkey anti-rabbit Cy5® conjugates (1:500, Jackson Immuno Research) were used to detect GFAP in triple immunofluorescence stainings.

To evaluate axonal regrowth within the hydrogel implant after SCI, samples were immunolabeled with the neuronal marker mouse anti-βIII-tubulin (1:1,000; Promega). Descending serotonergic axons were labeled with rabbit anti-5-HT (5-Hydroxytryptamine, 1:2,000; Immunostar). Descending propriospinal axons were specifically traced via BDA injection 7 days prior to perfusion.

Axonal markers were visualized using donkey secondary antibodies conjugated to Alexa Fluor®-594 (1:300, Life Technologies) for βIII-tubulin and 5-HT and Alexa Fluor® 594-conjugated Streptavidin (1:500, Jackson Immuno Research) for BDA.

2.2.6.1 Quantification of host cell infiltration into alginate-based hydrogel implants

The spinal cords of all animals that received a hydrogel implant were immunohistochemically analyzed *post mortem*. Over the course of 4 weeks, host cells filled the lesion cavity as well and infiltrated the implants channels. Host cell infiltration was measured at the channel entries (100 µm) and central regions (500 µm) at a virtual line perpendicular to the rostrocaudal channel orientation by determining the number of channels that were densely filled with $DAPI^+$ nuclei of all hydrogel channels present on the tissue section. Channels that only contained single separated $DAPI^+$ nuclei were considered as non-cell filled. Host cells could migrate from the rostral as well as caudal host spinal cord into the hydrogel channels, hence, both areas were analyzed separately. Cellular filling was analyzed on 2 serial tissue sections per animal (intersectional space 210 µm) and afterwards averaged. Data were expressed as percentage of $DAPI^+$ channels of total hydrogel channels.

2.2.6.2 Quantification of astroglial and microglial responses

To measure the astroglial and microglial response to the implanted alginate-based hydrogel, immunolabeling density of the astrocyte-specific marker GFAP and microglia/macrophage-specific marker Iba I was analyzed. Immunolabeling for GFAP and Iba I was detected using epifluorescent illumination with a fluorescent microcope (Olympus BX53; Olympus Life Sciences) in 2 serial tissue sections for each animal that received either a non-coated or PLO/lam-coated hydrogel implant. Images were taken at 20x magnification with similar exposure time and resolution. Using ImageJ, a labeling threshold representing the labeling density on the uninjured contralateral side had been used to determine the labeling density of both markers on the injured side, rostrally and caudally to the implant. Data were expressed as percentage of positive labeling within the analyzed area for GFAP and Iba I.

2.2.6.3 Quantification of graft cell survival within alginate-based hydrogel implants

For each animal that received an astrocyte-seeded hydrogel implant, two serial tissue sections (intersectional space 210 µm) of the hydrogel implantation site were analyzed. Immunolabeling of GFP was detected using epifluorescent illumination with a fluorescence microscope (Olympus BX53; Olympus Life Sciences) and images captured using a XC30 camera (Olympus Life Sciences) with 10x magnification, similar exposure time and resolution. Afterwards, individual images were stitched together using the Cell^{P} imaging and processing software (Olympus Life Sciences) to gain an overview image of the entire hydrogel implant. Using ImageJ, channel filling with GFP-expressing grafted cells was analyzed separately at the channel entries (0 – 500 µm) and central regions (500 – 1000 µm) from both the rostral and caudal edge of the hydrogel implant. First, the area of all cell-filled (DAPI^{+} channels) in the different hydrogel areas was measured (total cell-filled area). Second, a labeling threshold minimizing background and reflecting the GFP labeling was set and the area of positive GFP area per channel was measured. Graft cell survival were expressed as percentage of GFP^{+} channel area from the total area of all cell-filled channels. Additionally, the percentage of GFP^{+} channels of all DAPI^{+} channels was determined.

2.2.6.4 Quantification of axonal growth within alginate-based hydrogel implants

For quantification of overall non-specific axonal growth, βIII-tubulin-labeled axons crossing virtual lines perpendicular to the rostrocaudal orientation of the hydrogel channels at 100 µm and 500 µm from the rostral and caudal hydrogel edge, respectively, were counted. Since axonal penetration of the hydrogel implant may have occurred independently on both sides of the implant, the rostral and caudal half of the implants were examined separately. For each animal, two serial tissue sections 210 µm apart, were analyzed. In none of the analyzed hydrogel implants was any axon could detected in a channel that did not contain cells (DAPI^{-} channel). Therefore, since cell filling is a prerequisite for axonal growth with the hydrogel channels, data were expressed as number of axons per DAPI^{+} channel (cell-filled channel).
Additionally, in animals that received astrocyte-seeded hydrogel implants, descending raphespinal axons were specifically labeled with an antibody for serotonin (5-HT) and descending propriospinal axons were labeled via injection of the anterograde tracer BDA and quantified at channel entries and central hydrogel regions.

To compensate varying numbers of channels per hydrogel implant, data of each axon labeling were again normalized to the entire implant area using the following equation:

$$N = \frac{\sum \text{axons}}{1{,}000{,}000 \times \text{section thickness [µm]} \times \sum \text{width of hydrogel at specific distance [µm]}}$$

2.2.6.5 Quantification of vascularization within alginate-based hydrogel implants

Along with infiltrating host cells, hydrogel implants were innervated by host-derived blood vessels. In animals that received either non-coated, PLO/lam-coated hydrogel implants or astrocyte-seeded implants without additional cell injections, endothelial cells and blood vessels were only qualitatively investigated using immunolabeling with rabbit anti-von Willebrand factor (1:1,000; Sigma Aldrich).

For animals that received astrocyte-seeded hydrogel implants combined with distal astrocyte injection, vascularization of the implant was quantified using immunolabeling of CD31. Two serial tissue sections (intersectional space 210 µm) per animal were analyzed. Immunolabeling was detected using epifluorescent illumination with a fluorescence microscope (Olympus BX53; Olympus Life Sciences) and images were taken with a XC30 camera (Olympus Life Sciences s) at 10x magnification with similar exposure time and resolution. Individual images were stitched using the Cell^{P} imaging and processing software (Olympus Life Sciences) and the resulting overview image analyzed with ImageJ. First, the total channel area of the hydrogel implant was measured. Second, a labeling threshold minimizing background and reflecting the CD31 labeling was set and the area of CD31-positive immunolabeling was measured. Data were expressed as percentage of positive CD31 area per channel.

2.2.6.6 Quantification of migration of caudally co-transplanted astrocytes

The spinal cords of animals that received astrocyte-seeded hydrogel implants and additionally a caudal astrocyte injection, were examined for the migratory behavior of the caudally grafted cells.

For each animal, 2 serial tissue sections (intersectional space 210 µm) were analyzed measuring the GFP labeling density in the caudal uninjured host spinal cord ipsilateral to the lesion. GFP immunolabeling was detected using epifluorescent illumination with a fluorescence microscope (Olympus BX53; Olympus Life Sciences) at 10x magnification with similar exposure

time and resolution. Images of the implantation site and the caudal host spinal cord were captured with a digital camera (XC30; Olympus Life Sciences). Individual images were stitched using the Cell^{P} software as stated above. Labeling density was measured with ImageJ by setting a threshold minimizing the background and accurately reflecting the GFP signal; the uninjured and therefore non-grafted contralateral side of the spinal cord served as a reference. The GFP labeling density was analyzed in 6 separate regions-of-interest (ROI, dimensions: 1300 µm in height, 500 µm in width) with the first ROI placed directly adjacent to the caudal hydrogel edge and the last one representing an area 3000 µm caudal to the implantation site. Data were expressed as percentage of positive GFP area per ROI.

2.2.6.7 Characterization of neonatal astrocytes in vivo

Immunolabeling was visualized using epifluorescence illumination with a confocal laser-scanning microscope with attached photon detectors (Olympus BX61; Olympus Life Sciences). Images of the transplantation site were taken at 20x magnification with the same exposure time per marker, resolution, optical aperture, and filter cube settings. Marker expression of the grafted neonatal astrocytes was quantified in confocal z stacks (30 µm depth, 1 µm/slice) of at least 5 tissue sections (intersection spacing 200 µm) per animal. The total number of grafted cells in a randomly selected field of 1 mm^2 was determined (number of GFP$^+$ nuclei) and the number of positive cells for the different markers counted using the CellCounter plug-in for ImageJ. The incidence of immunopositive cells is expressed as percentage of the total number of GFP$^+$/GFAP$^+$ cells per each tissue section.

2.2.6.8 Statistical analysis

In vitro results of cell attachment and axonal growth on surface-coated alginate-based hydrogels were analyzed by an ordinary One-Way analysis of variance (ANOVA) followed by Tukey's *post hoc* test to reveal overall group differences. Molecular marker expression of neonatal astrocytes *in vitro* were analyzed by an unpaired Student's t-test comparing different developmental stages (P1 or P3) of cells of the same tissue origin (cortex or spinal cord), and Two-Way ANOVA followed by Sidak's *post hoc* to reveal overall group differences between cortex- and spinal cord-derived astrocytes. Astrocyte morphological categories were analyzed via Two-Way ANOVA followed by Sidak's *post hoc* to reveal group differences between cells isolated at different developmental time points and tissues. Marker expression profiles of neonatal astrocytes injected into the intact spinal cord were compared by Two-Way ANOVA followed by Sidak's *post hoc* testing.

Cell filling ($DAPI^+$ channels) and axonal growth (βIII-tubulin and 5-HT) within hydrogel implants *in vivo* were analyzed via repeated measures Two-Way ANOVA to test for overall group differences at different distances from the hydrogel edges between uncoated and PLO/laminin-coated hydrogel implants with Sidak's *post hoc* test. The host immune response (GFAP and Iba I) was analyzed with Two-Way ANOVA followed by Sidak's *post hoc* analysis.
Similarly, after astrocyte seeding of the implants, results of cell filling and axonal growth were analyzed with repeated measures Two-Way ANOVA to reveal group differences between at different distances from the hydrogel edges between non-seeded control hydrogels and astrocyte-seeded samples. Astrocyte filling of the hydrogel implants was compared at different distances via repeated measures Two-Way ANOVA followed by Sidak's *post hoc* test. Astrocyte colonization at the hydrogel entries (0 – 500 µm) and the central areas (500 – 1000 µm) was compared by an unpaired Student's t-test.

In animals that received either non-seeded implants or hydrogel implants seeded with neonatal cortex- or spinal cord-derived astrocytes with additional astrocyte grafts into the surrounding host spinal cord, cell filling ($DAPI^+$ channels) as well as axonal growth (βIII-tubulin, 5-HT, BDA) were analyzed via repeated measures Two-Way ANOVA followed by Tukey's *post hoc test* to test for overall group differences at different distances from the hydrogel edges. Astrocyte filling and colonization were compared between hydrogel implants seeded with either cortex- or spinal cord-derived astrocytes using repeated measures Two-Way ANOVA followed by Sidak's *post hoc* analysis. Results of blood vessel ingrowth into hydrogel implants were compared between non-seeded controls and astrocyte-seeded implants by ordinary One-Way ANOVA with Tukey's *post hoc* test. In animals that received astrocyte-seeded hydrogel implants and only a caudal astrocyte graft, molecular marker expression and migration of the caudally injected astrocytes was analyzed by repeated measures Two-Way ANOVA followed by Sidak's *post hoc* test.

Detailed descriptions of each statistical analysis are provided in the supplement and noted accordingly in the text or figure legends. Data are expressed as mean ± standard error of the mean (SEM) unless otherwise noted. All statistical analysis was performed using Prism 8 (GraphPad Software). A significance criterion of $p < 0.05$ was used.

3 Results

3.1 Impact of surface coating on the biocompatibility of alginate-based hydrogels in vitro and in vivo

Previously, we and others have shown that the implantation of a physical biomaterial scaffold into acute SCI lesion sites is feasible (Pawar, Mueller et al. 2011, Gunther, Gunther et al. 2015), even in combination with co-transplantation of cells (Gunther, Weidner et al. 2015, Liu, Sandner et al. 2017). Nevertheless, significant hurdles for such tissue engineering approaches persist. On the one hand, the biocompatibility and integration of the implant itself requires further enhancement. On the other hand, the grafted cells struggle to survive in the harsh SCI lesion environment. To overcome these limitations, we aimed at cellular and physical modification of alginate-based anisotropic capillary hydrogels to improve their biocompatibility and thereby promote host-graft interactions as well as axonal growth through the hydrogel implant.

The experiments in this first section (**3.1**) were conducted together with Dr. rer. nat. Manuel Ingo Günther in the course of my Master's thesis project entitled "Surface modified hydrogels for stem cell therapy after spinal cord injury" and his Ph.D. project entitled "Biomaterial-based approaches for guided axon regeneration in the injured spinal cord". A manuscript written by myself, including these results along with my own work in the second sections (**3.2**), was recently published in the journal of Tissue Engineering Part A (Schackel, Kumar et al. 2019).

3.1.1 Cell adhesion and axonal growth on surface-coated alginate-based hydrogels in vitro

Alginate is a naturally occurring heteromeric polymer made of interconnected polysaccharide chains of α-L-guluronate and β-D-mannuronate. Under physiological conditions, the alginate is negatively charged due to free carboxyl groups of the polymer chains. Hence, cell adhesion, viability as well as axonal growth on non-functionalized alginate substrates remain limited (Dillon, Yu et al. 1998). Although we and others have shown that alginate-based hydrogel implants can facilitate axonal growth, the achieved axonal growth through the hydrogel implant was attributed to infiltrated host cells or co-transplanted trophic cells colonizing within the implants consequently serving as a growth substrate for penetrating axons rather than to the axonal growth-promoting effect of the hydrogel itself (Schackel, Kumar et al. 2019).

To improve cell adhesion to and viability on alginate-based hydrogels, we first sought to alter the negative surface charge of the hydrogel matrix to create a biologically permissive micro-environment. Therefore, slices of alginate-based hydrogels were coated with the positively charged poly-peptide poly-L-ornithine (PLO) to mask the negative surface charge of the alginate backbone and subsequently with the extracellular matrix component laminin (lam) to create a bioactive signal on the hydrogel surface.

To examine the feasibility of alginate-based hydrogels as growth substrates for cells *in vitro*, primary astrocytes derived from the cortices of neonatal Fischer-344 rats were cultured for 7 days, as well as DRG neurons obtained from adult Fischer-344 rats, on alginate-based hydrogels and fixed after 48 h. Afterwards, the impact of surface coating on cell survival and attachment was analyzed (**FIG 4**). Neonatal cortex-derived astrocytes attached to the surface of alginate-based hydrogels of all tested conditions (**FIG 4A – C**). Nevertheless, coating with either the polypeptide PLO alone (**FIG 4B**) or in combination with laminin (**FIG 4C**) induced a bi-/tripolar and process-bearing morphology with large cell bodies, whereas small cells showed a petite roundish morphology on uncoated control hydrogels (**FIG 4A**). Similarly, DRG neurons attached to hydrogels of all tested conditions, however neurons were detected only sporadically on non-coated hydrogels but more prominently on PLO- (**FIG 4F**) on PLO/laminin-coated hydrogels (**FIG 4G**). Independent of cell identity, surface-coating massively increased cell attachment and thereby survival of the plated cells compared with uncoated hydrogels (**FIG 4D, H**; $p < 0.0001$). Surprisingly, the addition of laminin did not further quantitatively increase cell attachment but induced a differentiated cell morphology in GFAP-expressing astrocytes and DRG neurons.

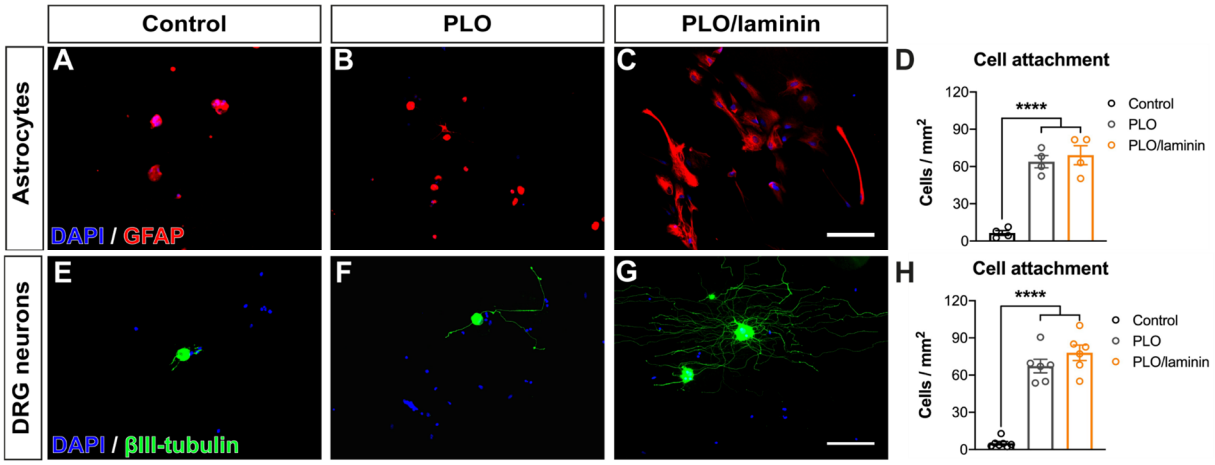

Figure 4: Surface coating of alginate-based hydrogels enhances cell adhesion and viability of neural cells. (A – D) Neonatal astrocytes derived from the cortex of P1 Fischer-344 rats (GFAP, red) and **(E – H)** DRG neurons (βIII-tubulin, green) isolated from adult Fischer-344 rats were seeded on uncoated (**A, E**), PLO-coated (**B, F**), or PLO/laminin-coated alginate-based hydrogels (**C, D**). On uncoated hydrogels, only a few cells attached to the hydrogel surface and astrocytes (**A**) as well as DRG neurons (**E**) showed roundish cell morphology. Both PLO- (**B, F**) and PLO/laminin-coating (**C, G**) massively improved cell attachment and induced a differentiated cell morphology in both cell types. (**D, H**) Quantification of attached cells revealed significantly higher cell numbers on surface-coated alginate-based hydrogels compared with uncoated control hydrogels (One-Way ANOVA $p < 0.0001$, with Tukey's *post hoc* ****$p < 0.0001$). Scale bar in **C, G**: 100 µm. Adapted from (Schackel, Kumar et al. 2019)

Since alginate-based hydrogels should serve as permissive guidance structures for regenerating axons within acute SCI lesion sites, the effect of surface coating on axonal growth was examined *in vitro* by plating adult DRG neurons onto either uncoated, PLO- or PLO/laminin-coated hydrogels and measuring the longest neurite after 48 h (**FIG 5**). Similar to cell attachment results, surface coating with either PLO or PLO together with laminin significantly affected neurite outgrowth of adult DRG neurons. Only a few DRG neurons developed neurites on uncoated hydrogels (**FIG 5A**). In contrast, coating with PLO increased neurite length (**FIG 5B, D**), while the addition of laminin resulted in more than a 10-fold increase in neurite length (**FIG 5C, D**; ***$p < 0.001$) in comparison to uncoated controls and an additional 3-fold increase when compared with PLO-coated hydrogels (***$p < 0.001$). Noteworthy, DRG neurons showed only single unbranched neurites on control and PLO-coated hydrogels, whereas DRG neurons on PLO/laminin-coated hydrogels developed multi-branched neurites (**FIG 5A – C**).

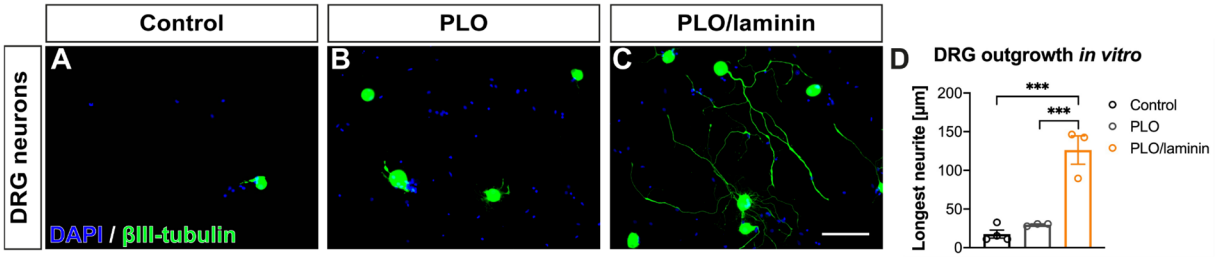

Figure 5: Surface coating of alginate-based hydrogels increases neurite outgrowth of adult DRG neurons. (**A – C**) Adult DRG neurons (βIII-tubulin, green) attached to the surface of all tested hydrogel conditions. (**D**) Quantification of the longest neurite per βIII-tubulin-labeled neuron revealed significantly longer neurites on PLO- and PLO/laminin-coated hydrogels (One-Way ANOVA $p < 0.001$, with Tukey's *post hoc* ***$p < 0.001$). Scale bar in **C**: 100 µm. Adapted from (Schackel, Kumar et al. 2019)

3.1.2 *Implantation of surface-coated alginate-based hydrogels into acute spinal cord injury sites*

The previous *in vitro* experiments underlined the feasibility of surface coating of alginate-based hydrogels with the synthetic polypeptide PLO and the biologically active protein laminin. To examine whether surface coating with PLO and laminin shows similar effects on neural cells and axonal growth *in vivo*, hydrogel cuboids (dimensions: 2 mm in height, 2 mm in length, 1.3 mm in width; fabricated with Sr^{2+} ions, channel diameter: 39.0 ± 1.6 µm) were coated with PLO (1 mg/ml) and laminin (10 µg/ml) and implanted into the lesion cavity of a unilateral hemisection SCI at cervical level 5/6 in adult female Fischer-344 rats (**FIG 6**). Uncoated hydrogel implants served as controls.

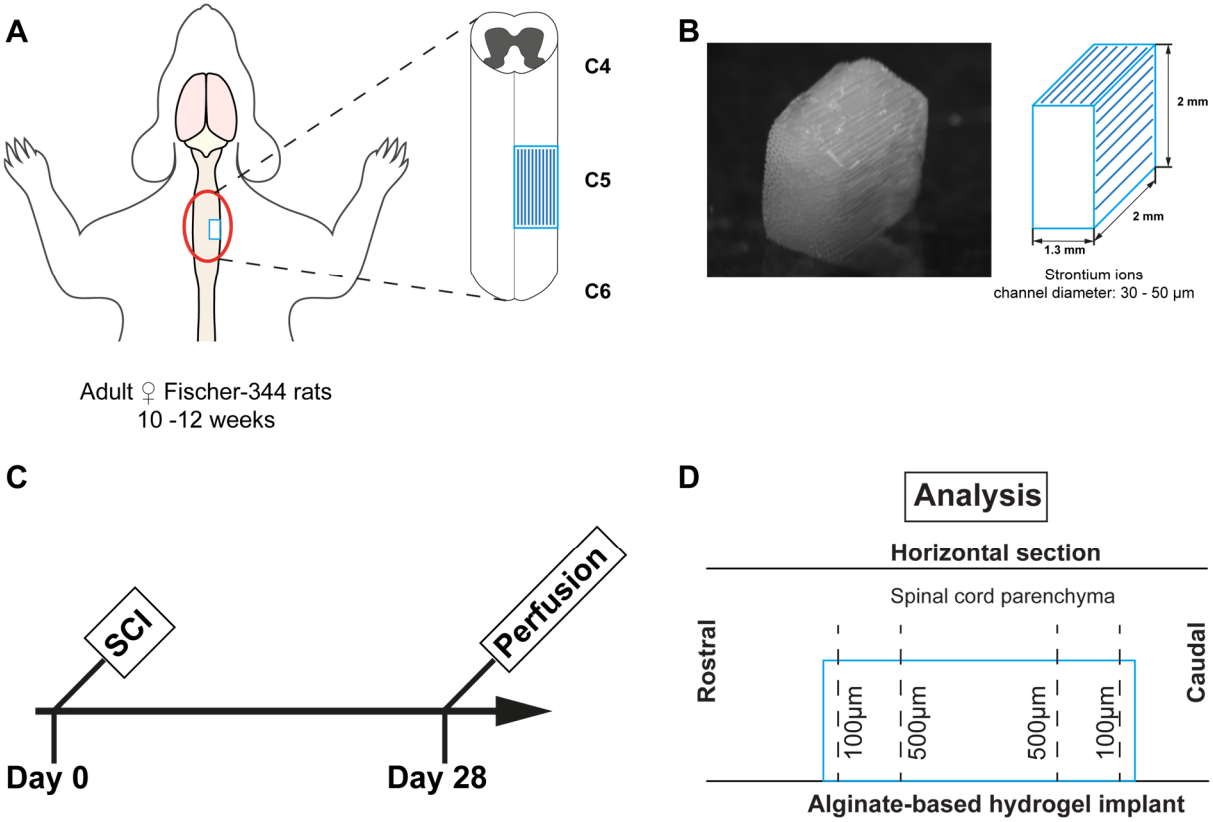

Figure 6: Experimental setup. (**A**) A total of 24 adult female Fischer-344 rats (wildtype) underwent a unilateral hemisection at cervical level C5. (**B**) Alginate-based hydrogel cuboids (dimensions: 2 mm in length, 2 mm in height, 1.3 mm in width) fabricated with Sr^{2+} (channel diameter: 39.0 ± 1.6 µm) were used as implants. (**C**) Animals were allowed to recover for 4 weeks and finally transcardially perfused. (**D**) Tissue sections (horizontal, 30 µm thick) of the hydrogel implantation site were immunohistochemically analyzed. Host cell infiltration, cell filling and axonal growth were examined in the rostral and caudal hydrogel half at 100 µm and 500 µm from the rostral or caudal hydrogel edge, respectively (control: n = 9, PLO/laminin: n = 10; 3 animals died after surgery; 2 were excluded from analysis **see Suppl. table 1**).

Four weeks after injury, the cervical spinal cord was immunohistochemically analyzed to assess structural integrity and cell filling of the hydrogel implant (**FIG 7**). Independent of coating conditions, the three-dimensional (3D) channel structure remained intact and in a rostrocaudal orientation. Implants of both groups were in close contact with the surrounding spinal parenchyma and integrated into the lesion cavity tightly without cavitation, although a small area of irregularly organized hypercellularity was present around the hydrogel implants. The ruptures on the right side of the hydrogel implants are most likely related to tissue processing artifacts (**FIG 7A, B**). Host cells (indicated by DAPI-labeled nuclei) infiltrated the channels of both, uncoated and coated hydrogel implants with significantly greater host cell infiltration into PLO/laminin-coated hydrogels (Two-Way ANOVA for overall group differences: $p < 0.0001$) both at channel entries (control: 58.58 ± 4.89% $DAPI^+$ channels vs. PLO/laminin: 83.4 ± 4.98% $DAPI^+$ channels) and central areas of the hydrogel (**FIG 7C**; control: 40.73 ± 5.88% $DAPI^+$ channels vs. PLO/laminin: 68.23 ± 7.23% $DAPI^+$ channels; Two-Way ANOVA for distance: $p < 0.01$). Noteworthy, astrocytes were present at the host/graft interface but surprisingly did not enter the hydrogel channels (**FIG 7D**).

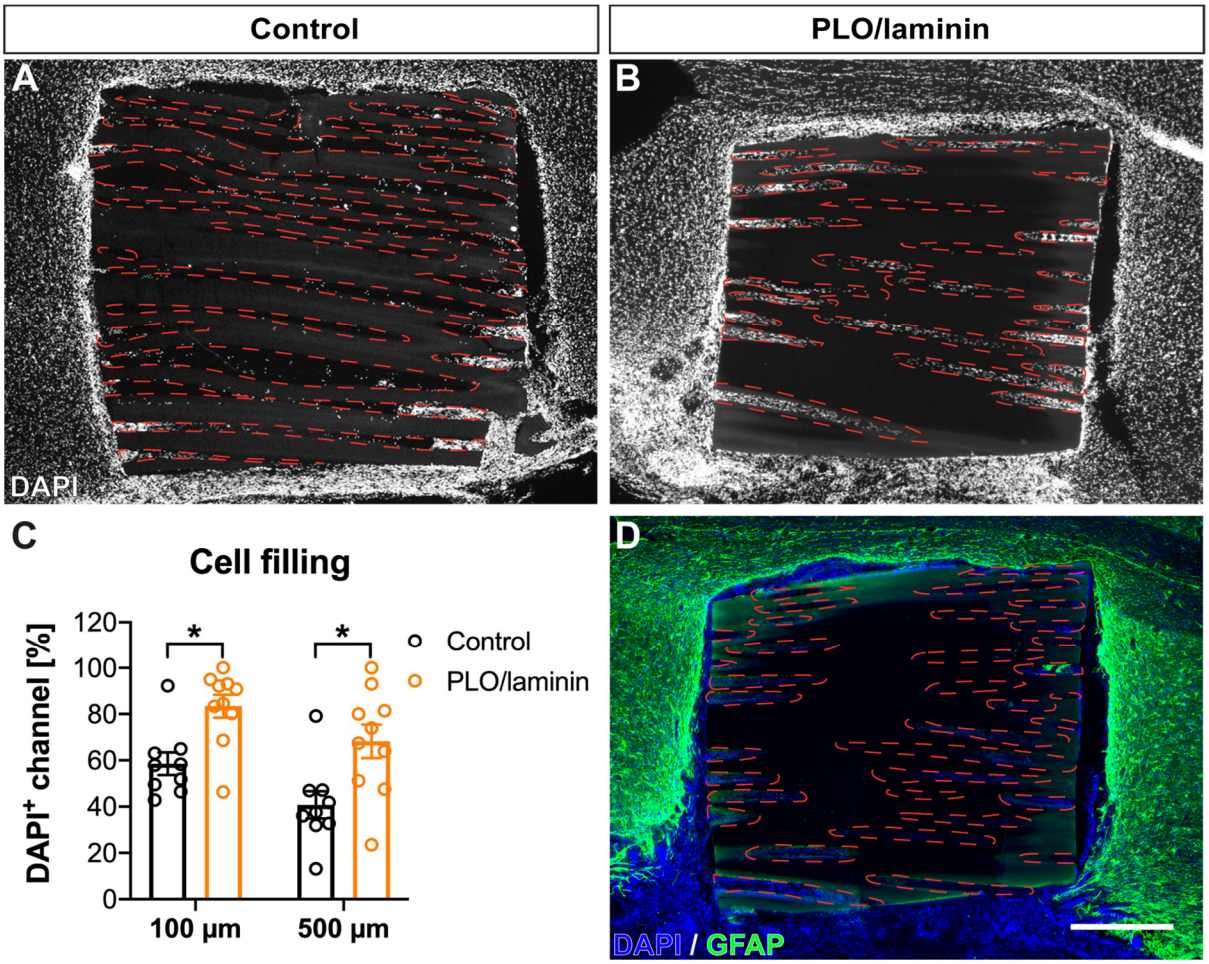

Figure 7: Surface coating improves host cell infiltration into alginate-based hydrogel implants 4 weeks after implantation. (**A**) Uncoated control hydrogels as well as (**B**) PLO/laminin-coated implants integrated tightly into the SCI lesion cavity. Implants of both groups showed no signs of degradation or structural collapse. Independent of surface coating, the implants channels (indicated by dashed lines) were infiltrated with host cells ($DAPI^+$ nuclei, white). Rostral is to the left, medial to the top, and caudal to the right. (**C**) Quantification of cell-filled hydrogel channels ($DAPI^+$ channels) revealed a significantly greater host cell infiltration and colonization of PLO/laminin-coated implants compared to uncoated control hydrogels (Two-Way ANOVA $p < 0.0001$, followed by Sidak's *post hoc* $^*p < 0.05$) both at channel entries (100 µm) and central regions (500 µm) of the implants (Two-Way ANOVA $p < 0.01$). (**D**) Host astrocytes (GFAP, green) were found at the host/graft interface surrounding the implantation site but were absent from the hydrogel channels (Control, n = 9; PLO/laminin, n = 10). Scale bar in **D**: 500 µm. Adapted from (Schackel, Kumar et al. 2019)

The higher host cell infiltration into PLO/laminin-coated hydrogel implants might be due to a stronger host immune response, thereby, hypercellularity at the lesion site. To assess the host immune response, immunoreactivity for the astrocyte marker GFAP and the microglia/macrophage marker Iba I was analyzed (**FIG 8**). Immunolabeling showed only sporadically $GFAP^+$ or

Iba I$^+$ cells on the uninjured contralateral side of the spinal cord (**FIG 8A, D**). In contrast, a strong upregulation of both markers was found directly adjacent to the hydrogel implantation site in the control (**FIG 8B, E**) as well as in the PLO/laminin-coated group (**FIG 8C, F**). By quantification of the GFAP labeling intensity, a significant upregulation of GFAP immunoreactivity directly at the implantation site in comparison to the uninjured contralateral spinal cord side in the same animal was found (**FIG 8G**; Two-Way ANOVA, $p < 0.0001$, followed by Tukey's *post hoc* ****$p < 0.0001$). More importantly, no difference between control and PLO/laminin-coated hydrogels was found (Two-Way ANOVA $p = 0.68$ for GFAP). Analysis of Iba I immunolabeling revealed similar results (**FIG 8H**; Two-Way ANOVA for group differences: $p = 0.11$, for location: $p < 0.0001$ followed by Tukey's *post hoc* ***$p < 0.001$, ****$p < 0.0001$). The host immune response, therefore, was not additionally enhanced by surface coating of the hydrogel implants.

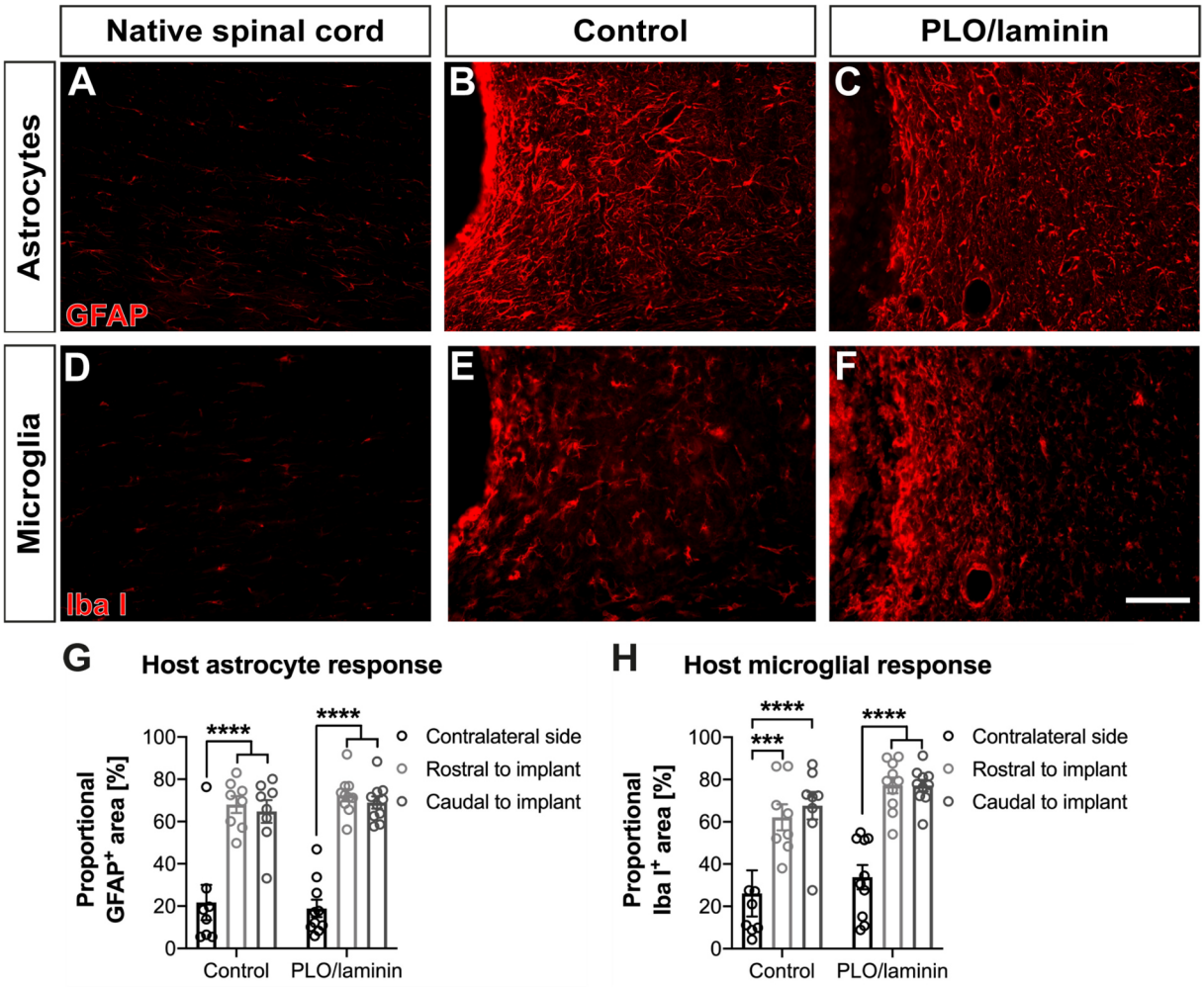

Figure 8: Surface coating of alginate-based hydrogel implants does not affect the host immune response. (**A – C**) Immunolabeling for astrocytes (GFAP) and (**D – F**) microglia/macrophages (Iba I) indicated an upregulation for both markers at the implantation site compared to the uninjured contralateral spinal cord in the same animal (**A, D**). (**G**) Quantification of labeling density revealed no significant difference for GFAP immunoreactivity between coated or uncoated hydrogel implants (Two-Way ANOVA for group differences: $p = 0.68$; for location: $p < 0.0001$, followed by Tukey's *post hoc* ****$p < 0.0001$). (**H**) Similarly, no difference in Iba I labeling density was found between controls and coated hydrogel implants (Two-Way ANOVA for group differences: $p = 0.11$; for location: $p < 0.0001$, with Tukey's *post hoc* ***$p < 0.001$, ****$p < 0.0001$; Control, n = 8; PLO/laminin, n = 10). Scale bar in **F**: 100 µm. Adapted from (Schackel, Kumar et al. 2019)

Consequently, the observed greater host cell infiltration into PLO/laminin-coated hydrogel channels was not exclusively based on infiltrating host immune cells such as astrocytes or microglia/macrophages. To further elucidate the identity of the infiltrated host cells, further immunohistological analysis was performed (**FIG 9**). The channel lumen of uncoated and PLO/laminin-coated hydrogel implants were filled predominantly with Iba I-expressing microglia/macrophages and p75-NTR-labeled Schwann cells (**FIG 9C, D**), whereas astrocytes were not found within the hydrogel channels. Surface coating did not effect on the type of infiltrated host cells.

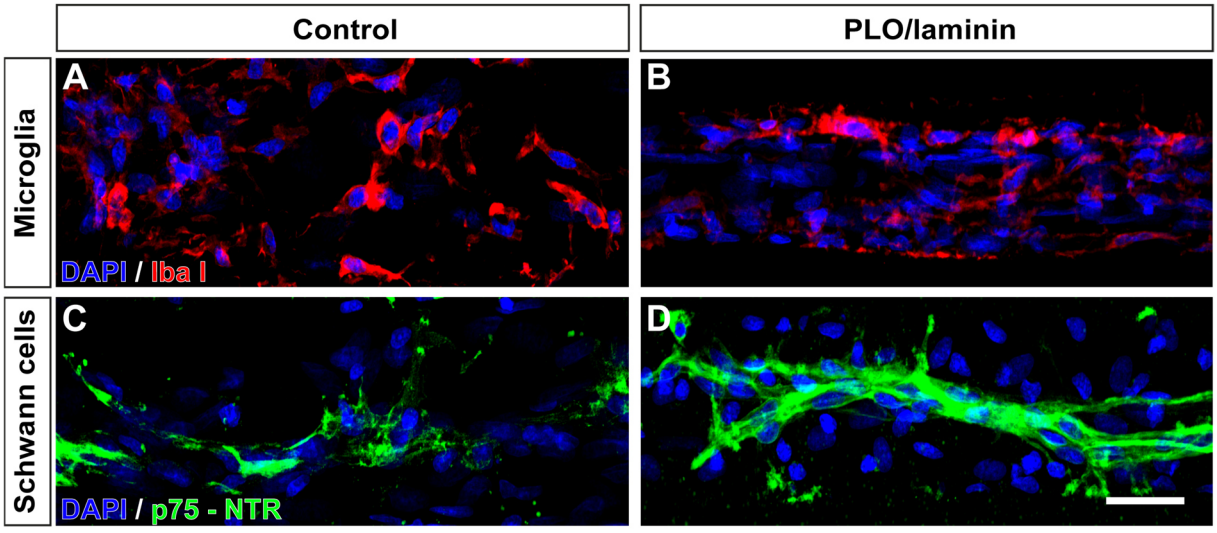

Figure 9: Microglia and Schwann cells predominantly fill the channels of alginate-based hydrogel implants. After 4 weeks, the channels of uncoated and PLO/laminin-coated hydrogel implants were predominantly filled with (**A, B**) microglia/macrophages (Iba I, red) and with (**C, D**) Schwann cells (p75-NTR, green). Scale bar in **D**: 30 µm. Adapted from (Schackel, Kumar et al. 2019)

3.1.3 Axonal growth into surface-coated alginate-based hydrogel implants

Besides integration and host cell infiltration, regrowth of spinal axons was examined within the hydrogel implants 4 weeks after SCI. Hence, tissue sections of animals that received either uncoated alginate-based hydrogel implant or implants that were previously coated with PLO and laminin were immunolabeled for the neuronal marker βIII-tubulin and the labeled axons were quantified at the channel entries (100 µm) and the central area (500 µm) of each hydrogel implant (**FIG 10**). Axons entered and extended within the channel of control as well as PLO/laminin-coated hydrogel implants (**FIG 10A, B**). Notably, independent of surface coating, axons were only found in channels that contained infiltrated host cells (defined as $DAPI^+$ channels). In surface coated hydrogels, axons were preferentially organized in thin axon bundles, whereas only single axons could be found in control hydrogels. This perhaps contributes to an underestimation of the axon numbers in surface coated alginate-based hydrogel implants. Quantification of βIII-tubulin-labeled axons showed comparable numbers of axons per cell-filled channels at the channel entries and central hydrogel (**FIG 10C**). In both groups, a significant reduction in axon numbers towards the center of the implants was observed (Two-Way ANOVA for distance: $p < 0.0001$, with Sidak's *post hoc* $^{***}p < 0.001$). Since the number of channels varies between samples, the number of axons per channel was normalized to the area of each individual hydrogel implant (**FIG 10D**). Importantly, more axons entered the channels of PLO/laminin-coated hydrogels from the rostral ($^*p < 0.05$) and caudal host spinal cord compared to uncoated controls. The total number of axons, however, significantly decreased towards the center of the implants in both groups (Two-Way ANOVA for distance: $p < 0.0001$, with Sidak's *post hoc* $^{###}p < 0.001$ for PLO/laminin, $^{+}p < 0.05$ for controls) which is consistent with the greater cell filling at the channel entries compared with the hydrogel center (**FIG 7**).

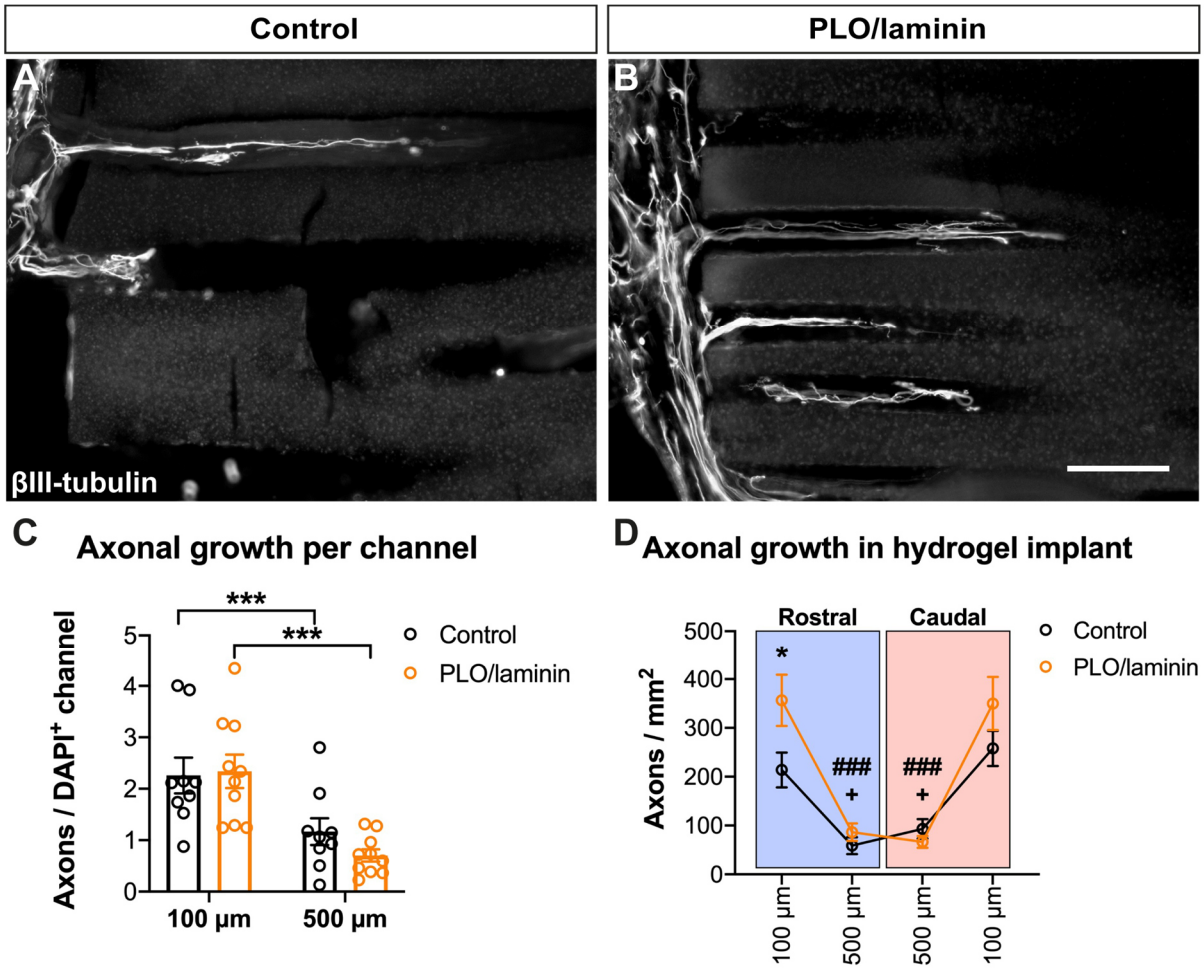

Figure 10: Axonal growth is enhanced in surface-coated alginate-based hydrogel implants after SCI. (**A, B**) After 4 weeks, βIII-tubulin-labeled axons (white) were found in channels of uncoated and PLO/laminin-coated hydrogels. Rostral is to the left, medial to the top, and caudal to the right. (**C**) Quantification of axon numbers per cell-filled channels (DAPI⁺ channel) at the channel entries (100 µm) or the central area of the implant (500 µm) revealed no significant difference between coated and uncoated implants (Two-Way ANOVA $p = 0.49$) but a decline of axons per channel towards the hydrogel center (Two-Way ANOVA $p < 0.0001$, with Sidak's *post hoc* ***$p < 0.001$). (**D**) Normalization to the entire hydrogel area revealed a significantly greater number of axons entering the channels in PLO/laminin-coated hydrogel implants compared to uncoated hydrogels (Two-Way ANOVA $p < 0.05$, with Sidak's *post hoc* *$p < 0.05$ at Rostral 100 µm). The number of axons significantly declined towards the center of the implant in both groups (Two-Way ANOVA $p < 0.0001$, followed by Sidak's *post hoc* ###$p < 0.001$ channel entries at 100 µm vs. central hydrogel at 500 µm for PLO/laminin; ⁺$p < 0.05$ comparing channel entries at 100 µm vs. central hydrogel at 500 µm for control; Control, n = 9; PLO/laminin, n = 10). The red and blue boxes indicate the rostral and caudal halves of the hydrogel implant, respectively. Scale bar in **B**: 100 µm. Adapted from (Schackel, Kumar et al. 2019)

Taken together, coating with the poly-peptide poly-L-ornithine and the ECM component laminin is applicable to the surface of alginate-based hydrogels. It significantly improves cell attachment, cell viability and axonal growth *in vitro* and host cell infiltration/colonization as well as regrowth of injured spinal axons *in vivo*. Although hydrogel implantation leads to an upregulation of GFAP and Iba I directly at the lesion site, no signs of excessive (neuro-)inflammation, cavitation or hydrogel degradation could be observed. In contrast to the *in vitro* results showing that PLO/laminin-coating of alginate-based hydrogels directly enhanced cell attachment and neurite outgrowth of DRG neurons, the *in vivo* data suggests that surface coating might only indirectly affect axonal growth. It instead provides a permissive molecular environment for attachment and colonization of host infiltrated cells within the hydrogel implant, creating a cellular growth substrate favorable for axon extension.

3.2 Impact of neonatal astrocytes as a cellular growth substrate within alginate-based hydrogel implants on axonal regeneration after traumatic spinal cord injury

Previous studies -including our own- using biomaterial scaffold implantation indicated that a permissive biological stimulus is essential to induce significant axonal regrowth into the hydrogel implant. In contrast, implantation of only a biomaterial into acute SCI sites resulted in only limited success (Nomura, Zahir et al. 2008, Wang, Zeng et al. 2011, Gunther, Weidner et al. 2015, Liu, Sandner et al. 2017).

Besides modification of the biomaterial itself by adding biologically active agents to its surface, the combination of the biomaterial implant with cell transplantation holds considerable promise in creating a growth-supportive environment at the lesion site. Among potential cell candidates, immature neurons, glia cells derived from NSCs, iPSCs or adult Schwann cells harbor great promise in restoring the lost spinal cord parenchyma and re-establishing lost axonal connections through the site of injury. These cells might have the capacity to improve the integration of the biomaterial implant into the host spinal cord and consequently improve the regrowth of spinal axons (Lu, Wang et al. 2012, Lu, Kadoya et al. 2014, Liu, Sandner et al. 2017, Koffler, Zhu et al. 2019). However, transplantation of Schwann cells and BMSCs have resulted in the formation of a glia limitans, clearly separating the cell grafts from the surrounding host spinal cord (Gunther, Weidner et al. 2015, Williams, Henao et al. 2015, Bunge 2016). This may be less likely the case for grafts containing CNS-derived glia cells.

Astrocytes facilitate structural and trophic support for neurons in both the developing as well as the adult CNS (Molofsky, Krencik et al. 2012, Chaboub and Deneen 2013). Moreover, networks of intermingled astrocytes were previously shown to serve as structural guidance matrices for axons similar to radial glia cells during cortical and spinal cord development (Joosten, Bar et al. 1995, Xu, Guenard et al. 1995, Guest, Hesse et al. 1997, Spilker, Yannas et al. 2001, Iseda, Nishio et al. 2004, Ma, Wei et al. 2004, Liu, Lu et al. 2010, Hurtado, Cregg et al. 2011, Zukor, Belin et al. 2013, Cregg, DePaul et al. 2014). Indeed, combining the natural scaffolding by immature astrocytes with a biomaterial implant with a defined microarchitecture might, therefore, provide physical support for growing axons enabling them to completely traverse extended SCI lesion sites. Hence, we seeded immature astrocytes derived from cortices of neonatal Fischer-344 rats into the channels of surface coated alginate-based hydrogel implants and examined their effect on implant integration assessed by analysis of host/graft interactions and revascularization, and -most importantly- axonal growth in adult rats after traumatic SCI.

3.2.1 Characterization of neonatal cortex-derived astrocytes from Fischer-344 rats

Astrocytes were isolated from neonatal Fischer-344 rats at postnatal day 1 (P1) with slight modifications as previously described (Albuquerque, Joseph et al. 2009). The primary neural culture was successfully cleared from contaminating non-astrocytic cells since barely any Iba I- or βIII-tubulin-positive cells could be detected after Ara-C treatment (**FIG 11A – D**). The vast majority of cells expressed additional markers of the astrocytic lineage (**FIG 11E**). Thus, enriched cortex-derived astrocyte cultures were obtained from neonatal rat pups and were used for *in vivo*-studies.

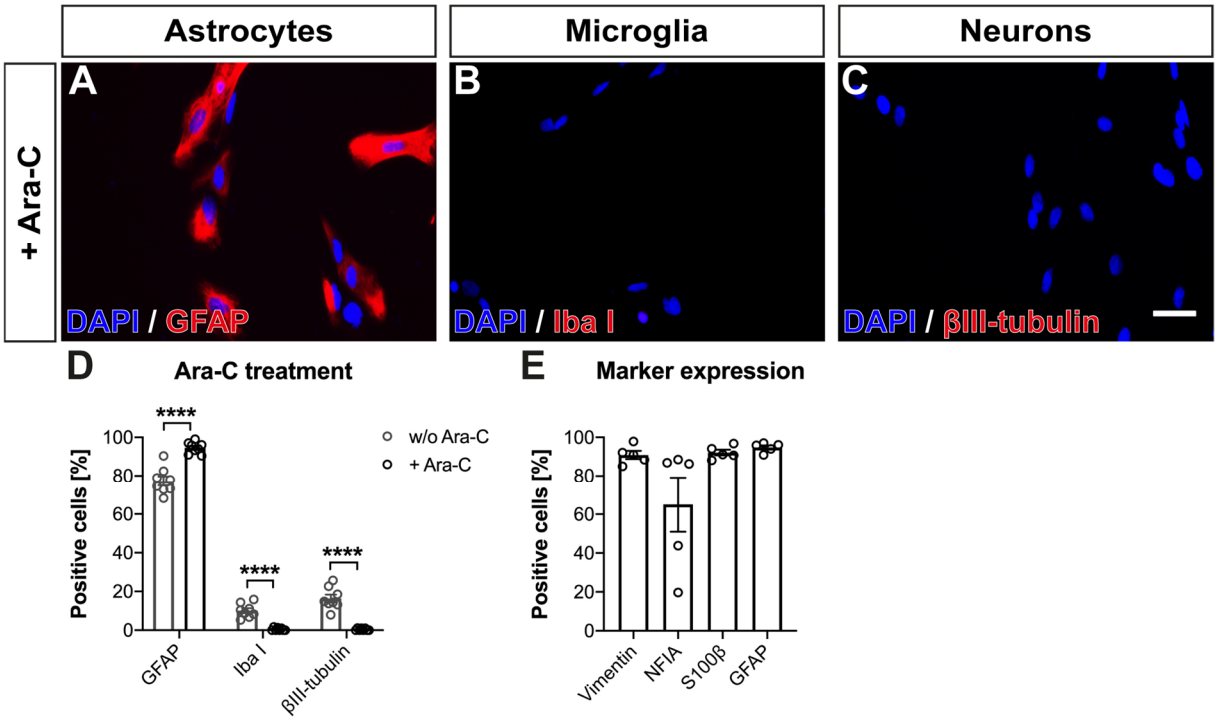

Figure 11: Neonatal cortex-derived astrocytes can be enriched *in vitro*. (**A – C**) Primary astrocyte cultures derived from the neonatal cortex were Ara-C-treated and immunolabeled for astrocytes (**A**, GFAP), microglia/macrophages (**B**, Iba I), and neurons (**C**, βIII-tubulin). (**D**) Ara-C treatment massively reduced the amount of contaminating non-astrocytic cells (Two-Way ANOVA $p < 0.05$, with Sidak's *post hoc* ****$p < 0.0001$). (**E**) Isolated and treated cells expressed markers of immature astrocyte precursors (Vimentin, NFIA) as well as of mature astrocytes (S100β, GFAP). Scale bar in **C**: 30 µm. Adapted from (Schackel, Kumar et al. 2019)

3.2.2 Implantation of astrocyte-seeded alginate-based hydrogel implants into the acutely injured spinal cord

To examine whether immature astrocytes could improve implant integration and provide a permissive cellular substrate for axonal growth, GFP-transgenic cortex-derived astrocytes were seeded into the channels of alginate-based hydrogels immediately before implantation into the lesion cavity of a unilateral hemisection injury at C5/6. Since surface coating with PLO and laminin had proven to strikingly enhance host cell infiltration and survival within the implant, PLO/laminin-coated implants were used as controls (**FIG 12**).

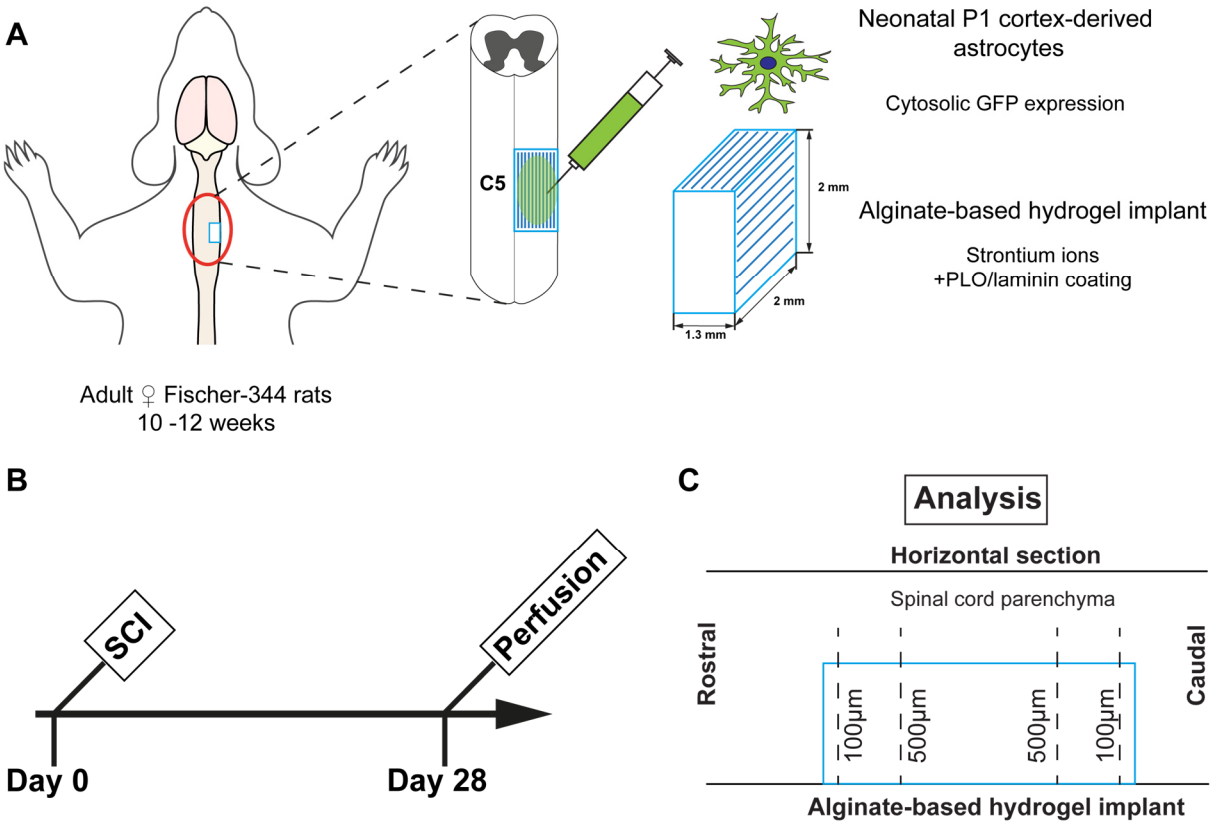

Figure 12: Experimental setup. (**A**) A total of 18 adult female *Fischer-344* rats were subjected to a unilateral C5 hemisection. The channels of PLO/laminin-coated alginate-based hydrogel implants were seeded with 200,000 GFP$^+$ neonatal P1 cortex-derived astrocytes. (**B**) Animals survived for 4 weeks and were finally transcardially perfused and (**C**) immunohistochemically analyzed at 100 µm and 500 µm from the rostral or caudal hydrogel edge, respectively (PLO/laminin: n = 6; + cortex-derived astrocytes: n = 10, see **Suppl. table 1**).

Both, non-seeded control implants (**FIG 13A**) as well as astrocyte-seeded implants (**FIG 13B**) were in close contact to the surrounding spinal parenchyma and densely filled with cells as indicated by DAPI-labeled nuclei within the implant. Cell filling of the implants was examined by quantifying the percentage of cell-filled (DAPI$^+$) of all hydrogel channels (**FIG 13C**). Overall, pre-seeding with cortex-derived astrocytes enhanced the cell filling of the implants both at the channel entries and at central regions on the hydrogel (Two-Way ANOVA for group differences $p < 0.001$). Cell filling significantly declined towards the hydrogel center in both groups (Two-Way ANOVA for distance $p < 0.0001$; see **Suppl. table 2**), however, still more hydrogel channels were filled with cells in pre-seeded implants compared to non-seeded controls (at rostral 500 µm: 78.78 ± 3.77% vs. 58.21 ± 10.57% cell-filled channels, $^*p < 0.05$; at caudal 500 µm: 75.97 ± 2.91% vs. 61.83 ± 4.64%, $p = 0.09$). Furthermore, a close association between cell grafting and distance was evident (Interaction between cell grafting and distance: $p = 0.04$). In astrocyte-seeded implants, the vast majority of all cell-filled channels were filled with GFP-

positive graft-derived cells that co-expressed the astrocyte marker GFAP (GFP⁺/GFAP⁺; **FIG 13D, E**). About 85% of all cell-filled channels per implant contained grafted GFP⁺ cells, also at the central regions of the implants (**FIG 13F**, One-Way ANOVA p = 0.52 for distance). Additionally, confocal imaging confirmed a dense filling of the implant channel lumen with GFP⁺/GFAP⁺ graft-derived astrocytes (**FIG 13G, H**). The astrocyte filling of the channels decreased towards the center of the hydrogel. Here, the grafted cells did not form a dense network but were occasionally organized in distinct cell clusters. Accordingly, the GFP⁺ channel area (area occupied with GFP-expressing graft cells) was significantly reduced at the hydrogel center compared to the channel entries (**FIG 13I**; unpaired Students' t-test ***p < 0.001).

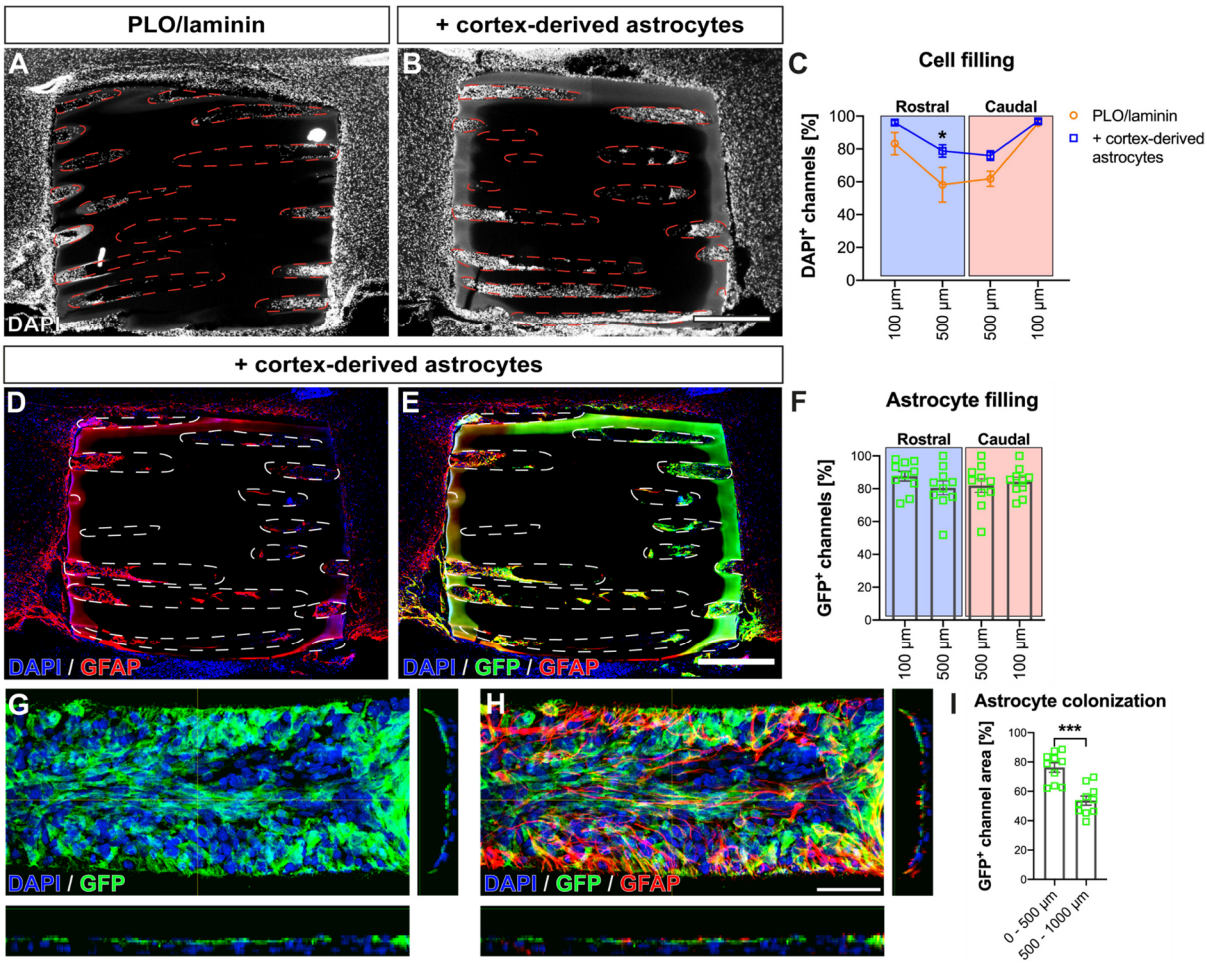

Figure 13: The seeded cortex-derived astrocytes robustly survive within surface-coated hydrogel implants. (**A, B**) All hydrogel implants remained structurally intact and in close contact with the host spinal cord. Channels (dashed lines) of non-seeded controls (**A**) and astrocyte-seeded hydrogel implants (**B**) were densely filled with cells ($DAPI^+$ nuclei, white). (**C**) Quantification of $DAPI^+$ channels revealed an overall increased cell filling in astrocyte-seeded implants compared to non-seeded controls (Two-Way ANOVA $p < 0.001$, followed by Sidak's *post hoc* $^*p < 0.05$ at 500 µm Rostral; interaction cell grafting x distance: $p = 0.04$; PLO/laminin, n = 6; + cortex-derived astrocytes, n = 10). Blue and red boxes indicate the rostral and caudal halves of the implant, respectively. Detailed statistical analysis is depicted in detail in **Suppl. table 2**. (**D, E**) The majority of channels in cell-seeded implants is filled with grafted GFP-positive astrocytes (GFAP) 4 weeks after implantation. (**F**) Quantification of GFP^+ channels of all $DAPI^+$ channels showed a homogenous cell filling throughout the implants with grafted GFP-expressing astrocytes (Two-Way ANOVA $p = 0.52$). (**G, H**) Within the hydrogel channels, the grafted GFP^+ cells (**G**) line the channel walls and co-express the astrocyte marker GFAP (**H**). XZ and YZ planes are shown underneath and to the right, respectively. (**I**) The seeded GFP^+ astrocytes were more densely packed at the channel entries (0 – 500 µm) in comparison with the central area of each implant (500 – 1000 µm; unpaired Students' t-test $^{***}p < 0.001$). Scale bars in **B**, **E**: 500 µm, in **H**: 50 µm. Adapted from (Schackel, Kumar et al. 2019)

To gain a more detailed view of implant integration, confocal imaging of the host/graft interface and the adjacent spinal cord parenchyma was performed (**FIG 14**). Again, the grafted GFP-transgenic astrocytes densely filled the channel lumen on the rostral as well as on the caudal side of the hydrogel implants (**FIG 14A, B**). They migrated into the host-graft interface on either side and extended protrusions into the adjacent uninjured host spinal cord intermingling with the host astrocytic network. Hence, graft- and host-derived astrocytes formed a continuous network-like guidance substrate connecting the implant with the host spinal parenchyma. Most importantly, host-derived spinal axons associated with the newly formed astrocytic network and were guided through the host/graft interface into the hydrogel implant (arrowheads in **FIG 14A, B**). Additionally, astrocyte-seeded implants were penetrated by tubular structures of von Willebrand factor-positive endothelial cells that might resemble host-derived blood vessels (**FIG 14C**). Within astrocyte-filled channels, the surface of the newly formed vasculature was covered with protrusions and potential endfeet of the grafted cortex-derived astrocytes.

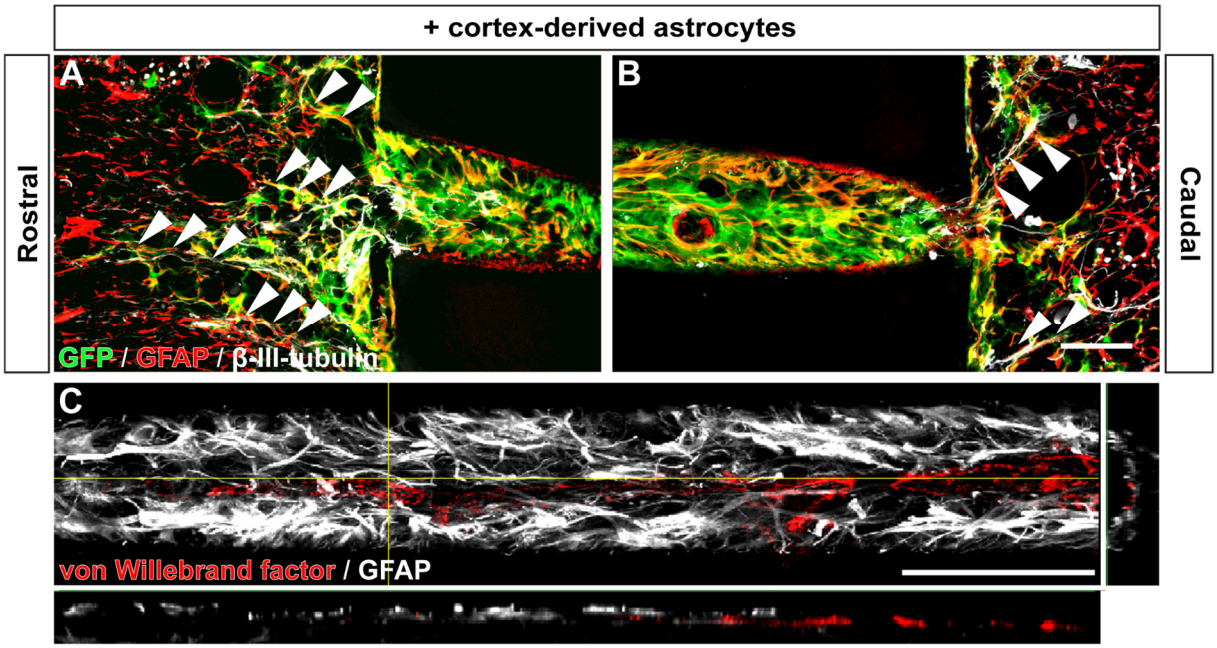

Figure 14: The grafted cortex-derived astrocytes intermingle with the host-derived astrocytic network and associate with endothelial cells and blood vessels within the hydrogel implants. (**A, B**) Graft-derived astrocytes (GFP, green) filled the channels of astrocyte-seeded hydrogels and migrated into the host/graft interface at the rostral (**A**) and caudal (**B**) side of the implants. GFP-positive graft-derived astrocytes ($GFP^+/GFAP^+$) extended protrusions into the host/graft interface and adjacent host spinal cord and intermingled with host-derived astrocytes (GFAP, red) forming continuous cellular guidance structures (arrowheads) for βIII-tubulin-labeled host axons (white) on both sides of the implant. (**C**) Immunolabeling for endothelial cells (von Willebrand factor, red) revealed tube-like structures within astrocyte-seeded hydrogel channels that were throughout the implant closely associated with grafted astrocytes (GFAP, white). XZ and YZ planes are shown underneath and to the right, respectively. Scale bar in **B, C**: 50 µm. Adapted from (Schackel, Kumar et al. 2019)

3.2.3 Axonal growth into astrocyte-seeded hydrogel implants 4 weeks after spinal cord injury

To assess whether astrocyte-seeding would improve axonal growth into and through the hydrogel implants, tissue sections were immunolabeled for βIII-tubulin and overall axonal growth was quantified at different distances within the hydrogel implant (**FIG 15**). Four weeks post-implantation, host axons were found throughout the entire length of channels in non-seeded controls and astrocyte-seeded hydrogel implants (**FIG 15A, B**). Quantification of axons per channel at the channel entries (100 µm from the rostral or caudal hydrogel edge) or the central area (500 µm from the rostral or caudal hydrogel edge) appeared to exhibit slightly greater

axonal growth in animals that received pre-seeded implants compared with animals that received a non-seeded implant. Unfortunately, this effect did not reach significance (**FIG 15C**; Two-Way ANOVA for overall group differences: $p = 0.09$). As previously reported, axons were exclusively found in channels that contained cells regardless of prior cell seeding (depicted in **FIG 10**). Further, axonal growth was significantly reduced at central hydrogel regions in both groups, comparable to the observed decrease in cell filling and graft cell survival at the central area of the implants (Two-Way ANOVA for distance $p < 0.0001$ **see Suppl. table 3**). Overall following normalization to the entire hydrogel implant area, more axons penetrated the astrocyte-seeded implants (**FIG 15D**; Two-Way ANOVA for overall group differences $p < 0.001$, followed by Sidak's *post hoc* $^{*}p < 0.05$ at rostral 100 µm), but, again, axon numbers significantly declined towards the central regions of the implants in both groups (Two-Way ANOVA for distance $p < 0.0001$, **see Suppl. table 4**). In addition, axonal growth responses were specifically analyzed in hydrogel implants of the astrocyte-seeded group. Here, the axon distribution between channels filled with the grafted cells and channels that only contained infiltrated host cells was determined (**FIG 15E – G**): the vast majority (86.05 ± 4.57%) of all axons were found in channels filled with the grafted cortex-derived astrocytes which is consistent throughout the entire implant (Two-Way ANOVA $p < 0.0001$).

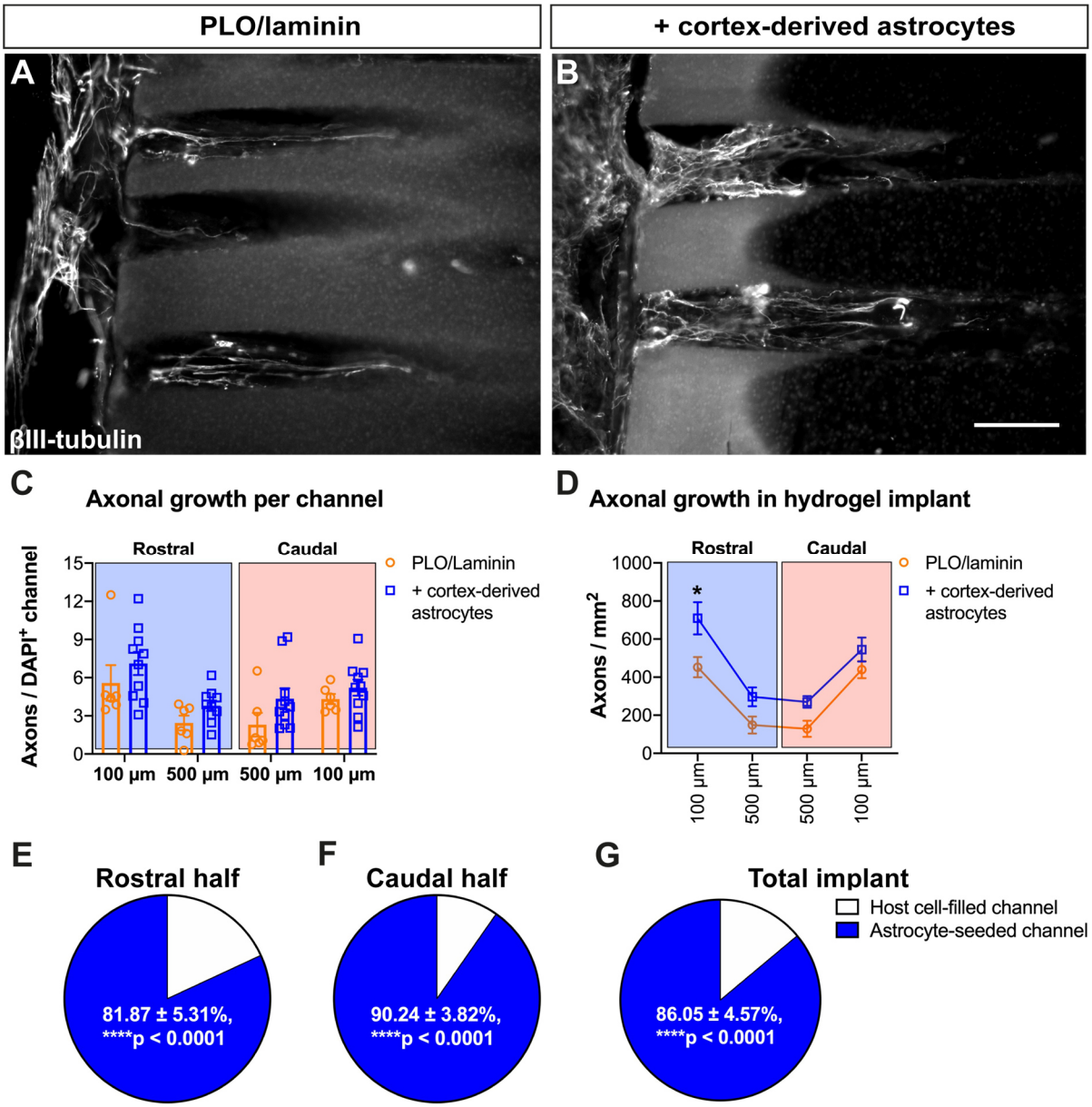
PLO/laminin
+ cortex-derived astrocytes
A
B
βIII-tubulin
C
Axonal growth per channel
Axons / DAPI+ channel
Rostral
Caudal
PLO/Laminin
+ cortex-derived astrocytes
100 µm
500 µm
500 µm
100 µm
D
Axonal growth in hydrogel implant
Axons / mm2
PLO/laminin
+ cortex-derived astrocytes
E
Rostral half
81.87 ± 5.31%,
****p < 0.0001
F
Caudal half
90.24 ± 3.82%,
****p < 0.0001
G
Total implant
Host cell-filled channel
Astrocyte-seeded channel
86.05 ± 4.57%,
****p < 0.0001

Figure 15: Seeding with cortex-derived astrocytes promotes axonal growth into alginate-based hydrogel implants. (**A, B**) βIII-tubulin-labeled axons (white) entered and extended within the channels of non-seeded control implants (**A**) and astrocyte-seeded implants (**B**). Single unbranched axons and thin axon bundles were found within the control group, whereas branched axons and thick bundles were seen within the channels of implants seeded with cortex-derived astrocytes. Rostral is to the left, medial to the top. (**C**) Axon numbers per $DAPI^+$ channels within the astrocyte-seeded implants appeared to be greater than in non-seeded controls (Two-Way ANOVA for overall group differences: $p = 0.09$), although axon numbers decreased towards the hydrogel center (Two-Way ANOVA for distance $p < 0.0001$, PLO/laminin, $n = 6$; + cortex-derived astrocytes, $n = 10$). Blue and red boxes indicate the rostral and caudal halves of the implant, respectively. Detailed statistical analysis is depicted in **Suppl. table 3**. (**D**) Throughout the implant, more axons were found in the astrocyte-seeded group compared with non-seeded controls (Two-Way ANOVA for overall group differences $p < 0.001$ followed by Sidak's *post hoc* $^*p < 0.05$ at Rostral 100 µm). Again, the amount of axonal growth within the implants declined towards the hydrogel center in both groups (Two-Way ANOVA for distance $p < 0.0001$). Detailed statistical analysis is depicted in **Suppl. table 4**. (**E – G**) Within the astrocyte-seeded implants, axons preferentially entered channels that contained the grafted GFP^+ astrocytes compared to channels that only contained infiltrated host cells at the rostral (**E**) or caudal half (**F**) as well as throughout the hydrogel implant (**G**, Two-Way ANOVA $p < 0.0001$, with Sidak's *post hoc* $^{****}p < 0.0001$). Scale bar in **B**: 25 µm. Adapted from (Schackel, Kumar et al. 2019)

To regain function after SCI, signal transmission between brain areas (e.g., somatosensory and motor cortex, brainstem nuclei) and their effector targets has to be re-established. Since βIII-tubulin labels both ascending and descending axons, a serotonin antibody (5-HT) was used to immunohistochemically detect descending serotonergic raphespinal axons and assess their contribution to the axonal growth within the hydrogel implants (**FIG 16**). Serotonergic axons were detected in non-seeded as well as astrocyte-seeded hydrogel implants (**FIG 16A, B**). In astrocyte-seeded implants, 5-HT-positive axons were found in close association with the grafted GFP-expressing astrocytes (**FIG 16B**). Further quantification revealed a not significant trend towards higher axon numbers in the astrocyte-seeded hydrogel implants. In both groups the largest number of serotonergic axons per $DAPI^+$ channel was present at the rostral side of the implants (**FIG 16C**, Two-Way ANOVA for group differences $p = 0.27$), but massively decreased towards the caudal side of the implants (Two-Way ANOVA for distance $p < 0.0001$; **see Suppl. table 5**). This was confirmed when the entire implant area was analyzed (**FIG 16D**, Two-Way ANOVA for overall group differences $p = 0.14$, for distance $p < 0.0001$, **see Suppl. table 6**) Consistent with βIII-tubulin-labeled axons, serotonergic axons preferentially entered implant channels filled with grafted astrocytes compared to channels containing only infiltrated host cells (**FIG 16E**, Two-Way ANOVA $p < 0.0001$).

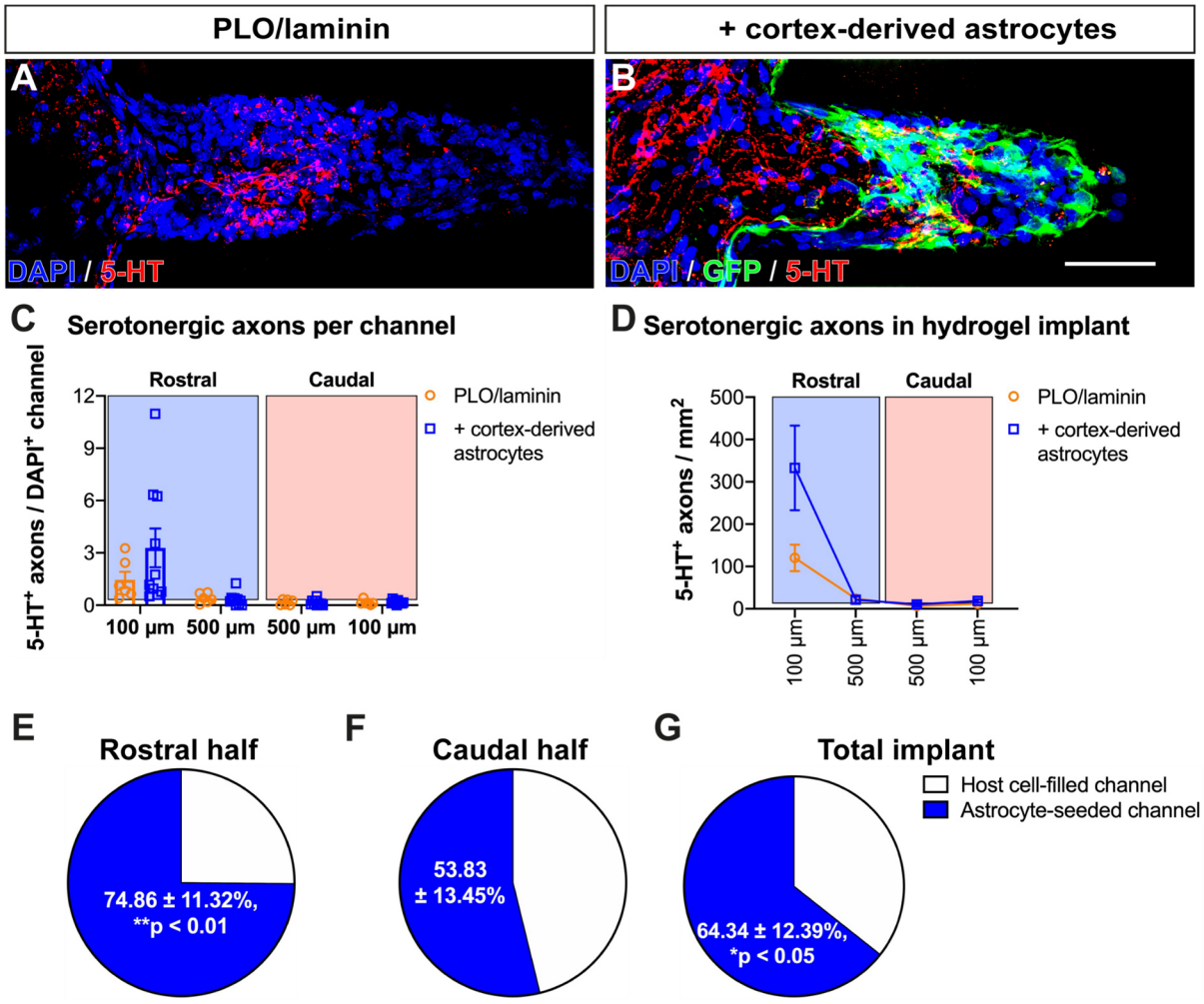
PLO/laminin
+ cortex-derived astrocytes
A
DAPI / 5-HT
B
DAPI / GFP / 5-HT
C
Serotonergic axons per channel
5-HT+ axons / DAPI+ channel
Rostral
Caudal
PLO/laminin
+ cortex-derived astrocytes
100 µm
500 µm
500 µm
100 µm
D
Serotonergic axons in hydrogel implant
5-HT+ axons / mm2
E
Rostral half
74.86 ± 11.32%,
**p < 0.01
F
Caudal half
53.83
± 13.45%
G
Total implant
Host cell-filled channel
Astrocyte-seeded channel
64.34 ± 12.39%,
*p < 0.05

Figure 16: Seeding with neonatal cortex-derived astrocytes enhances the growth of serotonergic axons into alginate-based hydrogel implants. (**A, B**) Descending serotonergic axons (5-HT, red) penetrated non-seeded controls (**A**) and astrocyte-seeded hydrogel implants (**B**) 4 weeks post-injury. 5-HT-labeled axons and graft-derived GFP-positive astrocytes were found aligned within the hydrogel channels. Rostral is to the left, medial to the top. (**C**) Quantification of 5-HT$^+$ axons per cell-filled channel showed a trend towards a slightly greater number of serotonergic axons in the astrocyte-seeded implants, but this did not reach significance (Two-Way ANOVA for overall group differences $p = 0.27$). Serotonergic axon numbers diminished towards the central and caudal part of the implants in both groups, but were more prominent in the astrocyte-seeded implants (Two-Way ANOVA for distance $p < 0.0001$, with Sidak's *post hoc* test ***$p < 0.001$ comparing rostral 100 µm with all other distances in the astrocyte-seeded group; PLO/laminin, n = 6; + cortex-derived astrocytes, n = 10). Detailed statistical analysis is depicted in **Suppl. table 5**. Blue and red boxes indicate the rostral and caudal hydrogel halves, respectively. (**D**) Similarly, a not significant trend towards enhanced ingrowth of raphespinal axons into implants pre-seeded with cortex-derived astrocytes was found but 5-HT$^+$ axon numbers dramatically decreased along the rostrocaudal extent of the hydrogels (Two-Way ANOVA for group differences $p = 0.14$, for distance $p < 0.0001$, with followed by Sidak's *post hoc* ****$p < 0.0001$ comparing rostral 100 µm with all other distances in the astrocyte-seeded group). Detailed statistical analysis is depicted in **Suppl. table 6**. (**E – G**) In the astrocyte-seeded implants, serotonergic axons entered and extended preferentially in channels that contained the grafted GFP-positive astrocytes. This effect was consistent throughout the entire hydrogel implants (Two-Way ANOVA $p < 0.0001$, with Sidak's *post hoc* **$p < 0.01$ for the rostral half, *$p < 0.05$). Scale bar in **B**: 50 µm. Adapted from (Schackel, Kumar et al. 2019)

Taken together, astrocytes can be isolated from neonatal cortical tissue from rats and used as a permissive cellular substrate within the channels of alginate-based hydrogel implants *in vivo*. Grafted astrocytes survived within the implants, filled the vast majority of the implants' channels and interacted with the host-derived vasculature and astrocytic network adjacent to the implantation site. Most importantly, cortex-derived grafted astrocytes served as a growth substrate for spinal axons at the host/graft interface and within the hydrogel implants.

3.3 Characterization of neonatal astrocytes in vitro and in vivo

In the previous study, neonatal cortex-derived astrocytes were used to provide a permissive growth substrate within the alginate-based hydrogel implant in hopes to improve axonal growth through the implantation site after traumatic SCI. The grafted cells filled the hydrogel implants, interacted with the host spinal cord, and slightly enhanced axonal growth (Schackel, Kumar et al. 2019). Noteworthy, astrocytes isolated from cortical tissue have a molecular identity that

suits the healthy and injured brain but might not necessarily be ideal for the injured spinal cord. Therefore, astrocytes obtained from neonatal spinal cord tissue could potentially harbor a greater pro-regenerative capacity in comparison to cortex-derived neonatal astrocytes after transplantation into acute SCI lesions. Thus, in the next set of experiments, we sought to examine whether neonatal spinal cord-derived astrocytes might represent a superior candidate for cell transplantation into acute SCI lesions.

3.3.1 Characterization of neonatal spinal cord-derived astrocytes

First, astrocytes were isolated from spinal cords of postnatal day 1 *Fischer-344* rats and were cultured. After Ara-C treatment, cells were immunolabeled for astrocytes (GFAP), microglia (Iba I), and neurons (βIII-tubulin) to determine the composition of the primary spinal cell culture (**FIG 17**). Similar to the isolation of cortex-derived astrocytes, the primary spinal cell culture contained neural as well as non-neural cells and had to be purified with Ara-C to obtain an enriched culture of spinal cord-derived astrocytes. About 10% of all cells were positively labeled for Iba I or βIII-tubulin, which decreased after Ara-C treatment (**FIG 17D**; Iba I: 0.53 ± 0.25%, βIII-tubulin: 0.42 ± 0.19%). However, only 50.99 ± 2.70% of all the remaining cells expressed GFAP and were therefore identified as astrocytes, which is much lower than the amount of GFAP-expressing cells obtained from neonatal cortical tissue (94.59 ± 1.05%, **FIG 11**).

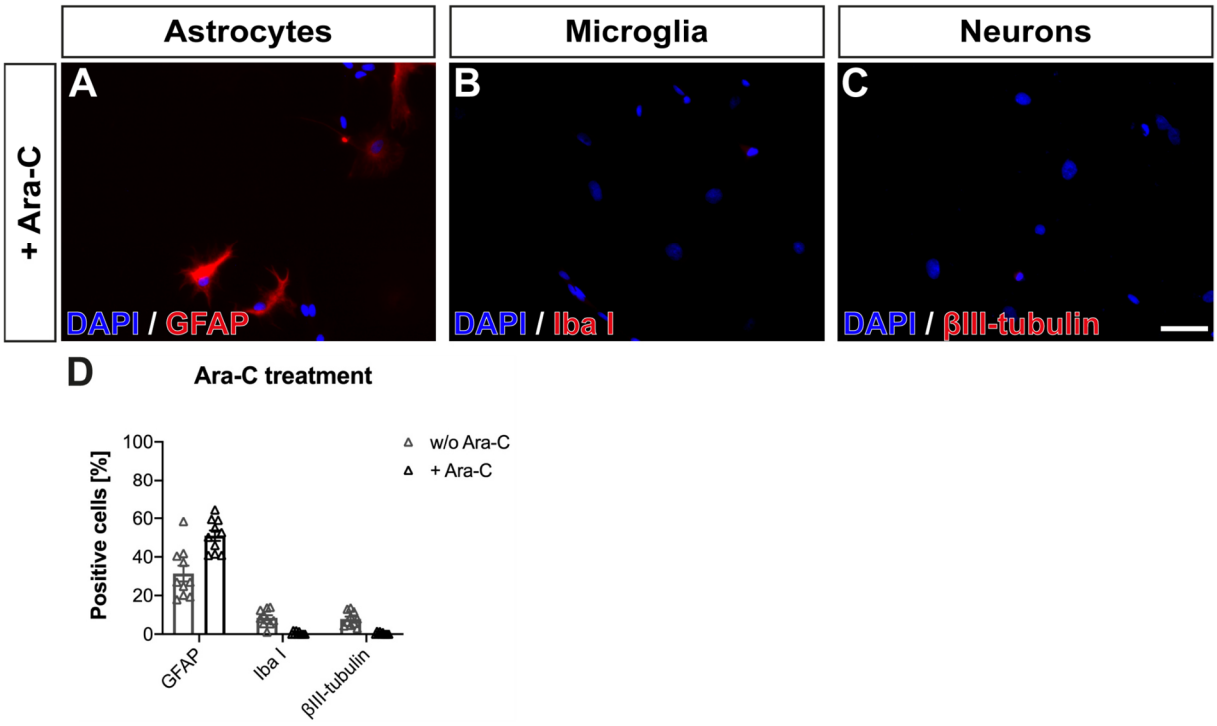

Figure 17: P1 spinal cord-derived astrocytes can be enriched *in vitro*. (**A – C**) Immunolabeling for astrocytes (**A**, GFAP), microglia (**B**, Iba I), and neurons (**C**, βIII-tubulin) of primary spinal cultures. (**D**) Ara-C treatment decreased the amount of contaminating microglia and neuronal cells in the culture (Two-Way ANOVA p = 0.48). Scale bar in **C**: 30 µm.

Since astrocyte development in the brain and spinal cord proceed along different time frames (Molofsky and Deneen 2015), we wondered whether more GFAP-expressing astrocytes could be obtained from the spinal cord of a later developmental timepoint. Further, immunolabeling for different molecular markers of neural stem cells, progenitor cells and cells of the astrocytic lineage was performed to phenotypically characterize purified astrocyte cultures generated from postnatal day 1 and 3 spinal cords (**FIG 18**). Both P1 and P3 spinal cord-derived cells showed strong immunolabeling for the cytoskeletal stem cell marker Vimentin (**FIG 18A – F**), Nestin (**FIG 18G – L**), and nuclear staining for Sox2 (**FIG 18M – O**). An equal percentage of P1 and P3 spinal cord-derived cells expressed the astrocyte marker GFAP (**FIG 18S**, 67.76 ± 2.53% at P1 vs. 72.29 ± 0.12% at P3; unpaired Students' t-test p = 0.14). Importantly, within the fraction of $GFAP^+$ cells, ~80% of all cells co-expressed Vimentin and Nestin, and a total of 40% of all GFAP-expressing cells were also found to be positive for Sox2, which labels proliferating progenitor cells. However, no significant differences were found between the marker expression profile of spinal cord-derived cells at postnatal day 1 and 3 (Two-Way ANOVA for developmental timepoint: p = 0.39). Conclusively, the large number of $GFAP^+$ cells co-expressing the tested stem cell and progenitor markers might be indicative of a rather immature or maturing phenotype of the isolated astrocytic cells. Since the morphology of cells of the astrocytic lineage changes during development (Freeman 2010, Vue, Kim et al. 2014, Zhao, Chen et al. 2014), $GFAP^+$ astrocytes were also morphologically examined at both developmental timepoints (**FIG 18U**). Overall cell morphology was defined in 4 different categories: bi-/tripolar, small fibrous, large fibrous, and stellate (Bushong, Martone et al. 2002, Holtje, Hoffmann et al. 2005, Sofroniew and Vinters 2010, Testen, Kim et al. 2020). At P1, significantly more GFAP-positive cells showed a tri-/bipolar morphology compared to P3 (44.49 ± 4.68% vs. 30.39 ± 0.73%; Two-Way ANOVA for morphological differences: $p < 0.001$, followed by Sidak's *post hoc* $^*p < 0.05$; Interaction between developmental timepoint and morphology: p = 0.0095). Further, the percentage of cells with a large fibrous and stellate cell shape increased from P1 to P3, but this trend did not yet reach significance.

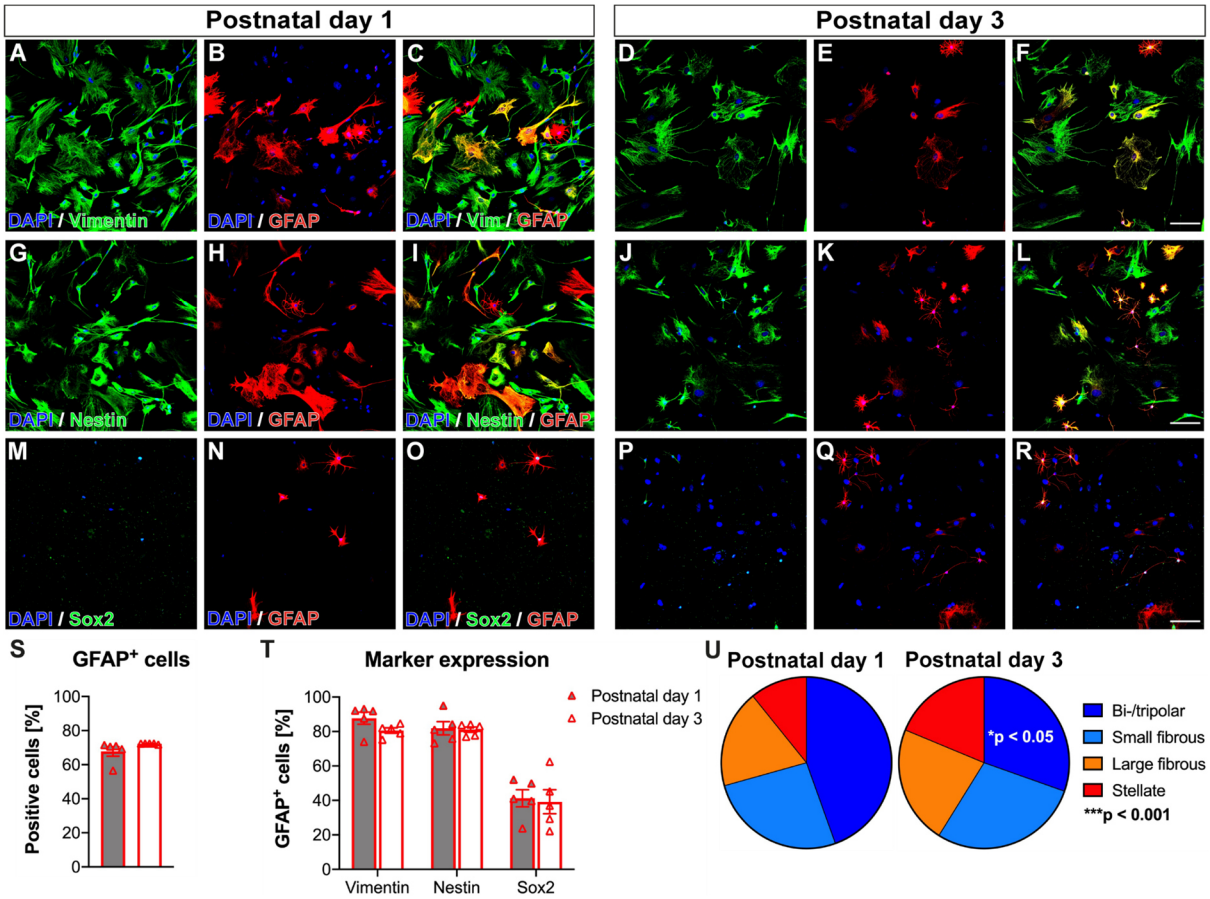

Figure 18: Spinal cord-derived astrocytes isolated at P1 and P3 show similar marker expression profiles but morphological differences *in vitro*. Ara-C-treated astrocyte cultures generated from postnatal days 1 and 3 were immunolabeled for the stem cell markers Vimentin (Vim, green, **A – F**), Nestin (green, **G – L**), and the progenitor marker Sox2 (green, **M – R**). (**S**) Quantification of GFAP expression revealed no significant difference between cells isolated at P1 and P3 (unpaired Students' t-test, p = 0.14). (**T**) The majority of GFAP⁺ cells similarly expressed Vimentin, Nestin and Sox2 at both developmental timepoints (Two-Way ANOVA for developmental timepoint: p = 0.39). (**U**) In contrast, the cell morphology of GFAP-expressing cells was significantly different between P1 and P3 (Two-Way ANOVA for morphological differences: p < 0.001, with Sidak's *post hoc* test *p < 0.05 comparing bi/tripolar cell morphology between P1 and P3). Scale bar in **F**, **L**, **R**: 100 µm.

To assess whether spinal cord-derived astrocytes shared characteristics of cortex-derived astrocytes, the same *in vitro*-characterization was done with cortex-derived astrocytes isolated at P1 and P3 (**FIG 19**). The vast majority of cortex-derived astrocytes at both developmental timepoints expressed Vimentin and Nestin together with GFAP (**FIG 19A – L**). The percentage of GFAP-expressing cells was unaltered between P1 and P3 (91.99 ± 1.21% at P1 vs. 94.92 ± 1.00% at P3, unpaired Students' t-test p = 0.13). Quantification of marker expression in GFAP⁺ (**FIG 19T**) indicated no change in Vimentin or Nestin, GFAP co-expression at P1 and P3, but a sharp decline in GFAP⁺/Sox2⁺-expressing cells (Two-Way ANOVA for developmental

timepoint: p < 0.0001, with Sidak's *post hoc* ****p < 0.0001). Further, a causal relation between developmental timepoints and marker expression might be present (Interaction between developmental timepoint and marker: p = 0.0002). Again, since more than 80% of all GFAP⁺ cells co-express stem cell markers, the isolated astrocytic cells might be in a maturing rather than a fully mature state. When cell morphology was examined, the vast majority of GFAP-expressing astrocytes showed either an undifferentiated bi-/tripolar or small fibrous morphology, which was consistent also at postnatal day 3 (**FIG 19U**).

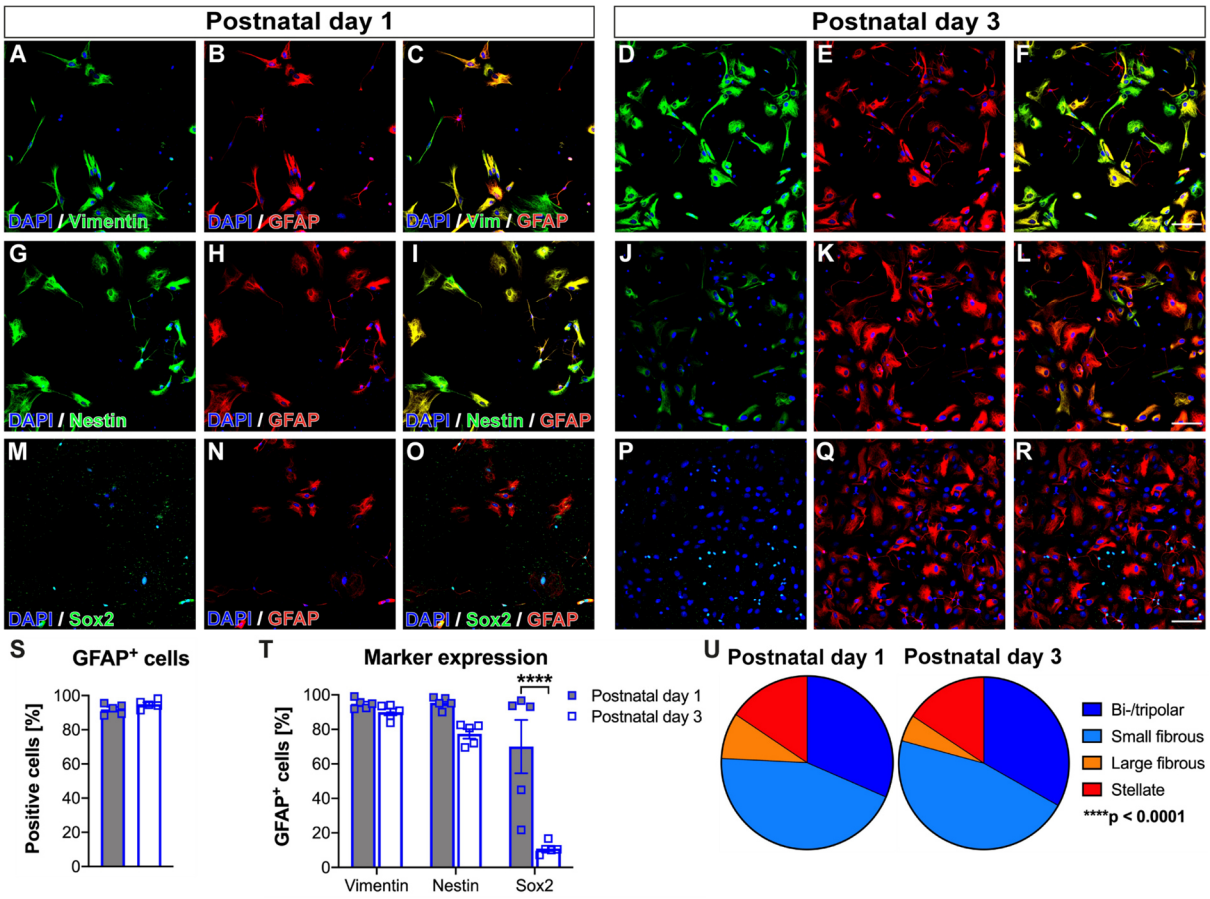

Figure 19: Cortex-derived astrocytes isolated at P1 express significantly less Sox2 compared with cortex-derived astrocytes isolated at P3. After Ara-C treatment, cortex-derived cells from P1 and P3 were immunolabeled for GFAP (red) and the stem cell markers Vimentin (green, **A – F**), Nestin (green, **G – L**), and Sox2 (green, **M – R**). (**S**) Similar to spinal cord-derived cells, no difference was observed in GFAP expression between P1 and P3 (unpaired Students' t-test p = 0.13). (**T**) At P1, most GFAP$^+$ cells co-expressed both Vimentin and Nestin, but their expression appeared slightly reduced at P3. Sox2 expression was, in contrast, strongly decreased at P3 (Two-Way ANOVA for developmental timepoint: p < 0.0001, followed by Sidak's *post hoc* test ****p < 0.0001 for Sox2; Interaction between developmental timepoint and marker expression: p = 0.0002). (**U**) Morphology analysis cells revealed ~75% of all GFAP-expressing cells to have either a bi-/tripolar or small fibrous cellular shape (Two-Way ANOVA for morphology differences: p < 0.0001; for developmental timepoint: p > 0.999). Scale bar in **F**, **L**, **M**: 100 µm.

For comparison, marker expression as well as the morphology *in vitro* of cortex- and spinal cord-derived astrocytes at P1 and P3 were directly examined (**FIG 20**). At both postnatal timepoints, the amount of GFAP$^+$ cells was significantly greater in cortex-derived samples (≥90% of all detected cells express GFAP) compared with spinal cord-derived samples (unpaired Students' t-test ****p < 0.0001). Within the fraction of GFAP-expressing cells -independent of cell origin and postnatal timepoint-, most cells co-express the stem cell markers Vimentin and Nestin. However, the percentage of GFAP$^+$/Sox$^+$ astrocytes derived from postnatal spinal cord was significantly higher than from cortex-derived astrocytes (**FIG 20D**, Two-Way ANOVA for cell type: p < 0.05, followed by Sidak's *post hoc* test *p < 0.05), which was reversed when cells from P3 were compared (Two-Way ANOVA for cell type: p < 0.05, followed by Sidak's *post hoc* test ****p < 0.05). Here, a causal relationship between cell type and marker expression was found (Interaction between cell type and marker: p = 0.0002). If cortex-derived P1 astrocytes with spinal cord-derived astrocytes P3 were compared, the fraction of GFAP$^+$/Vimentin$^+$ and GFAP$^+$/Nestin$^+$ was slightly but not significantly enhanced in cortex-derived astrocytes (**FIG 20F**). A more significant fraction of cortex-derived cells was co-labeled with GFAP and Sox2 (Two-Way ANOVA for cell type: p < 0.01, with Sidak's *post hoc* test *p < 0.05). If the different cell morphology categories were compared at P1, spinal cord-derived astrocytes appeared more often in a bi-/tripolar or large fibrous cell shape than cortex-derived cells. In contrast, a small fibrous cell shape was more prominent in the cortex-derived cells (Two-Way ANOVA for morphology. p < 0.0001, with Sidak's *post hoc* **p < 0.01 for bi-/tripolar, ****p < 0.0001 for small fibrous, *p < 0.05 for large fibrous; Interaction cell type x morphology: p < 0.0001). At postnatal day 3 (**FIG 20H**), only differences in the small and large fibrous fraction were detected (Two-Way ANOVA for morphology: p < 0.0001, with Sidak's *post hoc* ****p < 0.0001; Interaction between cell type and morphology: p < 0.0001), which was consistent

when cortex-derived astrocytes from P1 and spinal cord-derived astrocytes from P3 were compared with each other (**FIG 20I**) (Two-Way ANOVA for morphology: $p < 0.0001$, with Sidak's *post hoc* ****$p < 0.0001$; Interaction between cell type and morphology: $p < 0.0001$).

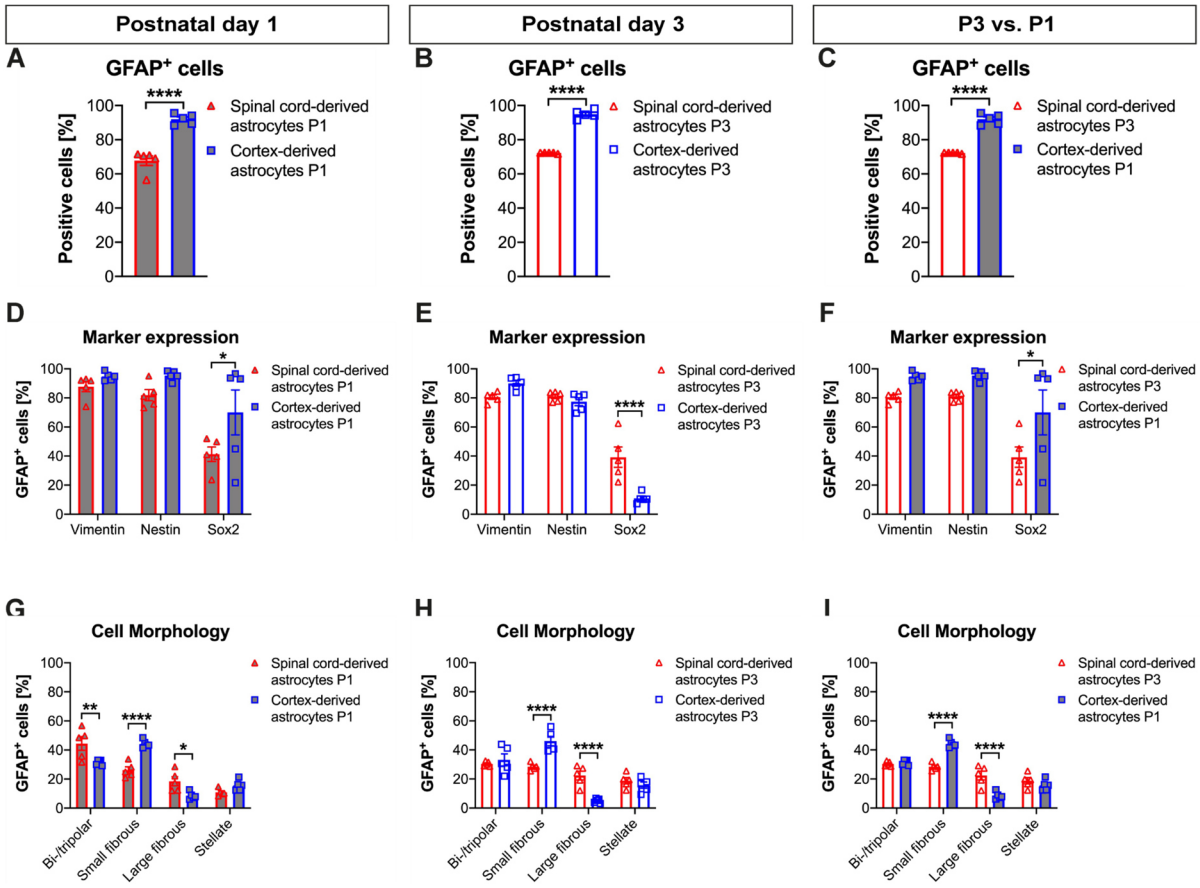

Figure 20: Cortex- and spinal cord-derived astrocytes isolated at P1 and P3 show differences in marker expression and cell morphology. (**A – C**) Quantification of GFAP⁺ cells at P1 (**A**), P3 (**B**) and the direct comparison of P3 vs. P1 (**C**) revealed an overall higher percentage of GFAP-expressing cells in cortex-derived cells (unpaired Students' t-test ****$p < 0.0001$). (**D – F**) Marker co-expression of GFAP⁺ cells at P1 (**D**) (Two-Way ANOVA for cell type: $p < 0.05$, with Sidak's *post hoc* *$p < 0.05$ for Sox2), P3 (**E**) (Two-Way ANOVA for cell type: $p < 0.05$, with Sidak's *post hoc* ****$p < 0.05$ for Sox2; Interaction between cell type and marker: $p = 0.0002$), and P1 vs. P3 (**F**)(Two-Way ANOVA for cell type: $p < 0.01$, with Sidak's *post hoc* *$p < 0.05$ for Sox2). (**G – I**) Cell morphology of GFAP⁺ cells at P1 (**G**) (Two-Way ANOVA for morphology: $p < 0.0001$, with Sidak's *post hoc* *$p < 0.05$, **$p < 0.01$, ****$p < 0.0001$ comparing spinal cord-derived astrocytes with cortex-derived astrocytes), at P3 (**H**) (Two-Way ANOVA for morphology: $p < 0.0001$, with Sidak's *post hoc* ****$p < 0.0001$ comparing spinal cord-derived astrocytes with cortex-derived astrocytes), and P1 vs. P3 (**I**) (Two-Way ANOVA for morphology: $p < 0.0001$, with Sidak's *post hoc* ****$p < 0.0001$).

To summarize, astrocytic cells can be obtained from spinal cords of neonatal *Fischer-344* rats, maintained in culture and enriched following Ara-C treatment. Importantly, the fraction of GFAP-expressing cells is significantly smaller in astrocyte cultures derived from the spinal cord compared to cortex-derived cultures. *In vitro*-characterization using immunolabeling revealed only minor differences between cortex- and spinal cord-derived astrocytes ($GFAP^+$), also when cells were isolated at later developmental timepoints. Similarly, the morphology of $GFAP^+$ astrocytes was comparable, although slight differences were found.

3.3.2 Transplantation of neonatal cortex-derived or spinal cord-derived astrocytes into the intact spinal cord

Since no striking differences between neonatal cortex- and spinal cord-derived astrocytes could be observed with the measured parameters, neonatal astrocytes derived from cortex at P1 and neonatal astrocytes derived from P3 spinal cord were used in the following *in vivo* studies. This decision was based upon previous studies that already successfully used transplantation of P1 cortex-derived astrocytes after SCI (Kliot, Smith et al. 1990, Olby and Blakemore 1996, Joosten, Veldhuis et al. 2004) as well as several practical considerations. More precisely, although GFAP-expressing astrocytes were successfully isolated from P1 spinal cord tissue, the overall cell yield per animal (~200,000 cells per spinal cord; ~60% $GFAP^+$ cells) and cell survival within the first days *in vitro* was minimal compared with the amount of cells that can be obtained from P1 cortical tissue (~2 x 10^6 cells per animal, more than 90% $GFAP^+$ cells). In contrast, if P3 spinal cords were used, a total of 500,000 cells per animal could be obtained with 60 to 65% of all cells expressing GFAP. Furthermore, P3 spinal cord cells appeared to be more robust *in vitro* and during the Ara-C treatment resulting in an overall greater amount of cells that could be used for further experiments.

In vitro-characterization of both, neonatal cortex-derived and spinal cord-derived cells, revealed an immature or maturing phenotype of the isolated astrocytes (**FIG 18 & 19**). To determine how these immature astrocytes respond to an *in vivo* environment, P3 spinal cord-derived astrocyte and P1 cortex-derived astrocytes were transplanted into the intact spinal cord at cervical level C5 (**FIG 21**).

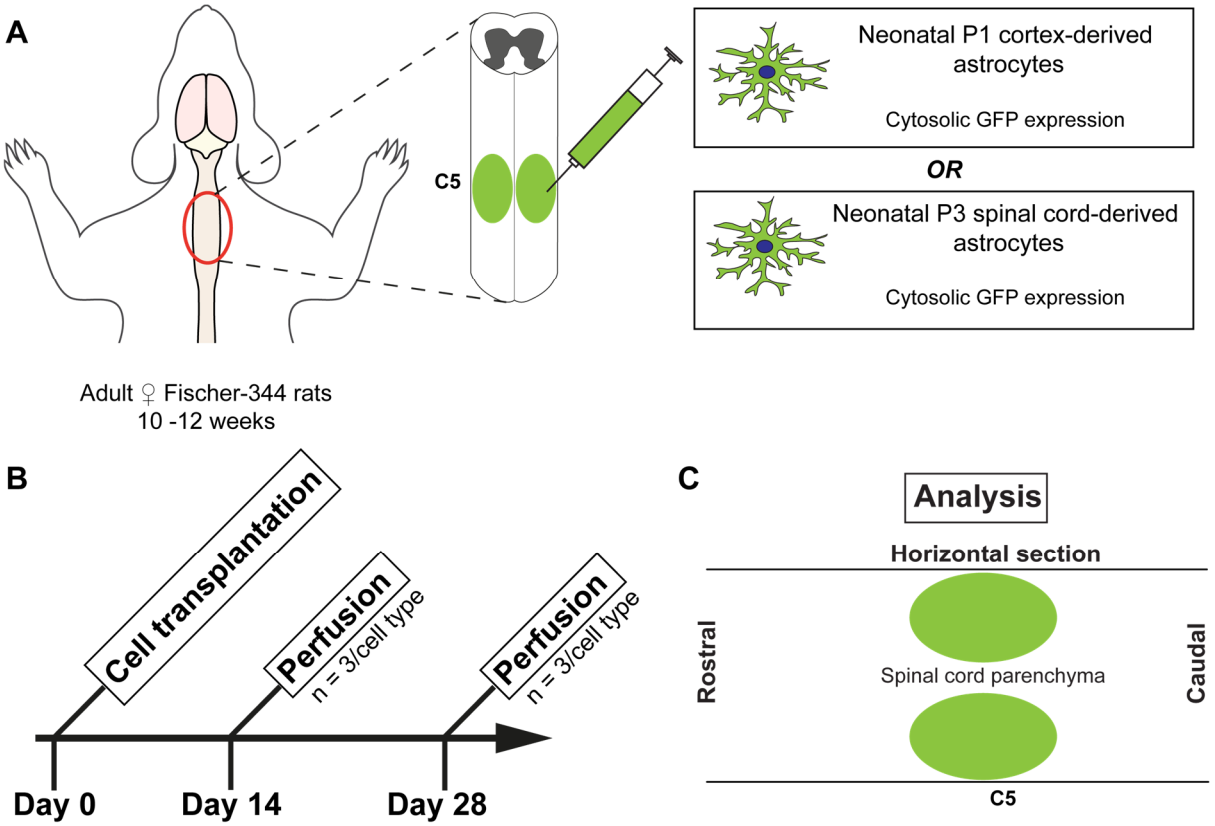

Figure 21: Experimental setup. (**A**) Neonatal P1 cortex-derived astrocytes (n = 6) or P3 spinal cord-derived astrocytes (n = 6) were transplanted into the intact spinal cord at cervical level C5. (**B**) Animals were sacrificed 2 or 4 weeks after cell transplantation (n = 3/timepoint) and their spinal cords immunohistochemically analyzed (**C**).

A total of 12 adult female Fischer-344 rats received cell injections of GFP-transgenic P3 spinal cord derived or P1 cortex-derived astrocytes (n = 6/cell type). In each group, a subgroup of animals was perfused 2 or 4 weeks after cell injection (n = 3/timepoint). Afterwards, their spinal cords were immunohistochemically analyzed to assess the expression of GFAP (**FIG 22**). The transplanted GFP^+ cells survived and integrated into the host spinal cord parenchyma with no distinct boundary between injected cells and surrounding host spinal parenchyma. Independent of tissue origin, most transplanted cells expressed the astrocyte marker GFAP already 2 weeks after transplantation (**FIG 22A – D, I**; P3 Spinal cord-derived astrocytes: 95.19 ± 3.34% $GFP^+/GFAP^+$ cells; P1 cortex-derived astrocytes: 99.09 ± 0.45% $GFP^+/GFAP^+$ cells) and continued to showed GFAP immunoreactivity also at 4 weeks post-transplantation (**FIG 22D – H, I** P3 Spinal cord-derived astrocytes: 96.41 ± 3.05% $GFP^+/GFAP^+$ cells; P1 cortex-derived astrocytes: 98.36 ± 0.51% $GFP^+/GFAP^+$ cells; Two-Way ANOVA for overall group differences: p = 0.24, for timepoints: p = 0.93).

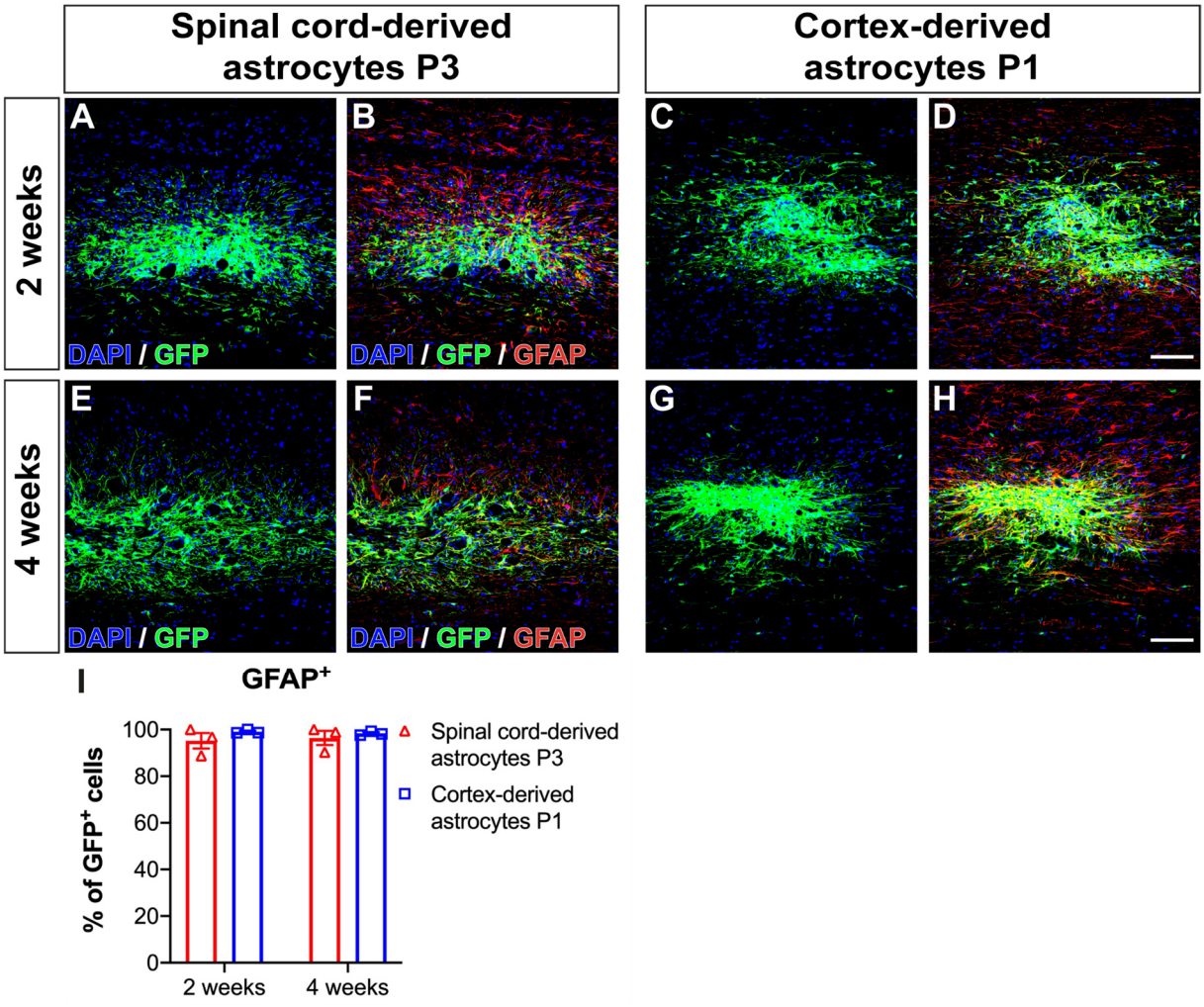

Figure 22: The majority of P3 spinal cord- and P1 cortex-derived astrocytes expresses GFAP 2 and 4 weeks after transplantation into the intact spinal cord. (**A – D**) Two weeks after transplantation, the vast majority of the grafted P3 spinal cord-derived (**A, B**) and P1 cortex-derived astrocytes (**C, D**; GFP, green) express the astrocyte marker GFAP (red), which was consistent also at 4 weeks post-transplantation (**E – H**). (**I**) Quantification of immunolabeling confirmed a constantly high fraction of the grafted GFP⁺ cells to express GFAP (Two-Way ANOVA for overall group differences: p = 0.24; for timepoints: p = 0.93; spinal cord-derived astrocytes P3, n = 3/timepoint; cortex-derived astrocytes P1, n = 3/timepoint). Scale bars in **D**, **H**: 100 µm.

Furthermore, co-expression of molecular markers of stem cells/progenitor cells (Vimentin, Nestin, Sox2), astrocyte precursors (Sox9) (**FIG 23**) and maturing or terminally differentiated astrocytes was determined (A2B5, AQP4, GLT-1, S100β) (**FIG 24**). About 80% of all transplanted astrocytes (GFP⁺/GFAP⁺) in both groups were positively labeled for Vimentin (**FIG 23A – E**) without any differences over time (Two-Way ANOVA p = 0.09). In contrast, Nestin expression appeared to be unaltered 2 and 4 weeks after transplantation (**FIG 23F – J**, Two-Way ANOVA for overall group differences: p = 0.85, for timepoint: p = 0.18). Sox2 expression was

surprisingly high in the P1 cortex-derived astrocytes at both timepoints (2 weeks: 40.24 ± 3.13%; 4 weeks: 57.59 ± 11.24% of $GFP^+/GFAP^+$ cells) compared to P3 Spinal cord-derived astrocytes (2 weeks: 9.83 ± 1.49%; 4 weeks: 18.09 ± 5.32% of $GFP^+/GFAP^+$ cells; Two-Way ANOVA $p < 0.01$ followed by Sidak's *post hoc* test $^*p < 0.05$). Additionally, Sox9 expression of the transplanted cells was examined and quantified (**FIG 23P – T**). Similar to the other markers, both cell types expressed moderate levels of Sox9, 2 and 4 weeks post-transplantation (Two-Way ANOVA for overall group differences: $p = 0.24$; for timepoints: $p = 0.95$).

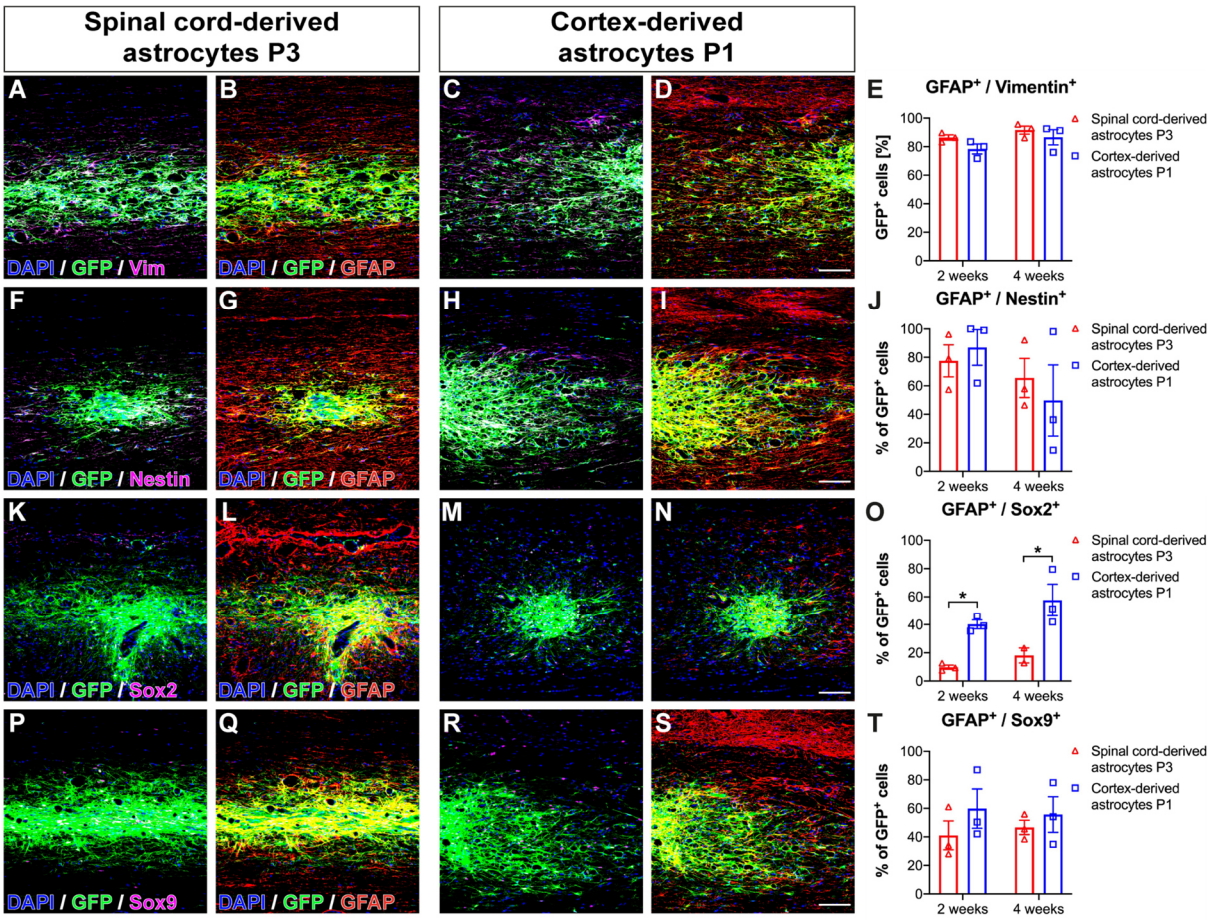

Figure 23: Neonatal P3 spinal cord- and P1 cortex-derived astrocytes still express stem cell and precursor cell markers 2 and 4 weeks after transplantation into the intact spinal cord. (**A – D**) Immunolabeling of transplanted GFP$^+$ astrocytes (GFP, green) derived from P3 spinal cord (**A, B**) or P1 cortex (**C, D**) showed strong Vimentin expression (Vim, magenta) 2 and 4 weeks after cell transplantation (spinal cord-derived astrocytes P3, n = 3/timepoint; cortex-derived astrocytes P1, n = 3/timepoint). (**E**) Most transplanted cells consistently co-expressed GFAP and Vimentin 2 and 4 weeks after cell transplantation (n = 3 for each timepoint/astrocyte population; Two-Way ANOVA for overall group differences: p = 0.11; for timepoint: p = 0.09). (**F – I**) Spinal cord- (**F, G**) as well as cortex-derived astrocytes (**H, I**) were positively labeled for Nestin (magenta). However, Nestin expression was unaltered 2 and 4 weeks after transplantation (**J**; Two-Way ANOVA for overall group differences: p = 0.85; for timepoint: p = 0.18). (**K – N**) Sox2 expression (magenta) was present in both P3 Spinal cord-derived (**K, L**) and P1 cortex-derived (**M, N**) astrocytes but significantly elevated in cortex-derived astrocytes (**O**; Two-Way ANOVA for overall group differences: p < 0.001, with Sidak's *post hoc* *p < 0.05; for timepoints: p = 0.11). (**P – S**) Both cell types equally expressed the transcription factor Sox9 (magenta) 2 and 4 weeks (**T**; Two-Way ANOVA for overall group differences: p = 0.24; for timepoints: p = 0.95). Scale bars in **D**, **I**, **N**, **S**: 100 µm.

More than 95% of all transplanted GFP$^+$ cells expressed the astrocyte marker GFAP early as 2 weeks and constantly expressed GFAP$^+$ 4 weeks after transplantation what perhaps indicate progressing astrocyte maturation. Surprisingly, the expression of the stem cell markers Vimentin and Nestin were found to be unaltered post-transplantation, whereas in contrast, Sox2 expression appeared to be elevated after transplantation and was significantly greater in P1 cortex-derived astrocytes.

Thus, to further examine the maturation state of the grafted astrocytes, the expression of molecular markers specific for maturing and functional astrocytes was immunohistochemically analyzed (**FIG 24**). Besides molecular markers for stem cells (Vimentin, Nestin) and progenitor cells (Sox2, Sox9), astrocytes derived from P3 spinal cord and P1 cortex displayed on overall high expression of markers indicative for mature and functional astrocytes *in vivo*. In particular, immunolabeling analysis revealed that expression of A2B5 may increase in P3 Spinal cord-derived astrocytes from 2 to 4 weeks post-transplantation (**FIG 24A – D**; 52.77 ± 16.52% at 2 weeks vs. 66.61 ± 8.07% of GFP$^+$/GFAP$^+$ cells at 4 weeks, Two-Way ANOVA p = 0.33), whereas A2B5 expression was unaltered in GFP$^+$/GFAP$^+$ cells derived from P1 cortex (Two-Way ANOVA p = 0.91). Similarly, about ~50% of all grafted cells were labeled for AQP4, independent of cell type and timepoint (Two-Way ANOVA p = 0.85), whereas a slightly lower percentage of P1 cortex-derived astrocytes were AQP4$^+$ 4 weeks post-transplantation (Two-Way ANOVA p = 0.37). Analysis of the glutamate transporter GLT-1 (**FIG 24K – O**) revealed a trend

towards an elevating expression in both cell types over time (Two-Way ANOVA p = 0.14). Finally, independent of cell type and time after transplantation, ~80% of all transplanted astrocytes showed immunoreactivity for S100β (**FIG 24P – T**).

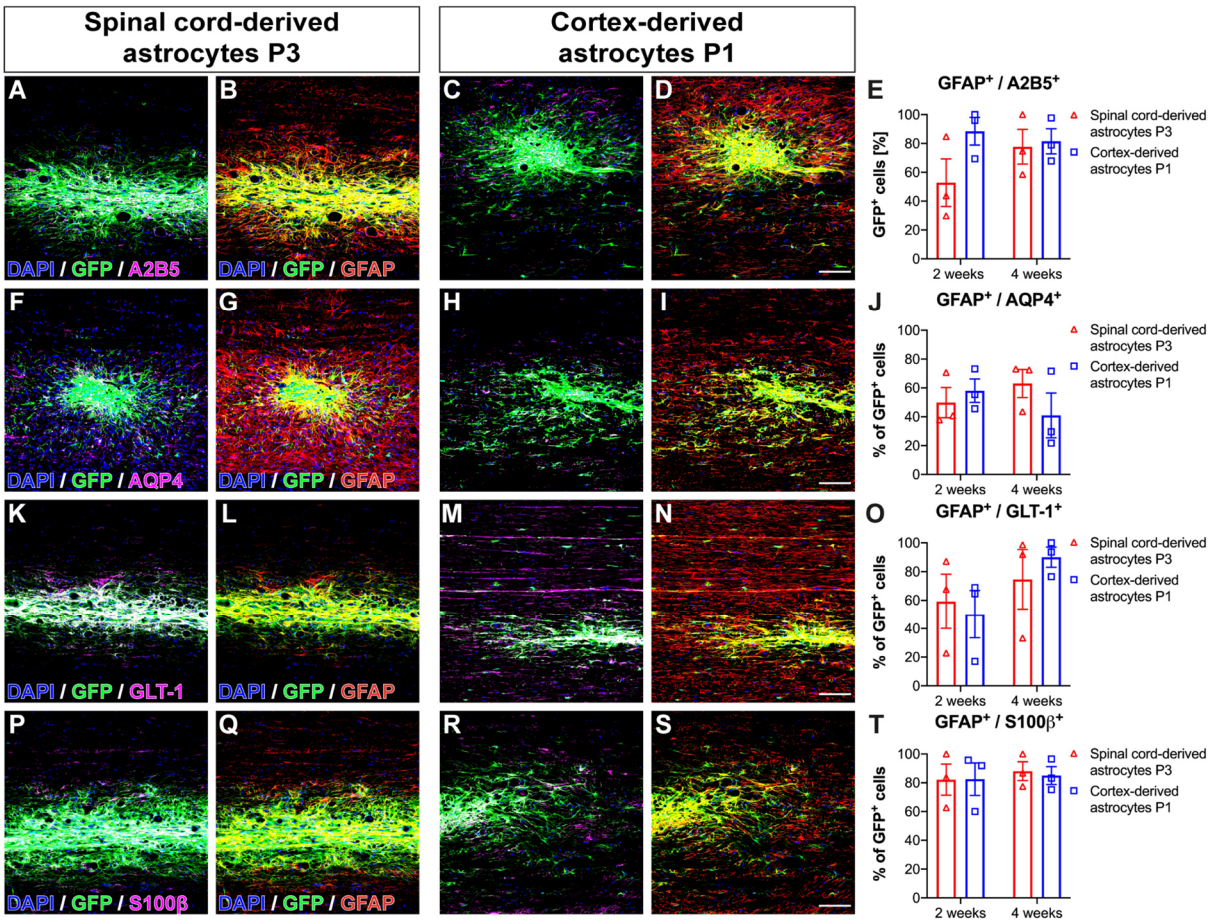

Figure 24: Neonatal P3 spinal cord- and P1 cortex-derived astrocytes express functional astrocyte markers 2 and 4 weeks after transplantation into the intact spinal cord. (**A – E**) Immunolabeling of the transplanted (GFP, green) astrocytes (GFAP, red) for A2B5 (magenta) pointed towards a trend for an increased expression from 2 weeks to 4 weeks after transplantation in P3 Spinal cord-derived astrocytes, whereas the expression was unaltered in P1 cortex-derived astrocytes (Two-Way ANOVA for overall group differences: p = 0.14; for timepoints: p = 0.48; spinal cord-derived astrocytes P3, n = 3/timepoint; cortex-derived astrocytes P1, n = 3/timepoint)). (**F – I**) Both cell types equally showed immunoreactivity for AQP4 (magenta) 2 and 4 weeks post-transplantation (**J**, Two-Way ANOVA for overall group differences: p = 0.56; for timepoints: p = 0.87). (**K – O**) More GFP$^+$/GFAP$^+$ astrocytes from both groups co-expressed GLT-1 4 weeks after transplantation compared to 2 weeks post-transplantation (Two-Way ANOVA for overall group differences: p = 0.85; for timepoints: p = 0.13). (**P – T**) S100β colocalized with GFP$^+$/GFAP$^+$ transplanted astrocytes both derived from spinal cord (**P, Q**) and cortex (**R, S**) and its expression remained unaltered between 2 and 4 weeks post-transplantation independent of the transplanted cell type (**T**, Two-Way ANOVA for overall group differences: p = 0.89; for timepoint: p = 0.66). Scale bars in **D**, **I**, **N**, **S**: 100 µm.

High-resolution confocal imaging of individual GFP$^+$ transplanted cells allowed for qualitative assessment of cell morphology and interaction with the host spinal tissue. Specifically, co-labeling with Connexin-43 (CX43) was used to visualize sites of direct cell-cell contact between astrocytes (Ezan, Andre et al. 2012, Lien, Tuszynski et al. 2019), whereas co-labeling with βIII-tubulin showed astrocyte-axon interactions (**FIG 25**). Both, P3 spinal cord- as well as P1 cortex-derived astrocytes (GFP$^+$), developed process-bearing stellate morphology *in vivo* (**FIG 25A, C**). More importantly, graft-derived astrocytes formed cell-cell contacts to host-derived astrocytes as indicated by the close association of GFP$^+$/CX43$^+$ cell processes (originating from transplanted cells) with GFP$^-$/CX43$^+$ cell processes (originating from the host astrocytic network) (arrowheads, **FIG 25B, D**). Further, transplanted GFP$^+$ astrocyte of both origins extended processes along host axons (arrowheads in **FIG 25F, H**).

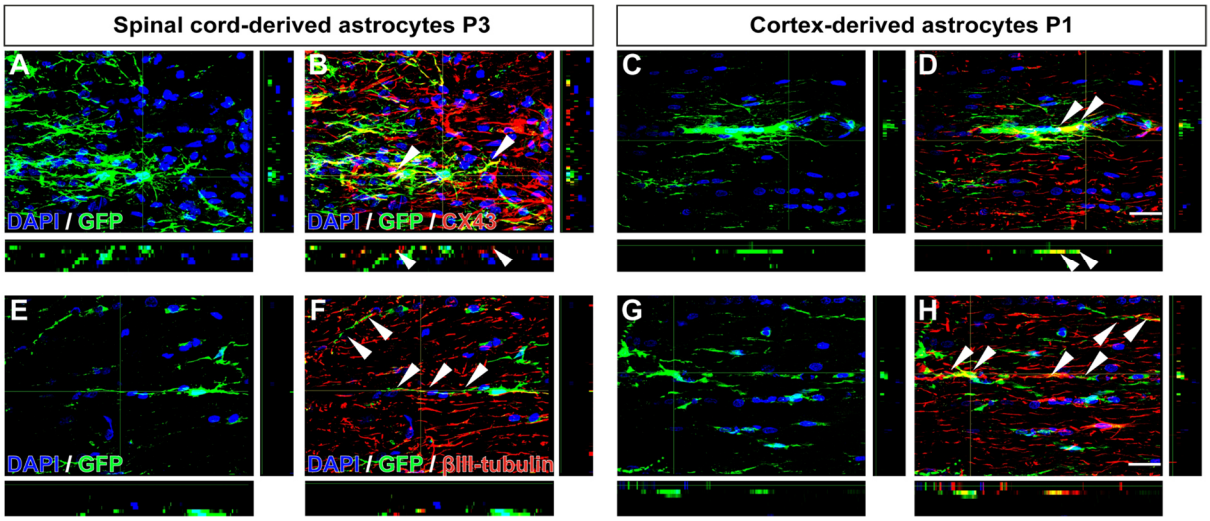

Figure 25: Neonatal P3 spinal cord- and P1 cortex-derived astrocytes associate with the host astrocytic network and align with host axons. (**A – D**) GFP-positive transplanted spinal cord P3- (**A, B**) and P1 cortex-derived astrocytes (**C, D**) and co-expressed CX43 (red) and formed direct cell contact sites with the host astrocytic network (arrowheads, GFP$^-$/CX43$^+$ cells). (**E – H**) Transplanted astrocytes aligned with host axons (βIII-tubulin, red). XZ and YZ planes are shown to underneath and to the right, respectively. Scale bars in **D**, **H**: 25 µm.

Taken together, independent of tissue origin, neonatal astrocytes can be successfully transplanted into the intact spinal cord. The transplanted cells survived for at least 4 weeks and distributed themselves into the adjacent spinal parenchyma without the formation of distinct borders between cell graft and host as previously reported for BMSC- and Schwann cell-containing grafts (Gunther, Weidner et al. 2015, Williams, Henao et al. 2015, Liu, Sandner et al. 2017). Although *in vitro*-characterization revealed a rather immature phenotype for both cell

types, P3 spinal cord- and P1 cortex-derived astrocytes equally expressed GFAP and developed a stellate cell morphology *in vivo* indicating progressing astrocyte maturation. However, most grafted cells still were positively labeled for Vimentin, Nestin and Sox2 2 and 4 weeks post-transplantation but started to additionally express markers specific for differentiating and functional mature astrocytes (A2B5, AQP4, GLT-1, S100β). CX43-positive cell processes of graft- and host-derived astrocytes were found in direct contact with each other, indicating an integration of the grafted cells into the host astrocytic network. In line with this, grafted cells aligned with host axons (**FIG 25F, H**).

3.4 Impact of neonatal spinal cord- derived astrocytes as a cellular growth substrate within alginate-based hydrogel implants and in the surrounding host spinal cord on axonal regeneration after traumatic spinal cord injury

Since astrocytes can be successfully obtained from neonatal spinal cord tissue and afterwards used for transplantation *in vivo*, we sought to test whether they represent a cellular growth substrate within alginate-based hydrogel implants superior to cortex-derived astrocytes used in the previous study (**see 3.2**). As stated in the last section, astrocytes derived from cortex as well as spinal cord harbor the capacity to adopt a mature morphology, express adult astrocyte markers and potentially integrate into the host astrocytic network *in vivo*.

To further improve the integration of the hydrogel implants into the lesion site and thereby maximize axonal growth, the implantation paradigm was modified by combining the results of the previous *in vivo* study and another implantation study parallelly performed in our laboratory (Liu, Sandner et al. 2017). Instead of hydrogel implants with a mean channel diameter of 39.0 $\pm$ 1.6 µm, new alginate-based hydrogels fabricated with Zinc ions (Zn^{2+}) were used resulting in a mean channel diameter of 78.2 $\pm$ 1.7 µm. Thus, the volume of each hydrogel channel was increased providing more space for the seeded astrocytes, infiltrating host cells and penetrating spinal axons. Additionally, the study by Liu et al. provided strong evidence that a continuous cellular substrate spanning the caudal host-graft interface is essential for re-entry of regrowing descending axons into the caudal spinal cord (Liu, Sandner et al. 2017). Hence, we grafted immature astrocytes either derived from P3 spinal cord or P1 cortex 1 mm caudal to the astrocyte-seeded hydrogel implants. Thereby, we sought to improve tissue penetration and consequently improve implant integration into the SCI lesion site.

3.4.1 *Implantation of astrocyte-seeded alginate-based hydrogel implants with additional caudal astrocyte transplantation after traumatic spinal cord injury*

In this study, P1 cortex- and P3 spinal cord-derived astrocytes were used for seeding of the implant as well as caudal cell transplantation (**FIG 26**) and their impact on implant integration as assessed via host-graft interactions and revascularization, and axonal growth were quantitatively and qualitatively analyzed.

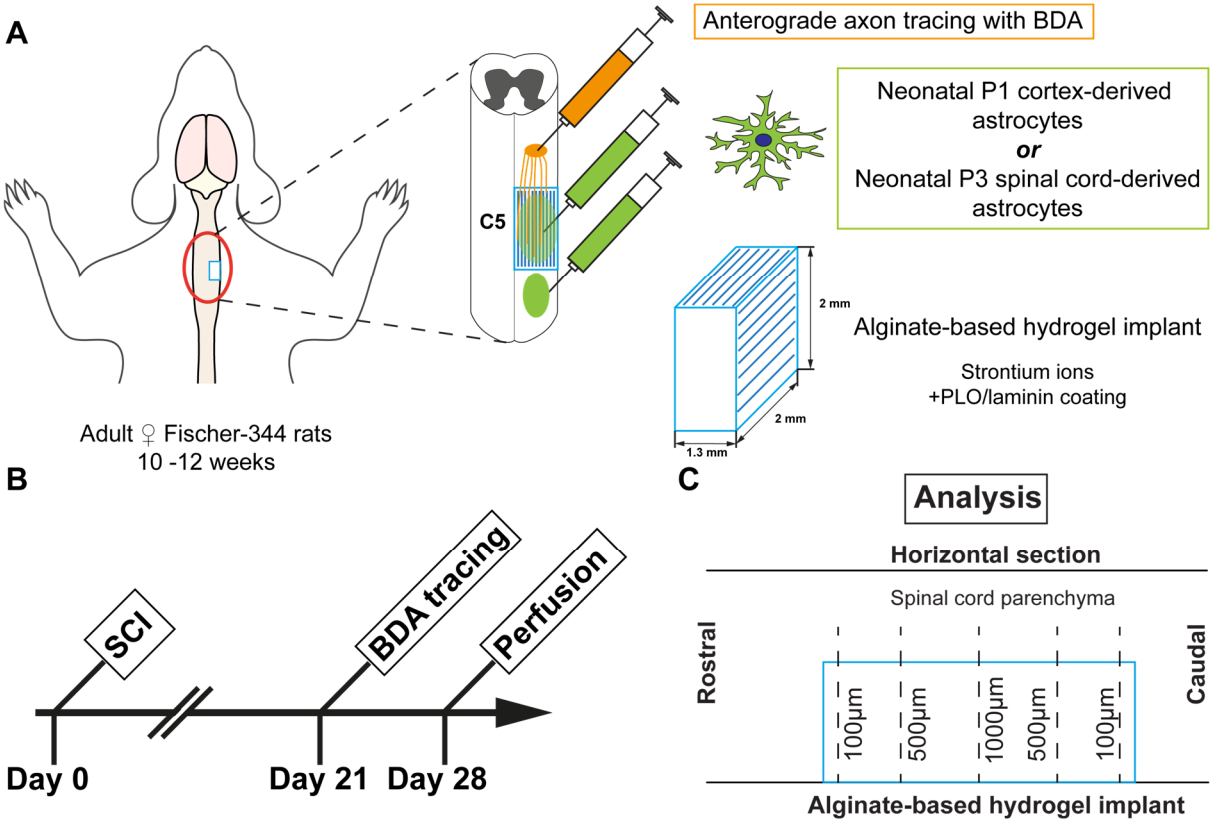

Figure 26: Experimental setup. (**A**) A total of 18 adult female Fischer-344 underwent a unilateral C5 hemisection with immediate implantation of an alginate-based hydrogel implant pre-seeded with either neonatal P1 cortex-derived (GFP^+) or P3 spinal cord-derived astrocytes (GFP^+). Additionally, 100,000 GFP^+ neonatal astrocytes were transplanted into the uninjured host spinal cord 1 mm caudal to the implantation site. After 3 weeks, the anterograde axon tracer BDA (10 kDa) was injected into the cervical spinal cord at C2 to label specifically label descending spinal axons. (**B**) Animals were allowed to survive for 4 weeks, transcardially perfused and (**C**) their spinal cords were immunohistochemically analyzed at 100 µm and 500 µm from the rostral or caudal hydrogel edge, respectively, and at the hydrogel center (1000 µm) (PLO/Laminin, n = 5 (1 animal excluded); + cortex-derived astrocytes, n = 6(1 animal excluded); + spinal cord-derived astrocytes, n = 6; see **Suppl. table 1**).

3.4.1.1 Cell filling and graft cell survival in astrocyte-seeded hydrogel implants in combination with additional astrocyte grafting into the caudal host spinal cord

To assess whether the neonatal spinal cord-derived astrocytes possess superior implant integration capacities and thereby increase axonal regrowth after SCI in comparison to cortex-derived astrocytes, alginate-based hydrogel implants were seeded with neonatal P3 spinal cord- (n = 6) or P1 cortex-derived astrocytes (n = 6, 1 animal had to be excluded from analysis due to destruction of the hydrogel during cryosectioning) and implanted directly into the lesion cavity of a unilateral hemisection injury at C5/6. Additionally, neonatal astrocytes were transplanted into the uninjured host spinal cord 1 mm caudal to the lesion site. Surface coated hydrogels without cell seeding or additional cell grafts served as controls (n = 6, 1 died immediately after SCI). Animals were allowed to recover and finally perfused 4 weeks after SCI; their spinal cords immunohistochemically analyzed (**FIG 27**). Similar to the previous *in vivo*-studies, hydrogel implants of all groups remained structurally intact with no signs of degradation and were integrated into the lesion site without cavitation (**FIG 27A – C**). Independent of cell seeding, most implant channels (> 80% $DAPI^+$ channels) were filled with cells particularly at the channel entries (**FIG 27D**; 100 µm from rostral/caudal hydrogel edge; Two-Way ANOVA for overall group differences: $p = 0.51$). In all groups, cell filling decreased towards the central area of each hydrogel implant, but surprisingly, this decline was most significant in implants seeded with cortex-derived astrocytes (Two-Way ANOVA for distance: $p < 0.0001$, followed by Tukey's *post hoc* $^{**}p < 0.01$ comparing the hydrogel edges with the hydrogel center in the cortex-derived astrocyte group; **see Suppl. table 7**). Within both astrocyte-seeded groups, the survival of the grafted GFP^+ astrocytes was quantified by determining the percentage of $DAPI^+/GFP^+$ channels (**FIG 27E**), and via measuring the GFP-covered channel area (**FIG 27F**). Both methods indicated an overall moderate graft cell survival, since 89.26 ± 0.69% of all cell-filled channels per implant contained GFP-expressing spinal cord-derived graft cells and 81.48 ± 2.51% of all cell-filled channels per implant contained GFP-expressing cortex-derived astrocytes. Noteworthy, in the cortex-derived astrocyte group the fraction of GFP^+ channels might have dropped at the hydrogel center (73.82 ± 8.31% GFP^+ channels) similar to the percentage of $DAPI^+$ channels, whereas, it was constant throughout the rostrocaudal extent in implants seeded with spinal cord-derived cells (**FIG 27E**). Nonetheless, both astrocyte populations equally filled the hydrogel channels as no significant group differences were found when channel area occupied by GFP-expressing graft cells was examined (**FIG 27F**; Two-Way ANOVA $p = 0.33$). Again, less grafted cells were detected at the hydrogel center in both groups (Two-Way ANOVA for distance: $p < 0.001$, followed by Tukey's *post hoc* test $^{**}p < 0.01$ for cortex-

derived astrocytes, *p < 0.05 for spinal cord-derived astrocytes). Finally, most GFP-positive grafted cells from both groups co-expressed GFAP, filled the channel lumen and lined the channel walls within the hydrogel implants 4 weeks after injury (**FIG 27G, H**).

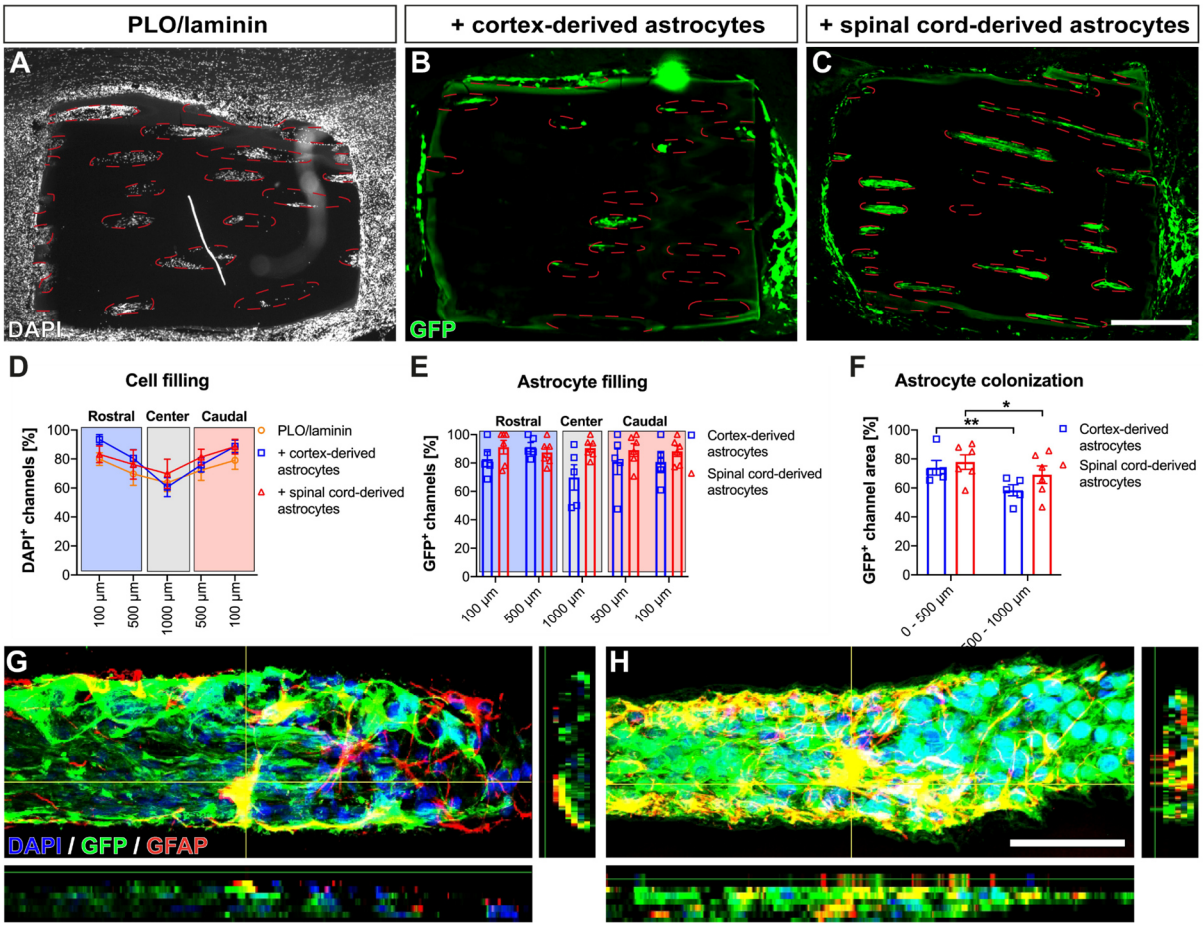

Figure 27: Neonatal P3 spinal cord- and P1 cortex-derived astrocytes fill alginate-based hydrogel implants and survive for at least 4 weeks *in vivo*. (**A – C**) Four weeks after implantation, non-seeded hydrogel implants (**A**), and implants seeded either with neonatal cortex-derived astrocytes (**B**) or spinal cord-derived astrocytes (**C**) were tightly integrated into the lesion cavity with their channels infiltrated with host cells as indicated by DAPI-labeled nuclei (DAPI, white) (**A**) or filled with graft-derived GFP^+ cells (GFP, green) (**B**, **C**). Dashed lines indicate hydrogel channels. Rostral is to the left, medial to the top and caudal to the right. (**D**) Quantification of $DAPI^+$ channels revealed a dense cell filling at the rostral and caudal channel entries and a strong decline towards the hydrogel center in all groups (Two-Way ANOVA for overall group differences: $p = 0.51$; PLO/Laminin, n = 5; + cortex-derived astrocytes, n = 5; + spinal cord-derived astrocytes, n = 6). This decline was most prominent in implants seeded with cortex-derived astrocytes (Two-Way ANOVA for distance: $p < 0.0001$, with Tukey's *post hoc* $^{**}p < 0.001$ comparing channel entries on both sides with hydrogel center). Detailed statistical analysis is depicted in **Suppl. table 7**. (**E**) In hydrogel implants seeded with spinal cord-derived astrocytes, about 86% of all channels were filled with grafted GFP-expressing cells, whereas the percentage of $DAPI^+/GFP^+$ channels in the cortex-derived astrocyte group appeared to be lower at the hydrogel center (Two-Way ANOVA for overall group differences: $p = 0.17$; for distance: $p = 0.28$). (**F**) Similarly, the channel area covered by GFP-positive cells was significantly higher at the channel entries (0 – 500 µm) and decreased towards the hydrogel center (500 – 1000 µm) (Two-Way ANOVA for overall group differences: $p = 0.33$; for distance: $p < 0.001$ with Tukey's *post hoc* $^{**}p < 0.01$ for cortex-derived astrocytes and $^{*}p < 0.05$ for spinal cord-derived astrocytes comparing channel entries and hydrogel center). Blue, red and grey boxes indicate the rostral and caudal hydrogel halves, and the hydrogel center, respectively. (**G, H**) Both, cortex-derived as well as spinal cord-derived astrocytes (GFP, green), primarily co-expressed GFAP (red) and densely filled the hydrogel implants and lined the channel walls. XZ and YZ planes are shown underneath and to the right, respectively. Scale bars in **C**: 500 µm, in **H**: 50 µm.

3.4.1.2 Characterization of neonatal astrocytes transplanted into the caudal host spinal cord

In this study, neonatal astrocytes were also transplanted into the uninjured host spinal cord 1 mm caudal to the implantation site to establish a continuous cellular bridge spanning the caudal host-graft interface (**FIG 28**). Both astrocyte populations survived after injection into the caudal host spinal cord and distributed themselves into the surrounding host spinal parenchyma (**FIG 28A, E**). High-resolution confocal imaging showed that cortex-derived astrocytes adopted a process-bearing cell morphology, whereas spinal cord-derived astrocytes adopted a longitudinal cell shape (**FIG 28B, F**). Moreover, both astrocyte populations distributed themselves into the host astrocytic network. The transplanted cells surprisingly showed a slightly different migratory behavior: neonatal cortex-derived astrocytes spread out widely in rostral and caudal direction from the injection site and were found up to 2 mm caudal from the injection

site. In contrast, astrocytes derived from neonatal spinal cords migrated preferentially in the rostral direction towards the hydrogel implant and only individual cells migrated into the more caudal areas of the host spinal cord (**FIG 28I**). Both astrocyte populations aligned into longitudinal cellular bridges towards the hydrogel implant, forming physical guidance structures for host axons (**FIG 28C, D & G, H**).

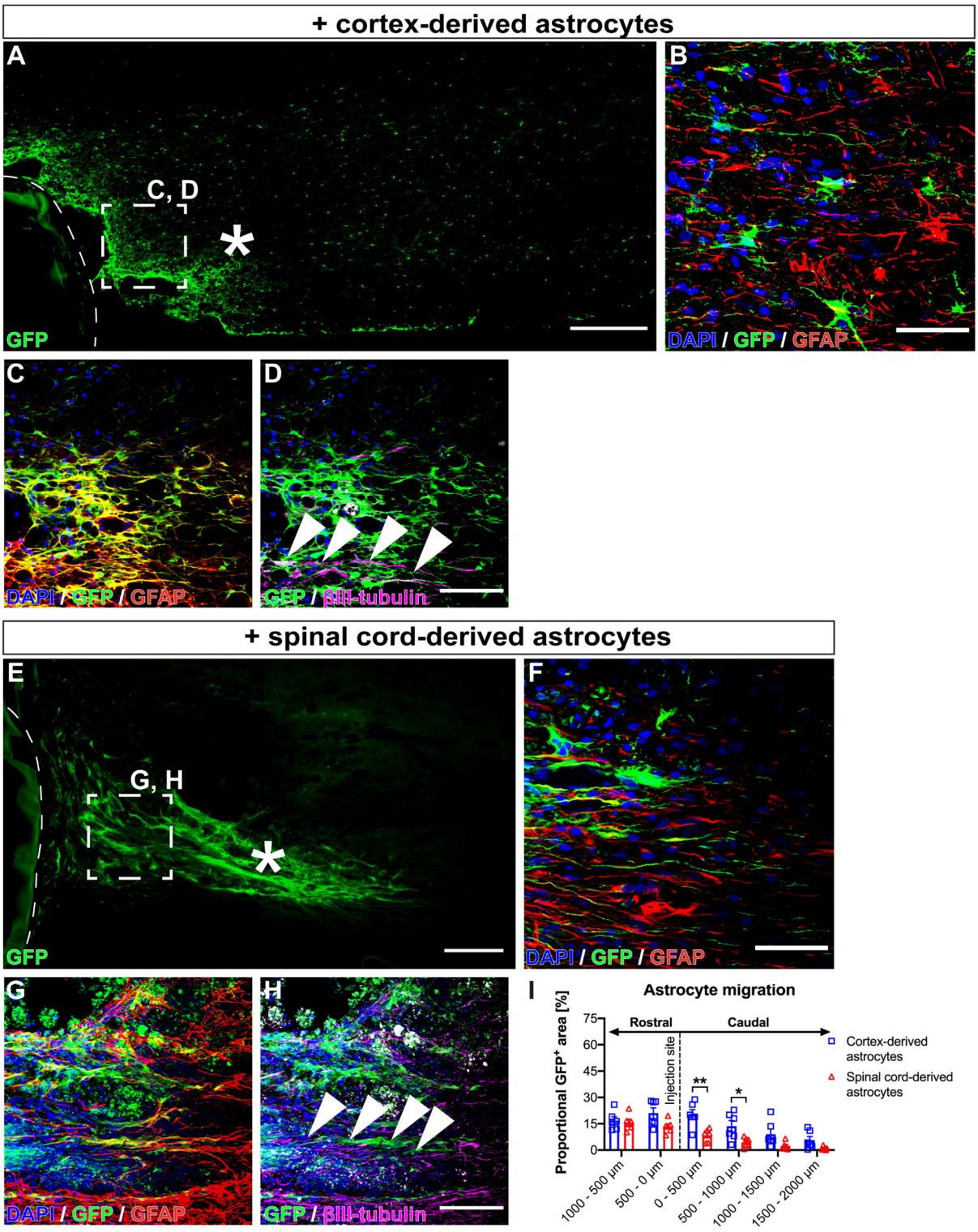

Figure 28: Caudally transplanted neonatal astrocytes spread out into the host spinal parenchyma and bridge the caudal host graft interface. (**A – D**) GFP-labeled neonatal cortex-derived astrocytes (GFP, green) spread out widely into the surrounding host parenchyma (**A**; asterisk indicate injection site). Dashed lines indicate the hydrogel implant. Inlay in **A** is shown at a higher magnification in **C**, **D**. Rostral is to the left, medial to the top and caudal to the right. (**B**) Cortex-derived astrocytes co-expressed GFAP (red), adopted a star-like morphology and distributed themselves into the host astrocytic network ($GFP^-/GFAP^+$). (**C**, **D**) The grafted cortex-derived astrocytes aligned into longitudinal tissue bridges (arrowheads in **D**) and were associated with host axons (βIII-tubulin, magenta). (**E – H**) GFP^+ spinal cord-derived astrocytes preferentially spread towards the hydrogel implant and only for short distances caudally. (**E**; asterisk indicate injection site). Dashed lines indicate the hydrogel implant. Inlay in **E** is shown at a higher magnification in **G**, **H**. Rostral is to the left, medial to the top, and caudal to the right. (**F**) Spinal cord-derived astrocytes co-expressed GFAP and adopted an elongated cell morphology. (**G**, **H**) Similar to cortex-derived astrocytes, they aligned longitudinally and were associated with host axons. (**I**) Graft cell migration was assessed by quantification of the proportional GFP^+ area in the host spinal parenchyma (Two-Way ANOVA for cell type: $p < 0.001$, with Sidak's *post hoc* $^{**}p < 0.01$ comparing both cell types at 0 – 500 µm and $^{*}p < 0.05$ caudal from the injection site; + cortex-derived astrocytes, n = 6; + spinal cord-derived astrocytes, n = 6). Individual GFP-labeled astrocytes from both groups were found within a 3 mm wide interval caudal from the cell injection site (Two-Way ANOVA for distance: $p < 0.0001$). Detailed statistical analysis is depicted in **Suppl. table 8**. Scale bars in **A**, **E:** 500 µm, in **B, F**: 50 µm, in **D**, **H**: 100 µm.

Although both astrocyte populations survived within the host spinal cord, they still exhibited a slightly different cell morphology and migratory behavior after transplantation. Given the rather immature phenotype of both astrocyte populations *in vitro*, their GFAP and Vimentin expression was assessed *in vivo* to determine whether the possibly observed morphological differences might be due to a differing maturation and/or reactivity states following transplantation (**FIG 29**). Independent of their tissue origin, the vast majority of all transplanted GFP^+ neonatal astrocytes expressed GFAP (**FIG 29A – L, M**; cortex-derived astrocytes: 93.78 ± 1.5% $GFP^+/GFAP^+$ cells, spinal cord-derived astrocytes: 92.11 ± 1.58% $GFP^+/GFAP^+$ cells, unpaired Students' t-test $p = 0.46$). Additionally, more than 70% of the grafted $GFAP^+$ astrocytes were co-labeled with Vimentin in both groups (unpaired Students' t-test $p = 0.55$). Similarly, proliferation capacity was not different between the cortex- and spinal cord-derived astrocytes (cortex-derived astrocytes: 15.54 ± 3.39% $GFP^+/GFAP^+/Ki67^+$ cells vs. spinal cord-derived astrocytes: 22.8 ± 5.66% $GFP^+/GFAP^+/Ki67^+$ cells, unpaired Students' t-test $p = 0.3$). Surprisingly, the percentage of Vimentin-expressing $GFAP^+$ astrocytes was remarkably lower compared with the fraction of $GFP^+/GFAP^+/Vim^+$ graft-derived cells after transplantation into the intact spinal cord (**FIG 29E**; cortex-derived astrocytes: 86.64 ± 5.31% $GFP^+/GFAP^+/Vim^+$ cells, spinal cord-derived astrocytes: 91.61 ± 2.81% $GFP^+/GFAP^+/Vim^+$ cells).

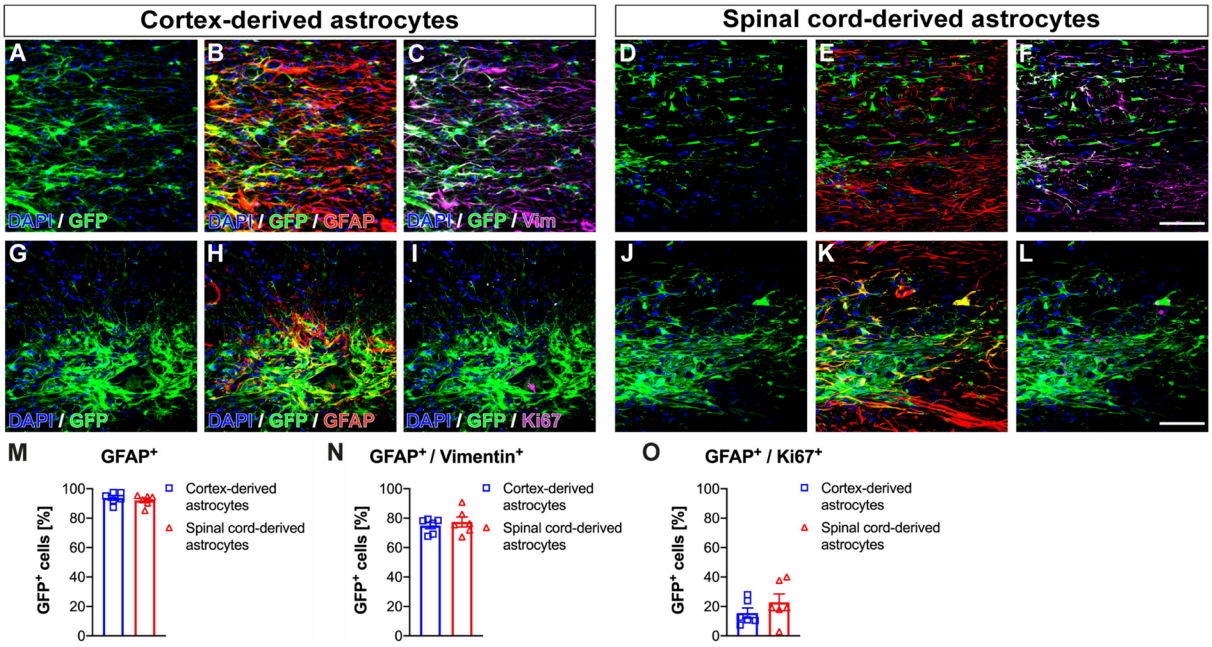

Figure 29: Caudally transplanted neonatal astrocytes co-express Vimentin and are partially proliferative. (**A – C**) Cortex-derived and (**D – F**) spinal cord-derived neonatal astrocytes (GFP, green) co-expressed GFAP (red) as well as Vimentin (magenta) 4 weeks after transplantation into the caudal host spinal cord. (**G – L**) Additionally, ~20% of the grafted astrocytes ($GFP^+/GFAP^+$) were proliferative as indicated by Ki67 (magenta) expression. Rostral is to the left, medial to the top, and caudal to the right. (**M**) Quantification of immunolabeling showed that >90 % of all transplanted cells expressed GFAP (unpaired Students' t-test p = 0.46; + cortex-derived astrocytes, n = 6; + spinal cord-derived astrocytes, n = 6) and a great fraction additionally co-expressed Vimentin (**N**, unpaired Students' t-test p = 0.55). (**O**) Quantification of Ki67 immunolabeling revealed no significant differences between cortex- and spinal cord-derived astrocytes (unpaired Students' t-test p = 0.3). Scale bars in **F**, **B**: 75 µm.

3.4.1.3 Vascularization of astrocyte-seeded hydrogel implants

Previously, thin blood vessels were found within the channels of astrocyte-seeded alginate-based hydrogel implants previously (**FIG 14**), therefore, vascularization was immunohistologically analyzed for implants seeded with either neonatal cortex- or spinal cord-derived astrocytes as well (**FIG 30**). Instead of anti-von Willebrand factor, an antibody against the endothelial cell marker CD31 was used to detect endothelial cells and thereby blood vessels. The CD31 antibody and the according tissue processing protocol were kindly provided by the laboratory of Carmen Ruiz de Almodovar (University of Mannheim). In particular, endothelial cells and blood vessels were detected in all hydrogel implants independent of astrocyte co-transplantation (**FIG 30A – C**). However, the channel area that was occupied with CD31-labeled endothelial cells was enhanced in astrocyte-seeded implants (**FIG 30D**, One-Way

ANOVA $p < 0.05$) and reached significance in implants seeded with astrocytes derived from neonatal spinal cord (*$p < 0.05$) but not for implants seeded with cortex-derived cells due to the high variance in this group ($p = 0.06$). Nevertheless, vascularization was similar in both astrocyte-seeded groups ($p = 0.98$). Within astrocyte-seeded implants, the grafted GFP^+ astrocytes were found in close spatial association with the CD31-labeled blood vessels. Hence, the tubular blood vessels seemed to be partially enwrapped by the grafted astrocytes (arrowheads in **FIG 30B, C**), which becomes even more evident when examining the respective XZ planes.

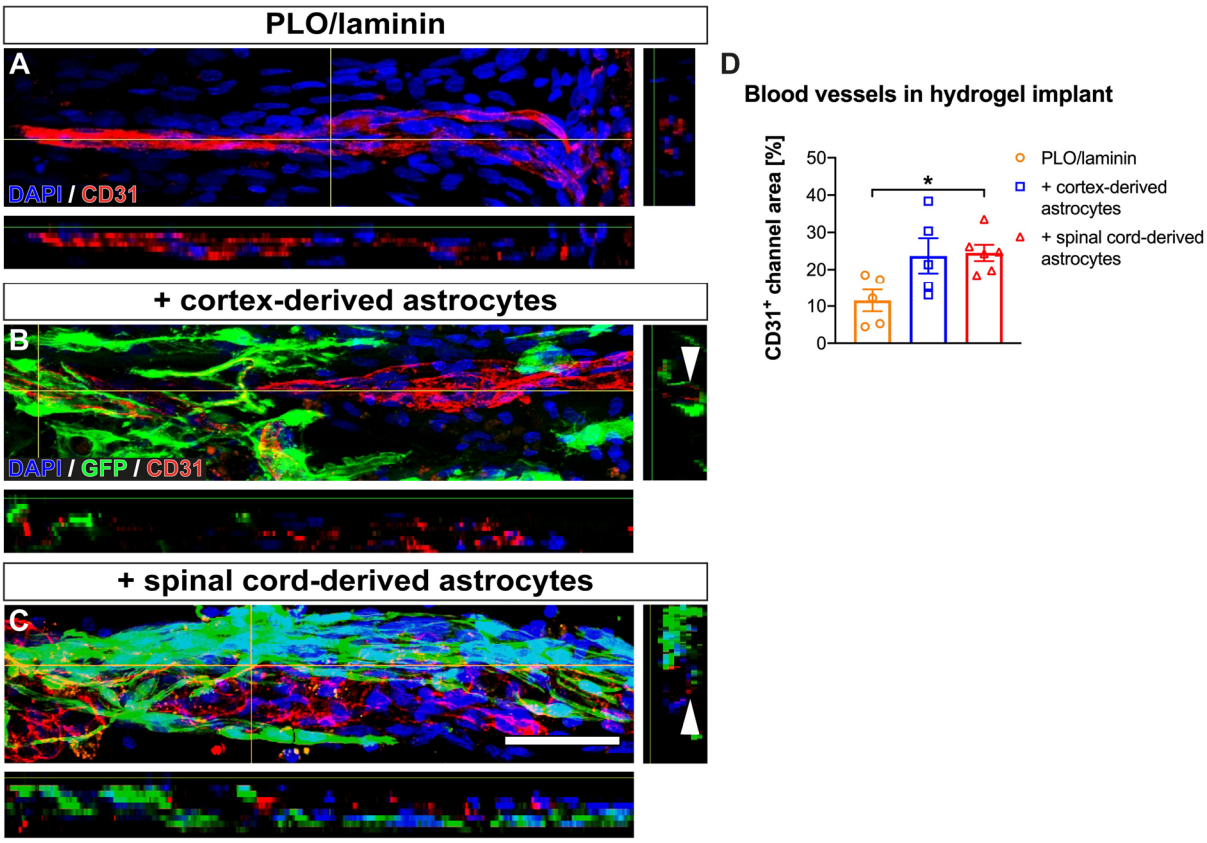

Figure 30: Newly formed vasculature is predominantly found in alginate-based hydrogel implants seeded with neonatal astrocytes. (**A – C**) Immunolabeling with CD31 (red) indicated tubular aggregates of endothelial cells representing thin blood vessels within the channels of control hydrogels (**A**), implants seeded with neonatal cortex-derived astrocytes (**B**), and astrocytes derived from neonatal spinal cord (**C**) 4 weeks after SCI. The XY and XZ planes are shown underneath and to the right, respectively. Both, cortex- as well as spinal cord-derived astrocytes were found in direct contact with $CD31^+$ endothelial cells and lined blood vessels within the hydrogel channels (arrowheads in **B**, **C**). (**D**) Quantification of $CD31^+$ area per hydrogel channel revealed a greater vascularization of astrocyte-seeded hydrogel implants compared to non-seeded controls (One-Way ANOVA $p < 0.05$, with Tukey's *post hoc* *$p < 0.05$ comparing controls with +spinal cord-derived astrocytes; PLO/Laminin, n = 5; + cortex-derived astrocytes, n = 5; + spinal cord-derived astrocytes, n = 6). Scale bar in **C**: 50 µm.

3.4.1.4 Axonal growth into astrocyte-seeded alginate-based hydrogel implants with additional caudal astrocytic grafts

Growth responses of host spinal axons were investigated to assess whether (1) the combination of cell-seeded hydrogel implants with additional caudal cell transplantation, and/or (2) neonatal spinal cord-derived astrocytes, positively affect axonal regeneration. First, immunolabeling with the neuronal marker βIII-tubulin was used to detect overall axonal growth within the channels of hydrogel implants 4 weeks post-injury (**FIG 31**). Consistent with previous observations, host spinal axons could be found in non-seeded controls as well as astrocyte-seeded hydrogel implants. Only individual axons and thin axon bundles were found in non-seeded implants (**FIG 31A**), whereas, in implants that were seeded with either neonatal cortex-derived astrocytes (**FIG 31B**) or spinal cord-derived astrocytes (**FIG 31C**) prior to implantation, thick axon bundles were detected. Quantitatively, astrocyte-seeded hydrogel implants showed a greater number of axons per cell-filled ($DAPI^+$ channel) (**FIG 31D**). In particular, the axon number was greatest at the channel entries, especially on the rostral side of the implant, but appeared to be reduced at the central area of the implants (Two-Way ANOVA for distance: $p = 0.21$). At the rostral channel entries, significantly more axons per channel were detected in implants seeded with spinal cord-derived astrocytes compared to all other implants (Two-Way ANOVA for overall group differences: $p < 0.05$, with Tukey's *post hoc* $^{**}p < 0.01$ comparing spinal cord-derived astrocytes with cortex-derived astrocytes and with controls, see **Suppl. table 9**). Unfortunately, this effect diminished towards the central area of the implants. When the axonal growth within the entire hydrogel implant was analyzed, the greater axonal growth in both astrocyte-seeding groups was confirmed (**FIG 31E**). At all analyzed distances within the implants, the axonal growth was at least 2-fold greater in the spinal cord-derived astrocyte group compared with control hydrogels and 1.5-fold higher than in the cortex-derived astrocyte group (Two-Way ANOVA for overall group differences: $p < 0.05$ with Tukey's *post hoc* test $^{*}p < 0.05$ comparing spinal cord-derived astrocytes with controls, **see Suppl. table 10**). Axonal growth in implants seeded with cortex- and spinal cord-derived astrocyte remained constant throughout the implants. Although, axonal growth in controls appeared to have declined at the hydrogel center but this effect did not reach significance (Two-Way ANOVA for distance: $p = 0.07$). Most important, axons showed a strong preference for both grafted astrocyte populations as their growth substrate compared to infiltrated host cells within the same implant in all analyzed areas of the implants (**FIG 31F**). More precisely, in implants containing cortex-derived astrocytes, 90.44 ± 1.61% of all axons were found in channels filled with the grafted cells; in the spinal cord-derived astrocyte group, 90.9 ± 0.17% of all axons preferentially extended on grafted cells rather than on infiltrated host cells (Two-Way ANOVA $p < 0.001$). In comparison

to the previous study, in which immature cortex-derived astrocytes were only seeded into the alginate-based hydrogels (**FIG 15**), the number of βIII-tubulin-labeled axons per cell-filled channels was enhanced by approximately 27% in implants seeded with P1 cortex-derived astrocytes with additional caudal cell grafts (astrocyte seeding only: 7.11 ± 0.91 axons/cell-filled channel at Rostral 100 µm vs. astrocytes seeding + caudal astrocytic graft: 9.01 ± 2.51 axons at Rostral 100 µm) and even more intriguingly by 315% when P3 Spinal cord-derived astrocytes were used. At the rostral channel entries, implants seeded with P1 cortex-derived astrocytes from the previous study contained on average 7.11 ± 0.91 axons/cell-filled channel, whereas implants of the P3 spinal-cord derived astrocyte contained 29.56 ± 15.22 axons. Similarly, also the overall axonal growth per hydrogel implant could be further enhanced when astrocyte-seeded implants were combined with additional caudal astrocytic grafts compared with the results of the previous study (+ 37% for cortex-derived astrocytes, + 140% for spinal cord-derived astrocytes).

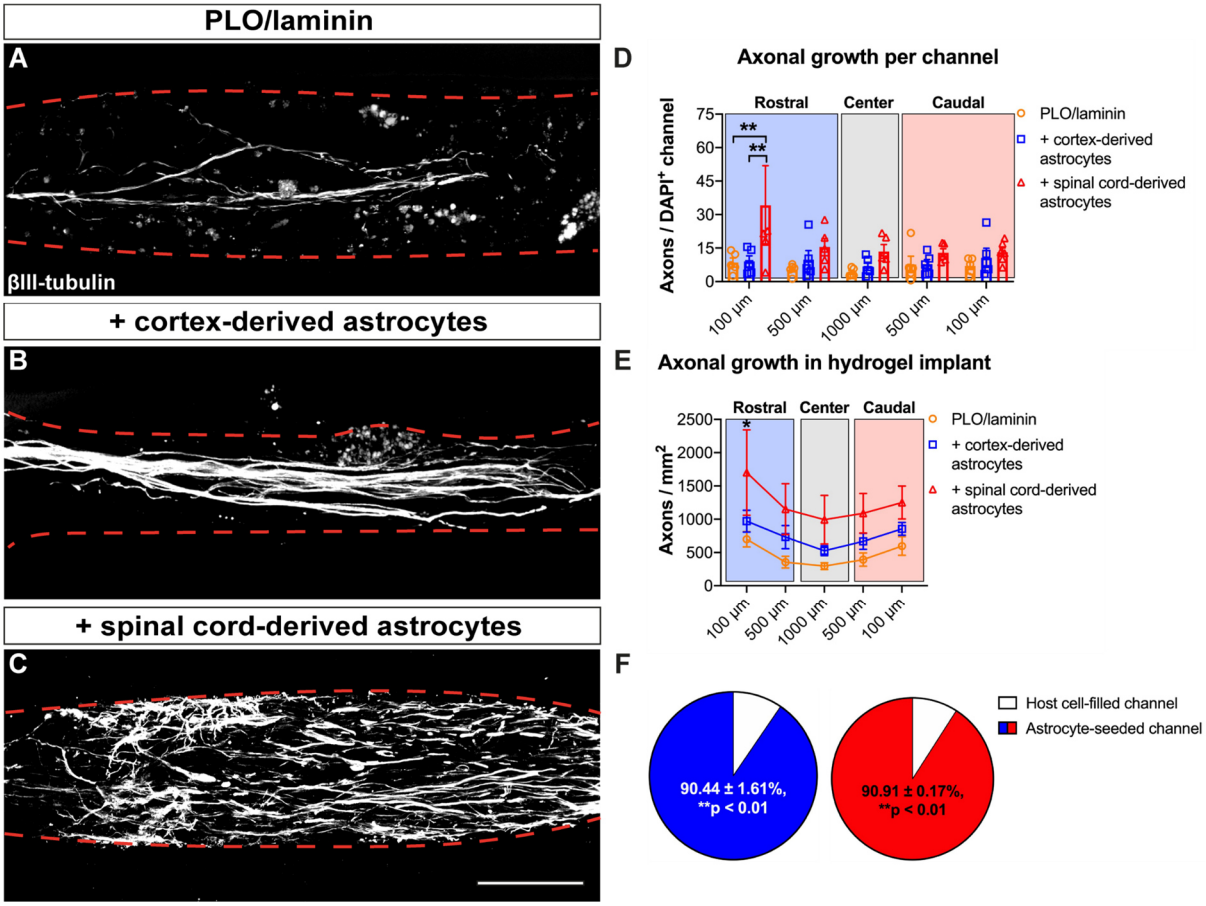

Figure 31: Seeded neonatal astrocytes together with additional caudal astrocytic grafts improve axonal growth within alginate-based hydrogel implants. (**A, B**) βIII-tubulin-labeled host axons (white) entered and extended within the channels of hydrogel implants without cell seeding (**A**), implants seeded with either neonatal cortex-derived astrocytes (**B**) or spinal cord-derived astrocytes (**C**). Dashed lines indicate channel walls. Rostral is to the left, medial to the top, and caudal to the right. (**D**) Quantification of axons per $DAPI^+$ channel depicted an overall greater axonal growth within astrocyte-seeded hydrogel implants compared to non-seeded controls (Two-Way ANOVA for overall group differences: $p < 0.05$, followed by Tukey's *post hoc* test $^{**}p < 0.01$ comparing spinal cord-derived astrocytes with cortex-derived astrocytes and with controls at Rostral 100 µm; PLO/Laminin, n = 5; + cortex-derived astrocytes, n = 5; + spinal cord-derived astrocytes, n = 6). However, the number of axons per channel may have declined towards the hydrogel center in all groups (Two-Way ANOVA for distance: $p = 0.21$). Detailed statistical analysis is depicted in **Suppl. table 9**. Blue, red and grey boxes indicate the rostral and caudal hydrogel halves, and the hydrogel center, respectively. (**E**) Overall, constantly more axons were found over the entire extent in astrocyte-seeded hydrogel implants compared with control implants (Two-Way ANOVA for overall group differences: $p < 0.05$, followed by Tukey's *post hoc* $^{*}p < 0.05$ comparing spinal-cord-derived astrocytes with controls at Rostral 100 µm, for distance: $p = 0.07$). Detailed statistical analysis is depicted in **Suppl. table 10**. (**F**) Axons preferentially entered hydrogel channels filled with the grafted neonatal cortex-derived astrocytes (blue) or spinal cord-derived astrocytes (red) compared to channels containing only infiltrated host cells (white) in each hydrogel implant (Two-Way ANOVA for cell substrate within channels: $p < 0.0001$, with Tukey's *post hoc* $^{**}p < 0.01$ comparing axons in $DAPI^+/GFP^-$ channels with axons in $DAPI^+/GFP^+$ channels). Scale bar in **C**: 50 µm.

Analogous to previous studies, regrowth of the raphespinal tract was assessed by immunolabeling using an antibody specific for serotonin (5-HT) (**FIG 32**). In line with the results for overall axonal growth within the hydrogel implants, a greater number of 5-HT-labeled axons were detected in implants seeded with cortex- or spinal cord-derived astrocytes compared with non-seeded control hydrogels (**FIG 32A – C**; Two-Way ANOVA $p < 0.05$), however, this was mostly restricted to the rostral half of the hydrogel implants (Two-Way ANOVA for distance: $p < 0.0001$). This observation was consistent for the number of axons per cell-filled channel as well as the overall number of serotonergic axons per hydrogel implant (**FIG 32D, E**). At the rostral end (100 µm), significantly more $5\text{-}HT^+$ axons per channel were found in both astrocyte-seeded groups ($^{*}p < 0.05$ for cortex-derived astrocytes: 4.92 ± 1.35 $5\text{-}HT^+$ axons/$DAPI^+$ channels; $^{**}p < 0.01$ for spinal cord-derived astrocytes: 5.01 ± 2.26 $5\text{-}HT^+$ axons/$DAPI^+$ channels vs. control: 1.51 ± 0.39 $5\text{-}HT^+$ axons/$DAPI^+$ channels). When the central and caudal areas of the implants were examined, only single $5\text{-}HT^+$ axons per channel were found in all groups. Overall, about 1.5- to 2-fold more $5\text{-}HT^+$ axons entered implants that were seeded with neonatal astrocytes (Two-Way ANOVA $p < 0.05$). In particular, the differences between non-seeded controls and implants seeded with cortex-derived astrocytes ($^{\#\#\#\#}p < 0.0001$) and spinal cord-

derived astrocytes (*p < 0.05) were strongest at the rostral channel entries and diminished with rising distance from the rostral hydrogel edge (Two-Way ANOVA for distance: p < 0.0001, see **Suppl. table 11**; Interaction between cell type and distance: p < 0.05) (**FIG 32E**). Importantly, similar to βIII-tubulin-labeled axons, serotonergic axons also preferred graft-derived astrocytes containing channels over channels that were filled with infiltrated host cells. This effect was consistently observed for both astrocyte populations (Two-Way ANOVA p < 0.001, followed by Tukey's *post hoc* *p < 0.05 for cortex-derived astrocytes vs. infiltrated host cells; **p < 0.01 for spinal cord-derived astrocytes vs. infiltrated host cells). Similar to the βIII-tubulin-labeled axons, by combining astrocyte seeding of the hydrogel implant with additional caudal astrocytic grafts, growth of serotonergic axons was further enhanced compared to the previous study (**FIG 16**). For example, at the rostral hydrogel edge, animals that received implants seeded with cortex-derived astrocytes and additional caudal grafts contained about 50% more 5-HT-labeled axons per channel (astrocyte seeding only: 3.28 ± 1.11 5-HT$^+$ axons/cell-filled channel at Rostral 100 µm vs. astrocyte seeding + caudal graft: 4.91 ± 1.48 5-HT$^+$ axons/cell-filled channel at Rostral 100 µm). This effect was comparably strong when the data obtained for seeding and co-transplantation of spinal cord-derived astrocytes were compared with the results of the initial astrocyte seeding study (astrocyte seeding + caudal graft: 5.01 ± 2.26 5-HT$^+$ axons/cell-filled channel at Rostral 100 µm).

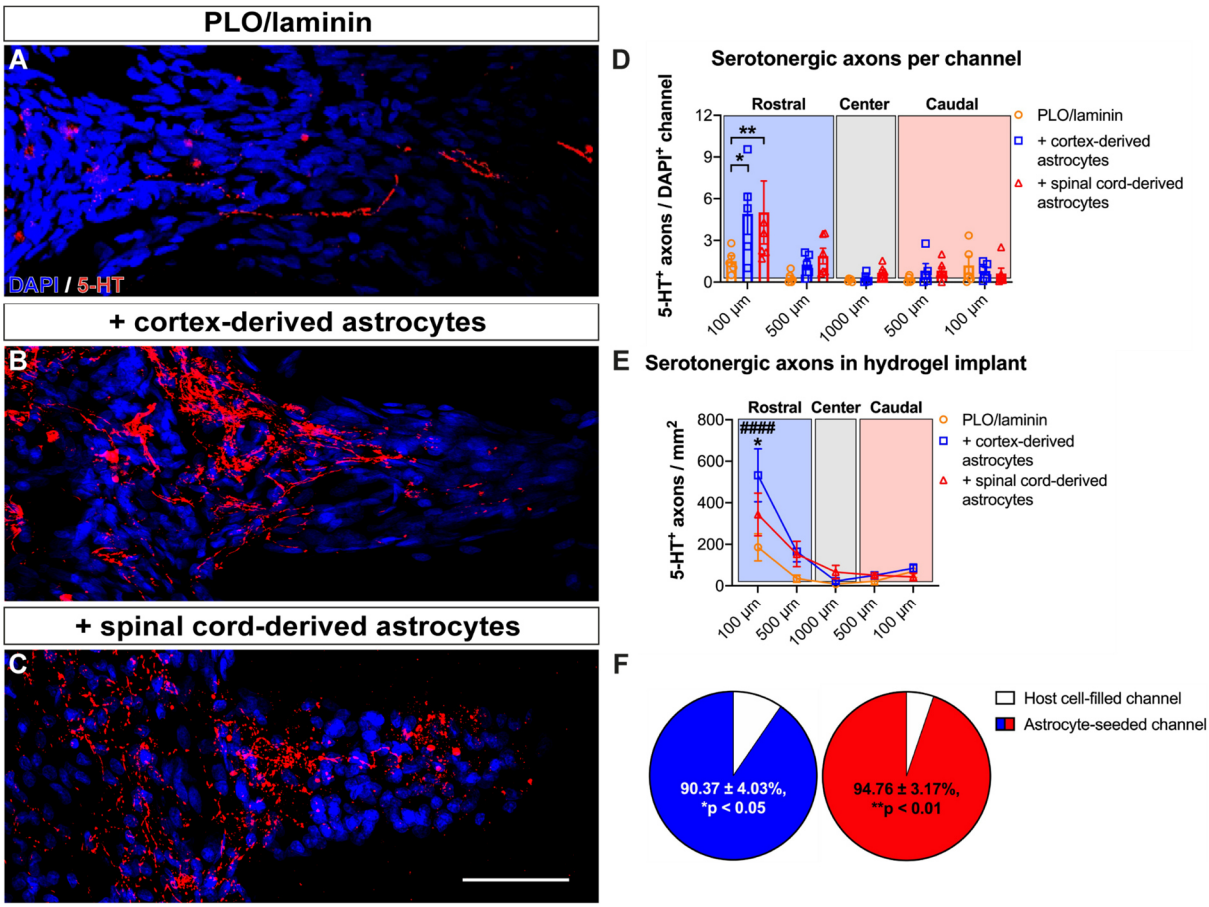

Figure 32: Growth of serotonergic axons is increased within astrocyte-seeded hydrogel implants with additional caudal astrocytic grafts. (**A – C**) Immunolabeling with 5-HT (red) showed serotonergic axons entering and extending within the channels of non-seeded hydrogel implants (**A**) or implants seeded with cortex-derived astrocytes (**B**) or seeded with spinal cord-derived astrocytes (**C**). (**D**) Per cell-filled channel, more 5-HT-labeled axons were detected in both astrocyte-seeded groups compared to controls (Two-Way ANOVA for overall group differences: $p < 0.05$, with Tukey's *post hoc* at rostral 100 µm: *$p < 0.05$ comparing control with cortex-derived astrocytes; **$p < 0.01$ comparing controls with spinal cord-derived astrocytes; PLO/Laminin, n = 5; + cortex-derived astrocytes, n = 5; + spinal cord-derived astrocytes, n = 6). However, the 5-HT$^+$ axons failed to extend over longer distances within the hydrogel channels (Two-Way ANOVA for distance: $p < 0.0001$), which was most prominent in both astrocyte-seeded groups. Detailed statistical analysis is depicted in **Suppl. table 11**. Blue, red and grey boxes indicate the rostral and caudal hydrogel halves, and the hydrogel center, respectively. (**E**) Quantification of the entire hydrogel implants revealed a significantly greater number of 5-HT-labeled axons, especially at the rostral channel entries in astrocyte-seeded implants (Two-Way ANOVA for overall group differences: $p < 0.05$) which became similar to controls at the central and caudal areas of the implants (Two-Way ANOVA for distance: $p < 0.0001$. Detailed statistical analysis is depicted in **Suppl. table 12**. (**F**) Consistent with previous observations, significantly more serotonergic axons were found in channels containing the grafted astrocytes than in channels that only contained infiltrated host cells in the same hydrogel implant (Two-Way ANOVA for cell substrate within channels: $p < 0.001$, with Tukey's *post hoc* *$p < 0.05$, **$p < 0.01$ comparing axons in DAPI$^+$/GFP$^-$ channels with axons in DAPI$^+$/GFP$^+$ channels). Scale bar in **C**: 50 µm.

Descending spinal axons were specifically labeled with the anterograde tracer BDA (10 kDa) rostral to the hydrogel, therefore, BDA-traced axons were primarily found at the rostral end of the hydrogel implants (**FIG 33**). Although BDA-labeled axons were present in the hydrogels of all 3 groups, a slightly greater number of them were found in astrocyte-seeded implants, especially in the spinal cord-derived astrocyte groups (**FIG 33D**; Two-Way ANOVA for overall group differences: $p < 0.05$, with Tukey's *post hoc* test *$p < 0.05$ comparing controls with spinal cord-derived astrocytes at Rostral 100 µm, see **Suppl. table 13**). In the central and caudal areas of the hydrogel channels, BDA-traced axons were occasionally detected independent of group identity, in the more central and caudal areas of the hydrogel channels, no significant differences were found (Two-Way ANOVA for distance: $p = 0.12$). When normalized to the entire hydrogel implant area, overall slightly more BDA-traced axons were present in both astrocyte-seeded groups compared to non-seeded control implants (**FIG 33E**, see **Suppl. table 14**). Although this effect appeared to be strongest in the rostral halves of the implants, due to high variability, no significant differences were observed between groups (Two-Way ANOVA $p = 0.28$). Consistent with the reduced number of BDA-axons per channel, the total number of BDA-traced descending axons was dramatically decreased at the center and caudal half of the

implants (Two-Way ANOVA for distance: $p < 0.05$). Similar to previous results, BDA-traced axons strikingly preferred the seeded astrocyte populations as their growth substrate over host cells within the hydrogel channels (**FIG 33F**; Two-Way ANOVA $p < 0.0001$).

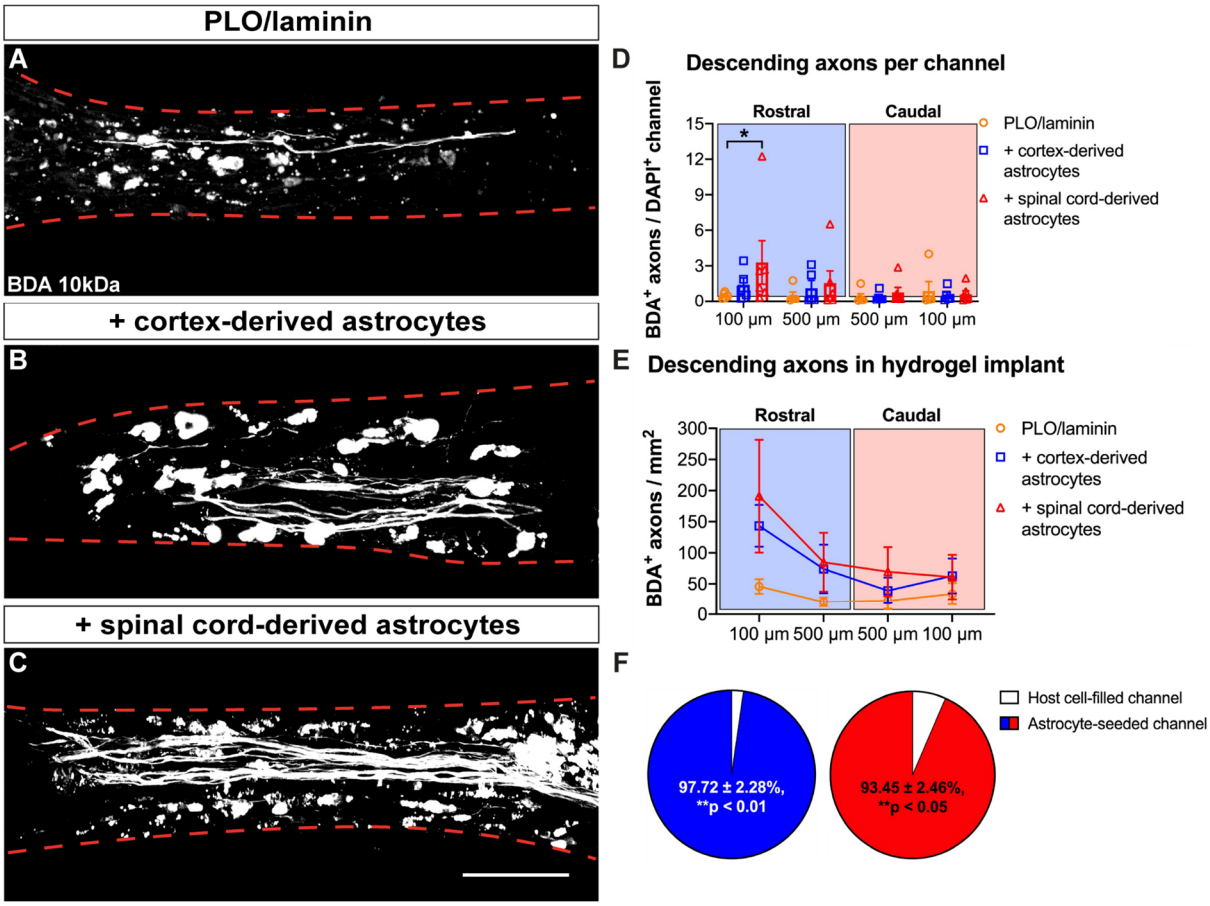

Figure 33: Growth of descending axons is enhanced within astrocyte-seeded hydrogel implants with additional caudal astrocytic grafts. (**A – C**) Descending spinal axons entered the channels of non-seeded controls (**A**) and implants seeded with neonatal cortex-derived astrocytes (**B**) or spinal cord-derived astrocytes (**C**). Dashed lines indicate channel walls. Rostral is to the left, medial to the top and caudal to the right. (**D**) Throughout the implants, a greater number of BDA-labeled axons per individual cell-filled channel was observed in astrocyte-seeded implants (Two-Way ANOVA for overall group differences: $p < 0.05$, with Tukey's *post hoc* $^{*}p < 0.05$ comparing spinal cord-derived astrocytes vs. controls at rostral 100 µm), although at the center and caudal areas of the implants no differences were observed (Two-Way ANOVA for distance: $p = 0.12$; PLO/laminin, $n = 5$; + cortex-derived astrocytes, $n = 5$; + spinal cord-derived astrocytes, $n = 6$). Detailed statistical analysis is depicted in **Suppl. table 13**. Blue and red boxes indicate the rostral and caudal hydrogel halves, respectively. (**E**) Although, a trend towards an elevated number of BDA-traced axons in both astrocyte-seeded groups was found, this did not reach significance due to the high variability (Two-Way ANOVA for overall group differences: $p = 0.28$). However, only a small number of BDA^{+} axons extended over long distances within the hydrogel channels (Two-Way ANOVA for distance: $p < 0.05$). This decline in axon numbers towards the hydrogel center was most prominent in the implants that contained spinal cord-derived astrocytes ($^{*}p < 0.05$ comparing rostral 100 µm with the caudal half of the implant). Detailed statistical analysis is depicted in **Suppl. table 14**. (**E**) Within both astrocyte-seeded groups, BDA^{+} axons showed a strong preference for the grafted astrocytes as growth substrate within the channels compared to infiltrated host cells (Two-Way ANOVA for cell substrate within channels: $p < 0.001$, with Tukey's *post hoc* $^{**}p < 0.01$ comparing axons in $DAPI^{+}/GFP^{-}$ channels with axons in $DAPI^{+}/GFP^{+}$ channels) Scale bar in **C**: 50 µm.

In summary, the results of the previous *in vivo* study (Schackel, Kumar et al. 2019) could be confirmed with neonatal cortex- as well as spinal cord-derived astrocytes used for seeding of the hydrogel implants. The additional caudal astrocyte grafts facilitated improved host-graft interactions as assessed by migration of the grafted cells into the surrounding host spinal parenchyma, establishment of a continuous cellular bridge spanning the caudal host-graft interface, and vascularization of the hydrogel implants. Importantly, both astrocyte populations equally supported axonal growth into and within the alginate-based hydrogel implants with only minor differences found between them.

3.5 Implantation of astrocyte-seeded alginate-based hydrogel implants together with additional astrocytic grafts into the rostral and caudal host spinal cord after traumatic spinal cord injury

Since the previous *in vivo* studies underlined the importance of a tight hydrogel integration into the lesion site and given that additional cell grafts into the caudal host spinal cord improved host-graft interactions, we conducted a study in which PLO/laminin-coated alginate-based hydrogel implants (Zn^{2+}, channel diameter: 88.6 ± 2.9 µm) were seeded with either GFP-expressing neonatal P1 cortex-derived astrocytes or P3 spinal cord-derived astrocytes and implanted into the cavity of a C5 hemisection lesion. In addition, astrocytes were grafted 1 mm rostral and caudal to the implantation site to maximize host-graft interactions and thereby further improve axonal growth through the hydrogel implant. Moreover, in contrast to the previous experiments, animals were allowed to survive for 8 weeks to test whether a longer survival time would enable descending spinal axons to completely traverse the injury site and re-enter the caudal host spinal cord (**FIG 34**).

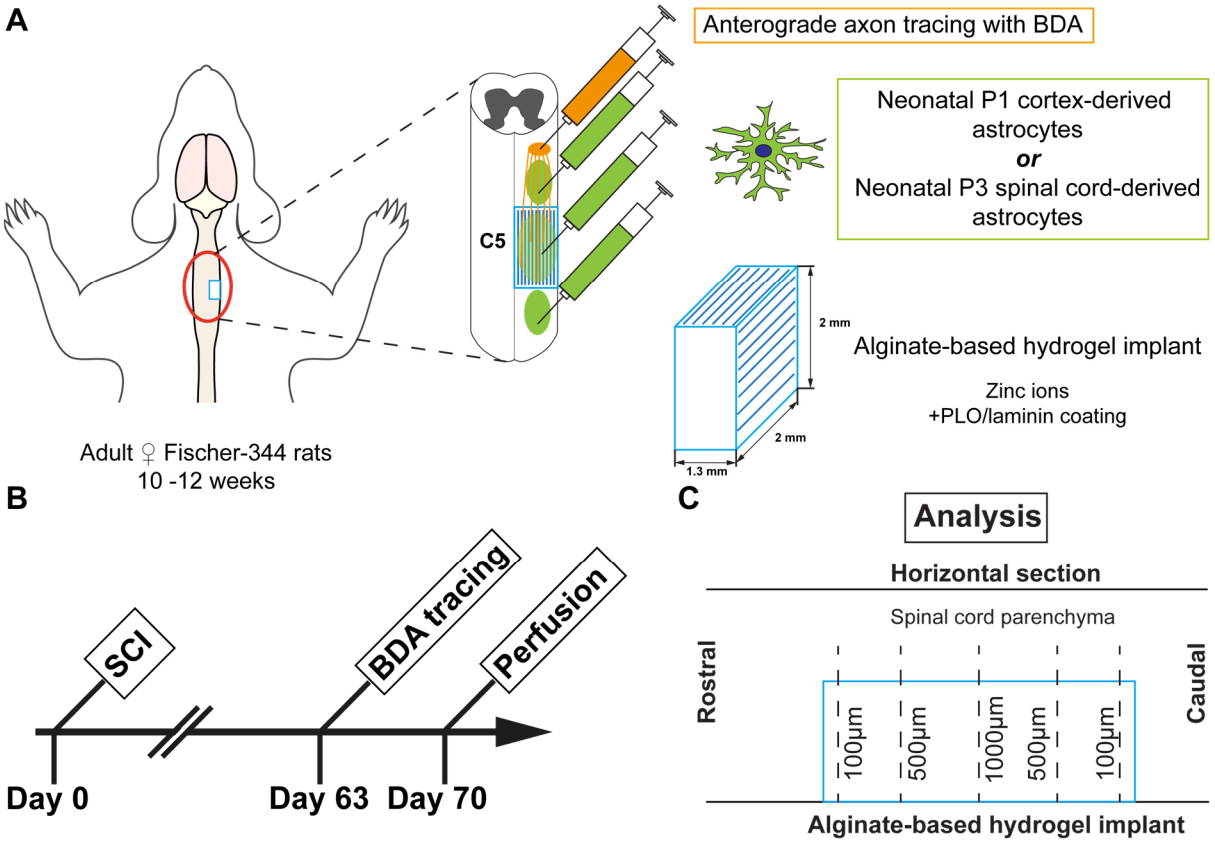

Figure 34: Experimental setup. (**A**) A total of 22 adult female Fischer-344 rats underwent a unilateral hemisection at C5 with immediate implantation of an astrocyte-seeded alginate-based hydrogel implant (fabricated with Zn^{2+}; channel diameter: 88.6 ± 2.9 µm). Additionally, neonatal astrocytes were injected 1 mm rostral and 1 mm caudal to the implantation site. (**B**) In contrast to all previous studies, survival time was extended to 8 weeks post-SCI. BDA was injected 1 week before transcardial perfusion to trace descending spinal axons. (**C**) After perfusion, the implantation site was immunohistochemically analyzed at 100 µm and 500 µm from the rostral or caudal hydrogel edge, respectively, and at the hydrogel center (1000 µm) (PLO/Laminin; n = 6; + cortex-derived astrocytes; n = 6 (2 died after SCI); + spinal cord-derived astrocytes; n = 6 (2 died after SCI); see **Suppl. table 1**).

3.5.1 Cell filling and graft cell survival within astrocyte-seeded hydrogel implants after additional astrocyte transplantation into the surrounding host spinal cord

To determine cell filling and survival of the GFP^+ grafted neonatal astrocytes, tissue sections of the cervical spinal cord containing the hydrogel implantation site and the surrounding host spinal cord were immunohistochemically analyzed (**FIG 35**). After 8 weeks, all analyzed hydrogel implants were structurally intact, in close contact with the surrounding host spinal cord and their channels were filled with cells (**FIG 35A – C**). While in both astrocyte-seeded groups ~90% of all hydrogel channel showed cell filling (indicated by $DAPI^+$ nuclei within the channels lumen), the overall cell filling in control implants was significantly lower throughout the implants (Two-Way ANOVA for overall group differences: $p < 0.0001$, followed by Tukey's *post hoc* test at rostral 100 µm: $^{\#}p < 0.05$ comparing controls with cortex-derived astrocytes; at the 1000 µm: $^{\#\#\#\#}p < 0.0001$ comparing controls with cortex-derived astrocytes, $^{****}p < 0.0001$ comparing controls with spinal cord-derived astrocytes; at caudal 500 µm: $^{\#}p < 0.05$ comparing controls with cortex-derived astrocytes, $^{*}p < 0.05$ comparing controls with spinal cord-derived astrocytes; at caudal 100 µm: $^{\#\#}p < 0.05$ comparing controls with cortex-derived astrocytes, $^{**}p < 0.05$ comparing controls with spinal cord-derived astrocytes). Additionally, in control hydrogels, cell filling significantly decreased with increasing distance from the hydrogel edges (Two-Way ANOVA for distance: $p < 0.001$). This effect was not found in astrocyte-seeded implants (**FIG 35D**, see **Suppl. table 15**). The grafted GFP-expressing neonatal astrocytes survived within the hydrogel channels (**FIG 35B, C**), and the majority of the cell-filled channels within these implants contained the grafted GFP^+ cells (**FIG 35E**). Within these implants, the seeded astrocytes occupied a great portion of the hydrogel channel area. Consistent with the overall cell filling, significantly less channel area was filled with GFP^+ with increasing distance from the rostral and caudal hydrogel edge (Two-Way ANOVA for distance: $p < 0.01$) equally for both

astrocyte populations (Two-Way ANOVA for overall group differences: p = 0.47). Cortex- as well as spinal cord-derived astrocytes expressed GFAP and densely filled the channel lumen of the hydrogel implants (**FIG 35G, H**).

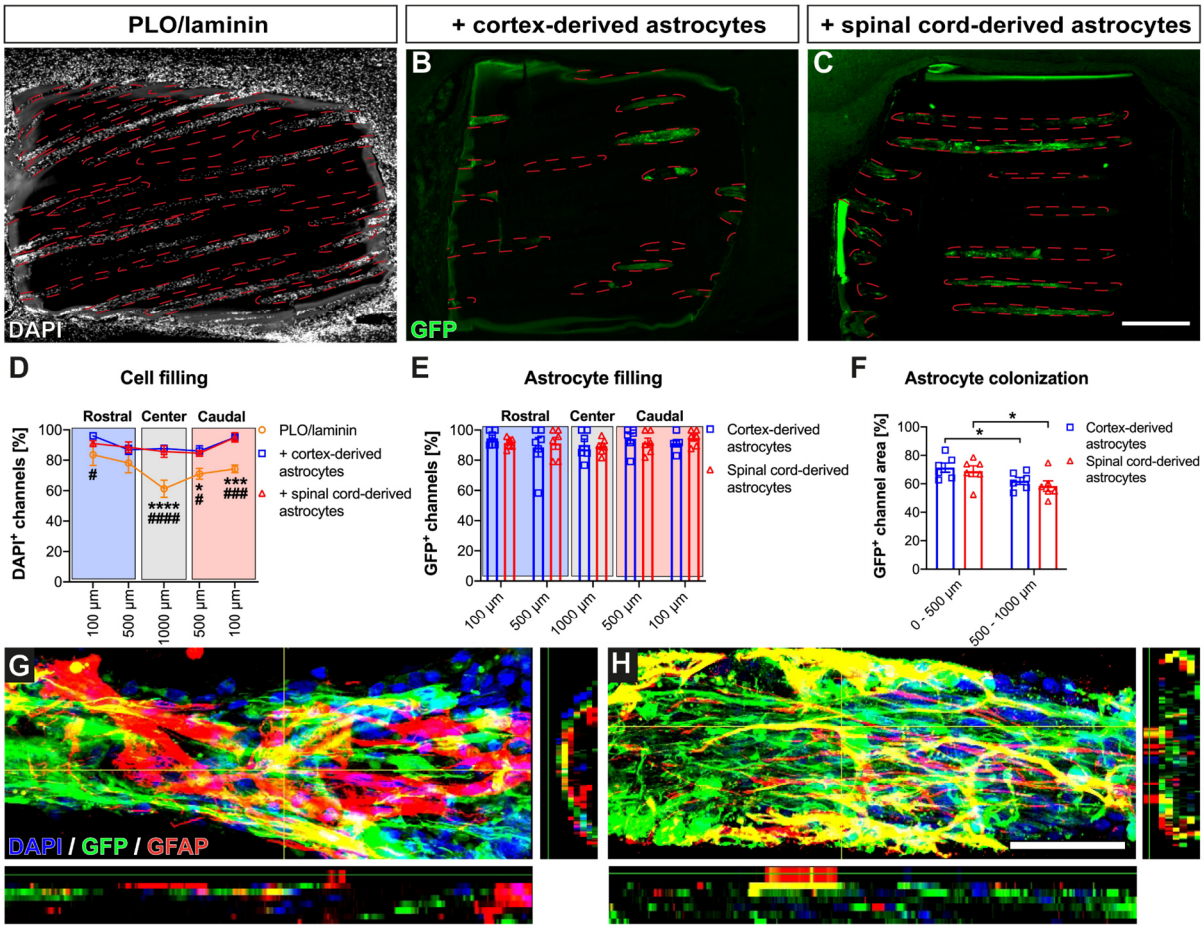

Figure 35: Neonatal spinal cord- and cortex-derived astrocytes fill alginate-based hydrogel implants and survive for at least 8 weeks *in vivo*. (**A – C**) Hydrogel implants without cell seeding (**A**) and implants seeded with neonatal cortex-derived astrocytes (**B**) or spinal cord-derived astrocytes (**C**) remained structurally intact and were in direct contact with the surrounding host spinal parenchyma 8 weeks after injury. Dashed lines indicate channel walls. Rostral is to the left, medial to the top, and caudal to the right. (**D**) Throughout the entire hydrogel implants, a greater percentage of channels were filled with cells in astrocyte-seeded implants (Two-Way ANOVA for overall group differences: $p < 0.0001$; PLO/Laminin; n = 6; + cortex-derived astrocytes; n = 6; + spinal cord-derived astrocytes; n = 6). Further, consistent with previous results, the hydrogel center showed a significantly smaller number of cell-filled channels in the control group (Two-Way ANOVA for distance: $p < 0.001$, with Tukey's *post hoc* ***$p < 0.001$ comparing rostral 100 µm with 1000 µm, *$p < 0.05$ comparing rostral 500 µm with 1000 µm). Detailed statistical analysis is depicted in **Suppl. table 15**. Blue, red and grey boxes indicate the rostral and caudal hydrogel halves, and the hydrogel center, respectively. (**E**) Within the astrocyte-seeded groups, consistently ~85% of all cell-filled channels contained the grafted GFP-expression neonatal astrocytes throughout the entire hydrogel (Two-Way ANOVA for overall group differences: $p = 0.98$; for distance: $p = 0.6$). (**F**) Both astrocytic populations equally occupied more than 70% of the channel area at the hydrogel entries and about 50% at the hydrogel center (Two-Way ANOVA for overall group differences: $p = 0.47$; for distance: $p < 0.01$ with Sidak's *post hoc* *$p < 0.05$ comparing 0 – 500 µm and 500 – 1000 µm in both groups). (**G, H**) The grafted GFP^+ cortex-derived (**G**) and spinal cord-derived astrocytes (**H**) co-expressed GFAP (red), lined the walls and filled the lumen of the hydrogel channels. XZ and YZ planes are shown underneath and to the right, respectively. Scale bar in **C**: 500 µm, in **H**: 50 µm.

As a further advancement of the previous implantation study, each animal that was implanted with an astrocyte-seeded hydrogel additionally received astrocyte grafts rostral and caudal to the implantation site into the uninjured host spinal cord to establish a continuous astrocytic bridge traversing the SCI site (**FIG 36**). The rostrally and caudally transplanted GFP-expressing neonatal astrocytes survived within the host spinal cord adjacent to the implantation site for 8 weeks and -independent of cell type- spread out into the surrounding intact host spinal parenchyma (**FIG 36A, B & H, I**). However, consistent with the previous results, cortex-derived astrocytes tended to migrate over longer distances (> 3 mm caudal from implantation site) within the host spinal cord (**FIG 36B**). In contrast, spinal cord-derived astrocytes did not spread far into the distal host spinal cord but rather migrated towards the implanted hydrogel. High-resolution confocal microscopy was used to determine the cell morphology of the grafted astrocytes: cortex-derived astrocytes adopted a differentiated cell morphology with long and branched $GFAP^+$ processes, whereas spinal cord-derived astrocytes appeared again in a rather elongated bipolar morphology with only a few long and thin processes (**FIG 36C, J**). Most important, both astrocyte populations intermingled with the host astrocytic network and aligned

into longitudinal bridges on both sides of the hydrogel implantation site (**FIG 36D – G, K – N**). Moreover, these astrocytic bridges were found in close spatial association with growing host axons confirming previous observations (**FIG 28**).

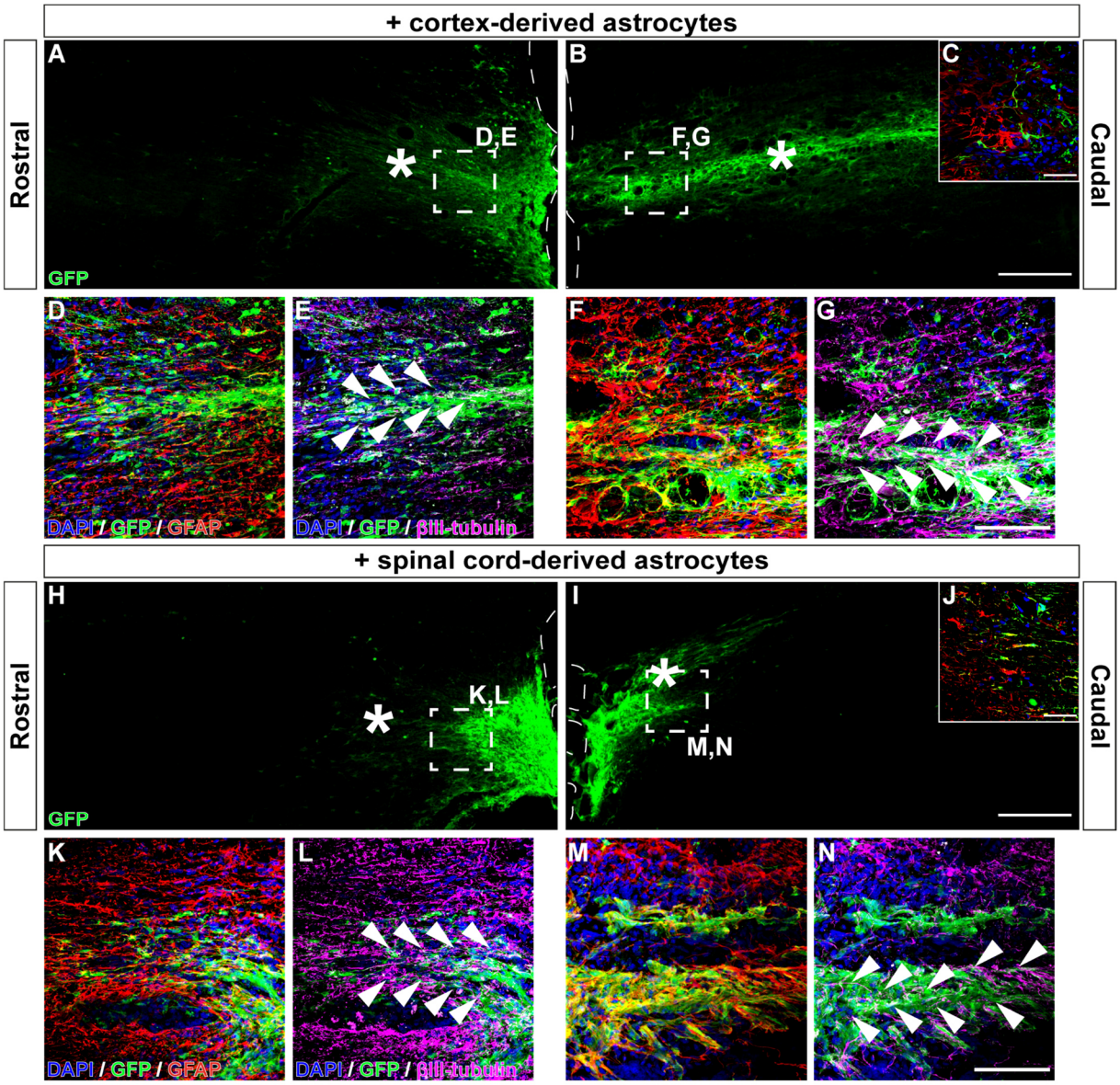

Figure 36: Rostrally and caudally co-transplanted astrocytes spread out into the surrounding host spinal parenchyma and form tissue bridges at the host-graft interface. The co-transplanted immature astrocytes (GFP, green) derived from the cortex (**A – G**) and spinal cord of neonatal rats (**H – N**) survived in the intact host tissue adjacent to the SCI site. They spread out into the surrounding rostral (**A, H**) and caudal spinal parenchyma (**B, I**). Asterisks indicate the cell injection site, while dashed lines the hydrogel implants and channel entries. Inserts in **A**, **B** are shown in **D – G**. Rostral is to the left, medial to the top and caudal to the right. (**C**) Cortex-derived astrocytes (GFP, green) expressed GFAP (red) and adopted a complex process-bearing morphology. (**D – G**) Adjacent to the hydrogel implantation site, the grafted astrocytes were in close contact with the host astrocytic network and aligned into longitudinal bundles (arrowheads in **E**, **G**) associated with host axons (βIII-tubulin, magenta) on the rostral (**D**, **E**) as well as the caudal side of the implant (**F**, **G**). Similarly, spinal cord-derived astrocytes distributed themselves into the rostral (**H**) and caudal (**I**) host spinal tissue. Boxed regions in **H**, **I** are shown in **K – N**. (**J**) In contrast to the grafted cortex-derived cells, spinal cord-derived astrocytes appeared to have an elongated cell shape with only a few thin processes. (**K – N**) Grafted spinal cord-derived astrocytes also aligned into longitudinal tissue bridges that served as a physical substrate for growing host axons (arrowheads in **L**, **N**) on both sides of the hydrogel implantation site. Scale bars in **B**, **I**: 500 µm; in **C**, **J**: 50 µm; in **G**, **N**: 100 µm.

3.5.2 Vascularization of hydrogel implants after astrocyte seeding and additional astrocyte transplantation into the surrounding host spinal cord

To investigate vascularization of the hydrogel implants 8 weeks after SCI, immunolabeling with a CD31 antibody was performed (**FIG 37**). CD31-labeled blood vessels entered and extended within the channels of control implants and, to a greater extent, within the channels of hydrogel implants that were seeded with neonatal astrocytes prior to implantation (**FIG 37A – C**). While 19.61 ± 6.2% of the channel area of control implants were covered with CD31-positive endothelial cells and blood vessels, twice as much channel area was filled with blood vessels in cortex-derived astrocyte-seeded implants (40.02 ± 5.7%; $p < 0.05$) and slightly less channel area in the spinal cord-derived astrocyte group (33.42 ± 2.41%) (One-Way ANOVA $p < 0.05$). Moreover, blood vessels were in close spatial association with the grafted GFP^+ astrocytes and seemed to be at least partially enveloped by them (arrowheads in **FIG 37B, C**).

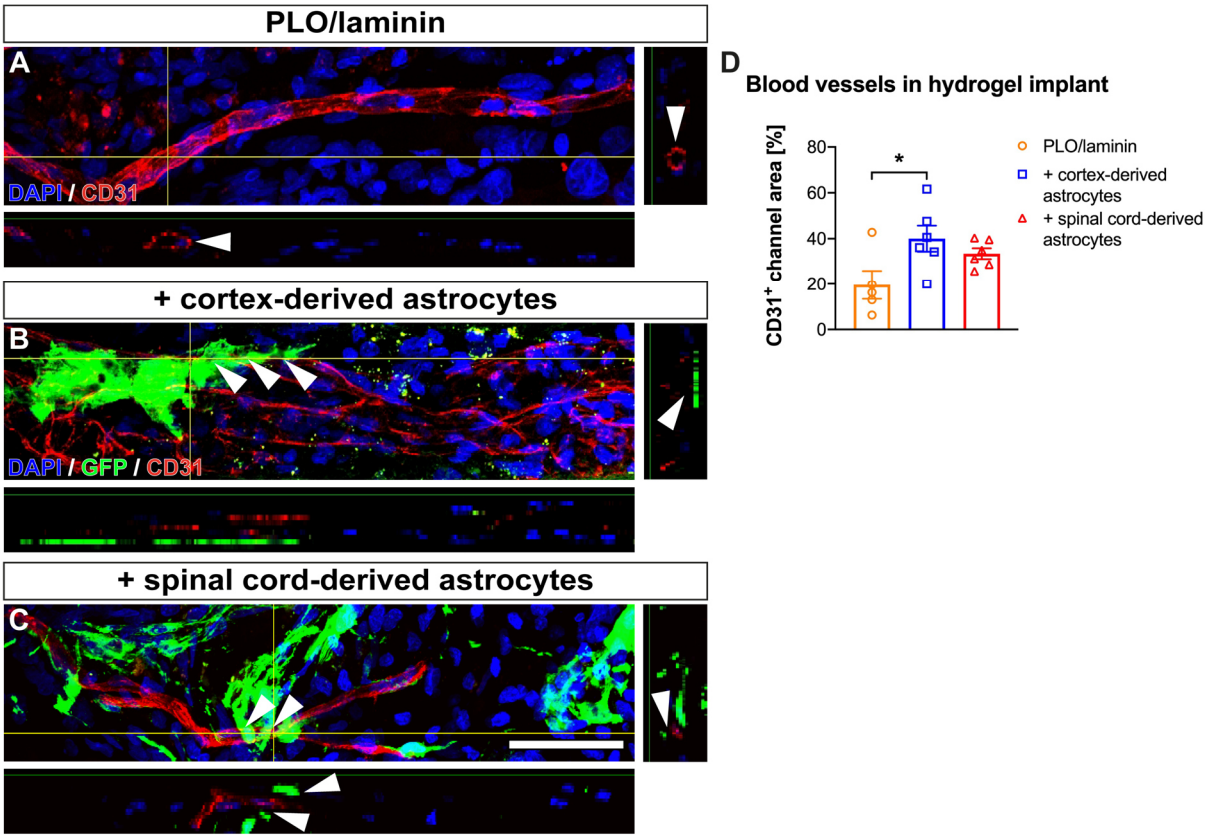

Figure 37: Seeding with neonatal astrocytes improves vascularization within alginate-based hydrogel implants. (**A – C**) CD31⁺ endothelial cells (red) formed tubular blood vessels (arrowheads in **A**) and were detected in the channels of control implants (**A**), in implants seeded with GFP-expressing neonatal cortex-derived (**B**) or spinal cord-derived astrocytes (**C**). XY and XZ planes are shown underneath and to the right, respectively. The grafted astrocytes partially enveloped the ingrowing blood vessels (arrowheads in **B**, **C**). (**D**) Importantly, a significantly greater channel area was occupied with CD31-positive blood vessels in both astrocyte-seeded groups compared to non-seeded controls (One-Way ANOVA $p < 0.05$, with Tukey's *post hoc* *$p < 0.05$ control vs. cortex-derived astrocytes; PLO/Laminin; n = 6; + cortex-derived astrocytes; n = 6; + spinal cord-derived astrocytes; n = 6). Scale bar in **C**: 50 µm.

3.5.3 Axonal growth into astrocyte-seeded hydrogel implants after additional astrocyte transplantation into the adjacent host spinal cord

To assess axonal regrowth at the implantation site and within the hydrogel implants, spinal axons were immunolabeled with βIII-tubulin and analyzed at different areas within each hydrogel implant (**FIG 38**). In line with the previous results, seeding with neonatal astrocytes promoted axonal growth into the hydrogel implants in comparison to non-seeded hydrogel implants (**FIG 38A – C**, Two-Way ANOVA for overall group differences: $p < 0.05$). However, no differences between cortex-derived and spinal cord-derived astrocytes were observed for the

number of axons per channel (**FIG 38D**) or the overall axonal growth within the implants (**FIG 38E**). In particular, an almost equal amount of axons extended within the channels of cortex- (38.91 ± 6.99 axons/DAPI$^+$ channel) and spinal cord-derived astrocyte-seeded hydrogels (38.06 ± 7.6 axons/DAPI$^+$ channel) in the rostral halves of the implants, whereas 70% fewer axons were present in non-seeded in the same area of the hydrogel (Two-Way ANOVA for overall group differences: $p < 0.05$, followed by Tukey's *post hoc* $^{**}p < 0.01$ comparing controls vs. astrocyte-seeded implants). The same trend was found in the caudal halves of the implants, as both astrocyte-seeded groups were found to contain significantly more axons in each channel than controls ($^{**}p < 0.01$ for cortex-derived astrocytes vs. controls; $^{*}p < 0.05$ for spinal cord-derived astrocytes vs. controls). Although the axon number per channel in control implants was consistent along the rostrocaudal extent of the implants, it varied in both astrocyte groups (Two-Way ANOVA for distance: $p < 0.0001$, see **Suppl. table 16**). Notably, a statistically significant caudal relation between cell type and distance was found (Interaction between cell type and distance: $p < 0.05$). Thus, when the entire hydrogel implants were analyzed, a similar axonal growth pattern was observed. While both astrocyte-seeded groups showed an equal amount of axons in the rostral, central and caudal area of the implant, only a few axons were present in non-seeded controls (Two-Way ANOVA for overall group differences: $p < 0.01$, see **Suppl. table 17**). This difference reached statistical significance especially at the rostral ($^{###}p < 0.001$ for controls vs. cortex-derived astrocytes, $^{**}p < 0.01$ controls vs. spinal cord-derived astrocytes) and at the caudal channel entries ($^{####}p < 0.0001$ for controls vs. cortex-derived astrocytes, $^{**}p < 0.01$ controls vs. spinal cord-derived astrocytes), while no significant difference at the hydrogel center was observed (**FIG 38E**). However, similar to the number of axons per DAPI$^+$ channel, the overall axonal growth was massively reduced at the central area of the implants in controls compared with both astrocyte-seeded groups (Two-Way ANOVA for distance: $p < 0.0001$). Again, a much greater number of axons were present at the rostral and caudal channel entries compared to the hydrogel center (Rostral 100 µm vs. 1000 µm: $^{##}p < 0.01$ for cortex-derived astrocytes, $^{**}p < 0.01$ for spinal cord-derived astrocytes). Surprisingly, although ~20% more axons appeared to be present at the caudal hydrogel half than the rostral hydrogel half in both astrocyte-seeded groups, this effect did not reach significance (rostral 100 µm vs. caudal 100 µm for cortex-derived astrocytes: $p = 0.2$; for spinal cord-derived astrocytes: $p = 0.93$). Controls showed similarly no change in overall axon numbers at the caudal hydrogel edge ($p = 0.99$). Additionally, the distribution of axons within the astrocyte-seeded hydrogel was determined (**FIG 38F**). Consistent with all previous results, the vast majority of axons were found in graft cell-filled channels compared to channels that only contained infiltrated host cells (Two-Way ANOVA for cell substrate within channels: $p < 0.0001$) independent of the tissue origin of the seeded astrocytes (Two-Way ANOVA for overall group differences: p

= 0.74). Consequently, 95.94 ± 1.43% of all axons were present in astrocyte-containing channels in the cortex-derived astrocyte group (****p < 0.0001) and 97.3 ± 0.86% entered astrocyte-containing channels in the spinal cord-derived astrocyte group (***p < 0.001) compared to channels filled only with infiltrated host cells.

In comparison with the previous study, where immature astrocytes were seeded into the hydrogel implants and additionally grafted caudally (**FIG 31**), axonal growth into the hydrogel implants could be even further increased by a factor of 4 for implants containing cortex-derived astrocytes (astrocyte seeding + caudal graft: 9.01 ± 2.51 βIII-tubulin$^+$ axons/cell-filled channel at Rostral 100 µm vs. astrocyte seeding + rostral/caudal grafts: 38.91 ± 6.99 βIII-tubulin$^+$ axons/cell-filled channel at Rostral 100 µm). For implants seeded with spinal cord-derived astrocytes, axonal growth was further enhanced by 30% compared with the previous study (astrocyte seeding + caudal graft: 29.56 ± 15.22 βIII-tubulin$^+$ axons/cell-filled channel at Rostral 100 µm vs. astrocyte seeding + rostral/caudal grafts: 38.06 ± 7.59 βIII-tubulin$^+$ axons/cell-filled channel at Rostral 100 µm).

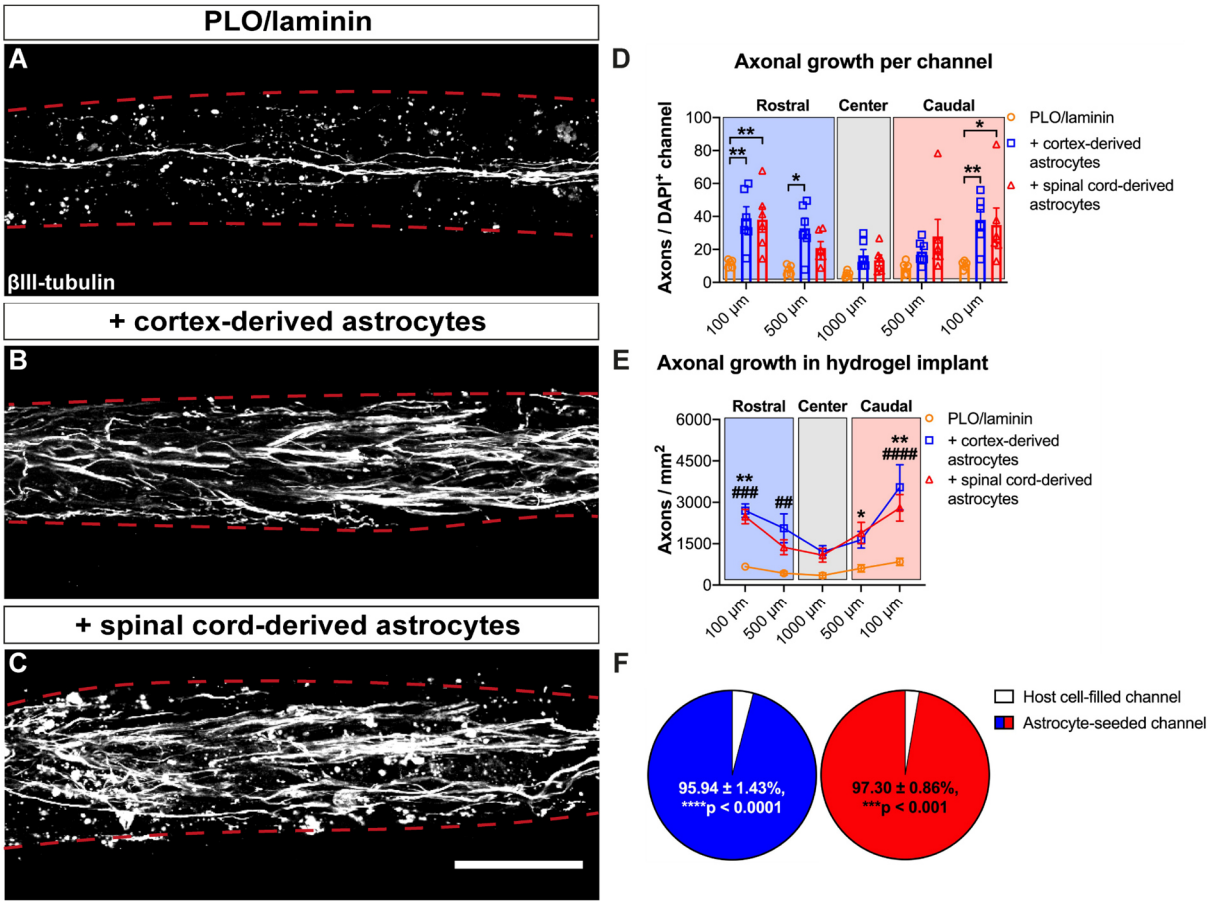

Figure 38: Axonal growth is enhanced within astrocyte-seeded alginate-based hydrogel implants after additional astrocyte transplantation into the surrounding host spinal cord. (**A – C**) Eight weeks post-injury, individual axons and thin axon bundles (βIII-tubulin, white) were found in non-seeded control implants (**A**), whereas thick axon bundles were present within the channels of hydrogel implants seeded either with neonatal cortex-derived astrocytes (**B**) or spinal cord-derived astrocytes (**C**). Dashed lines indicate channel walls. Rostral is to the left, medial to the top and caudal to the right. (**D**) Especially in the rostral half of the implants, equal axon numbers per cell-filled channel were detected in both astrocyte-seeded groups, whereas only a small number was found in controls (Two-Way ANOVA for overall group differences: $p < 0.05$; PLO/Laminin; n = 6; + cortex-derived astrocytes; n = 6; + spinal cord-derived astrocytes; n = 6). The number of axons decreased in both astrocyte-seeded groups towards the hydrogel center and elevated again in the caudal hydrogel half (Two-Way ANOVA for distance: $p < 0.0001$; Interaction between cell type and distance: $p < 0.05$). Detailed statistical analysis is depicted in **Suppl. table 16**. Blue, red and grey boxes indicate the rostral and caudal hydrogel halves, and the hydrogel center, respectively. (**E**) Overall, implants of both astrocyte-seeded groups contained a significantly greater number of βIII-tubulin-labeled axons compared to controls (Two-Way ANOVA for overall group differences: $p < 0.01$), although axonal growth was dramatically reduced at the hydrogel center in both astrocyte-seeded groups (Two-Way ANOVA for distance: $p < 0.0001$). Detailed statistical analysis is depicted in **Suppl. table 17.** (**F**) Within the astrocyte-seeded hydrogel implants, axons were almost exclusively found in channels containing the grafted cortex-derived astrocytes (blue) and spinal cord-derived astrocytes (red) and not in channels filled with only host cells (white) throughout the entire hydrogel implant (Two-Way ANOVA for cell substrate within channels: $p < 0.0001$ with Tukey's *post hoc* ****$p < 0.0001$ comparing axons in $DAPI^+/GFP^-$ channels with axons in $DAPI^+/GFP^+$ channels for cortex-derived astrocytes, ***$p < 0.001$ comparing axons in $DAPI^+/GFP^-$ channels with axons in $DAPI^+/GFP^+$ channels for spinal cord-derived astrocytes). Scale bar in **C**: 50 µm.

To determine whether descending raphespinal axons contributed to the observed axonal growth within the hydrogel implants, serotonergic axons were immunolabeled with 5-HT and quantified at the hydrogel edges and center (**FIG 39**). Descending raphespinal axons entered the hydrogel implants of all 3 groups from the rostral host spinal cord leading to high axon numbers per cell-filled channel at the rostral hydrogel edge in all groups (**FIG 39A – C**). However, astrocyte-seeded hydrogels contained significantly more 5-HT-labeled axons than non-seeded controls (**FIG 39D**, Two-Way ANOVA for overall group differences: $p < 0.05$, with Tukey's *post hoc* $^{\#\#}p < 0.01$ comparing controls vs. cortex-derived astrocytes, ****$p < 0.0001$ comparing controls vs. spinal cord-derived astrocytes at Rostral 100 µm, see **Suppl. table 18**). Across the different tested distances from the hydrogel edge, the number of $5\text{-}HT^+$ axons/$DAPI^+$ channels declined (Two-Way ANOVA for distance: $p < 0.0001$). In particular, the number of axons per channel dramatically decreased in both astrocyte-seeded groups from the rostral channel entries towards the hydrogel center (Two-Way ANOVA $p < 0.0001$, with Tukey's *post*

hoc for cortex-derived astrocytes: ####p < 0.0001 comparing Rostral 100 µm and Center 1000 µm; for spinal cord-derived astrocytes: ****p < 0.0001) and compared to the caudal hydrogel edge (Two-Way ANOVA p < 0.0001, with Tukey's *post hoc* for cortex-derived astrocytes: ####p < 0.0001 comparing Rostral 100 µm vs Caudal 100 µm; for spinal cord-derived astrocytes: ****p < 0.0001 comparing Rostral 100 µm vs Caudal 100 µm). The number of serotonergic axons in non-seeded controls slightly declined towards the hydrogel center and remained very limited throughout the central and caudal areas of the implants. Notably, an association between astrocyte seeding and axon number over distance within the hydrogel implants was found (Interaction between cell type and distance: p < 0.01). Generally, astrocyte-seeded implants contained a strikingly greater number of 5-HT-labeled axons than non-seeded control implants, for instance, 3 times as much 5-HT-positive axons were detected at the rostral hydrogel edge in astrocyte-seeded implants (Two-Way ANOVA for overall group differences: p < 0.05, followed by Tukey's *post hoc* test at rostral 100 µm: ####p < 0.0001 control vs. cortex-derived astrocytes; ****p < 0.0001 control vs- spinal cord-derived astrocytes) (**FIG 39E**, see **Suppl. table 19**). However, axon numbers fell towards the hydrogel center but surprisingly raised again at the caudal hydrogel edge in the cell-seeded implants (cortex-derived astrocytes: 790.426 ± 107.496 5-HT$^+$ axons/mm^2; spinal cord-derived astrocytes: 896.246 ± 133.734 5-HT$^+$ axons/mm^2), whereas this increase in 5-HT-labeled axon numbers was absent in controls (277.343 ± 64.978 5-HT$^+$ axons/mm^2) resulting in a significant difference between groups ($^{\#}$p < 0.05 for control vs. cortex-derived astrocytes; **p < 0.01 for control vs. spinal cord-derived astrocytes). Unfortunately, the axon density within implants decreased in all groups with rising distance from the rostral channel entries (Two-Way ANOVA for distance: p < 0.0001). This decline was again most prominent in implants seeded with immature astrocytes (Two-Way ANOVA p < 0.0001, with Tukey's *post hoc* test comparing Rostral 100 µm with Hydrogel center at 1000 µm: ####p < 0.0001 for cortex-derived astrocytes, ****p < 0.0001 for spinal cord-derived astrocytes). Contrary to βIII-tubulin-labeled axons, the number of serotonergic axons was significantly altered in control implants across different distances within the implants (Two-Way ANOVA p < 0.0001, with Tukey's *post hoc* $^{+++}$p < 0.001 comparing Rostral 100 µm with 1000 µm). Remarkably, at the caudal hydrogel edge, more serotonergic axons were found in both astrocyte-seeded groups compared with the hydrogel center (Center 1000 µm vs. Caudal 100 µm: $^{\#}$p < 0.05 for cortex-derived astrocytes; ****p < 0.0001 for spinal cord-derived astrocytes), whereas there was no effect in controls (p = 0.78). Noteworthy, a significant interaction between astrocyte seeding and distance was found (p < 0.0001) indicating a strong association between the two parameters. If the axon distribution in astrocyte-seeded implants was examined (**FIG 39F**), a strong preference of the 5-HT$^+$ axons for the grafted astrocytes as the cellular growth substrate within the hydrogel channels was found, comparable to the results

obtained for βIII-tubulin-labeled axons. More precisely, 94.73 ± 1.79 % of all axons present in the cortex-derived astrocyte-seeded implants were found in channels filled with the grafted astrocytes and, consistently, 94.38 ± 5.62% of all 5-HT-labeled axons entered spinal cord-derived astrocyte-filled channels (Two-Way ANOVA $p < 0.01$, with Sidak's *post hoc* test comparing axon number in astrocyte-filled channels vs. axon numbers in channels only containing host cells: $^{###}p < 0.001$ for cortex-derived astrocytes; $^{***}p < 0.001$ for spinal cord-derived astrocytes). Moreover, the addition of a rostral astrocytic graft further increased the ingrowth of serotonergic axons compared with the previous study, where astrocytic co-grafts were transplanted only caudally. Notably, more 5-HT$^+$ axons were detected in the present study compared to the previous experiment (**FIG 32**), e.g., 5-HT$^+$ axon numbers per channel were elevated by 500% in the cortex-derived astrocyte group (25.28 ± 5.66 5-HT$^+$ axons/channel vs. 4.91 ± 1.48 5-HT$^+$ axons/channel at Rostral 100 µm). Axon numbers in the spinal cord-derived astrocyte group were even further enhanced by more than 6-fold (5.01 ± 2.26 5-HT$^+$ axons/channel vs. 33.16 ± 5.99 5-HT$^+$ axons/channel at Rostral 100 µm). Accordingly, the overall number of serotonergic axons per hydrogel implant was enhanced as well.

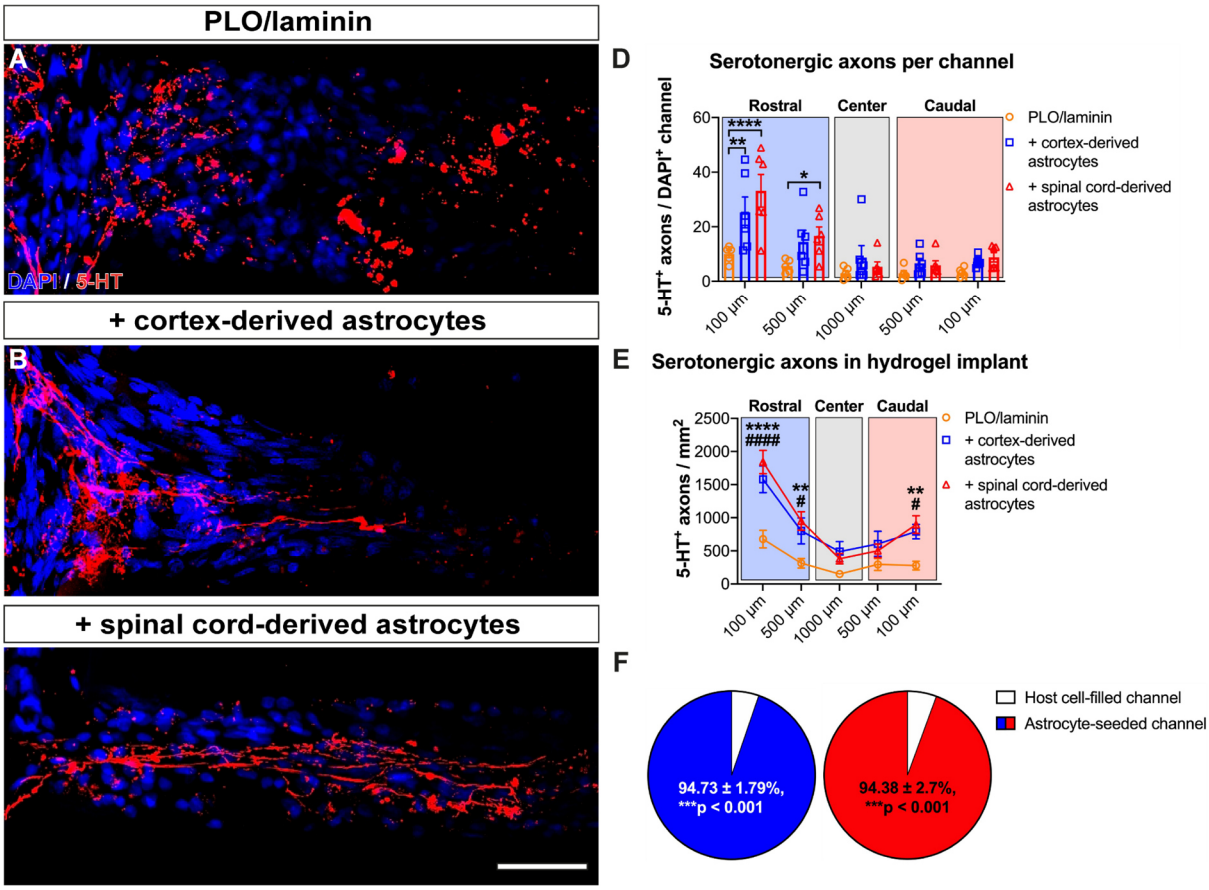

Figure 39: Growth of serotonergic axons is enhanced within astrocyte-seeded hydrogel implants after additional astrocyte transplantation into the surrounding spinal cord. (**A – C**) Serotonergic axons grew within the hydrogel channels of controls (**A**), implants seeded with cortex-derived astrocytes (**B**) or spinal cord-derived astrocytes (**C**). (**D**) Significantly more 5-HT-labeled axons were found in the rostral fraction of the channels in astrocyte-seeded implants compared to non-seeded controls (Two-Way ANOVA for overall group differences: $p < 0.05$, with Tukey's *post hoc* **$p < 0.01$ comparing controls vs. cortex-derived astrocytes, ****$p < 0.0001$ comparing controls vs. spinal cord-derived astrocytes at rostral 100 µm; *$p < 0.05$ comparing controls vs. spinal cord-derived astrocytes at Rostral 500 µm; PLO/Laminin; n = 6; + cortex-derived astrocytes; n = 6; + spinal cord-derived astrocytes; n = 6). However, this effect diminished towards the hydrogel center where all groups were equal (Two-Way ANOVA for distance: $p < 0.0001$). Detailed statistical analysis is depicted in **Suppl. table 18**. Blue, red and grey boxes indicate the rostral and caudal hydrogel halves, and the hydrogel center, respectively. (**E**) Similarly, the overall axon numbers were significantly greater in implants containing the grafted astrocytes (Two-Way ANOVA for overall group differences: $p < 0.05$) but serotonergic axons failed to extend over longer distances within the implants (Two-Way ANOVA for distance: $p < 0.0001$). Detailed statistical analysis is depicted in **Suppl. table 19**. Again, the number of axons were increased at the caudal end of the hydrogel implants. (**F**) Within both astrocyte-seeded groups, serotonergic axons preferentially entered channels which were filled with the grafted cells instead of channels that were filled with host cells (Two-Way ANOVA $p < 0.01$). Scale bar in **C**: 50 µm.

Descending spinal axons were specifically labeled *in vivo* with BDA injection into the cervical spinal cord at C2 one week before perfusion. Afterwards, regrown BDA-labeled axons were quantified at different distances within the hydrogel implants (**FIG 40**). Similar to 5-HT^+ axons, BDA-traced axons entered the hydrogel implants in all groups (**FIG 40A – C**). The number of BDA-labeled axons per channel was highest in all groups at the rostral hydrogel edge (100 µm), but throughout the hydrogels, the channels of astrocyte-seeded implants contained more traced axons (Two-Way ANOVA for overall group differences: $p < 0.01$) with implants seeded with cortex-derived astrocytes showing the greatest number of BDA^+ axons in the rostral hydrogel halves (Two-Way ANOVA $p < 0.01$, with Tukey's *post hoc* at rostral 100 µm: ****$p < 0.0001$ controls vs. cortex-derived astrocytes; *$p < 0.05$ controls vs. spinal cord-derived astrocytes) (**FIG 40D**). Moreover, cortex-derived astrocyte-seeded implants contained significantly more axons than spinal cord-derived astrocyte-seeded hydrogels (**$p < 0.01$). This same effect was consistent in the rostral but also caudal halves of the hydrogels but was diminished at the hydrogel center (Two-Way ANOVA for distance: $p < 0.0001$, see **Suppl. table 20**). Surprisingly, in the caudal hydrogel halves, BDA axon numbers increased again in the cortex-derived astrocyte-seeded implants, whereas BDA-traced axons were only sparsely seen in controls (Two-Way ANOVA $p < 0.01$ with Tukey's *post hoc* at Caudal 100 µm: **$p < 0.0001$ controls vs. cortex-derived astrocytes). However, the number of BDA-labeled axons in the spinal cord-derived

astrocyte-seeded group appeared to be constant throughout the entire length of the hydrogels. Again, a statistical interaction between cell seeding and distance was found ($p < 0.01$). Overall, both astrocyte-seeded groups contained a remarkably greater number of BDA-labeled axons compared with non-seeded controls (Two-Way ANOVA for overall group differences: $p < 0.01$), but with significant differences across the rostrocaudal extent of the implants (**FIG 40E**, Two-Way ANOVA for distance: $p < 0.0001$; see **Suppl. table 21**). At the rostral hydrogel edge, the number of BDA-traced axons was about 3x greater in cortex-derived astrocyte-seeded implants compared to controls and thereby even greater than in implants seeded with spinal cord-derived astrocytes (Two-Way ANOVA $p < 0.01$, with Tukey's *post hoc* at rostral 100 µm: ####$p < 0.0001$ control vs. cortex-derived astrocytes; ***$p < 0.001$ cortex-derived astrocytes vs. spinal cord-derived astrocytes). Hence, BDA-labeled axon numbers were significantly enhanced in cortex-derived astrocyte-seeded implants throughout the entire length of the implants compared with controls. Similar to BDA axon numbers per channel, an interaction between distance and cell seeding was identified ($p < 0.01$). Finally, the previously observed strong preference of re-growing axons towards graft astrocyte-filled hydrogel channels was again confirmed when descending BDA-traced axons were tested since more than 90% of all detected BDA^+ axons were found in channels containing the grafted cortex- (**$p < 0.01$) or spinal cord-derived astrocytes (**$p < 0.01$) (**FIG 40F**). Importantly, regrowth of descending BDA-traced axons was enhanced in comparison with the previous experiment (**FIG 33**). Especially in the cortex-derived astrocyte group, growth of descending BDA-labeled axons was elevated by a factor of 6.5 compared with the previous study (astrocyte seeding + caudal graft: 1.41 ± 0.57 BDA^+ axons/cell-filled channel at Rostral 100 µm vs. astrocyte seeding + rostral/caudal grafts: 9.19 ± 1.56 BDA^+ axons/cell-filled channel at Rostral 100 µm). In the spinal cord-derived astrocyte group, the BDA axon numbers were increased by additional 60% more BDA-traced axons (astrocyte seeding + caudal graft: 3.29 ± 1.83 BDA^+ axons/cell-filled channel at Rostral 100 µm vs. astrocyte seeding + rostral/caudal grafts: 5.33 ± 1.12 BDA^+ axons/cell-filled channel at Rostral 100 µm).

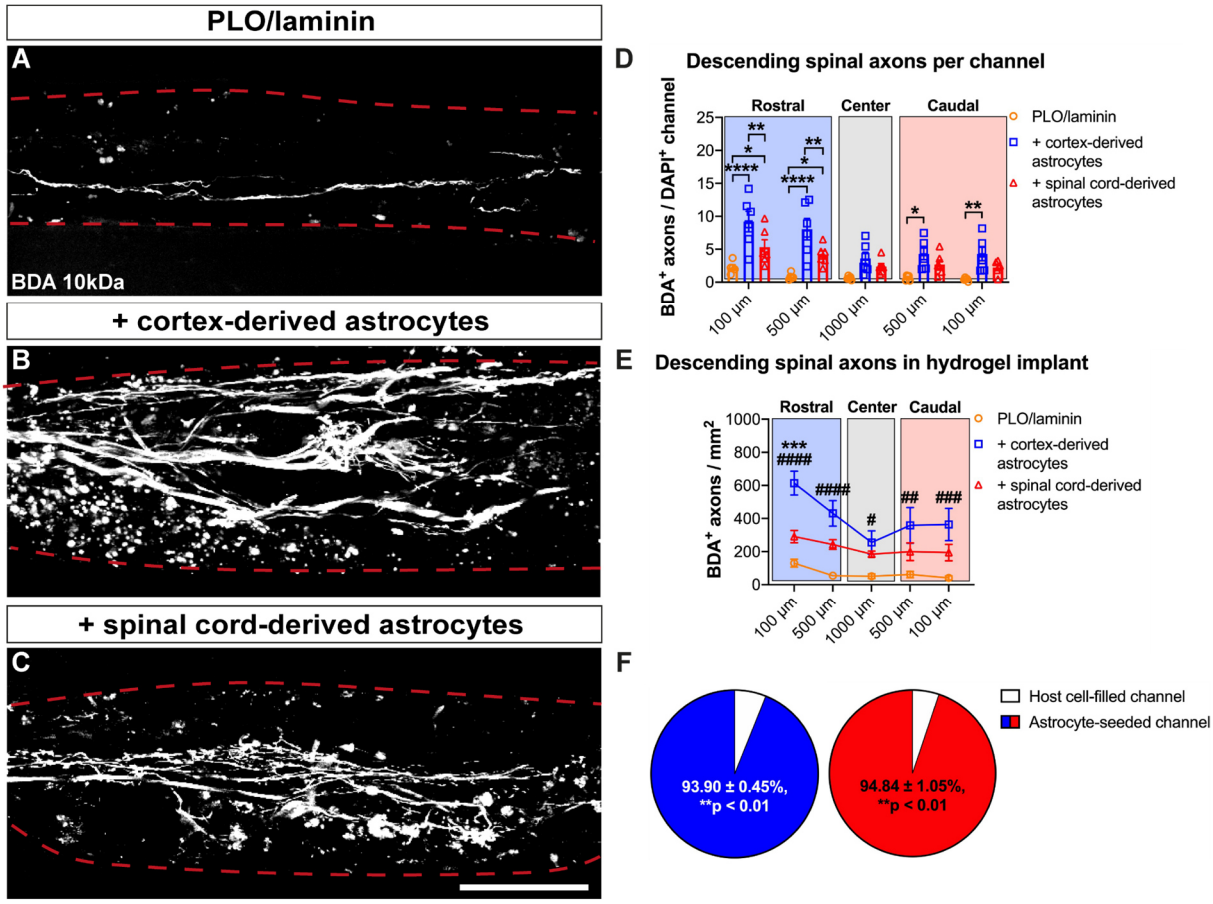
PLO/laminin
A
BDA 10kDa
+ cortex-derived astrocytes
B
+ spinal cord-derived astrocytes
C
D
Descending spinal axons per channel
BDA+ axons / DAPI+ channel
Rostral
Center
Caudal
PLO/laminin
+ cortex-derived astrocytes
+ spinal cord-derived astrocytes
100 µm
500 µm
1000 µm
E
Descending spinal axons in hydrogel implant
BDA+ axons / mm2
F
Host cell-filled channel
Astrocyte-seeded channel
93.90 ± 0.45%,
**p < 0.01
94.84 ± 1.05%,
**p < 0.01

Figure 40: Growth of descending axons is enhanced in astrocyte-seeded hydrogel implants after additional astrocyte transplantation into the surrounding host spinal cord. (**A – C**) Descending BDA^+ axons entered and extended within the channels of control hydrogels (**A**), implants seeded with astrocytes derived from the neonatal cortex (**B**) or spinal cord (**C**). Dashed lines indicate channel walls. Rostral is to the left, medial to the top, and caudal to the right. (**D**) Per cell-filled channel, a significantly greater number of BDA-traced axons in astrocyte-seeded implants was found compared with non-seeded controls in the rostral halves of the implants (Two-Way ANOVA for overall group differences: $p < 0.01$; PLO/laminin; n = 6; + cortex-derived astrocytes; n = 6; + spinal cord-derived astrocytes; n = 6), whereas at the hydrogel center, no significant differences were observed. In the caudal hydrogel halves, implants seeded with cortex-derived astrocytes showed promoted growth of BDA-labeled axons. These differences were highly significant across all distances within the hydrogel implant (Two-Way ANOVA for distance: $p < 0.0001$; Interaction between cell grafting and distance: $p < 0.01$). Detailed statistical analysis is depicted in **Suppl. table 20**. Blue, red and grey boxes indicate the rostral and caudal hydrogel halves, and the hydrogel center, respectively. (**E**) Overall, implants of both astrocyte-seeded groups contained at least the double amount of BDA-traced axons than the non-seeded controls at all analyzed distances (Two-Way ANOVA for overall group differences: $p < 0.01$), however, with rising distance from the rostral hydrogel edge, axon numbers appeared to slightly decline. In particular, axon numbers in implants seeded with cortex-derived astrocytes dramatically declined from the rostral channel entries towards the central area of the implants (Two-Way ANOVA for distance: $p < 0.0001$, with Tukey's *post hoc* $^{\#\#\#\#}p < 0.0001$ comparing rostral 100 µm and 1000 µm in the cortex-derived astrocyte group; Interaction between cell grafting and distance: $p < 0.01$). Detailed statistical analysis is depicted in **Suppl. table 21**. (**F**) The vast majority of BDA-labeled axons were found in astrocyte-containing channels throughout the entire implants (Two-Way ANOVA $p < 0.05$). Scale bar in **C**: 50 µm.

Taken together, previous results regarding implant integrity, cell filling, graft cell survival and host-graft interactions were confirmed. Moreover, the addition of an astrocyte graft rostral to the hydrogel implantation and -in parallel- prolonging the survival time of the animals to 8 weeks, further increased axonal growth into and through the hydrogel implants. Although no or only minor differences between neonatal astrocytes derived from cortex or spinal cord were found in the first set of experiments, cortex-derived astrocytes seemed to strongly promote regrowth of descending spinal axons and slightly improve vascularization of the implantation site compared with spinal cord-derived astrocytes in this 8-week study. Consequently, the combination of cell-seeded implants and additional cellular grafts was again proven to be superior over the implantation of only a non-seeded hydrogel without any further trophic intervention. Axonal re-entry into the caudal host spinal cord, however, was not achieved, and therefore, additional trophic attraction of the growing axons within the caudal spinal parenchyma might be required.

4 Discussion

The present study demonstrates that the implantation of a biocompatible alginate-based hydrogel implant in combination with co-transplantation of immature astrocytes into the biomaterial and the surrounding host spinal cord massively supports axonal growth after a unilateral hemisection injury in the adult rat spinal cord. The biocompatibility of the hydrogel implants is improved by surface coating with the polypeptide PLO and the ECM component laminin. Seeding of the surface-coated hydrogel implants with immature cortex-derived astrocytes facilitates host-graft interactions and promotes axonal growth into the implants. Furthermore, the grafted astrocytes establish a cellular bridge connecting the hydrogel implants with the surrounding host spinal cord. However, axons do not cross the caudal host graft interface and reinnervate the caudal host spinal cord four weeks after SCI (Schackel, Kumar et al. 2019).
To assess if further enhanced integration would promote reinnervation of the host spinal cord, we examined immature astrocytes of spinal cord origin in addition to cell transplantation within the uninjured tissue surrounding the hydrogel implant. No striking differences between the immature cortex-and spinal cord-derived astrocytes could be found *in vitro* or *in vivo*. Cortex- as well as spinal cord-derived astrocytes form tissue bridges spanning the host-graft interface, even though minor differences in their morphology and migratory behavior with the spinal parenchyma were observed. Moreover, either immature astrocytes equally facilitate vascularization of the injury site and superior axonal regrowth compared to previous astrocyte seeding experiments. An additional rostral astrocytic graft combined with a prolonged survival time of 8 weeks resulted in an overall additional improvement of vascularization and axonal growth within the hydrogel implants. This combinatorial treatment further enhances the regrowth of descending spinal axons by 400% compared with the previous co-transplantation studies, where immature astrocytes were only grafted caudal to the astrocyte-seeded hydrogel implant for a 4 week study. Nonetheless, axonal re-entry into the caudal host spinal cord was still not evident.
The results suggest that the creation of a molecularly and cellularly permissive environment within biomaterial implants crucially affects the integration of the biomaterial implant into the host spinal cord, thereby increasing host-graft interactions and axonal growth within the implantation site. A continuous cellular substrate connecting the uninjured host spinal cord and the hydrogel implant represents a prerequisite for axonal crossing of extended SCI sites. In this context, immature astrocytes can be used to bridge the interface between the hydrogel implant and the host spinal cord and facilitate vascularization and superior axonal growth of descending spinal tracts into and throughout the hydrogel implants without adopting *per se* a detrimental phenotype after transplantation into the hostile environment of acute SCI sites.

4.1 Biocompatibility of natural hydrogel biomaterials

The success of each transplantation approach crucially relies on the biocompatibility between the implant and the host tissue. In particular, the host spinal cord will initiate an immune response against each kind of implant. The hosts' response to a biomaterial implants highly depends upon the chemical formulation; physical properties, such as surface charge and elasticity and stiffness; structural properties, like surface texture and porosity; and finally size as well as the shape of the implant. In addition, biodegradation of the biomaterial implant and potentially toxic byproducts might contribute to the host immune response (Badylak 2015).
Hydrogels were shown to have numerous advantages over other biomaterial types, such as synthetic hollow tube conduits. Especially hydrogels that are derived from natural polymers have superior capacities as implants for biomedical applications due to their low intrinsic toxicity and immunogenicity, variable mechanical properties and microstructure. Hydrogels allow for rapid gas, liquid and nutrient diffusion/osmosis making them specifically predestinated as carrier matrices for cell transplantation and factor release approaches. Additionally, their inherent microstructure resembles (depending upon the basic chemical formulation) the natural microstructure of the mammalian ECM which further enhances their inherent biocompatibility (Fuhrmann, Anandakumaran et al. 2017, Liu, Schackel et al. 2017, Griffin and Bradke 2020).
In the present study, solid hydrogel implants fabricated from the heteromeric polysaccharide alginate were tested as biocompatible biomaterials *in vitro* and *in vivo*. Naturally, mammals do not possess specific cell surface receptors nor alginate-specific antibodies against the alginate polymers. Hence, a specific adverse immune response against alginate *per se* can most likely be neglected but a general foreign body response may be present (Orive, Ponce et al. 2002, Lee and Lee 2009). Additionally, alginate is inherently non-degradable in mammals since they lack specific enzymes, such as alginase, to degrade the alginate chains. Based upon this inherent biocompatibility and low toxicity, various chemical formulations of alginate are used for numerous biomedical applications, e.g., dental restoration composite (Torres, Mailart et al. 2020), wound dressings (Sweeney, Miraftab et al. 2012) or sealing agents for gastroesophageal mucosa microlesions (Uemura, Oda et al. 2019); and as an additive for pharmacological compounds, like Gaviscon alginate-antacid in the treatment of gastroesophageal reflux disease (Coyle, Crawford et al. 2017), and in nutritional science as e.g., thickening agent (Lee and Mooney 2012).
Nonetheless, alginate is biologically inert under physiological conditions due to a negative surface charge of the alginate backbone (Dillon, Yu et al. 1998). In some instances, this characteristic is advantageous for some biomedical applications; for example, non-adhesive wound dressings, where alginate-based hydrogels create a physiologically moist, absorb fluids from

and seal the wound, thereby preventing pathogen entry (Queen, Orsted et al. 2004, Sweeney, Miraftab et al. 2012, Dumville, Keogh et al. 2015). The non-permissive surface of pure alginate-based hydrogels does not allow for cell adhesion; hence, alginate surfaces need to be ectopically modified to be feasible growth substrates for cells and neurites.

To improve permissiveness and cell viability on alginate-based hydrogels, we applied surface coating with the synthetic polypeptide PLO to mask the negative surface charge and the ECM component laminin to introduce a biologically active signal to our alginate biomaterials (Dhoot, Tobias et al. 2004). In particular, masking the negative surface charge alone significantly improved cell adhesion to alginate-based hydrogels. However, an additional biological stimulus of laminin was necessary to induce a differentiated cell morphology in immature cortex-derived astrocytes as well as neurite outgrowth from DRG neurons. Any cell adhesion on the uncoated hydrogels might be attributed to ECM protein deposition from the seeded cells rather than permissiveness of the alginate substrate itself (McLeod and Mauck 2016, Loebel, Mauck et al. 2019).

Most importantly, we tested whether PLO/laminin-coating would similarly improve biocompatibility of alginate-based hydrogels *in vivo* after traumatic SCI in adult rats. Non-coated and coated hydrogel implants were in direct physical contact with the surrounding host spinal cord and minor cystic cavitation was occasionally observed around non-coated hydrogel implants. Still, the hydrogel implants were surrounded by an area of hypercellularity indicating a host-graft interface that mainly contained infiltrated fibroblasts, Schwann cells, microglia and macrophages, as has been commonly observed after implantation of a biomaterial into SCI lesions (Guo, Zahir et al. 2012, Gao, Lu et al. 2013, Badylak 2015). Infiltration of SCI sites by non-neural stromal cells, perivascular and meningeal fibroblasts as well as resident and blood-derived immune cells is a component of the naturally occurring regeneration process after SCI (Norenberg, Smith et al. 2004). Hence, hypercellularity around the hydrogel implants indicates the natural hosts' response to spinal cord damage *per* se and not a specific immune reaction against the biomaterial (Burda and Sofroniew 2014, Badylak 2015). Accordingly, surface coating did not affect the host immune response since astrocytes and macrophages/microglia were equally present at the lesion site in non-coated controls and animals that received surface-coated hydrogels.

Most intriguingly, surface coating significantly improved infiltration into and survival within the hydrogel implants of host-derived macrophages/microglia and Schwann cells. Thus, the PLO/laminin-coating remained stable and biologically active for at least 4 weeks *in vivo*, extending the previous *in vitro* results of two weeks (Schackel, Kumar et al. 2019). This is even more remarkable considering the presence of proteases and matrix metalloproteases at acute SCI lesion sites (Noble, Donovan et al. 2002, Zhang, Chang et al. 2011). Similar results were

obtained when a xyloglucan hydrogel was functionalized with poly-D-lysine (PDL) and transplanted into a lesion of the caudate putamen (Nisbet, Rodda et al. 2010).

Cell filling was found most prominently at the hydrogel edges and significantly reduced in the central areas of the implant. This may be caused by an insufficient nutritional support of the infiltrated cells at the more central hydrogel areas resulting in cell migration from the hydrogel center towards the periphery. To examine whether the cell filling at the hydrogel center varies over time, timeline experiments at earlier timepoints post-injury (1- and 2-weeks after SCI) are required. Alternatively, cells might be apoptotic due to a hostile environment at the central hydrogel area, which could be assessed via Live/Dead assays as previously done *in vitro* (Schackel, Kumar et al. 2019).

Along with greater host cell infiltration and survival, axonal growth was enhanced at channel entries in PLO/laminin-coated hydrogel implants compared with non-coated controls but equally decreased in both groups towards the hydrogel center. Since surface coating was sufficient for cell attachment throughout the entire length of the hydrogel channels *in vitro*, the decrease in axonal growth might be attributed to the lower cell filling at the hydrogel center rather than to insufficient surface coating (Schackel, Kumar et al. 2019). Although there is a possibility for a shift in the cellular composition at the central hydrogel areas, our immunolabeling data indicate a rather homogenous cellular composition of macrophages/microglia and Schwann cells throughout the entire hydrogel.

An obstacle for axonal regeneration through biomaterial implants represents astroglial scarring around the implantation site. In our study, we found an area of irregular hypercellular tissue around the hydrogel implants but, surprisingly, this host-graft interface was devoid of astrocytes and only individual $GFAP^+$ processes were extended from host astrocytes at the boundary between host and implant. However, host astrocytes formed thin but distinct borders at the boundary between the implant and the adjacent spinal cord, indicating astroglial scarring around the implantation site. This may hinder growing axons to cross the host-graft boundary due to the expression of axon growth-repulsive molecules such as CSPGs by reactive astrocytes and/or cells directly at the host-graft interface. Additionally, CSPG upregulation is also evident in the uninjured host spinal cord adjacent to the implantation site potentially impeding axonal re-entry (Silver and Miller 2004, Cregg, DePaul et al. 2014, Schwab and Strittmatter 2014, Sofroniew 2015). Nonetheless, there is growing evidence that an astroglial scar and high CSPG expression levels around the SCI lesion site *per se* do not ultimately prevent axonal crossing of SCI sites (Kawaja and Gage 1991, Zukor, Belin et al. 2013, Anderson, Burda et al. 2016). In line with this, we found βIII-tubulin-labeled axons enter the hydrogel implants from the rostral as well as caudal host spinal cord what contradicts an impermeable scar around the implantation site.

Most importantly, axons were not found extending in channels that were devoid of cells in any of the analyzed animals. In cell-filled channels, extending axons were mostly located centrally in the channel lumen and never found in direct contact with the alginate-based hydrogel itself. Consequently, it appears that the infiltrated host cells serve as cellular substrates for growing axons within the hydrogel channels; hence, surface coating alone does not affect axonal growth directly but indirectly by improving host cell viability within the alginate-based hydrogels. This differs from the *in vitro* results, where PLO/laminin-coating leads to neurite outgrowth of DRG neurons. However, this suggests that a cellular growth substrate may possess a greater axonal growth-promoting effect surface protein-coating itself. Further support comes from the fact that axonal growth during development is mediated via interaction of cell surface receptors with various components of the ECM which are present on cellular surfaces (Volpato, Fuhrmann et al. 2013, Fawcett and Verhaagen 2018). Most likely, the infiltrated Schwann cells might have served as an axonal growth-promoting cellular substrate in the hydrogel implants rather than the co-infiltrated macrophages and microglia (Weidner, Blesch et al. 1999, Pearse, Sanchez et al. 2007). Indeed, activated macrophages and microglia were found to be somewhat detrimental for axonal regeneration (Lang, Cregg et al. 2015, Anderson, Burda et al. 2016, van Niekerk, Tuszynski et al. 2016). In comparison to previous work from our laboratory, axonal growth within surface-coated hydrogel implants was 40% greater than in hydrogels seeded with BMSCs expressing GFP (~350 axons/mm^2 in PLO/laminin-coated hydrogels vs. ~250 axons/mm^2 in BMSC-seeded hydrogels at Rostral 100 µm) (Gunther, Weidner et al. 2015). Thus, the data indicate that a biologically active protein coating of the hydrogel surface helps to establish a substrate of infiltrated host cells within the hydrogel channels which is more effective in promoting axonal regrowth than a cellular substrate consistent of pre-seeded autologous BMSCs.

Thus, our data suggest that surface coating of alginate-based hydrogels improves their biocompatibility, thereby enhancing cell viability *in vitro* and *in vivo.* Surface coating, however, does not directly promote axonal growth through the hydrogel implants *in vivo* but instead creates a favorable molecular environment for host cell colonization within the implants. Hence, the infiltrated host cells, mainly Schwann cells, serve as a cellular growth substrate for the regrowing spinal axons. These findings further underline the notion that the combination of biomaterial implants with additional cell transplantation and/or factor delivery show great pro-regenerative potential (Suzuki, Kitaura et al. 2002, Teng, Lavik et al. 2002, Joosten, Veldhuis et al. 2004, Deumens, Koopmans et al. 2006, Nomura, Baladie et al. 2008, Olson, Rooney et al. 2009, Rauch, Hynes et al. 2009, Gao, Lu et al. 2013, Li, Xiao et al. 2013, Zeng, Qiu et al. 2015). In particular, cell transplantation and biomaterial implants act synergistically to overcome some limitations of each individual approach. For example, low survival rates of grafted

cells as well as inappropriate filling of the lesion cavity after transplantation into acute SCI sites can be solved when the cells are delivered via a biomaterial (Olson, Rooney et al. 2009, Bozkurt, Mothe et al. 2010, Park, Lee et al. 2012). Notably, the biomaterial serves as a physical adherence matrix for the grafted cells and protects them in parallel from the hostile acute lesion environment. Surface coating and other biofunctionalization methods of biomaterial implants may serve as additional parameters to enhance graft cell survival. Since laminin displays a generally permissive biological signal for growing cells and neurites, surface coating with other ECM components such as hyaluronic acid, collagen, fibronectin or Matrigel might transduce an even stronger bioactive signal (Fouad, Schnell et al. 2005, Novikova, Mosahebi et al. 2006, Wang, Zhao et al. 2006, Tonge, de Burgh et al. 2012, Volpato, Fuhrmann et al. 2013). However, surface modification with full length proteins might potentially be problematic since bioactivity of several cell surface proteins requires a distinct 3D orientation and/or steric constellation.
In our hands, surface coating with PLO and laminin was sufficient enough to support survival of the seeded immature astrocytes within the alginate-based hydrogel implants for at least 4 weeks post-injury. When immature astrocytes were additionally grafted into the surrounding uninjured host spinal cord, the transplanted astrocytes survived even more robustly within the hydrogel implants. In contrast, other transplantation studies used additional growth factors or calpain inhibitor to ensure survival of grafted NSCs/NPCs (Fuhrmann, Tam et al. 2016) (Johnson, Tatara et al. 2010). Intrinsically, NSCs have a greater proliferative capacity than differentiated precursors populations such as our grafted immature astrocytes. However, the robust survival of the grafted astrocytes remains remarkable, especially when compared with the low survival rates reported for adult brain- or spinal cord derived NPCs/NPCs within chitosan channel implants without additional trophic support (Kim, Tator et al. 2011, Guo, Zahir et al. 2012).

4.2 The permissive astrocytic cellular substrate for axonal regeneration within biomaterial implants

Surface-coated alginate-based hydrogels were primarily filled with mainly Schwann cells and macrophages/microglia 4 weeks post-injury. Although Schwann cells support axonal regeneration, tissue sparing and remyelination after SCI, they are not endogenous to the naïve spinal cord (Weidner, Blesch et al. 1999, Pearse, Sanchez et al. 2007). This raises the question of whether CNS endogenous cells would provide an even more permissive cellular substrate for axonal growth within our hydrogel implants. Previously, we successfully showed that our alginate-based hydrogel implants could be used in combination with the transplantation of BMSCs

(Gunther, Weidner et al. 2015) and syngeneic adult Schwann cells (Liu, Sandner et al. 2017). Similar to Schwann cells, BMSCs are not natural residents to the naïve spinal cord, and cellular grafts containing BMSCs or SCs tend to form distinct boundaries and therefore poorly integrate into the host spinal cord (Weidner, Blesch et al. 1999, Vroemen, Caioni et al. 2007, Gunther, Weidner et al. 2015, Williams, Henao et al. 2015). Hence, the BMSC- and SC-seeded hydrogel implants remain separated from the surrounding host spinal cord, which may essentially contribute to the failure of axons to easily cross the implantation site and re-enter the host spinal cord in the previous studies. We, therefore, sought to examine whether proper integration of our alginate-based hydrogel implants can be achieved by co-transplantation of cells that are endogenous to the CNS, thereby enhancing axonal growth through the SCI lesion. Consequently, we selected immature astrocytes as cellular candidates for hydrogel seeding and co-transplantation, which were previously shown to structurally support axonal growth similar to radial glia cells during development (Mason, Edmondson et al. 1988, Kliot, Smith et al. 1990, Hasegawa, Chang et al. 2005, Raper and Mason 2010, Wanner, Anderson et al. 2013, Shih, Lacagnina et al. 2014, Zhang, Burda et al. 2015, Rigby, Gomez et al. 2020). Grafts of immature astrocytes were previously shown to mediate neuroprotective as well as axonal growth-promoting capacities. For example, fetal E13.4 spinal cord-derived astrocytes improved survival of dopaminergic neurons and parvalbumin^{+} interneurons after 4 weeks-delayed transplantation into 6-hydroxy-dopamine (6-OHDA) hemiparkinsonian rats (Proschel, Stripay et al. 2014). Similarly, grafted fetal spinal cord-derived astrocytes facilitated neuroprotection of phrenic motor neuron pools in an amyotrophic lateral sclerosis (ALS) model in mice (SOD^{G93A}) by re-establishment of neurotransmitter homeostasis and amelioration of microglia activation (Lepore, Rauck et al. 2008). After SCI, transplanted human GRPs differentiated into functional astrocytes and supported regrowth of ascending sensory axons and descending raphe- and reticulospinal axons across both, cervical hemisection as well as DCL injuries (Jin, Neuhuber et al. 2011, Jin, Shumsky et al. 2018). Hence, the transplantation of immature astrocytes can lead to neuroprotective and axonal growth-promoting effects in the severed CNS without a potential risk of tumor formation as reported for undifferentiated stem cell grafts (Lee, Tang et al. 2009, Priest, Manley et al. 2015).

Transplantation of undifferentiated GRPs, however, did not have any effect on axonal growth or even detrimental effects (Davies, Proschel et al. 2008). Thus, transplantation of uncommitted glia precursors may harbor the potential for negative side effects which can be avoided when only cells that are terminally committed to the astrocytic lineage are transplanted. Indeed, *in vitro* pre-differentiation of fetal or ESC-derived GRPs with factors associated with astrocyte differentiation and maturation *in vivo* (e.g., BMP-4 or CNTF), resulted in functionally distinct astrocyte precursor (GDAs) subpopulations (Davies, Proschel et al. 2008, Davies, Shih et al.

2011, Haas, Neuhuber et al. 2012, Haas and Fischer 2013). Controversially, only GDA^{BMP} were shown to support regrowing spinal axons as well as transiently decrease neurocan expression at acute SCI sites (Davies, Huang et al. 2006, Davies, Proschel et al. 2008, Davies, Shih et al. 2011), whereas Haas et al. did not find differences between BMP- or CNTF-GDAs after grafting into the injured spinal cord (Haas, Neuhuber et al. 2012, Haas and Fischer 2013). This discrepancy might be explained by slightly different cell sources and *in vitro*-differentiation protocols (Chu, Zhou et al. 2014). Given that our immature astrocytes were obtained from a later developmental stage (postnatal day 1 or 3) than the GRPs in the above-mentioned studies (E13.5 fetal spinal cord or ESCs), they most likely are already terminally committed to the astroglial lineage. Moreover, our grafted cells showed terminal astrocyte differentiation *in vivo*; hence, they do not represent undifferentiated GRPs but rather resemble pre-differentiated GDAs used by the previous studies (Davies, Huang et al. 2006, Haas, Neuhuber et al. 2012). Indeed, seeding of PLO/laminin-coated alginate-based hydrogel implants with immature cortex-derived astrocytes leads to improved tissue penetration of the implantation site and host-graft interactions as assessed by intermingled graft-derived and host-derived astrocytes at the host-graft interface, penetration of newly formed vasculature into the hydrogel channels, and most importantly, a striking enhancement of axonal growth within the hydrogel implants. Thus, immature cortex-derived astrocytes represent a permissive cellular substrate for axonal growth within biomaterial implants, which is in line with previous reports (Kliot, Smith et al. 1990, Wang, Chuah et al. 1995, Joosten, Veldhuis et al. 2004). Notably, pro-regenerative effects of immature astrocytes after transplantation into SCI sites were mostly observed when the astrocytes were grafted within a biomaterial implant, for instance a Millipore pennant (Kliot, Smith et al. 1990) or a collagen matrix (Wang, Chuah et al. 1995, Joosten, Veldhuis et al. 2004). Particularly, the grafted astrocytes reduced the volume of the astroglial scar around the implantation site (Wang, Chuah et al. 1995) and established cellular continuity between graft and the surrounding host spinal cord across already formed astroglial scars (Joosten, Veldhuis et al. 2004). In contrast, when graft and host tissue were spatially separated by dense scar tissue, axonal growth into the implants was limited (Wang, Chuah et al. 1995). Even without astrocyte grafting, irregular astrocyte interface borders between lesion site and surrounding host tissue were found to facilitate greater regrowth of brain stem-derived spinal axons (vestibular, reticular, serotonergic, noradrenergic) compared with animals, which showed sharp distinct borders of GFAP-labeled astrocyte protrusions around a SC-seeded PAN/PVC channel implant at a thoracic full transection lesion (Williams, Henao et al. 2015). Likewise, linearly aligned PLA fiber conduits mediated aligned of host astrocytes at the margins of the implantation site which improved axonal growth into the conduits after Th9 transection (Hurtado, Cregg et al. 2011). Astrocyte alignment between lesion site and adjacent uninjured host spinal cord was also

found when different astrocyte population derived from either fetal spinal cord-derived GRPs or human ESCs were transplanted into acute cervical DCL injuries (Davies, Huang et al. 2006, Davies, Proschel et al. 2008, Davies, Shih et al. 2011). Similarly, Hasegawa et al. found tissue re-organization at the penumbra of a thoracic contusion injury after implantation of an immortalized radial glia-like cell line derived from fetal spinal cord-GRPs (Hasegawa, Chang et al. 2005). Most intriguingly, alignment of astrocytes across SCI sites was associated with greater regrowth of rubrospinal and ascending sensory axons and finally robust locomotion recovery on the horizontal ladder test (Davies, Huang et al. 2006, Davies, Proschel et al. 2008). These findings suggest that alignment of either grafted or host astrocytes at the lesion margins crucially contributes to axonal growth through SCI sites. In our study, the seeded immature astrocytes formed longitudinal bundles of astrocytic processes with the host astrocytic network spanning the host-graft interface. Host-derived axons were found closely associated with these astrocytic processes indicating alignment of graft- and host-derived astrocytes similar to those observed in previous studies (Hurtado, Cregg et al. 2011, Williams, Henao et al. 2015).

Thus, the combination of astrocyte grafting with the defined channel structure of our alginate-based hydrogel implants may have led to longitudinal tissue re-organization and alignment across the entire SCI lesion site, whereas cell grafts alone did result only in alignment at the lesion margins (Davies, Huang et al. 2006). Further evidence arises from other studies that delivered astrocytes and astrocyte precursor cells into SCI lesion cavities without a supportive biomaterial matrix and barely saw any effect at all or even detrimental effects. Notably, negative outcomes were mainly observed, when the grafted astrocytes formed dense clusters instead of loose grafts with extended astrocytic processes into the surrounding spinal parenchyma as seen for neonatal P1 forebrain-derived astrocytes transplanted into focal infarct lesions of the dorsal funiculus (Hayashi, Hashimoto et al. 2011, Olby and Blakemore 1996). In another study, iPSC-derived astrocytes were grafted into the epicenter of a moderate Th8 contusion injury in adult rats. Although the grafted cells penetrated the host astrocytic network, they did not align longitudinally with host astrocytic processes nor with spinal axons (Hayashi, Hashimoto et al. 2011). Most importantly, misaligned astrocyte grafts did not support axonal growth after SCI and were additionally associated with the induction of thermal and mechanical allodynia due to pathologic sprouting of $CGRP^{+}$ axons in the dorsal horn caudal to the injury (Davies, Proschel et al. 2008).

To summarize, immature astrocytes serve as a permissive cellular substrate within hydrogel implants, strikingly promoting axonal growth, specifically in comparison with previous work using autologous BMSCs (Lu, Yang et al. 2004, Gunther, Weidner et al. 2015) or syngeneic adult SCs without any further ectopic trophic factor delivery after traumatic SCI (Plant, Bates et al. 2001, Liu, Sandner et al. 2017). Regrowing spinal axons preferentially enter and extend within

hydrogel channels that contained the grafted astrocytes rather than channels that were filled with infiltrated host cells. Furthermore, the grafted astrocytes established interactions and aligned with the host astrocytic network across the host-graft interface. Thus, immature astrocytes seeded into an alginate-based hydrogel implants can promote axonal regrowth and facilitate host-graft interactions after SCI.

4.3 Differences between astrocyte populations

Astrocytes represent a highly adaptive and plastic cell population with complex functional and morphological patterns. Accordingly, astrocytes display an enormous degree of heterogeneity across the entire CNS during development, health and disease (Westergard and Rothstein 2020). In the first transplantation study, we co-transplanted immature cortex-derived astrocytes together with alginate-based hydrogel implants into a cervical SCI lesion. Although promising results in terms of host-graft interactions and promoted axonal regrowth were obtained with cortex-derived astrocytes, we wondered whether spinal cord-derived astrocytes further enhance implant integration and axonal growth. Consequently, we tested immature spinal cord-derived astrocytes as potential candidates for biomaterial-supported cell transplantation into acute SCI sites.

Developmentally, astrocytes arise from NSCs and glia-restricted precursors in different stem cell and precursor niches in the brain and spinal cord. In rodents, astrocyte specification starts at E10 to E12.5 in the spinal cord and slightly later in the forebrain, where it occurs from E16 to E18 (Deneen, Ho et al. 2006). Astrocyte specification is immediately followed by a stage in which maturing APCs migrate along radial glia-like processes towards their final destination in the CNS. Importantly, APC migration happens extensively in the developing and postnatal brain, whereas it is restricted to individual spinal segments in the developing spinal cord (Jacobsen and Miller 2003). However, the temporal sequence of astrocyte specification and maturation are still incompletely understood (Hochstim, Deneen et al. 2008). Thus, those developmental differences may have implications on maturation stages of neonatal cortex- and spinal cord-derived astrocytes.

Thus, to elucidate potential developmental differences, we isolated primary astrocytes from the cortex and the spinal cord of neonatal rats at postnatal days 1 and 3 and phenotypically characterized them *in vitro* as well as *in vivo*. Indeed, we found a differing marker expression pattern *in vitro* between cortex- and spinal cord-derived astrocytes at both tested postnatal timepoints. The difference in the expression of the astrocytic marker GFAP was most prominent between the two astrocyte subpopulations, since > 95% of all cortex-derived cells ex-

pressed GFAP, whereas only about 60 to 65% GFAP$^+$ were detected in primary cultures derived from postnatal spinal cord independent from the developmental timepoint. However, after transplantation into the intact spinal cord, no difference in GFAP expression was present indicating terminal differentiation of the grafted immature astrocytes *in vivo*. Nearly all grafted cells expressed GFAP already 2 weeks after transplantation, which was consistent through the 4 week timepoint identifying the grafted cells as late astrocyte precursors or terminally differentiated astrocytes (Allaman, Belanger et al. 2011). In line with this, Sox2 and Sox 9 expression were elevated in grafted cortex- and spinal cord-derived astrocytes. Previously, transcriptome analysis found *Sox2* expression to be enriched in purified mouse cortex-derived astrocytes (Cahoy, Emery et al. 2008, Zhang, Chen et al. 2014). Although Sox2 is thought to be responsible for cellular maintenance and maintenance of embryonic stem cell pluripotency (Kiefer 2007, Matsushima, Heavner et al. 2011), Kautzman et al. were able to link persistent *Sox2* expression to astrocyte maturation in the neonatal mouse retina (Kautzman, Keeley et al. 2018). This idea is further supported by high Sox9 expression in both astrocyte populations after transplantation. Similar to Sox2, Sox9 is expressed by neural stem/progenitor cells to maintain stemness and involved, first, in the onset of gliogenesis by inducing NFIA/B expression, and second, in the initiation of astrocyte specification/migration (Stolt, Lommes et al. 2003, Kang, Lee et al. 2012). However, high *Sox9* levels were also found as a hallmark of reactive astrocytes by Hara et al. but the ability to induce reactivity could also be seen as an indicator for full maturity of the grafted cells (Hara, Kobayakawa et al. 2017). Hence, elevated Sox2 and high Sox9 expression levels might reflect ongoing astrocyte maturation of the grafted astrocytic cells. Surprisingly, the expression profiles of the intermediate filament proteins Vimentin and Nestin were not altered *in vivo* compared with the *in vitro* results. Although both markers label NSCs (Sancho-Tello, Valles et al. 1995, Gilyarov 2008) expression profiling on astrocytes isolated either from intact or injured spinal cords of mice showed enhanced mRNA levels for Nestin and Vimentin at 7 dpi but decreased levels at later timepoints (Hara, Kobayakawa et al. 2017). Given that Nestin and Vimentin levels were analyzed exclusively on the protein level via immunolabeling in our study, both proteins might be detectable even at later timepoints post-injury than their respective mRNA. Moreover, enhanced Vimentin and Nestin levels were associated with an increased reactivity state of the astrocytes but not involved with astroglial scarring (Hara, Kobayakawa et al. 2017). Thus, our data might partially reflect the reactive astrocyte phenotype that Hara and colleagues identified after transplantation, since even minimal manipulations like cell injections produce a small injury to the spinal cord. Accordingly, Nestin expression was not exclusively elevated in the grafted GFP-labeled cells but also in neighboring host-derived astrocytes (GFP$^-$/GFAP$^+$).

The corresponding changes in the molecular milieu at the injection site might eventually induce a status of reactivity in the grafted astrocytes. Furthermore, about 80% of all grafted astrocytes co-expressed GFAP and A2B5, which labels different NPC populations during development but in adulthood, $GFAP^+/A2B5^+$ astrocytes were identified as terminally differentiated fibrous astrocytes (Raff, Abney et al. 1983, Bonaguidi, McGuire et al. 2005). Additionally, a subclass of $GFAP^+/A2B5^+$ astrocytes were found to retain a certain degree of stem cell-like pluripotency representing a quiescent progenitor pool potentially capable of adult neurogenesis (Kondo and Raff 2000, Imura, Kornblum et al. 2003, Morshead, Garcia et al. 2003, Garcia, Doan et al. 2004). The fibrous astrocyte identity of the grafted cells is further supported by the observed prominent fibrous cell morphology of the cortex- and spinal cord-derived astrocytes *in vitro*. *In vivo*, both astrocyte populations similarly adopted a differentiated morphology with long and thin $GFAP^+$ processes resembling the classical fibrous astrocyte morphology found throughout the WM of mammals (Bushong, Martone et al. 2002, Sofroniew and Vinters 2010).

Finally, the grafted cells expressed molecular markers of functional, terminally differentiated astrocytes, namely GLT-1/EAAT2, S100β, and AQP4. The glutamate transporter GLT-1/EAAT2 is the major astrocytic glutamate transporter in the mature CNS. Its expression appears to increase from 2 to 4 weeks *in vivo*, pointing towards the functionality of the grafted astrocytes and a potential involvement in glio-/neurotransmitter homeostasis (Furuta, Rothstein et al. 1997, Schreiner, Durry et al. 2014). S100β is expressed by late astrocyte precursors and fully mature astrocytes (Seri, Garcia-Verdugo et al. 2004). Additionally, about 50% of all grafted cells were $GFAP^+/AQP4^+$. Under healthy conditions, AQP4 is expressed in the endfeet of terminally differentiated astrocytes and involved in water and ion homeostasis, astrocyte migration and maintenance of the blood-brain/spinal cord-barrier (Camassa, Lunde et al. 2015, Ikeshima-Kataoka 2016). However, AQP4 is predominantly expressed by perivascular astrocytes in direct contact with blood vessels and endothelial cells, so a moderate percentage of AQP4-positive labeling does not necessarily point towards an immature state of the grafted astrocytes. Both astrocyte populations formed $CX43^+$ contact sites with host-derived astrocytes. CX43-labeled contact sites between astrocytes can be taken as signs for integration of the grafted cells into the perivascular astrocytic network of the host (Ezan, Andre et al. 2012, Chen, Qian et al. 2015, Lien, Tuszynski et al. 2019). Additionally, our grafted GFP-expressing cells aligned with host spinal axons similar to the results of Davies et al., where fetal spinal cord-derived and ESC-derived immature astrocytes aligned with host-derived axons after transplantation into a dorsal column lesion in adult Sprague-Dawley rats (Davies, Huang et al. 2006, Davies, Proschel et al. 2008). Thus, our data suggest that although minor differences

between immature cortex- and spinal cord-derived astrocytes exist *in vitro*, both astrocyte populations equally harbor the potential to differentiate into fully mature and functional astrocytes *in vivo*.

Another line of evidence arises from the characterization of both astrocyte populations after transplantation into the acutely injured spinal cord. Similarly, most of the grafted cortex- and spinal cord-derived astrocytes co-expressed GFAP (> 95% $GFP^+/GFAP^+$) and Vimentin (~ 80% $GFP^+/GFAP^+/Vim^+$) 4 weeks after SCI. Importantly, after transplantation into the uninjured spinal cord, Vimentin expression was mostly restricted to the grafted astrocytes, whereas after SCI, Vimentin is overall elevated in the injured spinal cord. In particular, grafted GFP^+ but also host-derived GFP^- astrocytes were co-labeled with $GFAP^+/Vim^+$, but only a small fraction of the grafted cells were proliferative (~ 20% $GFP^+/GFAP^+/Ki67^+$). Proliferative GFAP-expressing astrocytes are, in general, considered as reactive and potentially scar-forming (Sofroniew and Vinters 2010). However, live imaging studies showed only ~ 10% of the $GFAP^+$ astrocytes were proliferating and not necessarily associated with astrocyte scarring after traumatic stab wound injury of the brain (Bardehle, Kruger et al. 2013). Hence, both host- and graft-derived astrocytes may be in a reactive state under injury conditions. In concordance, recent transcriptome analysis revealed striking differences within the pool of “reactive astrocytes”: although Vimentin and GFAP overexpression are typical indicators for a state of reactivity in astrocytes, detrimental reactivity states (e.g., neurotoxicity, scar-formation) as well as beneficial reactivity states (e.g., ROS buffering, sealing of BSCB leakage) can be classified by the expression of specific transcripts (Hara, Kobayakawa et al. 2017). Liddelow et al. referred to these bimodal reactivity states as neurotoxic A1 astrocytes and rather pro-regenerative A2 astrocytes, respectively, based upon a panel of 10 differentially expressed genes after stimulation of isolated primary astrocytes with potent molecular triggers of astrocyte reactivity (Liddelow, Guttenplan et al. 2017). However, since no signs for severe astrocyte reactivity such as extensive cellular hypertrophy and formation of a distinct astrocytic scar by the grafted or host astrocytes around the implantation site were found, both astrocyte populations might be in a beneficial reactive state.

Interestingly, the grafted astrocyte populations showed a differing migration behavior at the SCI lesion site. While grafted cortex-derived astrocytes spread out widely into the surrounding host spinal parenchyma (up to > 2 mm caudal from their injection site), the grafted spinal cord-astrocytes migrated preferentially towards the injury. Although it remains unclear why this difference exists, it may be due to the tissue origin of the transplanted cells. Extensive migration of cortex-residential astrocytes was evident after brain injury (Elvira, Garcia et al. 2015) which was also seen after transplantation of primary cortex-derived or human NSC-derived astro-

cytes into SCI lesions (Pencalet, Serguera et al. 2006, Lien, Tuszynski et al. 2019), while others reported a somewhat restricted host astrocyte migration after brain injury (Bardehle, Kruger et al. 2013). Likewise, endogenous spinal cord astrocytes appear to be rather restricted to their spatial domain after stab wound injury of the spinal cord. Perhaps, the grafted spinal cord-derived astrocytes might be more sensitive to the milieu of an acute SCI lesion, thereby directly attracted to the lesion site, while cortex-derived astrocytes might harbor a greater intrinsic migratory potential. Accordingly, immature cortex-derived astrocytes migrated over several millimeters within *ex vivo* postnatal brain slices (Jacobsen and Miller 2003).

To summarize, P1 cortex- and P3 spinal cord-derived astrocytes show minor phenotypical differences *in vitro* but equally mature and terminally differentiated *in vivo* within the intact and injured adult spinal cord. Immunolabeling by various molecular astrocyte markers elucidated the heterogeneous character of the transplanted astrocytes. Although, nearly all grafted cells could be associated with the astrocytic lineage, subgroups were identified as late astrocyte precursor cells/maturing astrocytes, while others were terminally differentiated fully mature astrocytes expressing functional astrocyte markers (e.g., AQP4, GLT-1). Hence, the environment of the acutely injured spinal cord equally induced terminal differentiation and progressing maturation in the grafted cortex- and spinal cord-derived astrocytes. Moreover, both grafted astrocyte populations may have adopted a state of reactivity after SCI as indicated by elevated Vimentin expression 4 weeks post-injury. The ability to induce astrocyte reactivity can be taken as another indicator for a mature and functional phenotype of the grafted astrocytes. These findings are in line with previous work showing that the microenvironment of the transplantation site can override the astrocyte-intrinsic differentiation program and drive astrocyte maturation and phenotypical plasticity (Hara, Kobayakawa et al. 2017, Li, Khankan et al. 2019).

Nonetheless, some constraints persist since the exact molecular and temporal mechanisms of astrocyte specification, maturation as well as astrocyte reactivity are still not fully understood and remain objects of ongoing research (Sofroniew 2014, Molofsky and Deneen 2015, Ceyzeriat, Abjean et al. 2016, Hara, Kobayakawa et al. 2017, Liddelow and Barres 2017). Firstly, GFAP is widely used as a universal astrocyte marker but its marker potential is limited and not exclusively restricted to astrocytic cells, for instance, DRG satellite cells or NPCs in the olfactory bulb also show a certain degree of GFAP expression (Allaman, Belanger et al. 2011). Moreover, its induction and expression level varies between species, CNS insult conditions, and even between individual astrocytes (Liddelow, Guttenplan et al. 2017, Pekny, Wilhelmsson et al. 2019). Hence, defining reliable molecular markers of astrocytic cells throughout development, during maturation, and into adulthood, as well as their interpretation remains extraordinarily challenging. Given that *GFAP* remains, however, the most consistently

induced gene in the astrocyte transcriptome, its combination with various markers and/or transgenic reporter lines harbor the potential to reliably label the majority of all astrocytic cells and to identify different astrocyte populations during health and disease (Emsley and Macklis 2006, Allaman, Belanger et al. 2011, Molofsky, Krencik et al. 2012, Zeisel, Hochgerner et al. 2018, Morel, Men et al. 2019, Pekny, Wilhelmsson et al. 2019). Even more intriguing, transcriptional analysis of astrocytes form intact and damaged spinal cord convincingly revealed that most markers that were classically associated with astrocyte development become upregulated again during reactivity, especially Vimentin and Nestin (Zamanian, Xu et al. 2012, Hara, Kobayakawa et al. 2017, Liddelow, Guttenplan et al. 2017). Secondly, it has to be noted that all procedures of cell isolation, cultivation and final transplantation change the molecular phenotype of the primary astrocytes. In this context, Foo et al. demonstrated that cortex-derived astrocytes can be consistently isolated in large quantities with stable marker expression profiles via immunopanning. These astrocytes were found to closely resemble astrocytes *in vivo* (Foo, Allen et al. 2011). Additionally, cultivating primary astrocytes under serum-containing conditions affects GFAP expression and potentially reactive behavior (Chaboub and Deneen 2013). Therefore, the obtained marker expression data of the isolated immature astrocytes might not entirely reflect the expression pattern of astrocytes in their natural environment (Cahoy, Emery et al. 2008, Doyle, Dougherty et al. 2008). Thirdly and most importantly, astrocytes are a highly adaptive and plastic cell population during development, adulthood and during the CNS response to insults. Various astrocyte subpopulations with differing functional phenotypes exist throughout the mammalian CNS which might have implications to their behavior after isolation and/or transplantation into the intact and severed spinal cord (John Lin, Yu et al. 2017, Morel, Chiang et al. 2017, Zeisel, Hochgerner et al. 2018). Furthermore, astrocytes respond to CNS insults in a finely tuned context-dependent manner; hence, reactivity states differ between SCI (Hara, Kobayakawa et al. 2017), Alzheimer's disease (Ceyzeriat, Ben Haim et al. 2018), ischemia (Liddelow, Guttenplan et al. 2017), and multiple sclerosis (Itoh, Itoh et al. 2018). Strikingly, quiescent and reactivity states of astrocytes are plastic and reversible dependent upon their molecular environment (Hara, Kobayakawa et al. 2017) making a precise definition and comparison of astrocytic phenotypes and reactivity states in response to a multi-faceted pathology, such as SCI, difficult.

4.4 Distal cellular grafts to improve host-graft interactions and tissue bridging after biomaterial implantation

Since the spinal cord is a highly organized anatomic structure, its regeneration benefits from defined physical guidance systems to ensure proper organization and guidance of the repaired tissues through the lesion site (Miller, Jeftinija et al. 2002, Gunther, Gunther et al. 2015, Koffler, Zhu et al. 2019). Although no excessive inflammatory reaction around surface-coated alginate-based hydrogel implants was observed, the implants were surrounded by irregular hypercellular tissue, while penetration of regenerating tissue (e.g., vascularization) through the implants was limited. Therefore, a direct structural connection between the surrounding uninjured host spinal cord and hydrogel implant should support regeneration across extended SCI sites. By combining a biomaterial implant with cell transplantation, a continuous cellular substrate spanning the SCI lesion cavity can be established (Ramon-Cueto, Cordero et al. 2000, Fouad, Schnell et al. 2005, Deumens, Koopmans et al. 2006).

Indeed, seeding of immature cortex-derived astrocytes into the channels of PLO/laminin-coated alginate-based hydrogel implants mediated cellular interactions between the grafted astrocytes and the astrocytic network of the host. In particular, host- and graft-derived astrocytes intermingled and aligned longitudinally serving as astrocytic bridges for growing host spinal axons across the host-graft interface. Furthermore, endothelial cells and possibly blood vessels were found to extend mainly within the astrocyte-containing implant channels. Moreover, in consecutive experiments, we were able to further enhance tissue penetration of the alginate-hydrogel implants by adding grafts of either immature cortex- or spinal cord-derived astrocytes rostrally and caudally of the implantation site, further establishing structural continuity between biomaterial implant and surrounding host spinal parenchyma.

In particular, although the grafted immature astrocytes showed robust survival within the hydrogel implants, the central regions of the hydrogels displayed only modest cell filling, when the astrocytes were exclusively seeded into the hydrogel channels. When additional astrocytic grafts were provided within the surrounding host spinal cord, the hydrogel channels were densely filled with graft-derived cells and a smaller fraction of host-derived cells over their entire length at 8 weeks after implantation. This effect was not observed when the astrocytes were just grafted caudally to the hydrogel implant. Here, cell filling was similar to animals that were implanted with only astrocyte-seeded hydrogels. Hence, the greater cell filling could be correlated with the additional astrocyte grafting around the injury site. Noteworthy, the prolonged experimental timeframe might partially also account for the enhanced central cell filling, although cell filling within control hydrogels was unaltered between 4- and 8-weeks post-injury. Additionally, the grafted astrocytes might have migrated from the center towards the hydrogel

edges resulting in lower cell filling at the hydrogel center. Since the hydrogel edges were in direct contact with the damaged spinal cord tissue immediately after lesion, the lesion environment might have attracted the grafted astrocytes comparable to host astrocytes that at least locally migrate towards acute sites of CNS insults (Okada, Nakamura et al. 2006, Elvira, Garcia et al. 2015). This scenario is probably most relevant in animals that only received astrocyte-seeded implants, since the filling of the hydrogel channels with seeded astrocytes was rather continuous in animals with additional rostral and caudal grafts. Here, astrocytes derived from the additional grafts might have ameliorated the acute injury environment thereby inhibiting further recruitment of astrocytes to the injury site. Alternatively, astrocytes derived from the surrounding grafts may have migrated into the hydrogel channels. However, central cell filling was also reduced in animals that received astrocyte-seeded hydrogel implant together with only a caudal astrocytic graft. The differing survival periods of the animals have to be considered, since animals with only a caudal graft survived for 4 weeks post-SCI, whereas animals with rostral and caudal grafts survived for 8 weeks. Perhaps, a longer survival period facilitated either greater astrocyte migration into the channels or progressing proliferation of the seeded astrocytes, since a small fraction of about 20% of the grafted astrocytes were found to be proliferative.

Alternatively, the lack of vasculature at the implantation site and within the hydrogel implants might have contributed to the lower central hydrogel cell filling without additional astrocytic grafts. In comparison to the destruction and following degradation of blood vessels 2 to 3 days post-injury (Whetstone, Hsu et al. 2003, Ng, Stammers et al. 2011), our injury model completely removed a 2 mm-wide block of spinal tissue, which lead to an immediate void of the vasculature at the lesion site. Consequently, the lesion site as well as the hydrogel channel lumen were without blood supply immediately after implantation leading to elevated apoptosis at the hydrogel center. Studies focused on contusive SCI revealed that endothelial cells give rise to newly formed microvessels starting at 3 dpi and finally restore the microvessel density to the level of the uninjured spinal cord within the first week after SCI (Casella, Marcillo et al. 2002, Dray, Rougon et al. 2009, Zhou, Zheng et al. 2019). Hence, the freshly formed blood vessels restore oxygen and nutritional supply improving graft cell survival and potentially axonal growth at the implantation site. This notion is supported by the fact that re-vascularization of the hydrogel implants was increased by transplantation of immature astrocytes into and even further enhanced by co-transplantation of immature astrocytes into the surrounding adjacent spinal tissue. Perhaps, the increased density of CD31-labeled blood vessels within astrocyte-seeded hydrogel implants might be due to the secretion of pro-angiogenic factors such as VEGF and Shh by the grafted astrocytes (Alvarez, Dodelet-Devillers et al. 2011, Argaw, Asp et al. 2012).

The grafted astrocytes might have additionally provided a structural guidance network for vascularization of the implantation site. Likewise, in the developing mouse retina, an astrocytic scaffold is established that physically guides endothelial tip cell filopodia during blood vessel extension in a VEGF/VEGFR-dependent fashion (Gerhardt, Golding et al. 2003, Chappell, Darden et al. 2019). Host cells at the implantation site may also act pro-angiogenic. For example, activated M1 macrophages secrete factors that initiate sprouting of freshly formed microvessels and M2 macrophages positively affect microvessel maturation and stabilization after SCI (Lutton, Young et al. 2012, Spiller, Nassiri et al. 2015). Within the hydrogel implants, many microvessels were at least partially enwrapped by the grafted astrocytes, potentially indicating the formation of a functional BSCB (Whetstone, Hsu et al. 2003). In line with this, a moderate fraction of the grafted cortex- and spinal cord-derived astrocytes expressed the perivascular astrocyte marker AQP4 and integrated via $CX43^{+}$ gap junctions into the host astrocytic network, which might be indicative for the participation of the grafted cells in functioning BSCB (Attwell, Buchan et al. 2010, Langer, Gerkau et al. 2017). Given that blood vessels lacking association with the grafted astrocytes might be malfunctioning (Casella, Marcillo et al. 2002), the functionality of the observed re-vascularization could be assessed by perfusion tracing with i.v. injection of EvansBlue or Di I in future studies (Li, Song et al. 2008, Walchli, Mateos et al. 2015).

Besides a positive effect on cell filling and graft cell survival, promoted vascularization of the implantation site might have positively affected axonal growth as well. Intriguingly, blood vessels secrete factors such as VEGF, artemin and several neurotrophins to guide and attract growing axons (Carmeliet and Tessier-Lavigne 2005, Hatakeyama, Ninomiya et al. 2020). Accordingly, in the PNS, blood vessel formation precedes SC migration, formation of bands of Bügner and finally axonal growth across nerve gaps after sciatic nerve transection. Moreover, the delivery of VEGF enhanced SC migration into the lesion site, thereby promoting axonal regeneration from the proximal into the distal nerve stump (Hobson, Green et al. 2000). Later studies confirmed that migrating SCs used pioneer blood vessels at the injury site as physical tracks (Cattin, Burden et al. 2015). Similarly, in the CNS, vasculature networks were shown to guide migrating neuroblasts in a laminin-β1 integrin-dependent way after stroke (Fujioka, Kaneko et al. 2017). After SCI, migrating SCs form the PNS enter the spinal cord and infiltrate the lesion site along the local spinal cord microvasculature. During migration within uninjured spinal cord tissue, perivascular astrocytes confine SCs to the surface of blood vessels segregating them from WM tracts (Afshari, Kwok et al. 2010). In contrast, after demyelination injury to the thoracic spinal cord of mice, endothelial cells of blood vessel walls around the lesion site upregulate fibronectin as well as β1 integrin allowing SC migration into the WM and towards

the lesioned area. Although the exact molecular mechanisms remain elusive, Eph/ephrin signaling from pericytes and potentially perivascular astrocytes might be involved in controlling SC migration along blood vessels (Garcia-Diaz, Bachelin et al. 2019). Hence, blood vessels serve as physical guidance structures for cell migration and -although indirectly- for axonal growth after SCI. In our studies, vascularization of the hydrogel implants and the surrounding host-graft interface was greater after co-transplantation of either immature cortex- or spinal cord-derived astrocytes along with more axonal growth in the hydrogel implants. This data is in line with other reports that showed a positive correlation between blood vessel ingrowth and density with axonal growth within biomaterial implants after Th9 full transection in adult female Fischer and Sprague-Dawley rats (Madigan, Chen et al. 2014).

Another aspect that influenced the enhanced axonal growth into and through the alginate-based hydrogel implants may have been the longitudinal astrocytic bridges spanning the host-graft interface, thereby connecting the hydrogel implant with the adjacent spinal tissue. Although astrocytic bridges were also observed when the immature astrocytes were only seeded into the hydrogel implants, they appear more prominent when astrocytes were additionally grafted into the rostral and caudal host parenchyma. Host axons were often closely associated with these astrocyte bridges at the rostral and caudal host-graft interface, suggesting that the bridges provided physical guidance for the growing axons. Importantly, numerous studies identified the formation of astrocytic tissue bridges and tissue alignment at the periphery of SCI lesions as an anatomical predictor for axonal growth through SCI sites (Joosten, Bar et al. 1995, Xu, Guenard et al. 1995, Guest, Hesse et al. 1997, Spilker, Yannas et al. 2001, Iseda, Nishio et al. 2004, Ma, Wei et al. 2004, Liu, Lu et al. 2010, Hurtado, Cregg et al. 2011, Zukor, Belin et al. 2013, Cregg, DePaul et al. 2014). However, why such bridges form remains vastly unknown. Probably, since reactive astrocytes share some characteristics with immature astrocytes (Wanner, Anderson et al. 2013) and axons grow along radial glia trajectories or immature astrocytes during development (Mason, Edmondson et al. 1988, Hasegawa, Chang et al. 2005, Raper and Mason 2010), graft- and host-derived reactive astrocytes at the lesion site may recapitulate these developmental scaffolding properties. Immunolabeling analysis showed that subgroups of the grafted astrocytes still express differentiation markers after transplantation into the intact spinal cord; hence, their partially immature phenotype may allow them to act as they would during CNS development. Although the expression of maturation markers after transplantation into the acutely injured spinal cord was not specifically assessed in the present study, this might still be a possible explanation for the formation of the longitudinal astrocyte bridges. Likewise, *in vitro* studies showed stable longitudinal alignment of immature cortex-derived astrocytes (East, de Oliveira et al. 2010, Winter, Katiyar et al. 2016). Although astrocytes alignment as initiated by collagen-based hydrogel tubes in both studies, the

aligned astrocytic bundles retained their stability after removal of the hydrogel mold. Interestingly, DRG neurons were shown to grow along these astrocyte bundles (Winter, Katiyar et al. 2016). Moreover, in the study of Winter et al., the aligned astrocytes adopted an elongated bipolar cell shape (Winter, Katiyar et al. 2016), which was also observed for the co-grafted spinal cord-derived astrocytes in our study.

The astrocytic bundles at the rostral and caudal host-graft interface consisted of graft- as well as host-derived astrocytes. Since the grafted astrocytes harbor the potential to form $CX43^+$ direct contact sites with the host-astrocytic network, the mixed astrocyte population might have formed an astrocytic syncytium. Astrocytic responses to altered CNS conditions or insults are known to be orchestrated via cell-cell communication through CX43-positive gap junctions (Retamal, Froger et al. 2007, Orellana, Montero et al. 2013, Lagos-Cabre, Alvarez et al. 2017). Thus, the grafted astrocytes might have instructed host-derived astrocytes to align via those intercellular communication patterns. Although, whether an interconnected cellular network was formed after astrocyte co-transplantation was beyond the scope of this study, it can be examined via live imaging of Ca^{2+} wave dynamics and their propagation between graft- and host-derived astrocytes (Bazargani and Attwell 2016).

Within the alginate-based hydrogels, axonal growth was significantly improved by both grafted immature astrocyte populations, whereas axon numbers in the non-seeded control hydrogels were consistently lower at 4 and 8 weeks post-implantation. The greatest axonal growth in each study was found at the rostral end of the hydrogel implants suggesting growth promotion of descending spinal tracts. Axonal growth declined towards the hydrogel center in all experimental groups, nonetheless, with additional astrocytic grafts within the surrounding host spinal cord, we were able to ameliorate this decline partially. Noteworthy, the number of serotonergic raphespinal axons was especially high in hydrogels containing cortex-derived astrocytes in all studies. Since raphespinal axons originate from brainstem nuclei, cortex-derived astrocytes potentially preferentially attract them due to their brain origin. Accordingly, a study by Petit et al. demonstrated that neonatal cortex-derived astrocytes preferentially attracted $5\text{-}HT^+$ axons after transplantation into the striatum of adult rats (Petit, Pierret et al. 2001). In our study, the 5-HT-labeled axons appeared to have a rather branched than extended morphology within hydrogel channels seeded with immature cortex-derived astrocytes; hence, the astrocytic substrate within the hydrogel channels might have induced axonal branching or dendridization rather than long distance-growth. In concordance, Tom et al. showed that serotonergic axons tend to extend dendritic protrusions in areas of a high density of GFAP-expressing astrocytes in acute brain slice cultures *in vitro* (Tom, Steinmetz et al. 2004).

Surprisingly, axon numbers at the caudal hydrogel end were elevated 8 weeks post-injury. In comparison to the previous studies, axonal growth was more constant throughout the rostrocaudal extent of the implants, so the elevated axon numbers might account for axons that completely crossed the hydrogels. However, axon numbers were still significantly lower at the central hydrogel compared with the caudal edge; hence, the greater axonal growth at the caudal half may be rather due to the entry of ascending axons. Although the origin of these caudal axons remains unknown, they may account for regrowing sensory axons from the periphery. Likewise, Kliot et al. showed already in 1990 that grafts of immature astrocytes attract sensory axons from DRGs (Kliot, Smith et al. 1990). To clarify the origin of theses ascending axons, the retrograde tracer cholera toxin subunit B (CTB) could be used to label sensory fibers from the fore- and hindlimbs via injection into the ulnary nerve (Kathe, Hutson et al. 2016) and sciatic nerve, respectively (Massey, Hubscher et al. 2006, Alto, Havton et al. 2009). Alternatively, since the number of BDA-traced axons was increased in animals that received rostral and caudal astrocytic grafts at the caudal hydrogel edge as well, descending axons might have started to branch rather than further elongate at the caudal hydrogel halves. Due to the anatomical coordinates of the BDA tracer injection, a subfraction of the BDA-traced axons belongs to the corticospinal tract (CST). Previously, local sprouting of spared and severed descending spinal axons -including CST axons- was shown to contribute to limited spontaneous or treatment-induced functional restoration after SCI (Fouad, Pedersen et al. 2001, Weidner, Ner et al. 2001, Bareyre, Kerschensteiner et al. 2004, Ballermann and Fouad 2006, Kanagal and Muir 2008, Kanagal and Muir 2009). Hence, the greater number of BDA-traced axons within the implants could be attributed to sprouting of BDA-traced descending axons. A molecular reason for potential promoted branching of descending axons might be BDNF expression by the grafted astrocytes within the hydrogel channels. Indeed, reactive astrocytes were shown to express significant levels of BDNF in response to neuroinflammation, demyelination injury and compressive SCI (Ikeda, Murakami et al. 2001, Saha, Liu et al. 2006, Fulmer, VonDran et al. 2014, Hong, Zhao et al. 2016). Similarly, Sasaki et al. reported enhanced sprouting of descending axons after transplantation of BDNF-expressing MSCs into dorsal hemisection lesions in rats (Sasaki, Radtke et al. 2009), which is consistent with previous observations from our own laboratory (Gunther, Weidner et al. 2015). Alternatively, contralateral sprouting of descending axons might have caused the elevated BDA-labeled axon numbers at the caudal edge of the hydrogels. In particular, descending spinal axons might have passed the injury site on the contralesional spinal cord side and extended axonal sprouts into the lesioned side caudal to the lesion, which entered the hydrogel channels from the caudal side. Likewise, contralateral CST axons were shown to sprout to the lesioned side in the lumbar spinal cord several spinal segments caudal to a unilateral T7 hemisection in mice (Collyer, Catenaccio et al. 2014). This

possibility is rather unlikely, since BDA^+ axons were found only occasionally caudal to the lesion site. Alternatively, BDA-labeled axons on the ipsilateral spinal cord side approach the implantation site, do not enter the hydrogel channels but circumvent the implant medially or laterally. However, to determine the origin and identity of the axons at the caudal hydrogel edge, additional tract-specific tracing studies are necessary.

In summary, our data indicate that a continuous cellular substrate across an extended 2 mm-wide SCI lesion site can be established by implantation of an astrocyte-seeded alginate-based hydrogel implant and additional co-transplantation of immature astrocytes into the surrounding host spinal cord. Host- and graft-derived astrocytes intermingled and aligned across the host-graft interface providing physical guidance for regrowing axons. Furthermore, the grafted astrocytes improved vascularization and axonal growth into and through the alginate-based hydrogel implants.

4.5 Hurdles to axonal crossing at biomaterial implantation sites and axonal re-entry into the distal host spinal cord

Various experimental approaches have been developed to support and maximize axonal growth beyond biomaterial implants after SCI. However, axonal re-entry into the distal spinal cord after application of a biomaterial implant remains unseen or occasional at best. By incorporation of bioactive compounds (Pakulska, Vulic et al. 2013, Colello, Chow et al. 2016, Pakulska, Elliott Donaghue et al. 2016), trophic factors (Patist, Mulder et al. 2004, Stokols and Tuszynski 2006, Tsai, Dalton et al. 2006, Jain, McKeon et al. 2011, Rao, Zhao et al. 2018), and/or various cell populations (Gunther, Weidner et al. 2015, Liu, Sandner et al. 2017, Koffler, Zhu et al. 2019), axonal growth through biomaterial implants was successfully improved. However, functional recovery was only occasionally reported and modest at best (Teng, Lavik et al. 2002, Fouad, Schnell et al. 2005, Li, Yang et al. 2009, Du, Xiong et al. 2011, Wang, Sun et al. 2017, Rao, Zhao et al. 2018, Koffler, Zhu et al. 2019).

In the present study, we were able to consistently enhance axonal growth within alginate-based hydrogel implants (channel diameter: ~ 70 µm, + PLO/laminin) 4 and 8 weeks after SCI via co-transplantation of immature cortex- and spinal cord-derived astrocytes. Importantly, the astrocytes were grafted without additional trophic support of a growth factor cocktail (Lu, Wang et al. 2012) nor additional delivery or ectopic expression of bioactive molecules (Fuhrmann, Anandakumaran et al. 2018, Nori, Khazaei et al. 2018) and/or trophic factors (Ghosh, Wang et al. 2018, He, Zang et al. 2019). Previous studies from our own laboratory combined our algi-

nate-based hydrogel implants (channel diameter: ~ 50 µm, no PLO/lam) with co-transplantation of either BDNF-expressing BMSCs (Gunther, Weidner et al. 2015) or adult syngeneic Schwann cells together with inducible viral BDNF expression (Liu, Sandner et al. 2017). In direct comparison, axonal growth after astrocyte seeding of the hydrogel implants (**FIG 14D**, + cortex-derived astrocytes: ~ 710 axons/mm^2 at Rostral 100 µm) outnumbered the axonal growth responses observed after seeding with GFP-expressing BMSCs (~ 250 axons/mm^2 at Rostral 100 µm) by 2.5-fold, and nearly reached the level of axonal growth after seeding with constitutively BDNF-expressing BMSCs (~ 1000 axons/mm^2 at Rostral 100 µm) 4 weeks after SCI (Gunther, Weidner et al. 2015). Moreover, the seeded cortex-derived astrocytes doubled the amount of βIII-tubulin-labeled axons in hydrogel implants seeded with SCs (~ 350 axons/mm^2 at Rostral 100 µm, 4 weeks post-SCI) and showed an equal amount of axonal growth with SC-seeded implants with additional viral BDNF delivery in the caudal host parenchyma (~ 700 axons/mm^2) (Liu, Sandner et al. 2017). Most importantly, axonal growth was even further enhanced in alginate-based hydrogel implants when either cortex- or spinal cord-derived astrocytes were seeded into the implants and additionally grafted into the surrounding host spinal cord. In particular, both astrocyte populations (**FIG 37D**, ~ 2300 axons/mm^2 across the entire implant) surpassed the axonal growth found in implants seeded with SCs and sustained caudal BDNF expression 8 weeks after SCI (~ 750 axons/mm^2 across the entire implant). Unfortunately, although the axonal growth was strikingly enhanced by co-transplantation with immature astrocytes, axonal re-entry into the caudal host spinal cord was not observed, consistent with previous reports from our group (Gunther, Weidner et al. 2015).

The present data demonstrate, however, that co-transplantation of a continuous growth-permissive cellular substrate can strikingly enhance axonal growth into and through 2-mm long hydrogel implants, which is even greater than the BDNF-induced axonal growth of our previous studies. Intriguingly, either cortex- or spinal cord-derived astrocyte-seeded implants contained nearly 2x more axons than SC-seeded implants with additional SC grafts and constant BDNF-expression (~ 2300 axons/mm^2 vs. ~1 200 axons/mm^2 across the entire implant) 8 weeks after SCI. Nonetheless, why axons failed to re-enter the caudal host spinal cord remains elusive.

In our study, the observed axonal regrowth most likely accounts for neuroplasticity and axonal sprouting rather than long-distance regrowth of descending spinal tracts. A great fraction of the axons present in the hydrogel implants were serotonergic, hence, originate from the raphespinal tract. Additionally, due to its injection coordinates, BDA anterogradely traced axons of different descending spinal tracts, including the CST, reticulospinal and raphespinal tract. Previously, axonal sprouting of these spinal tracts was associated with spontaneous functional recovery after incomplete SCI (Courtine, Song et al. 2008, Takeoka, Vollenweider et al. 2014).

Alternatively, numerous studies that used biomaterial implants after SCI reported fibroglial and astrocyte scarring around the implantation hindering complete axonal crossing (Suzuki, Kitaura et al. 2002, Vroemen, Caioni et al. 2007, Grulova, Slovinska et al. 2015, Gunther, Weidner et al. 2015, Pawar, Prang et al. 2015). Thus, to reduce scarring, digestion of the growth inhibitory CSPGs at the scar tissue by delivery of ChABC (Fouad, Schnell et al. 2005). Although scarring was not explicitly analyzed in the present study, no obvious signs of a dense scar around the astrocyte-seeded implants (indicated by a distinct $GFAP^+$ border around the implantation site), especially when additional astrocytic grafts were placed in the adjacent host tissue. Moreover, axonal growth further enhanced from 4 to 8 weeks post-injury in the astrocyte transplantation groups counteracting the presence of an axon impermeable scar around the implants, at least in these animals. The combination of the astrocyte co-transplantation paradigm with additional ChABC delivery, however, harbors a prominent drawback, namely ChABCs' lack of specificity. In particular, ChABC degrades not only growth-inhibitory CSPGs but also ECM components such as hyaluronic acid (Prabhakar, Raman et al. 2005) and axonal growth-supportive CSPGs including aggrecan, CSPG 4 and CSPG 5 (Anderson, Burda et al. 2016), which could attenuate regenerative success by interfering with plasticity and neural reorganization in the uninjured spinal cord adjacent to the lesion (Garcia-Alias, Barkhuysen et al. 2009).

Alternatively, complete axonal crossing through biomaterial implantation sites can be achieved via the establishment of a cellular bridge between implant and host tissue (Ramon-Cueto, Cordero et al. 2000, Deumens, Koopmans et al. 2006, Williams, Henao et al. 2015) or a combination of biomaterial-supported cell transplantation and growth factor delivery (Fouad, Schnell et al. 2005, Deng, Hu et al. 2011, Liu, Sandner et al. 2017). Conversely, the formation of cellular bridges across the rostral and caudal host-graft interface was observed in the present study, especially after the co-transplantation of immature astrocytes into the rostral and caudal host tissue. Moreover, axons appeared to be closely associated with these cellular bridges, but hardly any BDA-traced descending axons were found at the caudal host-graft interface and the adjacent spinal parenchyma.

At more caudal spinal cord segments, individual BDA^+ axons were found on the lesioned side, however, since no BDA-labeled axons could be consistently followed from the hydrogel implant through the caudal host-graft interface and back into the caudal host tissue, contralateral sprouting cannot be excluded as the source of these BDA^+ axons. It has to be noted that tissue processing may have negatively influenced the axon tracing data. For example, since the hydrogel implant as well as host-graft interface are particularly fragile, sectioning procedures can generate ruptures within the tissue sections, which interfere with consistent tracing of individual axons on their way across the host-graft interface. Moreover, hydrogel channels and axons are not perfectly straight oriented and might not be entirely displayed on one tissue section.

They are found on one tissue section but proceed on the next adjacent tissue section and, therefore, cannot be traced consistently. In our study, descending axons were labeled by a BDA injection into the ipsilateral cervical spinal cord; hence, unspecific labeling of axons on the contralateral spinal cord side due to tracer diffusion cannot be excluded. Generally, specificity and reliability of axonal tracing can be enhanced by site-specific injection of BDA or AAV-based tracing vector systems into the contralateral motor cortex (Hutson, Verhaagen et al. 2012, Soderblom, Lee et al. 2015). Since the hydrogel implant and implantation site are highly fragile thereby vulnerable to damage and artifacts during standard tissue processing procedures, experiments to evaluate the feasibility of clearing protocols on our injury paradigm are currently underway in kindly collaboration with Dr. Carmen Ruiz de Aldomovar (University of Mannheim). Therefore, we hope to improve spatial resolution, thereby optimizing visualization of axonal tracing as well as interactions between the grafted astrocytes and host-derived cells by sophisticated imaging techniques including 2-photon and light-sheet microscopy (Soderblom, Lee et al. 2015).

Nonetheless, Liu et al. showed that BDA-traced axons can successfully traverse the implantation site and re-enter the caudal spinal cord, when SC-seeded hydrogel implants were combined with constant BDNF expression in the caudal host spinal cord and -most importantly- an additional SC graft adjacent to the implantation site (Liu, Sandner et al. 2017). Consequently, axonal re-entry essentially requires both, a continuous cellular substrate across the lesion site and caudal chemoattractance. Importantly, the growth of BDA-traced axons within the caudal host spinal cord was restricted to the areas of the caudal SC graft and BDNF expression and did not extend further into the distal spinal cord. Thus, long-distance axonal growth within the distal host spinal cord additionally relies upon persistent support of axonal growth. This notion is further supported by the elegant study of Anderson et al., where complete axonal crossing of a thoracic total crush injury was achieved via implantation of a synthetic hydrogel into the lesion epicenter, additional caudal growth factor delivery, and viral transduction of spinal axons (Anderson, O'Shea et al. 2018). Specifically, Anderson et al. transduced descending propriospinal axons with AVV vectors to either knock down PTEN or to overexpress insulin growth factor 1 (IGF1), osteopontin, and CNTF. Hence, the intrinsic growth capacity of these neurons was ectopically enhanced, which may explain the robust axonal growth across and caudally to the SCI site. Similarly, serial intraspinal injections of ChABC caudal to the unilateral C8 hemisection facilitated functional recovery of forelimb function in rhesus monkeys (Rosenzweig, Salegio et al. 2019). In contrast, Rao et al. reported robust axonal regeneration, restoring signal transduction and locomotion after implantation of a continuous NT3-releasing chitosan channel into a 1 cm-wide thoracic hemisection lesion in rhesus monkeys without additional manipulation of the distal spinal cord (Rao, Zhao et al. 2018).

However, persistent expression of neurotrophins after SCI was previously linked to detrimental side effects, including dysreflexia, neuropathic pain and spasticity. For example, administration of low doses of NT-3 were associated with temporal mechanical hypersensitivity in uninjured rats (White 1998, Zhou, Deng et al. 2000) and ectopic NGF expression either from genetically modified SCs or fibroblasts promoted sprouting of nociceptive axons after SCI (Tuszynski, Peterson et al. 1994, Tuszynski, Gabriel et al. 1996, Weidner, Blesch et al. 1999). Similarly, sustained BDNF overexpression caused spasticity in rats after partial or complete spinal cord transection (Lu, Blesch et al. 2012, Fouad, Bennett et al. 2013). Although the potential combination of the present astrocyte co-transplantation paradigm with virally delivered BDNF appears promising, however, BDNF has been shown to promote the activation of astrocytes and microglia, thereby aggravating neuroinflammation and mechanical allodynia (Coull, Beggs et al. 2005, Lu, Biggs et al. 2009, Zhang, Wang et al. 2011, Ding, Chen et al. 2020). In contrast, intrathecal NGF delivery attenuated reactive astrogliosis, neuroinflammation and pain after SNI (Cirillo, Cavaliere et al. 2010). Thus, the combination of the biomaterial-supported cell transplantation with additional manipulation such as growth factor or ChABC delivery might be useful to achieve axonal re-entry and sustained axonal extension within the caudal spinal cord but a finely graded balance has to be kept to avoid maladaptive plasticity. Perhaps, some of these risks can be circumvented by the use of ectopically regulatable viral vectors (Liu, Sandner et al. 2017). Finally, additional therapeutic interventions such as rehabilitative training and/or functional electrical stimulation (FES) might be necessary to regain sensorimotor function. Accordingly, Asboth et al. showed convincingly that even a small fraction of spared spinal tissue is sufficient to facilitate meaningful locomotion recovery when appropriate FES and locomotion training is applied (Asboth, Friedli et al. 2018). Hence, only a small number of axons that completely crossed the lesion and formed functionally relevant synapses in the distal spinal cord might be enough to restore function after SCI.

5 Conclusions and future perspectives

To conclude, the present study provides further evidence that a combinational approach consisting of an alginate-based hydrogel implant with a defined 3D microarchitecture and co-transplantation of a permissive cellular substrate is sufficient to robustly enhance axonal growth after a traumatic unilateral hemisection injury in adult female rats. Surface coating of the hydrogel implants with the synthetic polypeptide PLO and laminin improved their biocompatibility and positively affects cell viability of host and grafted cells. This may contribute to increasing graft cell survival rates thereby overcoming a major limitation of previous transplantation approaches. Moreover, co-transplantation of either immature cortex- or spinal cord-derived astrocytes facilitated implant integration in terms of host-graft interactions and improved vascularization thereby strikingly enhancing axonal growth compared with previous studies from our laboratory. Thus, a continuous cellular substrate across extended SCI and biomaterial implantation sites represents an essential component for proper implant integration and robust axonal growth into and through biomaterial implants.

Future studies will focus, firstly, on finely tuned additional manipulation of the implantation site on the physical, molecular and cellular level to maximize axonal growth through and finally beyond SCI sites, and, secondly, on translating the presented biomaterial-supported cell transplantation paradigm to more clinically relevant SCI models.

Consequently, excessive regrowth of descending axonal tracts has to be initiated, physically and trophically guided through the implantation site back into the uninjured host spinal cord to form functional synapses with their putative targets and, eventually, restore function. Experiments combining the present approach with additional interventions aiming at induction and maintenance of the intrinsic regenerative capacity of adult CNS neurons and chemoattraction/trophic support of regrowing spinal axons will be necessary. For example, delivery of neurotrophic factors may potentially lead to complete axonal crossing of the implantation site and re-entry into the caudal host spinal cord. Thus, growth factors could be released caudal to the SCI site from either deposits or regulatable viral expression vectors as done previously (Liu, Sandner et al. 2017, Anderson, O'Shea et al. 2018). Alternatively, partial neutralization of the growth-inhibitory environment at SCI lesion sites with finely graded administration of chondroitinase ABC might reduce detrimental CSPG expression around the lesion and allow for successful axonal crossing of SCI sites (Suzuki, Ahuja et al. 2017, Fuhrmann, Anandakumaran et al. 2018, Hu, Granger et al. 2018, Rosenzweig, Salegio et al. 2019).

Furthermore, the alginate-based hydrogel implant will be modified in terms of microarchitecture and mechanical properties. The currently used alginate-based hydrogels have a medium viscoelasticity of ~200 Pa*s, which is magnitudes stiffer than the surrounding spinal tissue (< 10

Pa*s). These stiffness differences might additionally affect implant integration and astroglial scarring (Moshayedi, Ng et al. 2014, Moeendarbary, Weber et al. 2017). CNS neurons particularly prefer growth substrates with physical characteristics of the natural ECM (Javid, Rezaei et al. 2014, Koser, Moeendarbary et al. 2015). Therefore, adjusting the viscoelasticity of the hydrogel implants to the mechanoproperties of the uninjured spinal cord may further support axonal growth within the implants and facilitate even greater implant integration and axonal growth (Javid, Rezaei et al. 2014, Koser, Moeendarbary et al. 2015, Koser, Thompson et al. 2016). Hence, ongoing studies with our collaboration partner Apl. Prof. Dr. Rainer Müller (University of Regensburg) focus on the modification of the viscoelasticity of the alginate-based hydrogel implants via alteration of the chemical stabilization process during hydrogel fabrication.

The present study further illustrates the potential of astrocytes to establish functional tissue connections between a biomaterial implant and the surrounding host tissue thereby providing a permissive and structurally continuous cellular substrate upon which damaged spinal axons can grow. Importantly, although transplantation of fetal-derived tissue in humans is *per se* legal, however, ethnical concerns remain. Therefore, graft cells have to be obtained from ESC- or iPSC-derived NSCs or generated via direct reprogramming of skin-derived fibroblasts (Kantawong, Saksiriwisitkul et al. 2018, Xiao, Liu et al. 2018). Thus, functional astrocyte subtypes can be obtained from ESC- or iPSC-derived NSCs using a plethora of differentiation protocols (Davies, Huang et al. 2006, Davies, Proschel et al. 2008, Davies, Shih et al. 2011, Krencik, Weick et al. 2011, Sloan, Darmanis et al. 2017, Tcw, Wang et al. 2017, Canals, Ginisty et al. 2018). With progress in understanding different molecular astrocyte phenotypes, differentiation protocols can be modified to generate distinct astrocytic subtypes with defined functions to meet the specific needs of acute SCI lesion sites.

Behavioral testing of potential functional recovery of sensorimotor function has not been done yet due to severe limitations of the SCI model used, namely the high severity of the hemisection injury and the resulting complete loss of neuronal circuitries essential for forelimb function and the lack or only minimal axonal re-entry into the caudal host spinal cord. Hence, potential functional improvements might exclusively rely on post-injury plasticity and compensatory mechanisms, such as contralateral sprouting or re-arrangement of local neuronal circuitries.

To overcome the limitations of the current SCI model, ongoing studies in the laboratory facilitated the implantation of a 1 mm-long alginate-based hydrogel with defined anisotropic channel structure in combination with co-transplantation of immature astrocytes to a full transection injury of the thoracic spinal cord at Th11. A full transection of the spinal cord completely abolishes all functions relying upon instructive or regulatory input from the motor cortex leaving only local circuitries below the level of injury intact that could mediate voluntary reflex-driven

function. Hence, potentially occurring functional improvements of locomotion and sensory function have to be necessarily based on functional axonal growth across the hydrogel implant. Moreover, the distance between lesion site and the putative targets of the regrowing axons in the lumbar motor neuron pools is minimal after a thoracic lesion. Hence, functional relevant reinnervation of the target regions is more likely to occur. Finally, by re-transection through the hydrogel implant and subsequent functional testing, a causal correlation between the observed functional improvements and axonal growth through the hydrogel implant can be determined.
Most important, since all kinds of transection injuries only represent a minor fraction of human SCI cases, the paradigm has to be adopted to the human condition where most SCIs account for compressive/contusive injuries with irregularly shaped lesion borders. So far, solid implants -like our alginate-based hydrogel implants- require physical space at the lesion site for implantation and cannot easily be trimmed to fit into a naturally occurring irregularly shaped lesion. Consequently, additional spinal tissue needs to be resected; thus, worsening the patients' outcome. Even after contusion injury and the resulting cyst formation at the lesion epicenter, implantation of a biocompatible implant requires resection of either scar and/or spinal cord tissue. By the use of fMRI scanning and 3D bioprinting, implants can be fabricated to match even irregular lesion borders (Koffler, Zhu et al. 2019). Furthermore, the timing of therapeutic interventions is essential. In the present study, the alginate-based hydrogel implants and immature astrocytes were implanted immediately after SCI and the grafted cells were confronted with the hostile inflammatory environment at the acute lesion site, which may have negatively affected regenerative success (Piltti, Salazar et al. 2013). Hence, a delayed transplantation paradigm needs to be considered, also in terms of the clinical setting where immediate transplantations are not feasible. For example, a 7 days delayed transplantation of immature OPCs lead to significant improvement in hindlimb locomotion (BBB motor scores) and electrophysiological signal transduction across thoracic contusion injuries, whereas the effect of immediate cell transplantation was very limited (Keirstead, Nistor et al. 2005, Wu, Sun et al. 2012). Likewise, pre-gelled fibrin hydrogels were successfully implanted 14 days after a dorsal hemisection injury of the Th9 spinal cord of Long Evans rats and lead to increased axonal density within the implants compared with fibrin implants that were immediately implanted (Johnson, Tatara et al. 2010).

Thus, to achieve efficacy, a biomaterial-based cell transplantation approach has to tackle multiple facets of the multifactorial SCI pathology, namely (1) physical and trophic support of the regrowing spinal axons, (2) establishment of a continuous cellular substrate across the implantation site, and (3) persistent chemoattractance and support of the growing spinal axons within the caudal host spinal cord. In the present work, we facilitated a structurally defined and biocompatible alginate-based hydrogel together with a continuous astrocytic substrate across an

extended SCI lesion, therefore, we addressed two of the above-mentioned facets. Moreover, we provided further evidence that regrowth of damaged axons at SCI sites can be enhanced by a physically guiding and biologically permissive biomaterial implant. Future studies will focus on persistent trophic support of regrowing axons at the lesion site and within the distal host spinal cord.

6 References

Afshari, F. T., J. C. Kwok and J. W. Fawcett (2010). "Astrocyte-produced ephrins inhibit schwann cell migration via VAV2 signaling." J Neurosci **30**(12): 4246-4255.

Ahuja, C. S., S. Nori, L. Tetreault, J. Wilson, B. Kwon, J. Harrop, D. Choi and M. G. Fehlings (2017). "Traumatic Spinal Cord Injury-Repair and Regeneration." Neurosurgery **80**(3S): S9-S22.

Albuquerque, C., D. J. Joseph, P. Choudhury and A. B. MacDermott (2009). "Dissection, plating, and maintenance of cortical astrocyte cultures." Cold Spring Harb Protoc **2009**(8): pdb prot5273.

All, A. H., P. Gharibani, S. Gupta, F. A. Bazley, N. Pashai, B. K. Chou, S. Shah, L. M. Resar, L. Cheng, J. D. Gearhart and C. L. Kerr (2015). "Early intervention for spinal cord injury with human induced pluripotent stem cells oligodendrocyte progenitors." PLoS One **10**(1): e0116933.

Allaman, I., M. Belanger and P. J. Magistretti (2011). "Astrocyte-neuron metabolic relationships: for better and for worse." Trends Neurosci **34**(2): 76-87.

Allen, N. J., M. L. Bennett, L. C. Foo, G. X. Wang, C. Chakraborty, S. J. Smith and B. A. Barres (2012). "Astrocyte glypicans 4 and 6 promote formation of excitatory synapses via GluA1 AMPA receptors." Nature **486**(7403): 410-414.

Alto, L. T., L. A. Havton, J. M. Conner, E. R. Hollis, 2nd, A. Blesch and M. H. Tuszynski (2009). "Chemotropic guidance facilitates axonal regeneration and synapse formation after spinal cord injury." Nat Neurosci **12**(9): 1106-1113.

Alvarez, J. I., A. Dodelet-Devillers, H. Kebir, I. Ifergan, P. J. Fabre, S. Terouz, M. Sabbagh, K. Wosik, L. Bourbonniere, M. Bernard, J. van Horssen, H. E. de Vries, F. Charron and A. Prat (2011). "The Hedgehog pathway promotes blood-brain barrier integrity and CNS immune quiescence." Science **334**(6063): 1727-1731.

Anderson, M. A., Y. Ao and M. V. Sofroniew (2014). "Heterogeneity of reactive astrocytes." Neurosci Lett **565**: 23-29.

Anderson, M. A., J. E. Burda, Y. Ren, Y. Ao, T. M. O'Shea, R. Kawaguchi, G. Coppola, B. S. Khakh, T. J. Deming and M. V. Sofroniew (2016). "Astrocyte scar formation aids central nervous system axon regeneration." Nature **532**(7598): 195-200.

Anderson, M. A., T. M. O'Shea, J. E. Burda, Y. Ao, S. L. Barlatey, A. M. Bernstein, J. H. Kim, N. D. James, A. Rogers, B. Kato, A. L. Wollenberg, R. Kawaguchi, G. Coppola, C. Wang, T. J. Deming, Z. He, G. Courtine and M. V. Sofroniew (2018). "Required growth facilitators propel axon regeneration across complete spinal cord injury." Nature **561**(7723): 396-400.

Andrews, E. M., R. J. Richards, F. Q. Yin, M. S. Viapiano and L. B. Jakeman (2012). "Alterations in chondroitin sulfate proteoglycan expression occur both at and far from the site of spinal contusion injury." Exp Neurol **235**(1): 174-187.

Ansorena, E., P. De Berdt, B. Ucakar, T. Simon-Yarza, D. Jacobs, O. Schakman, A. Jankovski, R. Deumens, M. J. Blanco-Prieto, V. Preat and A. des Rieux (2013). "Injectable alginate hydrogel loaded with GDNF promotes functional recovery in a hemisection model of spinal cord injury." Int J Pharm **455**(1-2): 148-158.

AOSPINE (2017). "Clinical Practice Guidelines - Management of Degenerative Cervical Myelopathy (DCM) and Acute Traumatic Spinal Cord Injury (SCI)." Global Spine J **7(3)**.

Araque, A. and M. Navarrete (2010). "Glial cells in neuronal network function." Philos Trans R Soc Lond B Biol Sci **365**(1551): 2375-2381.

Argaw, A. T., L. Asp, J. Zhang, K. Navrazhina, T. Pham, J. N. Mariani, S. Mahase, D. J. Dutta, J. Seto, E. G. Kramer, N. Ferrara, M. V. Sofroniew and G. R. John (2012). "Astrocyte-derived VEGF-A drives blood-brain barrier disruption in CNS inflammatory disease." J Clin Invest **122**(7): 2454-2468.

Asboth, L., L. Friedli, J. Beauparlant, C. Martinez-Gonzalez, S. Anil, E. Rey, L. Baud, G. Pidpruzhnykova, M. A. Anderson, P. Shkorbatova, L. Batti, S. Pages, J. Kreider, B. L. Schneider, Q. Barraud and G. Courtine (2018). "Cortico-reticulo-spinal circuit reorganization enables functional recovery after severe spinal cord contusion." Nat Neurosci **21**(4): 576-588.

Assinck, P., G. J. Duncan, B. J. Hilton, J. R. Plemel and W. Tetzlaff (2017). "Cell transplantation therapy for spinal cord injury." Nat Neurosci **20**(5): 637-647.

Assinck, P., G. J. Duncan, J. R. Plemel, M. J. Lee, J. A. Stratton, S. B. Manesh, J. Liu, L. M. Ramer, S. H. Kang, D. E. Bergles, J. Biernaskie and W. Tetzlaff (2017). "Myelinogenic Plasticity of Oligodendrocyte Precursor Cells following Spinal Cord Contusion Injury." J Neurosci **37**(36): 8635-8654.

Atala, A., R. Lanza, T. Mikos and R. Nerem (2018). Principles of Regenerative Medicine, Academic Press.

Attwell, D., A. M. Buchan, S. Charpak, M. Lauritzen, B. A. Macvicar and E. A. Newman (2010). "Glial and neuronal control of brain blood flow." Nature **468**(7321): 232-243.

Atwal, J. K., J. Pinkston-Gosse, J. Syken, S. Stawicki, Y. Wu, C. Shatz and M. Tessier-Lavigne (2008). "PirB is a functional receptor for myelin inhibitors of axonal regeneration." Science **322**(5903): 967-970.

Badylak, S. (2015). Host Response to Biomaterials. Academic Press
.

Bak, L. K., A. Schousboe and H. S. Waagepetersen (2006). "The glutamate/GABA-glutamine cycle: aspects of transport, neurotransmitter homeostasis and ammonia transfer." J Neurochem **98**(3): 641-653.

Bakshi, A., O. Fisher, T. Dagci, B. T. Himes, I. Fischer and A. Lowman (2004). "Mechanically engineered hydrogel scaffolds for axonal growth and angiogenesis after transplantation in spinal cord injury." J Neurosurg Spine **1**(3): 322-329.

Balgude, A. P., X. Yu, A. Szymanski and R. V. Bellamkonda (2001). "Agarose gel stiffness determines rate of DRG neurite extension in 3D cultures." Biomaterials **22**(10): 1077-1084.

Ballermann, M. and K. Fouad (2006). "Spontaneous locomotor recovery in spinal cord injured rats is accompanied by anatomical plasticity of reticulospinal fibers." Eur J Neurosci **23**(8): 1988-1996.

Bamber, N. I., H. Li, X. Lu, M. Oudega, P. Aebischer and X. M. Xu (2001). "Neurotrophins BDNF and NT-3 promote axonal re-entry into the distal host spinal cord through Schwann cell-seeded mini-channels." Eur J Neurosci **13**(2): 257-268.

Bardehle, S., M. Kruger, F. Buggenthin, J. Schwausch, J. Ninkovic, H. Clevers, H. J. Snippert, F. J. Theis, M. Meyer-Luehmann, I. Bechmann, L. Dimou and M. Gotz (2013). "Live imaging of astrocyte responses to acute injury reveals selective juxtavascular proliferation." Nat Neurosci **16**(5): 580-586.

Bareyre, F. M., N. Garzorz, C. Lang, T. Misgeld, H. Buning and M. Kerschensteiner (2011). "In vivo imaging reveals a phase-specific role of STAT3 during central and peripheral nervous system axon regeneration." Proc Natl Acad Sci U S A **108**(15): 6282-6287.

Bareyre, F. M., M. Kerschensteiner, O. Raineteau, T. C. Mettenleiter, O. Weinmann and M. E. Schwab (2004). "The injured spinal cord spontaneously forms a new intraspinal circuit in adult rats." Nat Neurosci **7**(3): 269-277.

Barnabe-Heider, F., J. A. Wasylnka, K. J. Fernandes, C. Porsche, M. Sendtner, D. R. Kaplan and F. D. Miller (2005). "Evidence that embryonic neurons regulate the onset of cortical gliogenesis via cardiotrophin-1." Neuron **48**(2): 253-265.

Barres, B. A. (2008). "The mystery and magic of glia: a perspective on their roles in health and disease." Neuron **60**(3): 430-440.

Basso, D. M., M. S. Beattie and J. C. Bresnahan (1996). "Graded histological and locomotor outcomes after spinal cord contusion using the NYU weight-drop device versus transection." Exp Neurol **139**(2): 244-256.

Basso, D. M., L. C. Fisher, A. J. Anderson, L. B. Jakeman, D. M. McTigue and P. G. Popovich (2006). "Basso Mouse Scale for locomotion detects differences in recovery after spinal cord injury in five common mouse strains." J Neurotrauma **23**(5): 635-659.

Batchelor, P. E., T. E. Wills, P. Skeers, C. R. Battistuzzo, M. R. Macleod, D. W. Howells and E. S. Sena (2013). "Meta-analysis of pre-clinical studies of early decompression in acute spinal cord injury: a battle of time and pressure." PLoS One **8**(8): e72659.

Batiuk, M. Y., A. Martirosyan, J. Wahis, F. de Vin, C. Marneffe, C. Kusserow, J. Koeppen, J. F. Viana, J. F. Oliveira, T. Voet, C. P. Ponting, T. G. Belgard and M. G. Holt (2020). "Identification of region-specific astrocyte subtypes at single cell resolution." Nat Commun **11**(1): 1220.

Bazargani, N. and D. Attwell (2016). "Astrocyte calcium signaling: the third wave." Nat Neurosci **19**(2): 182-189.

Belanger, M. and P. J. Magistretti (2009). "The role of astroglia in neuroprotection." Dialogues Clin Neurosci **11**(3): 281-295.

Bell, R. D., E. A. Winkler, I. Singh, A. P. Sagare, R. Deane, Z. Wu, D. M. Holtzman, C. Betsholtz, A. Armulik, J. Sallstrom, B. C. Berk and B. V. Zlokovic (2012). "Apolipoprotein E controls cerebrovascular integrity via cyclophilin A." Nature **485**(7399): 512-516.

Benson, M. D., M. I. Romero, M. E. Lush, Q. R. Lu, M. Henkemeyer and L. F. Parada (2005). "Ephrin-B3 is a myelin-based inhibitor of neurite outgrowth." Proc Natl Acad Sci U S A **102**(30): 10694-10699.

Bhatt, J. M. and P. H. Gordon (2007). "Current clinical trials in amyotrophic lateral sclerosis." Expert Opin Investig Drugs **16**(8): 1197-1207.

Bidarra, S. J., C. C. Barrias and P. L. Granja (2014). "Injectable alginate hydrogels for cell delivery in tissue engineering." Acta Biomater **10**(4): 1646-1662.

Blackmore, M. G., Z. Wang, J. K. Lerch, D. Motti, Y. P. Zhang, C. B. Shields, J. K. Lee, J. L. Goldberg, V. P. Lemmon and J. L. Bixby (2012). "Kruppel-like Factor 7 engineered for transcriptional activation promotes axon regeneration in the adult corticospinal tract." Proc Natl Acad Sci U S A **109**(19): 7517-7522.

Blakemore, W. F. and A. J. Crang (1989). "The relationship between type-1 astrocytes, Schwann cells and oligodendrocytes following transplantation of glial cell cultures into demyelinating lesions in the adult rat spinal cord." J Neurocytol **18**(4): 519-528.

Blesch, A., P. Lu, S. Tsukada, L. T. Alto, K. Roet, G. Coppola, D. Geschwind and M. H. Tuszynski (2012). "Conditioning lesions before or after spinal cord injury recruit broad genetic mechanisms that sustain axonal regeneration: superiority to camp-mediated effects." Exp Neurol **235**(1): 162-173.

Blesch, A. and M. H. Tuszynski (2009). "Spinal cord injury: plasticity, regeneration and the challenge of translational drug development." Trends Neurosci **32**(1): 41-47.

Blight, A. R., J. Hsieh, A. Curt, J. W. Fawcett, J. D. Guest, N. Kleitman, S. N. Kurpad, B. K. Kwon, D. P. Lammertse, N. Weidner and J. D. Steeves (2019). "The challenge of recruitment for neurotherapeutic clinical trials in spinal cord injury." Spinal Cord **57**(5): 348-359.

Bonaguidi, M. A., T. McGuire, M. Hu, L. Kan, J. Samanta and J. A. Kessler (2005). "LIF and BMP signaling generate separate and discrete types of GFAP-expressing cells." Development **132**(24): 5503-5514.

Bozkurt, G., A. J. Mothe, T. Zahir, H. Kim, M. S. Shoichet and C. H. Tator (2010). "Chitosan channels containing spinal cord-derived stem/progenitor cells for repair of subacute spinal cord injury in the rat." Neurosurgery **67**(6): 1733-1744.

Braccini, I. and S. Perez (2001). "Molecular basis of C(2+)-induced gelation in alginates and pectins: the egg-box model revisited." Biomacromolecules **2**(4): 1089-1096.

Bradbury, E. J., V. R. King, L. J. Simmons, J. V. Priestley and S. B. McMahon (1998). "NT-3, but not BDNF, prevents atrophy and death of axotomized spinal cord projection neurons." Eur J Neurosci **10**(10): 3058-3068.

Bradbury, E. J., L. D. Moon, R. J. Popat, V. R. King, G. S. Bennett, P. N. Patel, J. W. Fawcett and S. B. McMahon (2002). "Chondroitinase ABC promotes functional recovery after spinal cord injury." Nature **416**(6881): 636-640.

Brambilla, R., T. Persaud, X. Hu, S. Karmally, V. I. Shestopalov, G. Dvoriantchikova, D. Ivanov, L. Nathanson, S. R. Barnum and J. R. Bethea (2009). "Transgenic inhibition of astroglial NF-kappa B improves functional outcome in experimental autoimmune encephalomyelitis by suppressing chronic central nervous system inflammation." J Immunol **182**(5): 2628-2640.

Bregman, B. S., E. Kunkel-Bagden, L. Schnell, H. N. Dai, D. Gao and M. E. Schwab (1995). "Recovery from spinal cord injury mediated by antibodies to neurite growth inhibitors." Nature **378**(6556): 498-501.

Buffo, A., I. Rite, P. Tripathi, A. Lepier, D. Colak, A. P. Horn, T. Mori and M. Gotz (2008). "Origin and progeny of reactive gliosis: A source of multipotent cells in the injured brain." Proc Natl Acad Sci U S A **105**(9): 3581-3586.

Bundesen, L. Q., T. A. Scheel, B. S. Bregman and L. F. Kromer (2003). "Ephrin-B2 and EphB2 regulation of astrocyte-meningeal fibroblast interactions in response to spinal cord lesions in adult rats." J Neurosci **23**(21): 7789-7800.

Bunge, M. B. (2016). "Efficacy of Schwann cell transplantation for spinal cord repair is improved with combinatorial strategies." J Physiol **594**(13): 3533-3538.

Burda, J. E. and M. V. Sofroniew (2014). "Reactive gliosis and the multicellular response to CNS damage and disease." Neuron **81**(2): 229-248.

Burnside, E. R., F. De Winter, A. Didangelos, N. D. James, E. C. Andreica, H. Layard-Horsfall, E. M. Muir, J. Verhaagen and E. J. Bradbury (2018). "Immune-evasive gene switch enables regulated delivery of chondroitinase after spinal cord injury." Brain **141**(8): 2362-2381.

Bush, T. G., N. Puvanachandra, C. H. Horner, A. Polito, T. Ostenfeld, C. N. Svendsen, L. Mucke, M. H. Johnson and M. V. Sofroniew (1999). "Leukocyte infiltration, neuronal degeneration, and neurite outgrowth after ablation of scar-forming, reactive astrocytes in adult transgenic mice." Neuron **23**(2): 297-308.

Bushong, E. A., M. E. Martone, Y. Z. Jones and M. H. Ellisman (2002). "Protoplasmic astrocytes in CA1 stratum radiatum occupy separate anatomical domains." J Neurosci **22**(1): 183-192.

Buss, A., K. Pech, B. A. Kakulas, D. Martin, J. Schoenen, J. Noth and G. A. Brook (2009). "NG2 and phosphacan are present in the astroglial scar after human traumatic spinal cord injury." BMC Neurol **9**: 32.

Cahoy, J. D., B. Emery, A. Kaushal, L. C. Foo, J. L. Zamanian, K. S. Christopherson, Y. Xing, J. L. Lubischer, P. A. Krieg, S. A. Krupenko, W. J. Thompson and B. A. Barres (2008). "A transcriptome database for astrocytes, neurons, and oligodendrocytes: a new resource for understanding brain development and function." J Neurosci **28**(1): 264-278.

Cajal, R. y. (1928). "„Degeneration and Regeneration of the Nervous System“ Translated and edited by Dr. Raoul M. May." London: Oxford University Press **Vol. 2**: 397-769.

Cajal, R. y., J. DeFelipe and E. Jones, G. (1991). Cajal's Degeneration and Regeneration of the Nervous System. Oxford University Press
.

Calancie, B., M. R. Molano and J. G. Broton (2002). "Interlimb reflexes and synaptic plasticity become evident months after human spinal cord injury." Brain **125**(Pt 5): 1150-1161.

Camassa, L. M. A., L. K. Lunde, E. H. Hoddevik, M. Stensland, H. B. Boldt, G. A. De Souza, O. P. Ottersen and M. Amiry-Moghaddam (2015). "Mechanisms underlying AQP4 accumulation in astrocyte endfeet." Glia **63**(11): 2073-2091.

Canals, I., A. Ginisty, E. Quist, R. Timmerman, J. Fritze, G. Miskinyte, E. Monni, M. G. Hansen, I. Hidalgo, D. Bryder, J. Bengzon and H. Ahlenius (2018). "Rapid and efficient induction of functional astrocytes from human pluripotent stem cells." Nat Methods **15**(9): 693-696.

Cao, Q. L., Y. P. Zhang, R. M. Howard, W. M. Walters, P. Tsoulfas and S. R. Whittemore (2001). "Pluripotent stem cells engrafted into the normal or lesioned adult rat spinal cord are restricted to a glial lineage." Exp Neurol **167**(1): 48-58.

Carlen, M., K. Meletis, C. Goritz, V. Darsalia, E. Evergren, K. Tanigaki, M. Amendola, F. Barnabe-Heider, M. S. Yeung, L. Naldini, T. Honjo, Z. Kokaia, O. Shupliakov, R. M. Cassidy, O. Lindvall and J. Frisen (2009). "Forebrain ependymal cells are Notch-dependent and generate neuroblasts and astrocytes after stroke." Nat Neurosci **12**(3): 259-267.

Carmeliet, P. and M. Tessier-Lavigne (2005). "Common mechanisms of nerve and blood vessel wiring." Nature **436**(7048): 193-200.

Casella, G. T., A. Marcillo, M. B. Bunge and P. M. Wood (2002). "New vascular tissue rapidly replaces neural parenchyma and vessels destroyed by a contusion injury to the rat spinal cord." Exp Neurol **173**(1): 63-76.

Casha, S., D. Zygun, M. D. McGowan, I. Bains, V. W. Yong and R. J. Hurlbert (2012). "Results of a phase II placebo-controlled randomized trial of minocycline in acute spinal cord injury." Brain **135**(Pt 4): 1224-1236.

Cattin, A. L., J. J. Burden, L. Van Emmenis, F. E. Mackenzie, J. J. Hoving, N. Garcia Calavia, Y. Guo, M. McLaughlin, L. H. Rosenberg, V. Quereda, D. Jamecna, I. Napoli, S. Parrinello, T. Enver, C. Ruhrberg and A. C. Lloyd (2015). "Macrophage-Induced Blood Vessels Guide Schwann Cell-Mediated Regeneration of Peripheral Nerves." Cell **162**(5): 1127-1139.

Ceyzeriat, K., L. Abjean, M. A. Carrillo-de Sauvage, L. Ben Haim and C. Escartin (2016). "The complex STATes of astrocyte reactivity: How are they controlled by the JAK-STAT3 pathway?" Neuroscience **330**: 205-218.

Ceyzeriat, K., L. Ben Haim, A. Denizot, D. Pommier, M. Matos, O. Guillemaud, M. A. Palomares, L. Abjean, F. Petit, P. Gipchtein, M. C. Gaillard, M. Guillermier, S. Bernier, M. Gaudin, G. Auregan, C. Josephine, N. Dechamps, J. Veran, V. Langlais, K. Cambon, A. P. Bemelmans, J. Baijer, G. Bonvento, M. Dhenain, J. F. Deleuze, S. H. R. Oliet, E. Brouillet, P. Hantraye, M. A. Carrillo-de Sauvage, R. Olaso, A. Panatier and C. Escartin (2018). "Modulation of astrocyte reactivity improves functional deficits in mouse models of Alzheimer's disease." Acta Neuropathol Commun **6**(1): 104.

Chaboub, L. S. and B. Deneen (2013). "Astrocyte form and function in the developing central nervous system." Semin Pediatr Neurol **20**(4): 230-235.

Chapouly, C., A. Tadesse Argaw, S. Horng, K. Castro, J. Zhang, L. Asp, H. Loo, B. M. Laitman, J. N. Mariani, R. Straus Farber, E. Zaslavsky, G. Nudelman, C. S. Raine and G. R. John (2015). "Astrocytic TYMP and VEGFA drive blood-brain barrier opening in inflammatory central nervous system lesions." Brain **138**(Pt 6): 1548-1567.

Chappell, J. C., J. Darden, L. B. Payne, K. Fink and V. L. Bautch (2019). "Blood Vessel Patterning on Retinal Astrocytes Requires Endothelial Flt-1 (VEGFR-1)." J Dev Biol **7**(3).

Chen, H., K. Qian, W. Chen, B. Hu, L. W. t. Blackbourn, Z. Du, L. Ma, H. Liu, K. M. Knobel, M. Ayala and S. C. Zhang (2015). "Human-derived neural progenitors functionally replace astrocytes in adult mice." J Clin Invest **125**(3): 1033-1042.

Chen, L., H. Huang, H. Xi, F. Zhang, Y. Liu, D. Chen and J. Xiao (2014). "A prospective randomized double-blind clinical trial using a combination of olfactory ensheathing cells and Schwann cells for the treatment of chronic complete spinal cord injuries." Cell Transplant **23 Suppl 1**: S35-44.

Chen, M. S., A. B. Huber, M. E. van der Haar, M. Frank, L. Schnell, A. A. Spillmann, F. Christ and M. E. Schwab (2000). "Nogo-A is a myelin-associated neurite outgrowth inhibitor and an antigen for monoclonal antibody IN-1." Nature **403**(6768): 434-439.

Chen, Y., N. E. Vartiainen, W. Ying, P. H. Chan, J. Koistinaho and R. A. Swanson (2001). "Astrocytes protect neurons from nitric oxide toxicity by a glutathione-dependent mechanism." J Neurochem **77**(6): 1601-1610.

Christopherson, K. S., E. M. Ullian, C. C. Stokes, C. E. Mullowney, J. W. Hell, A. Agah, J. Lawler, D. F. Mosher, P. Bornstein and B. A. Barres (2005). "Thrombospondins are astrocyte-secreted proteins that promote CNS synaptogenesis." Cell **120**(3): 421-433.

Chu, T., H. Zhou, F. Li, T. Wang, L. Lu and S. Feng (2014). "Astrocyte transplantation for spinal cord injury: current status and perspective." Brain Res Bull **107**: 18-30.

Cirillo, G., C. Cavaliere, M. R. Bianco, A. De Simone, A. M. Colangelo, S. Sellitti, L. Alberghina and M. Papa (2010). "Intrathecal NGF administration reduces reactive astrocytosis and changes neurotrophin receptors expression pattern in a rat model of neuropathic pain." Cell Mol Neurobiol **30**(1): 51-62.

Colello, R. J., W. N. Chow, J. W. Bigbee, C. Lin, D. Dalton, D. Brown, B. S. Jha, B. E. Mathern, K. D. Lee and D. G. Simpson (2016). "The incorporation of growth factor and chondroitinase ABC into an electrospun scaffold to promote axon regrowth following spinal cord injury." J Tissue Eng Regen Med **10**(8): 656-668.

Collyer, E., A. Catenaccio, D. Lemaitre, P. Diaz, V. Valenzuela, F. Bronfman and F. A. Court (2014). "Sprouting of axonal collaterals after spinal cord injury is prevented by delayed axonal degeneration." Exp Neurol **261**: 451-461.

Conova, L., J. Vernengo, Y. Jin, B. T. Himes, B. Neuhuber, I. Fischer, A. Lowman, J. Vernengo, Y. Jin, B. T. Himes, B. Neuhuber, I. Fischer and A. Lowman (2011). "A pilot study of poly(N-isopropylacrylamide)-g-polyethylene glycol and poly(N-isopropylacrylamide)-g-methylcellulose branched copolymers as injectable scaffolds for local delivery of neurotrophins and cellular transplants into the injured spinal cord." J Neurosurg Spine **15**(6): 594-604.

Cote, M. P., A. A. Amin, V. J. Tom and J. D. Houle (2011). "Peripheral nerve grafts support regeneration after spinal cord injury." Neurotherapeutics **8**(2): 294-303.

Coull, J. A., S. Beggs, D. Boudreau, D. Boivin, M. Tsuda, K. Inoue, C. Gravel, M. W. Salter and Y. De Koninck (2005). "BDNF from microglia causes the shift in neuronal anion gradient underlying neuropathic pain." Nature **438**(7070): 1017-1021.

Courtine, G. and M. V. Sofroniew (2019). "Spinal cord repair: advances in biology and technology." Nat Med **25**(6): 898-908.

Courtine, G., B. Song, R. R. Roy, H. Zhong, J. E. Herrmann, Y. Ao, J. Qi, V. R. Edgerton and M. V. Sofroniew (2008). "Recovery of supraspinal control of stepping via indirect propriospinal relay connections after spinal cord injury." Nat Med **14**(1): 69-74.

Coyle, C., G. Crawford, J. Wilkinson, S. J. Thomas and P. Bytzer (2017). "Randomised clinical trial: addition of alginate-antacid (Gaviscon Double Action) to proton pump inhibitor therapy in patients with breakthrough symptoms." Aliment Pharmacol Ther **45**(12): 1524-1533.

Craig, A., Y. Tran and J. Middleton (2009). "Psychological morbidity and spinal cord injury: a systematic review." Spinal Cord **47**(2): 108-114.

Cregg, J. M., M. A. DePaul, A. R. Filous, B. T. Lang, A. Tran and J. Silver (2014). "Functional regeneration beyond the glial scar." Exp Neurol **253**: 197-207.

Curcio, M. and F. Bradke (2018). "Axon Regeneration in the Central Nervous System: Facing the Challenges from the Inside." Annu Rev Cell Dev Biol **34**: 495-521.

Davies, J. E., C. Huang, C. Proschel, M. Noble, M. Mayer-Proschel and S. J. Davies (2006). "Astrocytes derived from glial-restricted precursors promote spinal cord repair." J Biol **5**(3): 7.

Davies, J. E., C. Proschel, N. Zhang, M. Noble, M. Mayer-Proschel and S. J. Davies (2008). "Transplanted astrocytes derived from BMP- or CNTF-treated glial-restricted precursors have opposite effects on recovery and allodynia after spinal cord injury." J Biol **7**(7): 24.

Davies, S. J., M. T. Fitch, S. P. Memberg, A. K. Hall, G. Raisman and J. Silver (1997). "Regeneration of adult axons in white matter tracts of the central nervous system." Nature **390**(6661): 680-683.

Davies, S. J., D. R. Goucher, C. Doller and J. Silver (1999). "Robust regeneration of adult sensory axons in degenerating white matter of the adult rat spinal cord." J Neurosci **19**(14): 5810-5822.

Davies, S. J., C. H. Shih, M. Noble, M. Mayer-Proschel, J. E. Davies and C. Proschel (2011). "Transplantation of specific human astrocytes promotes functional recovery after spinal cord injury." PLoS One **6**(3): e17328.

Deneen, B., R. Ho, A. Lukaszewicz, C. J. Hochstim, R. M. Gronostajski and D. J. Anderson (2006). "The transcription factor NFIA controls the onset of gliogenesis in the developing spinal cord." Neuron **52**(6): 953-968.

Deng, L. X., J. Hu, N. Liu, X. Wang, G. M. Smith, X. Wen and X. M. Xu (2011). "GDNF modifies reactive astrogliosis allowing robust axonal regeneration through Schwann cell-seeded guidance channels after spinal cord injury." Exp Neurol **229**(2): 238-250.

des Rieux, A., P. De Berdt, E. Ansorena, B. Ucakar, J. Damien, O. Schakman, E. Audouard, C. Bouzin, D. Auhl, T. Simon-Yarza, O. Feron, M. J. Blanco-Prieto, P. Carmeliet, C. Bailly, F. Clotman and V. Preat (2014). "Vascular endothelial growth factor-loaded injectable hydrogel enhances plasticity in the injured spinal cord." J Biomed Mater Res A **102**(7): 2345-2355.

Deumens, R., G. C. Koopmans, W. M. Honig, F. P. Hamers, V. Maquet, R. Jerome, H. W. Steinbusch and E. A. Joosten (2006). "Olfactory ensheathing cells, olfactory nerve fibroblasts and biomatrices to promote long-distance axon regrowth and functional recovery in the dorsally hemisected adult rat spinal cord." Exp Neurol **200**(1): 89-103.

Deumens, R., G. C. Koopmans, W. M. Honig, V. Maquet, R. Jerome, H. W. Steinbusch and E. A. Joosten (2006). "Limitations in transplantation of astroglia-biomatrix bridges to stimulate corticospinal axon regrowth across large spinal lesion gaps." Neurosci Lett **400**(3): 208-212.

Dhoot, N. O., C. A. Tobias, I. Fischer and M. A. Wheatley (2004). "Peptide-modified alginate surfaces as a growth permissive substrate for neurite outgrowth." J Biomed Mater Res A **71**(2): 191-200.

Dietz, V., S. Grillner, A. Trepp, M. Hubli and M. Bolliger (2009). "Changes in spinal reflex and locomotor activity after a complete spinal cord injury: a common mechanism?" Brain **132**(Pt 8): 2196-2205.

Dillon, G. P., X. Yu, A. Sridharan, J. P. Ranieri and R. V. Bellamkonda (1998). "The influence of physical structure and charge on neurite extension in a 3D hydrogel scaffold." J Biomater Sci Polym Ed **9**(10): 1049-1069.

Ding, H., J. Chen, M. Su, Z. Lin, H. Zhan, F. Yang, W. Li, J. Xie, Y. Huang, X. Liu, B. Liu and X. Zhou (2020). "BDNF promotes activation of astrocytes and microglia contributing to neuroinflammation and mechanical allodynia in cyclophosphamide-induced cystitis." J Neuroinflammation **17**(1): 19.

Donnelly, D. J. and P. G. Popovich (2008). "Inflammation and its role in neuroprotection, axonal regeneration and functional recovery after spinal cord injury." Exp Neurol **209**(2): 378-388.

Downing, T. L., A. Wang, Z. Q. Yan, Y. Nout, A. L. Lee, M. S. Beattie, J. C. Bresnahan, D. L. Farmer and S. Li (2012). "Drug-eluting microfibrous patches for the local delivery of rolipram in spinal cord repair." J Control Release **161**(3): 910-917.

Doyle, J. P., J. D. Dougherty, M. Heiman, E. F. Schmidt, T. R. Stevens, G. Ma, S. Bupp, P. Shrestha, R. D. Shah, M. L. Doughty, S. Gong, P. Greengard and N. Heintz (2008). "Application of a translational profiling approach for the comparative analysis of CNS cell types." Cell **135**(4): 749-762.

Draget, K. I., G. Skjak-Braek and O. Smidsrod (1997). "Alginate based new materials." Int J Biol Macromol **21**(1-2): 47-55.

Dray, C., G. Rougon and F. Debarbieux (2009). "Quantitative analysis by in vivo imaging of the dynamics of vascular and axonal networks in injured mouse spinal cord." Proc Natl Acad Sci U S A **106**(23): 9459-9464.

Du, B. L., Y. Xiong, C. G. Zeng, L. M. He, W. Zhang, D. P. Quan, J. L. Wu, Y. Li and Y. S. Zeng (2011). "Transplantation of artificial neural construct partly improved spinal tissue repair and functional recovery in rats with spinal cord transection." Brain Res **1400**: 87-98.

Dulin, J. N., A. F. Adler, H. Kumamaru, G. H. D. Poplawski, C. Lee-Kubli, H. Strobl, D. Gibbs, K. Kadoya, J. W. Fawcett, P. Lu and M. H. Tuszynski (2018). "Injured adult motor and sensory axons regenerate into appropriate organotypic domains of neural progenitor grafts." Nat Commun **9**(1): 84.

Dumville, J. C., S. J. Keogh, Z. Liu, N. Stubbs, R. M. Walker and M. Fortnam (2015). "Alginate dressings for treating pressure ulcers." Cochrane Database Syst Rev(5): CD011277.

Duncan, G. J., S. B. Manesh, B. J. Hilton, P. Assinck, J. Liu, A. Moulson, J. R. Plemel and W. Tetzlaff (2018). "Locomotor recovery following contusive spinal cord injury does not require oligodendrocyte remyelination." Nat Commun **9**(1): 3066.

Duncan, I. D., A. B. Radcliff, M. Heidari, G. Kidd, B. K. August and L. A. Wierenga (2018). "The adult oligodendrocyte can participate in remyelination." Proc Natl Acad Sci U S A **115**(50): E11807-E11816.

Durkee, C. A. and A. Araque (2019). "Diversity and Specificity of Astrocyte-neuron Communication." Neuroscience **396**: 73-78.

Dyck, S. M., A. Alizadeh, K. T. Santhosh, E. H. Proulx, C. L. Wu and S. Karimi-Abdolrezaee (2015). "Chondroitin Sulfate Proteoglycans Negatively Modulate Spinal Cord Neural Precursor Cells by Signaling Through LAR and RPTPsigma and Modulation of the Rho/ROCK Pathway." Stem Cells **33**(8): 2550-2563.

East, E., D. B. de Oliveira, J. P. Golding and J. B. Phillips (2010). "Alignment of astrocytes increases neuronal growth in three-dimensional collagen gels and is maintained following plastic compression to form a spinal cord repair conduit." Tissue Eng Part A **16**(10): 3173-3184.

El-Kheir, W. A., H. Gabr, M. R. Awad, O. Ghannam, Y. Barakat, H. A. Farghali, Z. M. El Maadawi, I. Ewes and H. E. Sabaawy (2014). "Autologous bone marrow-derived cell therapy combined with physical therapy induces functional improvement in chronic spinal cord injury patients." Cell Transplant **23**(6): 729-745.

Elliott Donaghue, I., C. H. Tator and M. S. Shoichet (2015). "Sustained delivery of bioactive neurotrophin-3 to the injured spinal cord." Biomater Sci **3**(1): 65-72.

Elvira, G., I. Garcia, J. Gallo, M. Benito, P. Montesinos, E. Holgado-Martin, A. Ayuso-Sacido, S. Penades, M. Desco, A. Silva and J. A. Garcia-Sanz (2015). "Detection of mouse endogenous type B astrocytes migrating towards brain lesions." Stem Cell Res **14**(1): 114-129.

Emsley, J. G. and J. D. Macklis (2006). "Astroglial heterogeneity closely reflects the neuronal-defined anatomy of the adult murine CNS." Neuron Glia Biol **2**(3): 175-186.

Enes, J., N. Langwieser, J. Ruschel, M. M. Carballosa-Gonzalez, A. Klug, M. H. Traut, B. Ylera, S. Tahirovic, F. Hofmann, V. Stein, S. Moosmang, I. D. Hentall and F. Bradke (2010). "Electrical activity suppresses axon growth through Ca(v)1.2 channels in adult primary sensory neurons." Curr Biol **20**(13): 1154-1164.

Enomoto, M., M. B. Bunge and P. Tsoulfas (2013). "A multifunctional neurotrophin with reduced affinity to p75NTR enhances transplanted Schwann cell survival and axon growth after spinal cord injury." Exp Neurol **248**: 170-182.

Erturk, A., F. Hellal, J. Enes and F. Bradke (2007). "Disorganized microtubules underlie the formation of retraction bulbs and the failure of axonal regeneration." J Neurosci **27**(34): 9169-9180.

Ezan, P., P. Andre, S. Cisternino, B. Saubamea, A. C. Boulay, S. Doutremer, M. A. Thomas, N. Quenech'du, C. Giaume and M. Cohen-Salmon (2012). "Deletion of astroglial connexins weakens the blood-brain barrier." J Cereb Blood Flow Metab **32**(8): 1457-1467.

Fan, C., Y. Zheng, X. Cheng, X. Qi, P. Bu, X. Luo, D. H. Kim and Q. Cao (2013). "Transplantation of D15A-expressing glial-restricted-precursor-derived astrocytes improves anatomical and locomotor recovery after spinal cord injury." Int J Biol Sci **9**(1): 78-93.

Faulkner, J. R., J. E. Herrmann, M. J. Woo, K. E. Tansey, N. B. Doan and M. V. Sofroniew (2004). "Reactive astrocytes protect tissue and preserve function after spinal cord injury." J Neurosci **24**(9): 2143-2155.

Fawcett, J. W. (2020). "The Struggle to Make CNS Axons Regenerate: Why Has It Been so Difficult?" Neurochem Res **45**(1): 144-158.

Fawcett, J. W. and J. Verhaagen (2018). "Intrinsic Determinants of Axon Regeneration." Dev Neurobiol **78**(10): 890-897.

Fehlings, M. G., K. D. Kim, B. Aarabi, M. Rizzo, L. M. Bond, L. McKerracher, A. R. Vaccaro and D. O. Okonkwo (2018). "Rho Inhibitor VX-210 in Acute Traumatic Subaxial Cervical Spinal Cord Injury: Design of the SPinal Cord Injury Rho INhibition InvestiGation (SPRING) Clinical Trial." J Neurotrauma **35**(9): 1049-1056.

Fehlings, M. G., L. A. Tetreault, J. R. Wilson, B. K. Kwon, A. S. Burns, A. R. Martin, G. Hawryluk and J. S. Harrop (2017). "A Clinical Practice Guideline for the Management of Acute Spinal Cord Injury: Introduction, Rationale, and Scope." Global Spine J **7**(3 Suppl): 84S-94S.

Fehlings, M. G., N. Theodore, J. Harrop, G. Maurais, C. Kuntz, C. I. Shaffrey, B. K. Kwon, J. Chapman, A. Yee, A. Tighe and L. McKerracher (2011). "A phase I/IIa clinical trial of a recombinant Rho protein antagonist in acute spinal cord injury." J Neurotrauma **28**(5): 787-796.

Felix, E. R. and E. G. Widerstrom-Noga (2009). "Reliability and validity of quantitative sensory testing in persons with spinal cord injury and neuropathic pain." J Rehabil Res Dev **46**(1): 69-83.

Festoff, B. W., S. Ameenuddin, P. M. Arnold, A. Wong, K. S. Santacruz and B. A. Citron (2006). "Minocycline neuroprotects, reduces microgliosis, and inhibits caspase protease expression early after spinal cord injury." J Neurochem **97**(5): 1314-1326.

Field-Fote, E. C., S. D. Lindley and A. L. Sherman (2005). "Locomotor training approaches for individuals with spinal cord injury: a preliminary report of walking-related outcomes." J Neurol Phys Ther **29**(3): 127-137.

Filbin, M. T. (2003). "Myelin-associated inhibitors of axonal regeneration in the adult mammalian CNS." Nat Rev Neurosci **4**(9): 703-713.

Filous, A. R., J. H. Miller, Y. M. Coulson-Thomas, K. P. Horn, W. J. Alilain and J. Silver (2010). "Immature astrocytes promote CNS axonal regeneration when combined with chondroitinase ABC." Dev Neurobiol **70**(12): 826-841.

Finnerup, N. B. (2013). "Pain in patients with spinal cord injury." Pain **154 Suppl 1**: S71-76.

Finnerup, N. B., L. Sorensen, F. Biering-Sorensen, I. L. Johannesen and T. S. Jensen (2007). "Segmental hypersensitivity and spinothalamic function in spinal cord injury pain." Exp Neurol **207**(1): 139-149.

Flora, G., G. Joseph, S. Patel, A. Singh, D. Bleicher, D. J. Barakat, J. Louro, S. Fenton, M. Garg, M. B. Bunge and D. D. Pearse (2013). "Combining neurotrophin-transduced schwann cells and rolipram to promote functional recovery from subacute spinal cord injury." Cell Transplant **22**(12): 2203-2217.

Foo, L. C., N. J. Allen, E. A. Bushong, P. B. Ventura, W. S. Chung, L. Zhou, J. D. Cahoy, R. Daneman, H. Zong, M. H. Ellisman and B. A. Barres (2011). "Development of a method for the purification and culture of rodent astrocytes." Neuron **71**(5): 799-811.

Forostyak, S., P. Jendelova and E. Sykova (2013). "The role of mesenchymal stromal cells in spinal cord injury, regenerative medicine and possible clinical applications." Biochimie **95**(12): 2257-2270.

Fouad, K., D. J. Bennett, R. Vavrek and A. Blesch (2013). "Long-term viral brain-derived neurotrophic factor delivery promotes spasticity in rats with a cervical spinal cord hemisection." Front Neurol **4**: 187.

Fouad, K., V. Pedersen, M. E. Schwab and C. Brosamle (2001). "Cervical sprouting of corticospinal fibers after thoracic spinal cord injury accompanies shifts in evoked motor responses." Curr Biol **11**(22): 1766-1770.

Fouad, K., L. Schnell, M. B. Bunge, M. E. Schwab, T. Liebscher and D. D. Pearse (2005). "Combining Schwann cell bridges and olfactory-ensheathing glia grafts with chondroitinase promotes locomotor recovery after complete transection of the spinal cord." J Neurosci **25**(5): 1169-1178.

Franklin, R. J., A. J. Crang and W. F. Blakemore (1992). "Type 1 astrocytes fail to inhibit Schwann cell remyelination of CNS axons in the absence of cells of the O-2A lineage." Dev Neurosci **14**(2): 85-92.

Freeman, M. R. (2010). "Specification and morphogenesis of astrocytes." Science **330**(6005): 774-778.

Fuhrmann, T., P. N. Anandakumaran, S. L. Payne, M. M. Pakulska, B. V. Varga, A. Nagy, C. Tator and M. S. Shoichet (2018). "Combined delivery of chondroitinase ABC and human induced pluripotent stem cell-derived neuroepithelial cells promote tissue repair in an animal model of spinal cord injury." Biomed Mater **13**(2): 024103.

Fuhrmann, T., P. N. Anandakumaran and M. S. Shoichet (2017). "Combinatorial Therapies After Spinal Cord Injury: How Can Biomaterials Help?" Adv Healthc Mater **6**(10).

Fuhrmann, T., R. Y. Tam, B. Ballarin, B. Coles, I. Elliott Donaghue, D. van der Kooy, A. Nagy, C. H. Tator, C. M. Morshead and M. S. Shoichet (2016). "Injectable hydrogel promotes early survival of induced pluripotent stem cell-derived oligodendrocytes and attenuates longterm teratoma formation in a spinal cord injury model." Biomaterials **83**: 23-36.

Fujimoto, Y., M. Abematsu, A. Falk, K. Tsujimura, T. Sanosaka, B. Juliandi, K. Semi, M. Namihira, S. Komiya, A. Smith and K. Nakashima (2012). "Treatment of a mouse model of spinal cord injury by transplantation of human induced pluripotent stem cell-derived long-term self-renewing neuroepithelial-like stem cells." Stem Cells **30**(6): 1163-1173.

Fujioka, T., N. Kaneko, I. Ajioka, K. Nakaguchi, T. Omata, H. Ohba, R. Fassler, J. M. Garcia-Verdugo, K. Sekiguchi, N. Matsukawa and K. Sawamoto (2017). "beta1 integrin signaling promotes neuronal migration along vascular scaffolds in the post-stroke brain." EBioMedicine **16**: 195-203.

Fulmer, C. G., M. W. VonDran, A. A. Stillman, Y. Huang, B. L. Hempstead and C. F. Dreyfus (2014). "Astrocyte-derived BDNF supports myelin protein synthesis after cuprizone-induced demyelination." J Neurosci **34**(24): 8186-8196.

Furuta, A., J. D. Rothstein and L. J. Martin (1997). "Glutamate transporter protein subtypes are expressed differentially during rat CNS development." J Neurosci **17**(21): 8363-8375.

Gadea, A., S. Schinelli and V. Gallo (2008). "Endothelin-1 regulates astrocyte proliferation and reactive gliosis via a JNK/c-Jun signaling pathway." J Neurosci **28**(10): 2394-2408.

Gallo, V. and B. Deneen (2014). "Glial development: the crossroads of regeneration and repair in the CNS." Neuron **83**(2): 283-308.

Gao, M., P. Lu, B. Bednark, D. Lynam, J. M. Conner, J. Sakamoto and M. H. Tuszynski (2013). "Templated agarose scaffolds for the support of motor axon regeneration into sites of complete spinal cord transection." Biomaterials **34**(5): 1529-1536.

Garcia, A. D., N. B. Doan, T. Imura, T. G. Bush and M. V. Sofroniew (2004). "GFAP-expressing progenitors are the principal source of constitutive neurogenesis in adult mouse forebrain." Nat Neurosci **7**(11): 1233-1241.

Garcia-Alias, G., S. Barkhuysen, M. Buckle and J. W. Fawcett (2009). "Chondroitinase ABC treatment opens a window of opportunity for task-specific rehabilitation." Nat Neurosci **12**(9): 1145-1151.

Garcia-Alias, G., R. Lopez-Vales, J. Fores, X. Navarro and E. Verdu (2004). "Acute transplantation of olfactory ensheathing cells or Schwann cells promotes recovery after spinal cord injury in the rat." J Neurosci Res **75**(5): 632-641.

Garcia-Diaz, B., C. Bachelin, F. Coulpier, G. Gerschenfeld, C. Deboux, V. Zujovic, P. Charnay, P. Topilko and A. Baron-Van Evercooren (2019). "Blood vessels guide Schwann cell migration in the adult demyelinated CNS through Eph/ephrin signaling." Acta Neuropathol **138**(3): 457-476.

Gaub, P., Y. Joshi, A. Wuttke, U. Naumann, S. Schnichels, P. Heiduschka and S. Di Giovanni (2011). "The histone acetyltransferase p300 promotes intrinsic axonal regeneration." Brain **134**(Pt 7): 2134-2148.

Ge, W. P., A. Miyawaki, F. H. Gage, Y. N. Jan and L. Y. Jan (2012). "Local generation of glia is a major astrocyte source in postnatal cortex." Nature **484**(7394): 376-380.

Gensel, J. C. and B. Zhang (2015). "Macrophage activation and its role in repair and pathology after spinal cord injury." Brain Res **1619**: 1-11.

Gerhardt, H., M. Golding, M. Fruttiger, C. Ruhrberg, A. Lundkvist, A. Abramsson, M. Jeltsch, C. Mitchell, K. Alitalo, D. Shima and C. Betsholtz (2003). "VEGF guides angiogenic sprouting utilizing endothelial tip cell filopodia." J Cell Biol **161**(6): 1163-1177.

Ghosh, B., Z. Wang, J. Nong, M. W. Urban, Z. Zhang, V. A. Trovillion, M. C. Wright, Y. Zhong and A. C. Lepore (2018). "Local BDNF Delivery to the Injured Cervical Spinal Cord using an Engineered Hydrogel Enhances Diaphragmatic Respiratory Function." J Neurosci **38**(26): 5982-5995.

Gilyarov, A. V. (2008). "Nestin in central nervous system cells." Neurosci Behav Physiol **38**(2): 165-169.

Giuliani, F., S. A. Fu, L. M. Metz and V. W. Yong (2005). "Effective combination of minocycline and interferon-beta in a model of multiple sclerosis." J Neuroimmunol **165**(1-2): 83-91.

Giuseppe, M. D., N. Law, B. Webb, A. M. R, L. J. Liew, T. B. Sercombe, R. J. Dilley and B. J. Doyle (2018). "Mechanical behaviour of alginate-gelatin hydrogels for 3D bioprinting." J Mech Behav Biomed Mater **79**: 150-157.

Global Burden of Disease Study 2016: Traumatic brain Injury and Spinal Cord Injury Collaborators (2019). "Global, regional, and national burden of traumatic brain injury and spinal cord injury, 1990 - 2016: a systematic analysis for the Global Burden of Disease Study 2016." Lancet Neurol **18:** 56-87.

Goldberg, J. L., M. P. Klassen, Y. Hua and B. A. Barres (2002). "Amacrine-signaled loss of intrinsic axon growth ability by retinal ganglion cells." Science **296**(5574): 1860-1864.

Golden, K. L., D. D. Pearse, B. Blits, M. S. Garg, M. Oudega, P. M. Wood and M. B. Bunge (2007). "Transduced Schwann cells promote axon growth and myelination after spinal cord injury." Exp Neurol **207**(2): 203-217.

Gomez, R. M., M. Y. Sanchez, M. Portela-Lomba, K. Ghotme, G. E. Barreto, J. Sierra and M. T. Moreno-Flores (2018). "Cell therapy for spinal cord injury with olfactory ensheathing glia cells (OECs)." Glia **66**(7): 1267-1301.

Goritz, C., D. O. Dias, N. Tomilin, M. Barbacid, O. Shupliakov and J. Frisen (2011). "A pericyte origin of spinal cord scar tissue." Science **333**(6039): 238-242.

GrandPre, T., F. Nakamura, T. Vartanian and S. M. Strittmatter (2000). "Identification of the Nogo inhibitor of axon regeneration as a Reticulon protein." Nature **403**(6768): 439-444.

Griffin, J. M. and F. Bradke (2020). "Therapeutic repair for spinal cord injury: combinatory approaches to address a multifaceted problem." EMBO Mol Med **12**(3): e11505.

Grijalvo, S., M. Nieto-Diaz, R. M. Maza, R. Eritja and D. D. Diaz (2019). "Alginate Hydrogels as Scaffolds and Delivery Systems to Repair the Damaged Spinal Cord." Biotechnol J **14**(12): e1900275.

Gros, T., J. S. Sakamoto, A. Blesch, L. A. Havton and M. H. Tuszynski (2010). "Regeneration of long-tract axons through sites of spinal cord injury using templated agarose scaffolds." Biomaterials **31**(26): 6719-6729.

Grous, L. C., J. Vernengo, Y. Jin, B. T. Himes, J. S. Shumsky, I. Fischer and A. Lowman (2013). "Implications of poly(N-isopropylacrylamide)-g-poly(ethylene glycol) with codissolved brain-derived neurotrophic factor injectable scaffold on motor function recovery rate following cervical dorsolateral funiculotomy in the rat." J Neurosurg Spine **18**(6): 641-652.

Grulova, I., L. Slovinska, J. Blasko, S. Devaux, M. Wisztorski, M. Salzet, I. Fournier, O. Kryukov, S. Cohen and D. Cizkova (2015). "Delivery of Alginate Scaffold Releasing Two Trophic Factors for Spinal Cord Injury Repair." Sci Rep **5**: 13702.

Guest, J. and W. D. Dietrich (2015). "Commentary Regarding the Recent Publication by Tabakow et al., "Functional Regeneration of Supraspinal Connections in a Patient with Transected Spinal Cord following Transplantation of Bulbar Olfactory Ensheathing Cells with Peripheral Nerve Bridging"." J Neurotrauma **32**(15): 1176-1178.

Guest, J., A. J. Santamaria and F. D. Benavides (2013). "Clinical translation of autologous Schwann cell transplantation for the treatment of spinal cord injury." Curr Opin Organ Transplant **18**(6): 682-689.

Guest, J. D., D. Hesse, L. Schnell, M. E. Schwab, M. B. Bunge and R. P. Bunge (1997). "Influence of IN-1 antibody and acidic FGF-fibrin glue on the response of injured corticospinal tract axons to human Schwann cell grafts." J Neurosci Res **50**(5): 888-905.

Gunther, M. I., M. Gunther, M. Schneiders, R. Rupp and A. Blesch (2015). "AngleJ: A new tool for the automated measurement of neurite growth orientation in tissue sections." J Neurosci Methods **251**: 143-150.

Gunther, M. I., N. Weidner, R. Muller and A. Blesch (2015). "Cell-seeded alginate hydrogel scaffolds promote directed linear axonal regeneration in the injured rat spinal cord." Acta Biomater **27**: 140-150.

Guo, X., T. Zahir, A. Mothe, M. S. Shoichet, C. M. Morshead, Y. Katayama and C. H. Tator (2012). "The effect of growth factors and soluble Nogo-66 receptor protein on transplanted neural stem/progenitor survival and axonal regeneration after complete transection of rat spinal cord." Cell Transplant **21**(6): 1177-1197.

Haas, C. and I. Fischer (2013). "Human astrocytes derived from glial restricted progenitors support regeneration of the injured spinal cord." J Neurotrauma **30**(12): 1035-1052.

Haas, C., B. Neuhuber, T. Yamagami, M. Rao and I. Fischer (2012). "Phenotypic analysis of astrocytes derived from glial restricted precursors and their impact on axon regeneration." Exp Neurol **233**(2): 717-732.

Hackett, A. R., S. L. Yahn, K. Lyapichev, A. Dajnoki, D. H. Lee, M. Rodriguez, N. Cammer, J. Pak, S. T. Mehta, O. Bodamer, V. P. Lemmon and J. K. Lee (2018). "Injury type-dependent differentiation of NG2 glia into heterogeneous astrocytes." Exp Neurol **308**: 72-79.

Haggerty, A. E., I. Maldonado-Lasuncion and M. Oudega (2018). "Biomaterials for revascularization and immunomodulation after spinal cord injury." Biomed Mater **13**(4): 044105.

Halassa, M. M. and P. G. Haydon (2010). "Integrated brain circuits: astrocytic networks modulate neuronal activity and behavior." Annu Rev Physiol **72**: 335-355.

Hamby, M. E., G. Coppola, Y. Ao, D. H. Geschwind, B. S. Khakh and M. V. Sofroniew (2012). "Inflammatory mediators alter the astrocyte transcriptome and calcium signaling elicited by multiple G-protein-coupled receptors." J Neurosci **32**(42): 14489-14510.

Hammond, T. R., A. Gadea, J. Dupree, C. Kerninon, B. Nait-Oumesmar, A. Aguirre and V. Gallo (2014). "Astrocyte-derived endothelin-1 inhibits remyelination through notch activation." Neuron **81**(3): 588-602.

Han, Q., W. Jin, Z. Xiao, H. Ni, J. Wang, J. Kong, J. Wu, W. Liang, L. Chen, Y. Zhao, B. Chen and J. Dai (2010). "The promotion of neural regeneration in an extreme rat spinal cord injury model using a collagen scaffold containing a collagen binding neuroprotective protein and an EGFR neutralizing antibody." Biomaterials **31**(35): 9212-9220.

Han, S., J. Y. Lee, E. Y. Heo, I. K. Kwon, T. Y. Yune and I. Youn (2018). "Implantation of a Matrigel-loaded agarose scaffold promotes functional regeneration of axons after spinal cord injury in rat." Biochem Biophys Res Commun **496**(3): 785-791.

Hara, M., K. Kobayakawa, Y. Ohkawa, H. Kumamaru, K. Yokota, T. Saito, K. Kijima, S. Yoshizaki, K. Harimaya, Y. Nakashima and S. Okada (2017). "Interaction of reactive astrocytes with type I collagen induces astrocytic scar formation through the integrin-N-cadherin pathway after spinal cord injury." Nat Med **23**(7): 818-828.

Hasegawa, K., Y. W. Chang, H. Li, Y. Berlin, O. Ikeda, N. Kane-Goldsmith and M. Grumet (2005). "Embryonic radial glia bridge spinal cord lesions and promote functional recovery following spinal cord injury." Exp Neurol **193**(2): 394-410.

Hatakeyama, M., I. Ninomiya and M. Kanazawa (2020). "Angiogenesis and neuronal remodeling after ischemic stroke." Neural Regen Res **15**(1): 16-19.

Hatton, J. D., M. H. Nguyen and H. S. U (1993). "Differential migration of astrocytes grafted into the developing rat brain." Glia **9**(2): 113-119.

Hayashi, K., M. Hashimoto, M. Koda, A. T. Naito, A. Murata, A. Okawa, K. Takahashi and M. Yamazaki (2011). "Increase of sensitivity to mechanical stimulus after transplantation of murine induced pluripotent stem cell-derived astrocytes in a rat spinal cord injury model." J Neurosurg Spine **15**(6): 582-593.

He, Z. and Y. Jin (2016). "Intrinsic Control of Axon Regeneration." Neuron **90**(3): 437-451.

He, Z., H. Zang, L. Zhu, K. Huang, T. Yi, S. Zhang and S. Cheng (2019). "An anti-inflammatory peptide and brain-derived neurotrophic factor-modified hyaluronan-methylcellulose hydrogel promotes nerve regeneration in rats with spinal cord injury." Int J Nanomedicine **14**: 721-732.

Hellal, F., A. Hurtado, J. Ruschel, K. C. Flynn, C. J. Laskowski, M. Umlauf, L. C. Kapitein, D. Strikis, V. Lemmon, J. Bixby, C. C. Hoogenraad and F. Bradke (2011). "Microtubule stabilization reduces scarring and causes axon regeneration after spinal cord injury." Science **331**(6019): 928-931.

Hernigou, P., C. H. Flouzat-Lachaniette, J. Delambre, A. Poignard, J. Allain, N. Chevallier and H. Rouard (2015). "Osteonecrosis repair with bone marrow cell therapies: state of the clinical art." Bone **70**: 102-109.

Herrmann, J. E., T. Imura, B. Song, J. Qi, Y. Ao, T. K. Nguyen, R. A. Korsak, K. Takeda, S. Akira and M. V. Sofroniew (2008). "STAT3 is a critical regulator of astrogliosis and scar formation after spinal cord injury." J Neurosci **28**(28): 7231-7243.

Hervera, A., L. Zhou, I. Palmisano, E. McLachlan, G. Kong, T. H. Hutson, M. C. Danzi, V. P. Lemmon, J. L. Bixby, A. Matamoros-Angles, K. Forsberg, F. De Virgiliis, D. P. Matheos, J. Kwapis, M. A. Wood, R. Puttagunta, J. A. Del Rio and S. Di Giovanni (2019). "PP4-dependent HDAC3 dephosphorylation discriminates between axonal regeneration and regenerative failure." EMBO J **38**(13): e101032.

Hirabayashi, Y., Y. Itoh, H. Tabata, K. Nakajima, T. Akiyama, N. Masuyama and Y. Gotoh (2004). "The Wnt/beta-catenin pathway directs neuronal differentiation of cortical neural precursor cells." Development **131**(12): 2791-2801.

Hirabayashi, Y., N. Suzki, M. Tsuboi, T. A. Endo, T. Toyoda, J. Shinga, H. Koseki, M. Vidal and Y. Gotoh (2009). "Polycomb limits the neurogenic competence of neural precursor cells to promote astrogenic fate transition." Neuron **63**(5): 600-613.

Hobson, M. I., C. J. Green and G. Terenghi (2000). "VEGF enhances intraneural angiogenesis and improves nerve regeneration after axotomy." J Anat **197 Pt 4**: 591-605.

Hochstim, C., B. Deneen, A. Lukaszewicz, Q. Zhou and D. J. Anderson (2008). "Identification of positionally distinct astrocyte subtypes whose identities are specified by a homeodomain code." Cell **133**(3): 510-522.

Hofstetter, C. P., N. A. Holmstrom, J. A. Lilja, P. Schweinhardt, J. Hao, C. Spenger, Z. Wiesenfeld-Hallin, S. N. Kurpad, J. Frisen and L. Olson (2005). "Allodynia limits the usefulness of intraspinal neural stem cell grafts; directed differentiation improves outcome." Nat Neurosci **8**(3): 346-353.

Holtje, M., A. Hoffmann, F. Hofmann, C. Mucke, G. Grosse, N. Van Rooijen, H. Kettenmann, I. Just and G. Ahnert-Hilger (2005). "Role of Rho GTPase in astrocyte morphology and migratory response during in vitro wound healing." J Neurochem **95**(5): 1237-1248.

Hong, Y., T. Zhao, X. J. Li and S. Li (2016). "Mutant Huntingtin Impairs BDNF Release from Astrocytes by Disrupting Conversion of Rab3a-GTP into Rab3a-GDP." J Neurosci **36**(34): 8790-8801.

Hou, S. and A. G. Rabchevsky (2014). "Autonomic consequences of spinal cord injury." Compr Physiol **4**(4): 1419-1453.

Hu, H. Z., N. Granger, S. B. Pai, R. V. Bellamkonda and N. D. Jeffery (2018). "Therapeutic efficacy of microtube-embedded chondroitinase ABC in a canine clinical model of spinal cord injury." Brain **141**(4): 1017-1027.

Huang, D. W., L. McKerracher, P. E. Braun and S. David (1999). "A therapeutic vaccine approach to stimulate axon regeneration in the adult mammalian spinal cord." Neuron **24**(3): 639-647.

Hughes, C. S., L. M. Postovit and G. A. Lajoie (2010). "Matrigel: a complex protein mixture required for optimal growth of cell culture." Proteomics **10**(9): 1886-1890.

Hurlbert, R. J., M. N. Hadley, B. C. Walters, B. Aarabi, S. S. Dhall, D. E. Gelb, C. J. Rozzelle, T. C. Ryken and N. Theodore (2013). "Pharmacological therapy for acute spinal cord injury." Neurosurgery **72 Suppl 2**: 93-105.

Hurtado, A., J. M. Cregg, H. B. Wang, D. F. Wendell, M. Oudega, R. J. Gilbert and J. W. McDonald (2011). "Robust CNS regeneration after complete spinal cord transection using aligned poly-L-lactic acid microfibers." Biomaterials **32**(26): 6068-6079.

Hutson, T. H., J. Verhaagen, R. J. Yanez-Munoz and L. D. Moon (2012). "Corticospinal tract transduction: a comparison of seven adeno-associated viral vector serotypes and a non-integrating lentiviral vector." Gene Ther **19**(1): 49-60.

Hwang, D. H., H. M. Kim, Y. M. Kang, I. S. Joo, C. S. Cho, B. W. Yoon, S. U. Kim and B. G. Kim (2011). "Combination of multifaceted strategies to maximize the therapeutic benefits of neural stem cell transplantation for spinal cord repair." Cell Transplant **20**(9): 1361-1379.

Ide, C., Y. Nakai, N. Nakano, T. B. Seo, Y. Yamada, K. Endo, T. Noda, F. Saito, Y. Suzuki, M. Fukushima and T. Nakatani (2010). "Bone marrow stromal cell transplantation for treatment of sub-acute spinal cord injury in the rat." Brain Res **1332**: 32-47.

Ikeda, O., M. Murakami, H. Ino, M. Yamazaki, T. Nemoto, M. Koda, C. Nakayama and H. Moriya (2001). "Acute up-regulation of brain-derived neurotrophic factor expression resulting from experimentally induced injury in the rat spinal cord." Acta Neuropathol **102**(3): 239-245.

Ikeshima-Kataoka, H. (2016). "Neuroimmunological Implications of AQP4 in Astrocytes." Int J Mol Sci **17**(8).

Imura, T., H. I. Kornblum and M. V. Sofroniew (2003). "The predominant neural stem cell isolated from postnatal and adult forebrain but not early embryonic forebrain expresses GFAP." J Neurosci **23**(7): 2824-2832.

Iseda, T., T. Nishio, S. Kawaguchi, M. Yamanoto, T. Kawasaki and S. Wakisaka (2004). "Spontaneous regeneration of the corticospinal tract after transection in young rats: a key role of reactive astrocytes in making favorable and unfavorable conditions for regeneration." Neuroscience **126**(2): 365-374.

Ishibashi, T., K. A. Dakin, B. Stevens, P. R. Lee, S. V. Kozlov, C. L. Stewart and R. D. Fields (2006). "Astrocytes promote myelination in response to electrical impulses." Neuron **49**(6): 823-832.

Itoh, N., Y. Itoh, A. Tassoni, E. Ren, M. Kaito, A. Ohno, Y. Ao, V. Farkhondeh, H. Johnsonbaugh, J. Burda, M. V. Sofroniew and R. R. Voskuhl (2018). "Cell-specific and region-specific transcriptomics in the multiple sclerosis model: Focus on astrocytes." Proc Natl Acad Sci U S A **115**(2): E302-E309.

Jacobsen, C. T. and R. H. Miller (2003). "Control of astrocyte migration in the developing cerebral cortex." Dev Neurosci **25**(2-4): 207-216.

Jain, A., R. J. McKeon, S. M. Brady-Kalnay and R. V. Bellamkonda (2011). "Sustained delivery of activated Rho GTPases and BDNF promotes axon growth in CSPG-rich regions following spinal cord injury." PLoS One **6**(1): e16135.

Javid, S., A. Rezaei and G. Karami (2014). "A micromechanical procedure for viscoelastic characterization of the axons and ECM of the brainstem." J Mech Behav Biomed Mater **30**: 290-299.

Jin, D., Y. Liu, F. Sun, X. Wang, X. Liu and Z. He (2015). "Restoration of skilled locomotion by sprouting corticospinal axons induced by co-deletion of PTEN and SOCS3." Nat Commun **6**: 8074.

Jin, Y., B. Neuhuber, A. Singh, J. Bouyer, A. Lepore, J. Bonner, T. Himes, J. T. Campanelli and I. Fischer (2011). "Transplantation of human glial restricted progenitors and derived astrocytes into a contusion model of spinal cord injury." J Neurotrauma **28**(4): 579-594.

Jin, Y., J. S. Shumsky and I. Fischer (2018). "Axonal regeneration of different tracts following transplants of human glial restricted progenitors into the injured spinal cord in rats." Brain Res **1686**: 101-112.

John Lin, C. C., K. Yu, A. Hatcher, T. W. Huang, H. K. Lee, J. Carlson, M. C. Weston, F. Chen, Y. Zhang, W. Zhu, C. A. Mohila, N. Ahmed, A. J. Patel, B. R. Arenkiel, J. L. Noebels, C. J. Creighton and B. Deneen (2017). "Identification of diverse astrocyte populations and their malignant analogs." Nat Neurosci **20**(3): 396-405.

Johnson, P. J., S. R. Parker and S. E. Sakiyama-Elbert (2010). "Fibrin-based tissue engineering scaffolds enhance neural fiber sprouting and delay the accumulation of reactive astrocytes at the lesion in a subacute model of spinal cord injury." J Biomed Mater Res A **92**(1): 152-163.

Johnson, P. J., A. Tatara, D. A. McCreedy, A. Shiu and S. E. Sakiyama-Elbert (2010). "Tissue-engineered fibrin scaffolds containing neural progenitors enhance functional recovery in a subacute model of SCI." Soft Matter **6**(20): 5127-5137.

Jones, L. L., R. U. Margolis and M. H. Tuszynski (2003). "The chondroitin sulfate proteoglycans neurocan, brevican, phosphacan, and versican are differentially regulated following spinal cord injury." Exp Neurol **182**(2): 399-411.

Jones, L. L., D. Sajed and M. H. Tuszynski (2003). "Axonal regeneration through regions of chondroitin sulfate proteoglycan deposition after spinal cord injury: a balance of permissiveness and inhibition." J Neurosci **23**(28): 9276-9288.

Joosten, E. A., P. R. Bar and W. H. Gispen (1995). "Collagen implants and cortico-spinal axonal growth after mid-thoracic spinal cord lesion in the adult rat." J Neurosci Res **41**(4): 481-490.

Joosten, E. A. and A. A. Gribnau (1989). "Astrocytes and guidance of outgrowing corticospinal tract axons in the rat. An immunocytochemical study using anti-vimentin and anti-glial fibrillary acidic protein." Neuroscience **31**(2): 439-452.

Joosten, E. A., W. B. Veldhuis and F. P. Hamers (2004). "Collagen containing neonatal astrocytes stimulates regrowth of injured fibers and promotes modest locomotor recovery after spinal cord injury." J Neurosci Res **77**(1): 127-142.

Joset, A., D. A. Dodd, S. Halegoua and M. E. Schwab (2010). "Pincher-generated Nogo-A endosomes mediate growth cone collapse and retrograde signaling." J Cell Biol **188**(2): 271-285.

Joung, D., V. Truong, C. C. Neitzke, S. Guo, P. J. Walsh, J. R. Monat, F. Meng, S. H. Park, J. R. Dutton, A. M. Parr and M. C. McAlpine (2018). "3D Printed Stem-Cell Derived Neural Progenitors Generate Spinal Cord Scaffolds." Adv. Funct. Mater. **28**.

Kalpachidou, T., L. Spiecker, M. Kress and S. Quarta (2019). "Rho GTPases in the Physiology and Pathophysiology of Peripheral Sensory Neurons." Cells **8**(6).

Kanagal, S. G. and G. D. Muir (2008). "Effects of combined dorsolateral and dorsal funicular lesions on sensorimotor behaviour in rats." Exp Neurol **214**(2): 229-239.

Kanagal, S. G. and G. D. Muir (2009). "Task-dependent compensation after pyramidal tract and dorsolateral spinal lesions in rats." Exp Neurol **216**(1): 193-206.

Kang, P., H. K. Lee, S. M. Glasgow, M. Finley, T. Donti, Z. B. Gaber, B. H. Graham, A. E. Foster, B. G. Novitch, R. M. Gronostajski and B. Deneen (2012). "Sox9 and NFIA coordinate a transcriptional regulatory cascade during the initiation of gliogenesis." Neuron **74**(1): 79-94.

Kanno, H., Y. Pressman, A. Moody, R. Berg, E. M. Muir, J. H. Rogers, H. Ozawa, E. Itoi, D. D. Pearse and M. B. Bunge (2014). "Combination of engineered Schwann cell grafts to secrete neurotrophin and chondroitinase promotes axonal regeneration and locomotion after spinal cord injury." J Neurosci **34**(5): 1838-1855.

Kantawong, F., C. Saksiriwisitkul, C. Riyapa, S. Limpakdee, P. Wanachantararak and T. Kuboki (2018). "Reprogramming of mouse fibroblasts into neural lineage cells using biomaterials." Bioimpacts **8**(2): 129-138.

Karimi-Abdolrezaee, S., E. Eftekharpour, J. Wang, C. M. Morshead and M. G. Fehlings (2006). "Delayed transplantation of adult neural precursor cells promotes remyelination and functional neurological recovery after spinal cord injury." J Neurosci **26**(13): 3377-3389.

Karimi-Abdolrezaee, S., E. Eftekharpour, J. Wang, D. Schut and M. G. Fehlings (2010). "Synergistic effects of transplanted adult neural stem/progenitor cells, chondroitinase, and growth factors promote functional repair and plasticity of the chronically injured spinal cord." J Neurosci **30**(5): 1657-1676.

Kataoka, K., Y. Suzuki, M. Kitada, T. Hashimoto, H. Chou, H. Bai, M. Ohta, S. Wu, K. Suzuki and C. Ide (2004). "Alginate enhances elongation of early regenerating axons in spinal cord of young rats." Tissue Eng **10**(3-4): 493-504.

Kataoka, K., Y. Suzuki, M. Kitada, K. Ohnishi, K. Suzuki, M. Tanihara, C. Ide, K. Endo and Y. Nishimura (2001). "Alginate, a bioresorbable material derived from brown seaweed, enhances elongation of amputated axons of spinal cord in infant rats." J Biomed Mater Res **54**(3): 373-384.

Kathe, C., T. H. Hutson, S. B. McMahon and L. D. Moon (2016). "Intramuscular Neurotrophin-3 normalizes low threshold spinal reflexes, reduces spasms and improves mobility after bilateral corticospinal tract injury in rats." Elife **5**.

Katoh, H., K. Yokota and M. G. Fehlings (2019). "Regeneration of Spinal Cord Connectivity Through Stem Cell Transplantation and Biomaterial Scaffolds." Front Cell Neurosci **13**: 248.

Kautzman, A. G., P. W. Keeley, M. M. Nahmou, G. Luna, S. K. Fisher and B. E. Reese (2018). "Sox2 regulates astrocytic and vascular development in the retina." Glia **66**(3): 623-636.

Kawaja, M. D. and F. H. Gage (1991). "Reactive astrocytes are substrates for the growth of adult CNS axons in the presence of elevated levels of nerve growth factor." Neuron **7**(6): 1019-1030.

Keirstead, H. S., G. Nistor, G. Bernal, M. Totoiu, F. Cloutier, K. Sharp and O. Steward (2005). "Human embryonic stem cell-derived oligodendrocyte progenitor cell transplants remyelinate and restore locomotion after spinal cord injury." J Neurosci **25**(19): 4694-4705.

Kelley, K. W., L. Ben Haim, L. Schirmer, G. E. Tyzack, M. Tolman, J. G. Miller, H. H. Tsai, S. M. Chang, A. V. Molofsky, Y. Yang, R. Patani, A. Lakatos, E. M. Ullian and D. H. Rowitch (2018). "Kir4.1-Dependent Astrocyte-Fast Motor Neuron Interactions Are Required for Peak Strength." Neuron **98**(2): 306-319 e307.

Khaing, Z. Z., A. Ehsanipour, C. P. Hofstetter and S. K. Seidlits (2016). "Injectable Hydrogels for Spinal Cord Repair: A Focus on Swelling and Intraspinal Pressure." Cells Tissues Organs **202**(1-2): 67-84.

Khakh, B. S. and M. V. Sofroniew (2015). "Diversity of astrocyte functions and phenotypes in neural circuits." Nat Neurosci **18**(7): 942-952.

Khodagholi, F., B. Eftekharzadeh, N. Maghsoudi and P. F. Rezaei (2010). "Chitosan prevents oxidative stress-induced amyloid beta formation and cytotoxicity in NT2 neurons: involvement of transcription factors Nrf2 and NF-kappaB." Mol Cell Biochem **337**(1-2): 39-51.

Khor, E. and L. Y. Lim (2003). "Implantable applications of chitin and chitosan." Biomaterials **24**(13): 2339-2349.

Kiefer, J. C. (2007). "Back to basics: Sox genes." Dev Dyn **236**(8): 2356-2366.

Kigerl, K. A., J. C. Gensel, D. P. Ankeny, J. K. Alexander, D. J. Donnelly and P. G. Popovich (2009). "Identification of two distinct macrophage subsets with divergent effects causing either neurotoxicity or regeneration in the injured mouse spinal cord." J Neurosci **29**(43): 13435-13444.

Kim, H., C. H. Tator and M. S. Shoichet (2011). "Chitosan implants in the rat spinal cord: biocompatibility and biodegradation." J Biomed Mater Res A **97**(4): 395-404.

Kim, H., T. Zahir, C. H. Tator and M. S. Shoichet (2011). "Effects of dibutyryl cyclic-AMP on survival and neuronal differentiation of neural stem/progenitor cells transplanted into spinal cord injured rats." PLoS One **6**(6): e21744.

Kim, J., L. Shapiro and A. Flynn (2015). "The clinical application of mesenchymal stem cells and cardiac stem cells as a therapy for cardiovascular disease." Pharmacol Ther **151**: 8-15.

Kim, R. Y., A. S. Hoffman, N. Itoh, Y. Ao, R. Spence, M. V. Sofroniew and R. R. Voskuhl (2014). "Astrocyte CCL2 sustains immune cell infiltration in chronic experimental autoimmune encephalomyelitis." J Neuroimmunol **274**(1-2): 53-61.

Kim, Y. H., K. Y. Ha and S. I. Kim (2017). "Spinal Cord Injury and Related Clinical Trials." Clin Orthop Surg **9**(1): 1-9.

King, V. R., A. Alovskaya, D. Y. Wei, R. A. Brown and J. V. Priestley (2010). "The use of injectable forms of fibrin and fibronectin to support axonal ingrowth after spinal cord injury." Biomaterials **31**(15): 4447-4456.

Kitamura, K., K. Fujiyoshi, J. Yamane, F. Toyota, K. Hikishima, T. Nomura, H. Funakoshi, T. Nakamura, M. Aoki, Y. Toyama, H. Okano and M. Nakamura (2011). "Human hepatocyte growth factor promotes functional recovery in primates after spinal cord injury." PLoS One **6**(11): e27706.

Kliot, M., G. M. Smith, J. D. Siegal and J. Silver (1990). "Astrocyte-polymer implants promote regeneration of dorsal root fibers into the adult mammalian spinal cord." Exp Neurol **109**(1): 57-69.

Kobayashi, Y., Y. Okada, G. Itakura, H. Iwai, S. Nishimura, A. Yasuda, S. Nori, K. Hikishima, T. Konomi, K. Fujiyoshi, O. Tsuji, Y. Toyama, S. Yamanaka, M. Nakamura and H. Okano (2012). "Pre-evaluated safe human iPSC-derived neural stem cells promote functional recovery after spinal cord injury in common marmoset without tumorigenicity." PLoS One **7**(12): e52787.

Koffler, J., W. Zhu, X. Qu, O. Platoshyn, J. N. Dulin, J. Brock, L. Graham, P. Lu, J. Sakamoto, M. Marsala, S. Chen and M. H. Tuszynski (2019). "Biomimetic 3D-printed scaffolds for spinal cord injury repair." Nat Med **25**(2): 263-269.

Kokaia, Z., G. Martino, M. Schwartz and O. Lindvall (2012). "Cross-talk between neural stem cells and immune cells: the key to better brain repair?" Nat Neurosci **15**(8): 1078-1087.

Kondo, T. and M. Raff (2000). "Oligodendrocyte precursor cells reprogrammed to become multipotential CNS stem cells." Science **289**(5485): 1754-1757.

Kong, H., K. Y. Lee and D. J. Mooney (2002). "Decoupling the dependence of rheological/mechanical properties of hydrogels from solids concentration." Polymer **43**: 6239-6246.

Koprivica, V., K. S. Cho, J. B. Park, G. Yiu, J. Atwal, B. Gore, J. A. Kim, E. Lin, M. Tessier-Lavigne, D. F. Chen and Z. He (2005). "EGFR activation mediates inhibition of axon regeneration by myelin and chondroitin sulfate proteoglycans." Science **310**(5745): 106-110.

Koser, D. E., E. Moeendarbary, J. Hanne, S. Kuerten and K. Franze (2015). "CNS cell distribution and axon orientation determine local spinal cord mechanical properties." Biophys J **108**(9): 2137-2147.

Koser, D. E., A. J. Thompson, S. K. Foster, A. Dwivedy, E. K. Pillai, G. K. Sheridan, H. Svoboda, M. Viana, L. D. Costa, J. Guck, C. E. Holt and K. Franze (2016). "Mechanosensing is critical for axon growth in the developing brain." Nat Neurosci **19**(12): 1592-1598.

Kottis, V., P. Thibault, D. Mikol, Z. C. Xiao, R. Zhang, P. Dergham and P. E. Braun (2002). "Oligodendrocyte-myelin glycoprotein (OMgp) is an inhibitor of neurite outgrowth." J Neurochem **82**(6): 1566-1569.

Krencik, R., J. P. Weick, Y. Liu, Z. J. Zhang and S. C. Zhang (2011). "Specification of transplantable astroglial subtypes from human pluripotent stem cells." Nat Biotechnol **29**(6): 528-534.

Kucher, K., D. Johns, D. Maier, R. Abel, A. Badke, H. Baron, R. Thietje, S. Casha, R. Meindl, B. Gomez-Mancilla, C. Pfister, R. Rupp, N. Weidner, A. Mir, M. E. Schwab and A. Curt (2018). "First-in-Man

Intrathecal Application of Neurite Growth-Promoting Anti-Nogo-A Antibodies in Acute Spinal Cord Injury." Neurorehabil Neural Repair **32**(6-7): 578-589.

Kucukdereli, H., N. J. Allen, A. T. Lee, A. Feng, M. I. Ozlu, L. M. Conatser, C. Chakraborty, G. Workman, M. Weaver, E. H. Sage, B. A. Barres and C. Eroglu (2011). "Control of excitatory CNS synaptogenesis by astrocyte-secreted proteins Hevin and SPARC." Proc Natl Acad Sci U S A **108**(32): E440-449.

Kumamaru, H., P. Lu, E. S. Rosenzweig, K. Kadoya and M. H. Tuszynski (2019). "Regenerating Corticospinal Axons Innervate Phenotypically Appropriate Neurons within Neural Stem Cell Grafts." Cell Rep **26**(9): 2329-2339 e2324.

Kumar, R., J. Lim, R. A. Mekary, A. Rattani, M. C. Dewan, S. Y. Sharif, E. Osorio-Fonseca and K. B. Park (2018). "Traumatic Spinal Injury: Global Epidemiology and Worldwide Volume." World Neurosurg **113**: e345-e363.

Lagos-Cabre, R., A. Alvarez, M. Kong, F. Burgos-Bravo, A. Cardenas, E. Rojas-Mancilla, R. Perez-Nunez, R. Herrera-Molina, F. Rojas, P. Schneider, M. Herrera-Marschitz, A. F. G. Quest, B. van Zundert and L. Leyton (2017). "alphaVbeta3 Integrin regulates astrocyte reactivity." J Neuroinflammation **14**(1): 194.

Lang, B. T., J. M. Cregg, M. A. DePaul, A. P. Tran, K. Xu, S. M. Dyck, K. M. Madalena, B. P. Brown, Y. L. Weng, S. Li, S. Karimi-Abdolrezaee, S. A. Busch, Y. Shen and J. Silver (2015). "Modulation of the proteoglycan receptor PTPsigma promotes recovery after spinal cord injury." Nature **518**(7539): 404-408.

Langer, J., N. J. Gerkau, A. Derouiche, C. Kleinhans, B. Moshrefi-Ravasdjani, M. Fredrich, K. W. Kafitz, G. Seifert, C. Steinhauser and C. R. Rose (2017). "Rapid sodium signaling couples glutamate uptake to breakdown of ATP in perivascular astrocyte endfeet." Glia **65**(2): 293-308.

Lanjakornsiripan, D., B. J. Pior, D. Kawaguchi, S. Furutachi, T. Tahara, Y. Katsuyama, Y. Suzuki, Y. Fukazawa and Y. Gotoh (2018). "Layer-specific morphological and molecular differences in neocortical astrocytes and their dependence on neuronal layers." Nat Commun **9**(1): 1623.

Lee, A. S., C. Tang, F. Cao, X. Xie, K. van der Bogt, A. Hwang, A. J. Connolly, R. C. Robbins and J. C. Wu (2009). "Effects of cell number on teratoma formation by human embryonic stem cells." Cell Cycle **8**(16): 2608-2612.

Lee, H., R. J. McKeon and R. V. Bellamkonda (2010). "Sustained delivery of thermostabilized chABC enhances axonal sprouting and functional recovery after spinal cord injury." Proc Natl Acad Sci U S A **107**(8): 3340-3345.

Lee, J. and K. Y. Lee (2009). "Local and sustained vascular endothelial growth factor delivery for angiogenesis using an injectable system." Pharm Res **26**(7): 1739-1744.

Lee, J. K., R. Chow, F. Xie, S. Y. Chow, K. E. Tolentino and B. Zheng (2010). "Combined genetic attenuation of myelin and semaphorin-mediated growth inhibition is insufficient to promote serotonergic axon regeneration." J Neurosci **30**(32): 10899-10904.

Lee, J. K., C. G. Geoffroy, A. F. Chan, K. E. Tolentino, M. J. Crawford, M. A. Leal, B. Kang and B. Zheng (2010). "Assessing spinal axon regeneration and sprouting in Nogo-, MAG-, and OMgp-deficient mice." Neuron **66**(5): 663-670.

Lee, K. Y. and D. J. Mooney (2012). "Alginate: properties and biomedical applications." Prog Polym Sci **37**(1): 106-126.

Lee, K. Y., J. A. Rowley, P. Eiselt, E. M. Moy, K. H. Bouhadir and D. J. Mooney (2000). "Controlling Mechanical and Swelling Properties of Alginate Hydrogels Independently by Cross-Linker Type and Cross-Linking Density." Macromolecules **33**(11).

Lee, Y. S., C. Y. Lin, H. H. Jiang, M. Depaul, V. W. Lin and J. Silver (2013). "Nerve regeneration restores supraspinal control of bladder function after complete spinal cord injury." J Neurosci **33**(26): 10591-10606.

Lee, Y. S., S. Wu, T. L. Arinzeh and M. B. Bunge (2017). "Enhanced noradrenergic axon regeneration into schwann cell-filled PVDF-TrFE conduits after complete spinal cord transection." Biotechnol Bioeng **114**(2): 444-456.

Lepore, A. C., B. Rauck, C. Dejea, A. C. Pardo, M. S. Rao, J. D. Rothstein and N. J. Maragakis (2008). "Focal transplantation-based astrocyte replacement is neuroprotective in a model of motor neuron disease." Nat Neurosci **11**(11): 1294-1301.

Li, B. C., Y. Li, L. F. Chen, J. Y. Chang and Z. X. Duan (2011). "Olfactory ensheathing cells can reduce the tissue loss but not the cavity formation in contused spinal cord of rats." J Neurol Sci **303**(1-2): 67-74.

Li, H. Y., T. Fuhrmann, Y. Zhou and P. D. Dalton (2013). "Host reaction to poly(2-hydroxyethyl methacrylate) scaffolds in a small spinal cord injury model." J Mater Sci Mater Med **24**(8): 2001-2011.

Li, J., R. R. Khankan, C. Caneda, M. I. Godoy, M. S. Haney, M. C. Krawczyk, M. C. Bassik, S. A. Sloan and Y. Zhang (2019). "Astrocyte-to-astrocyte contact and a positive feedback loop of growth factor signaling regulate astrocyte maturation." Glia **67**(8): 1571-1597.

Li, S. and P. K. Stys (2000). "Mechanisms of ionotropic glutamate receptor-mediated excitotoxicity in isolated spinal cord white matter." J Neurosci **20**(3): 1190-1198.

Li, X., J. M. Newbern, Y. Wu, M. Morgan-Smith, J. Zhong, J. Charron and W. D. Snider (2012). "MEK Is a Key Regulator of Gliogenesis in the Developing Brain." Neuron **75**(6): 1035-1050.

Li, X., Z. Xiao, J. Han, L. Chen, H. Xiao, F. Ma, X. Hou, X. Li, J. Sun, W. Ding, Y. Zhao, B. Chen and J. Dai (2013). "Promotion of neuronal differentiation of neural progenitor cells by using EGFR antibody functionalized collagen scaffolds for spinal cord injury repair." Biomaterials **34**(21): 5107-5116.

Li, X., Z. Yang, A. Zhang, T. Wang and W. Chen (2009). "Repair of thoracic spinal cord injury by chitosan tube implantation in adult rats." Biomaterials **30**(6): 1121-1132.

Li, Y., Y. Song, L. Zhao, G. Gaidosh, A. M. Laties and R. Wen (2008). "Direct labeling and visualization of blood vessels with lipophilic carbocyanine dye DiI." Nat Protoc **3**(11): 1703-1708.

Li, Z. W., R. H. Tang, J. P. Zhang, Z. P. Tang, W. S. Qu, W. H. Zhu, J. J. Li, M. J. Xie, D. S. Tian and W. Wang (2011). "Inhibiting epidermal growth factor receptor attenuates reactive astrogliosis and improves functional outcome after spinal cord injury in rats." Neurochem Int **58**(7): 812-819.

Liauw, J., S. Hoang, M. Choi, C. Eroglu, M. Choi, G. H. Sun, M. Percy, B. Wildman-Tobriner, T. Bliss, R. G. Guzman, B. A. Barres and G. K. Steinberg (2008). "Thrombospondins 1 and 2 are necessary for synaptic plasticity and functional recovery after stroke." J Cereb Blood Flow Metab **28**(10): 1722-1732.

Liddelow, S. A. and B. A. Barres (2017). "Reactive Astrocytes: Production, Function, and Therapeutic Potential." Immunity **46**(6): 957-967.

Liddelow, S. A., K. A. Guttenplan, L. E. Clarke, F. C. Bennett, C. J. Bohlen, L. Schirmer, M. L. Bennett, A. E. Munch, W. S. Chung, T. C. Peterson, D. K. Wilton, A. Frouin, B. A. Napier, N. Panicker, M. Kumar, M. S. Buckwalter, D. H. Rowitch, V. L. Dawson, T. M. Dawson, B. Stevens and B. A. Barres (2017). "Neurotoxic reactive astrocytes are induced by activated microglia." Nature **541**(7638): 481-487.

Liedtke, W., W. Edelmann, F. C. Chiu, R. Kucherlapati and C. S. Raine (1998). "Experimental autoimmune encephalomyelitis in mice lacking glial fibrillary acidic protein is characterized by a more severe clinical course and an infiltrative central nervous system lesion." Am J Pathol **152**(1): 251-259.

Lien, B. V., M. H. Tuszynski and P. Lu (2019). "Astrocytes migrate from human neural stem cell grafts and functionally integrate into the injured rat spinal cord." Exp Neurol **314**: 46-57.

Lin, J. H., N. Lou, N. Kang, T. Takano, F. Hu, X. Han, Q. Xu, D. Lovatt, A. Torres, K. Willecke, J. Yang, J. Kang and M. Nedergaard (2008). "A central role of connexin 43 in hypoxic preconditioning." J Neurosci **28**(3): 681-695.

Liu, K., Y. Lu, J. K. Lee, R. Samara, R. Willenberg, I. Sears-Kraxberger, A. Tedeschi, K. K. Park, D. Jin, B. Cai, B. Xu, L. Connolly, O. Steward, B. Zheng and Z. He (2010). "PTEN deletion enhances the regenerative ability of adult corticospinal neurons." Nat Neurosci **13**(9): 1075-1081.

Liu, M., W. Wu, H. Li, S. Li, L. T. Huang, Y. Q. Yang, Q. Sun, C. X. Wang, Z. Yu and C. H. Hang (2015). "Necroptosis, a novel type of programmed cell death, contributes to early neural cells damage after spinal cord injury in adult mice." J Spinal Cord Med **38**(6): 745-753.

Liu, S., B. Sandner, T. Schackel, L. Nicholson, A. Chtarto, L. Tenenbaum, R. Puttagunta, R. Muller, N. Weidner and A. Blesch (2017). "Regulated viral BDNF delivery in combination with Schwann cells promotes axonal regeneration through capillary alginate hydrogels after spinal cord injury." Acta Biomater **60**: 167-180.

Liu, S., T. Schackel, N. Weidner and R. Puttagunta (2017). "Biomaterial-Supported Cell Transplantation Treatments for Spinal Cord Injury: Challenges and Perspectives." Front Cell Neurosci **11**: 430.

Loebel, C., R. L. Mauck and J. A. Burdick (2019). "Local nascent protein deposition and remodelling guide mesenchymal stromal cell mechanosensing and fate in three-dimensional hydrogels." Nat Mater **18**(8): 883-891.

Loy, D. N., D. S. Magnuson, Y. P. Zhang, S. M. Onifer, M. D. Mills, Q. L. Cao, J. B. Darnall, L. C. Fajardo, D. A. Burke and S. R. Whittemore (2002). "Functional redundancy of ventral spinal locomotor pathways." J Neurosci **22**(1): 315-323.

Lu, P., A. Blesch, L. Graham, Y. Wang, R. Samara, K. Banos, V. Haringer, L. Havton, N. Weishaupt, D. Bennett, K. Fouad and M. H. Tuszynski (2012). "Motor axonal regeneration after partial and complete spinal cord transection." J Neurosci **32**(24): 8208-8218.

Lu, P., L. L. Jones, E. Y. Snyder and M. H. Tuszynski (2003). "Neural stem cells constitutively secrete neurotrophic factors and promote extensive host axonal growth after spinal cord injury." Exp Neurol **181**(2): 115-129.

Lu, P., L. L. Jones and M. H. Tuszynski (2007). "Axon regeneration through scars and into sites of chronic spinal cord injury." Exp Neurol **203**(1): 8-21.

Lu, P., K. Kadoya and M. H. Tuszynski (2014). "Axonal growth and connectivity from neural stem cell grafts in models of spinal cord injury." Curr Opin Neurobiol **27**: 103-109.

Lu, P., Y. Wang, L. Graham, K. McHale, M. Gao, D. Wu, J. Brock, A. Blesch, E. S. Rosenzweig, L. A. Havton, B. Zheng, J. M. Conner, M. Marsala and M. H. Tuszynski (2012). "Long-distance growth and connectivity of neural stem cells after severe spinal cord injury." Cell **150**(6): 1264-1273.

Lu, P., G. Woodruff, Y. Wang, L. Graham, M. Hunt, D. Wu, E. Boehle, R. Ahmad, G. Poplawski, J. Brock, L. S. Goldstein and M. H. Tuszynski (2014). "Long-distance axonal growth from human induced pluripotent stem cells after spinal cord injury." Neuron **83**(4): 789-796.

Lu, P., H. Yang, L. L. Jones, M. T. Filbin and M. H. Tuszynski (2004). "Combinatorial therapy with neurotrophins and cAMP promotes axonal regeneration beyond sites of spinal cord injury." J Neurosci **24**(28): 6402-6409.

Lu, V. B., J. E. Biggs, M. J. Stebbing, S. Balasubramanyan, K. G. Todd, A. Y. Lai, W. F. Colmers, D. Dawbarn, K. Ballanyi and P. A. Smith (2009). "Brain-derived neurotrophic factor drives the changes in excitatory synaptic transmission in the rat superficial dorsal horn that follow sciatic nerve injury." J Physiol **587**(Pt 5): 1013-1032.

Luo, L. and D. D. O'Leary (2005). "Axon retraction and degeneration in development and disease." Annu Rev Neurosci **28**: 127-156.

Lutton, C., Y. W. Young, R. Williams, A. C. Meedeniya, A. Mackay-Sim and B. Goss (2012). "Combined VEGF and PDGF treatment reduces secondary degeneration after spinal cord injury." J Neurotrauma **29**(5): 957-970.

Ma, M., P. Wei, T. Wei, R. M. Ransohoff and L. B. Jakeman (2004). "Enhanced axonal growth into a spinal cord contusion injury site in a strain of mouse (129X1/SvJ) with a diminished inflammatory response." J Comp Neurol **474**(4): 469-486.

Macias, M. Y., M. B. Syring, M. A. Pizzi, M. J. Crowe, A. R. Alexanian and S. N. Kurpad (2006). "Pain with no gain: allodynia following neural stem cell transplantation in spinal cord injury." Exp Neurol **201**(2): 335-348.

Mackay-Sim, A., F. Feron, J. Cochrane, L. Bassingthwaighte, C. Bayliss, W. Davies, P. Fronek, C. Gray, G. Kerr, P. Licina, A. Nowitzke, C. Perry, P. A. Silburn, S. Urquhart and T. Geraghty (2008). "Autologous olfactory ensheathing cell transplantation in human paraplegia: a 3-year clinical trial." Brain **131**(Pt 9): 2376-2386.

Madigan, N. N., B. K. Chen, A. M. Knight, G. E. Rooney, E. Sweeney, L. Kinnavane, M. J. Yaszemski, P. Dockery, T. O'Brien, S. S. McMahon and A. J. Windebank (2014). "Comparison of cellular architecture, axonal growth, and blood vessel formation through cell-loaded polymer scaffolds in the transected rat spinal cord." Tissue Eng Part A **20**(21-22): 2985-2997.

Magnus, T., J. Carmen, J. Deleon, H. Xue, A. C. Pardo, A. C. Lepore, M. P. Mattson, M. S. Rao and N. J. Maragakis (2008). "Adult glial precursor proliferation in mutant SOD1G93A mice." Glia **56**(2): 200-208.

Martinez, F. O. and S. Gordon (2014). "The M1 and M2 paradigm of macrophage activation: time for reassessment." F1000Prime Rep **6**: 13.

Masahira, N., H. Takebayashi, K. Ono, K. Watanabe, L. Ding, M. Furusho, Y. Ogawa, Y. Nabeshima, A. Alvarez-Buylla, K. Shimizu and K. Ikenaka (2006). "Olig2-positive progenitors in the embryonic spinal cord give rise not only to motoneurons and oligodendrocytes, but also to a subset of astrocytes and ependymal cells." Dev Biol **293**(2): 358-369.

Mason, C. A., J. C. Edmondson and M. E. Hatten (1988). "The extending astroglial process: development of glial cell shape, the growing tip, and interactions with neurons." J Neurosci **8**(9): 3124-3134.

Massey, J. M., C. H. Hubscher, M. R. Wagoner, J. A. Decker, J. Amps, J. Silver and S. M. Onifer (2006). "Chondroitinase ABC digestion of the perineuronal net promotes functional collateral sprouting in the cuneate nucleus after cervical spinal cord injury." J Neurosci **26**(16): 4406-4414.

Matsushima, D., W. Heavner and L. H. Pevny (2011). "Combinatorial regulation of optic cup progenitor cell fate by SOX2 and PAX6." Development **138**(3): 443-454.

McDermott, K. W., D. S. Barry and S. S. McMahon (2005). "Role of radial glia in cytogenesis, patterning and boundary formation in the developing spinal cord." J Anat **207**(3): 241-250.

McKenna, M. C. (2007). "The glutamate-glutamine cycle is not stoichiometric: fates of glutamate in brain." J Neurosci Res **85**(15): 3347-3358.

McKerracher, L., S. David, D. L. Jackson, V. Kottis, R. J. Dunn and P. E. Braun (1994). "Identification of myelin-associated glycoprotein as a major myelin-derived inhibitor of neurite growth." Neuron **13**(4): 805-811.

McKinley, W. O., A. B. Jackson, D. D. Cardenas and M. J. DeVivo (1999). "Long-term medical complications after traumatic spinal cord injury: a regional model systems analysis." Arch Phys Med Rehabil **80**(11): 1402-1410.

McLeod, C. M. and R. L. Mauck (2016). "High fidelity visualization of cell-to-cell variation and temporal dynamics in nascent extracellular matrix formation." Sci Rep **6**: 38852.

Meeuwsen, S., C. Persoon-Deen, M. Bsibsi, R. Ravid and J. M. van Noort (2003). "Cytokine, chemokine and growth factor gene profiling of cultured human astrocytes after exposure to proinflammatory stimuli." Glia **43**(3): 243-253.

Mehta, S. T., X. Luo, K. K. Park, J. L. Bixby and V. P. Lemmon (2016). "Hyperactivated Stat3 boosts axon regeneration in the CNS." Exp Neurol **280**: 115-120.

Meirelles Lda, S., A. M. Fontes, D. T. Covas and A. I. Caplan (2009). "Mechanisms involved in the therapeutic properties of mesenchymal stem cells." Cytokine Growth Factor Rev **20**(5-6): 419-427.

Meletis, K., F. Barnabe-Heider, M. Carlen, E. Evergren, N. Tomilin, O. Shupliakov and J. Frisen (2008). "Spinal cord injury reveals multilineage differentiation of ependymal cells." PLoS Biol **6**(7): e182.

Mendonca, M. V., T. F. Larocca, B. S. de Freitas Souza, C. F. Villarreal, L. F. Silva, A. C. Matos, M. A. Novaes, C. M. Bahia, A. C. de Oliveira Melo Martinez, C. M. Kaneto, S. B. Furtado, G. P. Sampaio, M. B. Soares and R. R. dos Santos (2014). "Safety and neurological assessments after autologous transplantation of bone marrow mesenchymal stem cells in subjects with chronic spinal cord injury." Stem Cell Res Ther **5**(6): 126.

Miao, T., D. Wu, Y. Zhang, X. Bo, M. C. Subang, P. Wang and P. M. Richardson (2006). "Suppressor of cytokine signaling-3 suppresses the ability of activated signal transducer and activator of transcription-3 to stimulate neurite growth in rat primary sensory neurons." J Neurosci **26**(37): 9512-9519.

Miller, C., S. Jeftinija and S. Mallapragada (2002). "Synergistic effects of physical and chemical guidance cues on neurite alignment and outgrowth on biodegradable polymer substrates." Tissue Eng **8**(3): 367-378.

Miller, F. D. and A. S. Gauthier (2007). "Timing is everything: making neurons versus glia in the developing cortex." Neuron **54**(3): 357-369.

Mills Ko, E., J. H. Ma, F. Guo, L. Miers, E. Lee, P. Bannerman, T. Burns, D. Ko, J. Sohn, A. M. Soulika and D. Pleasure (2014). "Deletion of astroglial CXCL10 delays clinical onset but does not affect progressive axon loss in a murine autoimmune multiple sclerosis model." J Neuroinflammation **11**: 105.

Min, K. J., M. S. Yang, S. U. Kim, I. Jou and E. H. Joe (2006). "Astrocytes induce hemeoxygenase-1 expression in microglia: a feasible mechanism for preventing excessive brain inflammation." J Neurosci **26**(6): 1880-1887.

Miron, V. E., A. Boyd, J. W. Zhao, T. J. Yuen, J. M. Ruckh, J. L. Shadrach, P. van Wijngaarden, A. J. Wagers, A. Williams, R. J. M. Franklin and C. Ffrench-Constant (2013). "M2 microglia and macrophages drive oligodendrocyte differentiation during CNS remyelination." Nat Neurosci **16**(9): 1211-1218.

Mironova, Y. A. and R. J. Giger (2013). "Where no synapses go: gatekeepers of circuit remodeling and synaptic strength." Trends Neurosci **36**(6): 363-373.

Mitsui, T., I. Fischer, J. S. Shumsky and M. Murray (2005). "Transplants of fibroblasts expressing BDNF and NT-3 promote recovery of bladder and hindlimb function following spinal contusion injury in rats." Exp Neurol **194**(2): 410-431.

Moeendarbary, E., I. P. Weber, G. K. Sheridan, D. E. Koser, S. Soleman, B. Haenzi, E. J. Bradbury, J. Fawcett and K. Franze (2017). "The soft mechanical signature of glial scars in the central nervous system." Nat Commun **8**: 14787.

Molofsky, A. V. and B. Deneen (2015). "Astrocyte development: A Guide for the Perplexed." Glia **63**(8): 1320-1329.

Molofsky, A. V., K. W. Kelley, H. H. Tsai, S. A. Redmond, S. M. Chang, L. Madireddy, J. R. Chan, S. E. Baranzini, E. M. Ullian and D. H. Rowitch (2014). "Astrocyte-encoded positional cues maintain sensorimotor circuit integrity." Nature **509**(7499): 189-194.

Molofsky, A. V., R. Krencik, E. M. Ullian, H. H. Tsai, B. Deneen, W. D. Richardson, B. A. Barres and D. H. Rowitch (2012). "Astrocytes and disease: a neurodevelopmental perspective." Genes Dev **26**(9): 891-907.

Monnier, P. P., A. Sierra, J. M. Schwab, S. Henke-Fahle and B. K. Mueller (2003). "The Rho/ROCK pathway mediates neurite growth-inhibitory activity associated with the chondroitin sulfate proteoglycans of the CNS glial scar." Mol Cell Neurosci **22**(3): 319-330.

Moore, D. L., M. G. Blackmore, Y. Hu, K. H. Kaestner, J. L. Bixby, V. P. Lemmon and J. L. Goldberg (2009). "KLF family members regulate intrinsic axon regeneration ability." Science **326**(5950): 298-301.

Moore, M. J., J. A. Friedman, E. B. Lewellyn, S. M. Mantila, A. J. Krych, S. Ameenuddin, A. M. Knight, L. Lu, B. L. Currier, R. J. Spinner, R. W. Marsh, A. J. Windebank and M. J. Yaszemski (2006). "Multiple-channel scaffolds to promote spinal cord axon regeneration." Biomaterials **27**(3): 419-429.

Morawietz, C. and F. Moffat (2013). "Effects of locomotor training after incomplete spinal cord injury: a systematic review." Arch Phys Med Rehabil **94**(11): 2297-2308.

Moreau-Fauvarque, C., A. Kumanogoh, E. Camand, C. Jaillard, G. Barbin, I. Boquet, C. Love, E. Y. Jones, H. Kikutani, C. Lubetzki, I. Dusart and A. Chedotal (2003). "The transmembrane semaphorin Sema4D/CD100, an inhibitor of axonal growth, is expressed on oligodendrocytes and upregulated after CNS lesion." J Neurosci **23**(27): 9229-9239.

Morel, L., M. S. R. Chiang, H. Higashimori, T. Shoneye, L. K. Iyer, J. Yelick, A. Tai and Y. Yang (2017). "Molecular and Functional Properties of Regional Astrocytes in the Adult Brain." J Neurosci **37**(36): 8706-8717.

Morel, L., Y. Men, M. S. R. Chiang, Y. Tian, S. Jin, J. Yelick, H. Higashimori and Y. Yang (2019). "Intracortical astrocyte subpopulations defined by astrocyte reporter Mice in the adult brain." Glia **67**(1): 171-181.

Morshead, C. M., A. D. Garcia, M. V. Sofroniew and D. van Der Kooy (2003). "The ablation of glial fibrillary acidic protein-positive cells from the adult central nervous system results in the loss of forebrain neural stem cells but not retinal stem cells." Eur J Neurosci **18**(1): 76-84.

Moshayedi, P., G. Ng, J. C. Kwok, G. S. Yeo, C. E. Bryant, J. W. Fawcett, K. Franze and J. Guck (2014). "The relationship between glial cell mechanosensitivity and foreign body reactions in the central nervous system." Biomaterials **35**(13): 3919-3925.

Mothe, A. J., R. Y. Tam, T. Zahir, C. H. Tator and M. S. Shoichet (2013). "Repair of the injured spinal cord by transplantation of neural stem cells in a hyaluronan-based hydrogel." Biomaterials **34**(15): 3775-3783.

Muroyama, Y., Y. Fujiwara, S. H. Orkin and D. H. Rowitch (2005). "Specification of astrocytes by bHLH protein SCL in a restricted region of the neural tube." Nature **438**(7066): 360-363.

Myers, S. A., A. N. Bankston, D. A. Burke, S. S. Ohri and S. R. Whittemore (2016). "Does the preclinical evidence for functional remyelination following myelinating cell engraftment into the injured spinal cord support progression to clinical trials?" Exp Neurol **283**(Pt B): 560-572.

Nagoshi, N. and H. Okano (2018). "iPSC-derived neural precursor cells: potential for cell transplantation therapy in spinal cord injury." Cell Mol Life Sci **75**(6): 989-1000.

Nakamura, M., R. A. Houghtling, L. MacArthur, B. M. Bayer and B. S. Bregman (2003). "Differences in cytokine gene expression profile between acute and secondary injury in adult rat spinal cord." Exp Neurol **184**(1): 313-325.

Namihira, M., J. Kohyama, K. Semi, T. Sanosaka, B. Deneen, T. Taga and K. Nakashima (2009). "Committed neuronal precursors confer astrocytic potential on residual neural precursor cells." Dev Cell **16**(2): 245-255.

Nandoe Tewarie, R. S., A. Hurtado, R. H. Bartels, A. Grotenhuis and M. Oudega (2009). "Stem cell-based therapies for spinal cord injury." J Spinal Cord Med **32**(2): 105-114.

Neary, J. T. and H. Zimmermann (2009). "Trophic functions of nucleotides in the central nervous system." Trends Neurosci **32**(4): 189-198.

Neumann, S., F. Bradke, M. Tessier-Lavigne and A. I. Basbaum (2002). "Regeneration of sensory axons within the injured spinal cord induced by intraganglionic cAMP elevation." Neuron **34**(6): 885-893.

Ng, M. T., A. T. Stammers and B. K. Kwon (2011). "Vascular disruption and the role of angiogenic proteins after spinal cord injury." Transl Stroke Res **2**(4): 474-491.

Ning, L., Y. Xu, X. Chen and D. J. Schreyer (2016). "Influence of mechanical properties of alginate-based substrates on the performance of Schwann cells in culture." J Biomater Sci Polym Ed **27**(9): 898-915.

Nisbet, D. R., S. Pattanawong, N. E. Ritchie, W. Shen, D. I. Finkelstein, M. K. Horne and J. S. Forsythe (2007). "Interaction of embryonic cortical neurons on nanofibrous scaffolds for neural tissue engineering." J Neural Eng **4**(2): 35-41.

Nisbet, D. R., A. E. Rodda, M. K. Horne, J. S. Forsythe and D. I. Finkelstein (2010). "Implantation of functionalized thermally gelling xyloglucan hydrogel within the brain: associated neurite infiltration and inflammatory response." Tissue Eng Part A **16**(9): 2833-2842.

Noble, L. J., F. Donovan, T. Igarashi, S. Goussev and Z. Werb (2002). "Matrix metalloproteinases limit functional recovery after spinal cord injury by modulation of early vascular events." J Neurosci **22**(17): 7526-7535.

Noble, M., J. E. Davies, M. Mayer-Proschel, C. Proschel and S. J. Davies (2011). "Precursor cell biology and the development of astrocyte transplantation therapies: lessons from spinal cord injury." Neurotherapeutics **8**(4): 677-693.

Nogradi, A., A. Szabo, S. Pinter and G. Vrbova (2007). "Delayed riluzole treatment is able to rescue injured rat spinal motoneurons." Neuroscience **144**(2): 431-438.

Nomura, H., B. Baladie, Y. Katayama, C. M. Morshead, M. S. Shoichet and C. H. Tator (2008). "Delayed implantation of intramedullary chitosan channels containing nerve grafts promotes extensive axonal regeneration after spinal cord injury." Neurosurgery **63**(1): 127-141; discussion 141-123.

Nomura, H., H. Kim, A. Mothe, T. Zahir, I. Kulbatski, C. M. Morshead, M. S. Shoichet and C. H. Tator (2010). "Endogenous radial glial cells support regenerating axons after spinal cord transection." Neuroreport **21**(13): 871-876.

Nomura, H., T. Zahir, H. Kim, Y. Katayama, I. Kulbatski, C. M. Morshead, M. S. Shoichet and C. H. Tator (2008). "Extramedullary chitosan channels promote survival of transplanted neural stem and progenitor cells and create a tissue bridge after complete spinal cord transection." Tissue Eng Part A **14**(5): 649-665.

Norden, D. M., A. M. Fenn, A. Dugan and J. P. Godbout (2014). "TGFbeta produced by IL-10 redirected astrocytes attenuates microglial activation." Glia **62**(6): 881-895.

Norenberg, M. D., J. Smith and A. Marcillo (2004). "The pathology of human spinal cord injury: defining the problems." J Neurotrauma **21**(4): 429-440.

Nori, S., M. Khazaei, C. S. Ahuja, K. Yokota, J. E. Ahlfors, Y. Liu, J. Wang, S. Shibata, J. Chio, M. H. Hettiaratchi, T. Fuhrmann, M. S. Shoichet and M. G. Fehlings (2018). "Human Oligodendrogenic Neural Progenitor Cells Delivered with Chondroitinase ABC Facilitate Functional Repair of Chronic Spinal Cord Injury." Stem Cell Reports **11**(6): 1433-1448.

Nori, S., Y. Okada, A. Yasuda, O. Tsuji, Y. Takahashi, Y. Kobayashi, K. Fujiyoshi, M. Koike, Y. Uchiyama, E. Ikeda, Y. Toyama, S. Yamanaka, M. Nakamura and H. Okano (2011). "Grafted human-induced pluripotent stem-cell-derived neurospheres promote motor functional recovery after spinal cord injury in mice." Proc Natl Acad Sci U S A **108**(40): 16825-16830.

Novikova, L. N., A. Mosahebi, M. Wiberg, G. Terenghi, J. O. Kellerth and L. N. Novikov (2006). "Alginate hydrogel and matrigel as potential cell carriers for neurotransplantation." J Biomed Mater Res A **77**(2): 242-252.

Novikova, L. N., J. Pettersson, M. Brohlin, M. Wiberg and L. N. Novikov (2008). "Biodegradable poly-beta-hydroxybutyrate scaffold seeded with Schwann cells to promote spinal cord repair." Biomaterials **29**(9): 1198-1206.

Nucera, S., D. Biziato and M. De Palma (2011). "The interplay between macrophages and angiogenesis in development, tissue injury and regeneration." Int J Dev Biol **55**(4-5): 495-503.

O'Shea, T. M., J. E. Burda and M. V. Sofroniew (2017). "Cell biology of spinal cord injury and repair." J Clin Invest **127**(9): 3259-3270.

O'Toole, D. A., A. K. West and M. I. Chuah (2007). "Effect of olfactory ensheathing cells on reactive astrocytes in vitro." Cell Mol Life Sci **64**(10): 1303-1309.

Obara, M., M. Szeliga and J. Albrecht (2008). "Regulation of pH in the mammalian central nervous system under normal and pathological conditions: facts and hypotheses." Neurochem Int **52**(6): 905-919.

Oblinger, M. M. and R. J. Lasek (1984). "A conditioning lesion of the peripheral axons of dorsal root ganglion cells accelerates regeneration of only their peripheral axons." J Neurosci **4**(7): 1736-1744.

Oh, J., K. I. Lee, H. T. Kim, Y. You, D. H. Yoon, K. Y. Song, E. Cheong, Y. Ha and D. Y. Hwang (2015). "Human-induced pluripotent stem cells generated from intervertebral disc cells improve neurologic functions in spinal cord injury." Stem Cell Res Ther **6**: 125.

Ohta, M., Y. Suzuki, T. Noda, Y. Ejiri, M. Dezawa, K. Kataoka, H. Chou, N. Ishikawa, N. Matsumoto, Y. Iwashita, E. Mizuta, S. Kuno and C. Ide (2004). "Bone marrow stromal cells infused into the cerebrospinal fluid promote functional recovery of the injured rat spinal cord with reduced cavity formation." Exp Neurol **187**(2): 266-278.

Okada, S. (2016). "The pathophysiological role of acute inflammation after spinal cord injury." Inflamm Regen **36**: 20.

Okada, S., M. Nakamura, H. Katoh, T. Miyao, T. Shimazaki, K. Ishii, J. Yamane, A. Yoshimura, Y. Iwamoto, Y. Toyama and H. Okano (2006). "Conditional ablation of Stat3 or Socs3 discloses a dual role for reactive astrocytes after spinal cord injury." Nat Med **12**(7): 829-834.

Okano, H., M. Nakamura, K. Yoshida, Y. Okada, O. Tsuji, S. Nori, E. Ikeda, S. Yamanaka and K. Miura (2013). "Steps toward safe cell therapy using induced pluripotent stem cells." Circ Res **112**(3): 523-533.

Okubo, T., A. Iwanami, J. Kohyama, G. Itakura, S. Kawabata, Y. Nishiyama, K. Sugai, M. Ozaki, T. Iida, K. Matsubayashi, M. Matsumoto, M. Nakamura and H. Okano (2016). "Pretreatment with a gamma-Secretase Inhibitor Prevents Tumor-like Overgrowth in Human iPSC-Derived Transplants for Spinal Cord Injury." Stem Cell Reports **7**(4): 649-663.

Okubo, T., N. Nagoshi, J. Kohyama, O. Tsuji, M. Shinozaki, S. Shibata, Y. Kase, M. Matsumoto, M. Nakamura and H. Okano (2018). "Treatment with a Gamma-Secretase Inhibitor Promotes Functional Recovery in Human iPSC- Derived Transplants for Chronic Spinal Cord Injury." Stem Cell Reports **11**(6): 1416-1432.

Okuda, A., N. Horii-Hayashi, T. Sasagawa, T. Shimizu, H. Shigematsu, E. Iwata, Y. Morimoto, K. Masuda, M. Koizumi, M. Akahane, M. Nishi and Y. Tanaka (2017). "Bone marrow stromal cell sheets may promote axonal regeneration and functional recovery with suppression of glial scar formation after spinal cord transection injury in rats." J Neurosurg Spine **26**(3): 388-395.

Olby, N. J. and W. F. Blakemore (1996). "Reconstruction of the glial environment of a photochemically induced lesion in the rat spinal cord by transplantation of mixed glial cells." J Neurocytol **25**(8): 481-498.

Olsen, M. L., S. L. Campbell and H. Sontheimer (2007). "Differential distribution of Kir4.1 in spinal cord astrocytes suggests regional differences in K+ homeostasis." J Neurophysiol **98**(2): 786-793.

Olson, H. E., G. E. Rooney, L. Gross, J. J. Nesbitt, K. E. Galvin, A. Knight, B. Chen, M. J. Yaszemski and A. J. Windebank (2009). "Neural stem cell- and Schwann cell-loaded biodegradable polymer scaffolds support axonal regeneration in the transected spinal cord." Tissue Eng Part A **15**(7): 1797-1805.

Onifer, S. M., G. M. Smith and K. Fouad (2011). "Plasticity after spinal cord injury: relevance to recovery and approaches to facilitate it." Neurotherapeutics **8**(2): 283-293.

Orellana, J. A., T. D. Montero and R. von Bernhardi (2013). "Astrocytes inhibit nitric oxide-dependent Ca(2+) dynamics in activated microglia: involvement of ATP released via pannexin 1 channels." Glia **61**(12): 2023-2037.

Orive, G., S. Ponce, R. M. Hernandez, A. R. Gascon, M. Igartua and J. L. Pedraz (2002). "Biocompatibility of microcapsules for cell immobilization elaborated with different type of alginates." Biomaterials **23**(18): 3825-3831.

Orre, M., W. Kamphuis, L. M. Osborn, J. Melief, L. Kooijman, I. Huitinga, J. Klooster, K. Bossers and E. M. Hol (2014). "Acute isolation and transcriptome characterization of cortical astrocytes and microglia from young and aged mice." Neurobiol Aging **35**(1): 1-14.

Oudega, M., P. Hao, J. Shang, A. E. Haggerty, Z. Wang, J. Sun, D. J. Liebl, Y. Shi, L. Cheng, H. Duan, Y. E. Sun, X. Li and V. P. Lemmon (2019). "Validation study of neurotrophin-3-releasing chitosan facilitation of neural tissue generation in the severely injured adult rat spinal cord." Exp Neurol **312**: 51-62.

Pakulska, M. M., I. Elliott Donaghue, J. M. Obermeyer, A. Tuladhar, C. K. McLaughlin, T. N. Shendruk and M. S. Shoichet (2016). "Encapsulation-free controlled release: Electrostatic adsorption eliminates the need for protein encapsulation in PLGA nanoparticles." Sci Adv **2**(5): e1600519.

Pakulska, M. M., K. Vulic and M. S. Shoichet (2013). "Affinity-based release of chondroitinase ABC from a modified methylcellulose hydrogel." J Control Release **171**(1): 11-16.

Palmisano, I., M. C. Danzi, T. H. Hutson, L. Zhou, E. McLachlan, E. Serger, K. Shkura, P. K. Srivastava, A. Hervera, N. O. Neill, T. Liu, H. Dhrif, Z. Wang, M. Kubat, S. Wuchty, M. Merkenschlager, L. Levi, E. Elliott, J. L. Bixby, V. P. Lemmon and S. Di Giovanni (2019). "Epigenomic signatures underpin the axonal regenerative ability of dorsal root ganglia sensory neurons." Nat Neurosci **22**(11): 1913-1924.

Papadopoulos, M. C. and A. S. Verkman (2013). "Aquaporin water channels in the nervous system." Nat Rev Neurosci **14**(4): 265-277.

Park, E., A. A. Velumian and M. G. Fehlings (2004). "The role of excitotoxicity in secondary mechanisms of spinal cord injury: a review with an emphasis on the implications for white matter degeneration." J Neurotrauma **21**(6): 754-774.

Park, K. K., K. Liu, Y. Hu, P. D. Smith, C. Wang, B. Cai, B. Xu, L. Connolly, I. Kramvis, M. Sahin and Z. He (2008). "Promoting axon regeneration in the adult CNS by modulation of the PTEN/mTOR pathway." Science **322**(5903): 963-966.

Park, S. S., Y. J. Lee, S. H. Lee, D. Lee, K. Choi, W. H. Kim, O. K. Kweon and H. J. Han (2012). "Functional recovery after spinal cord injury in dogs treated with a combination of Matrigel and neural-induced adipose-derived mesenchymal Stem cells." Cytotherapy **14**(5): 584-597.

Pasterkamp, R. J., R. J. Giger, M. J. Ruitenberg, A. J. Holtmaat, J. De Wit, F. De Winter and J. Verhaagen (1999). "Expression of the gene encoding the chemorepellent semaphorin III is induced in the fibroblast component of neural scar tissue formed following injuries of adult but not neonatal CNS." Mol Cell Neurosci **13**(2): 143-166.

Pastrana, E., M. T. Moreno-Flores, E. N. Gurzov, J. Avila, F. Wandosell and J. Diaz-Nido (2006). "Genes associated with adult axon regeneration promoted by olfactory ensheathing cells: a new role for matrix metalloproteinase 2." J Neurosci **26**(20): 5347-5359.

Patel, V., G. Joseph, A. Patel, S. Patel, D. Bustin, D. Mawson, L. M. Tuesta, R. Puentes, M. Ghosh and D. D. Pearse (2010). "Suspension matrices for improved Schwann-cell survival after implantation into the injured rat spinal cord." J Neurotrauma **27**(5): 789-801.

Patist, C. M., M. B. Mulder, S. E. Gautier, V. Maquet, R. Jerome and M. Oudega (2004). "Freeze-dried poly(D,L-lactic acid) macroporous guidance scaffolds impregnated with brain-derived neurotrophic factor in the transected adult rat thoracic spinal cord." Biomaterials **25**(9): 1569-1582.

Pawar, K., B. J. Cummings, A. Thomas, L. D. Shea, A. Levine, S. Pfaff and A. J. Anderson (2015). "Biomaterial bridges enable regeneration and re-entry of corticospinal tract axons into the caudal spinal cord after SCI: Association with recovery of forelimb function." Biomaterials **65**: 1-12.

Pawar, K., R. Mueller, M. Caioni, P. Prang, U. Bogdahn, W. Kunz and N. Weidner (2011). "Increasing capillary diameter and the incorporation of gelatin enhance axon outgrowth in alginate-based anisotropic hydrogels." Acta Biomater **7**(7): 2826-2834.

Pawar, K., P. Prang, R. Muller, M. Caioni, U. Bogdahn, W. Kunz and N. Weidner (2015). "Intrinsic and extrinsic determinants of central nervous system axon outgrowth into alginate-based anisotropic hydrogels." Acta Biomater **27**: 131-139.

Pearse, D. D., A. R. Sanchez, F. C. Pereira, C. M. Andrade, R. Puzis, Y. Pressman, K. Golden, B. M. Kitay, B. Blits, P. M. Wood and M. B. Bunge (2007). "Transplantation of Schwann cells and/or olfactory ensheathing glia into the contused spinal cord: Survival, migration, axon association, and functional recovery." Glia **55**(9): 976-1000.

Pekny, M., U. Wilhelmsson, T. Tatlisumak and M. Pekna (2019). "Astrocyte activation and reactive gliosis-A new target in stroke?" Neurosci Lett **689**: 45-55.

Pencalet, P., C. Serguera, O. Corti, A. Privat, J. Mallet and M. Gimenez y Ribotta (2006). "Integration of genetically modified adult astrocytes into the lesioned rat spinal cord." J Neurosci Res **83**(1): 61-67.

Petit, A., P. Pierret, A. Vallee and G. Doucet (2001). "Astrocytes from cerebral cortex or striatum attract adult host serotoninergic axons into intrastriatal ventral mesencephalic co-grafts." J Neurosci **21**(18): 7182-7193.

Pfeifer, K., M. Vroemen, A. Blesch and N. Weidner (2004). "Adult neural progenitor cells provide a permissive guiding substrate for corticospinal axon growth following spinal cord injury." Eur J Neurosci **20**(7): 1695-1704.

Pfrieger, F. W. and B. A. Barres (1997). "Synaptic efficacy enhanced by glial cells in vitro." Science **277**(5332): 1684-1687.

Piantino, J., J. A. Burdick, D. Goldberg, R. Langer and L. I. Benowitz (2006). "An injectable, biodegradable hydrogel for trophic factor delivery enhances axonal rewiring and improves performance after spinal cord injury." Exp Neurol **201**(2): 359-367.

Pickett, G. E., M. Campos-Benitez, J. L. Keller and N. Duggal (2006). "Epidemiology of traumatic spinal cord injury in Canada." Spine (Phila Pa 1976) **31**(7): 799-805.

Piltti, K. M., D. L. Salazar, N. Uchida, B. J. Cummings and A. J. Anderson (2013). "Safety of epicenter versus intact parenchyma as a transplantation site for human neural stem cells for spinal cord injury therapy." Stem Cells Transl Med **2**(3): 204-216.

Plant, G. W., M. L. Bates and M. B. Bunge (2001). "Inhibitory proteoglycan immunoreactivity is higher at the caudal than the rostral Schwann cell graft-transected spinal cord interface." Mol Cell Neurosci **17**(3): 471-487.

Plemel, J. R., A. Chojnacki, J. S. Sparling, J. Liu, W. Plunet, G. J. Duncan, S. E. Park, S. Weiss and W. Tetzlaff (2011). "Platelet-derived growth factor-responsive neural precursors give rise to myelinating oligodendrocytes after transplantation into the spinal cords of contused rats and dysmyelinated mice." Glia **59**(12): 1891-1910.

Plunet, W., B. K. Kwon and W. Tetzlaff (2002). "Promoting axonal regeneration in the central nervous system by enhancing the cell body response to axotomy." J Neurosci Res **68**(1): 1-6.

Pomeshchik, Y., K. A. Puttonen, I. Kidin, M. Ruponen, S. Lehtonen, T. Malm, E. Akesson, O. Hovatta and J. Koistinaho (2015). "Transplanted Human Induced Pluripotent Stem Cell-Derived Neural

Progenitor Cells Do Not Promote Functional Recovery of Pharmacologically Immunosuppressed Mice With Contusion Spinal Cord Injury." Cell Transplant **24**(9): 1799-1812.

Poplawski, G. H. D., R. Kawaguchi, E. Van Niekerk, P. Lu, N. Mehta, P. Canete, R. Lie, I. Dragatsis, J. M. Meves, B. Zheng, G. Coppola and M. H. Tuszynski (2020). "Injured adult neurons regress to an embryonic transcriptional growth state." Nature **581**(7806): 77-82.

Powers, B. E., J. Lasiene, J. R. Plemel, L. Shupe, S. I. Perlmutter, W. Tetzlaff and P. J. Horner (2012). "Axonal thinning and extensive remyelination without chronic demyelination in spinal injured rats." J Neurosci **32**(15): 5120-5125.

Prabhakar, V., R. Raman, I. Capila, C. J. Bosques, K. Pojasek and R. Sasisekharan (2005). "Biochemical characterization of the chondroitinase ABC I active site." Biochem J **390**(Pt 2): 395-405.

Prang, P., R. Muller, A. Eljaouhari, K. Heckmann, W. Kunz, T. Weber, C. Faber, M. Vroemen, U. Bogdahn and N. Weidner (2006). "The promotion of oriented axonal regrowth in the injured spinal cord by alginate-based anisotropic capillary hydrogels." Biomaterials **27**(19): 3560-3569.

Priest, C. A., N. C. Manley, J. Denham, E. D. Wirth, 3rd and J. S. Lebkowski (2015). "Preclinical safety of human embryonic stem cell-derived oligodendrocyte progenitors supporting clinical trials in spinal cord injury." Regen Med **10**(8): 939-958.

Pritchard, C. D., J. R. Slotkin, D. Yu, H. Dai, M. S. Lawrence, R. T. Bronson, F. M. Reynolds, Y. D. Teng, E. J. Woodard and R. S. Langer (2010). "Establishing a model spinal cord injury in the African green monkey for the preclinical evaluation of biodegradable polymer scaffolds seeded with human neural stem cells." J Neurosci Methods **188**(2): 258-269.

Proschel, C., J. L. Stripay, C. H. Shih, J. C. Munger and M. D. Noble (2014). "Delayed transplantation of precursor cell-derived astrocytes provides multiple benefits in a rat model of Parkinsons." EMBO Mol Med **6**(4): 504-518.

Puttagunta, R., A. Tedeschi, M. G. Soria, A. Hervera, R. Lindner, K. I. Rathore, P. Gaub, Y. Joshi, T. Nguyen, A. Schmandke, C. J. Laskowski, A. L. Boutillier, F. Bradke and S. Di Giovanni (2014). "PCAF-dependent epigenetic changes promote axonal regeneration in the central nervous system." Nat Commun **5**: 3527.

Queen, D., H. Orsted, H. Sanada and G. Sussman (2004). "A dressing history." Int Wound J **1**(1): 59-77.

Radtke, C., Y. Akiyama, J. Brokaw, K. L. Lankford, K. Wewetzer, W. L. Fodor and J. D. Kocsis (2004). "Remyelination of the nonhuman primate spinal cord by transplantation of H-transferase transgenic adult pig olfactory ensheathing cells." FASEB J **18**(2): 335-337.

Raff, M. C., E. R. Abney, J. Cohen, R. Lindsay and M. Noble (1983). "Two types of astrocytes in cultures of developing rat white matter: differences in morphology, surface gangliosides, and growth characteristics." J Neurosci **3**(6): 1289-1300.

Raivich, G., M. Bohatschek, C. Da Costa, O. Iwata, M. Galiano, M. Hristova, A. S. Nateri, M. Makwana, L. Riera-Sans, D. P. Wolfer, H. P. Lipp, A. Aguzzi, E. F. Wagner and A. Behrens (2004). "The AP-1 transcription factor c-Jun is required for efficient axonal regeneration." Neuron **43**(1): 57-67.

Ramon-Cueto, A., M. I. Cordero, F. F. Santos-Benito and J. Avila (2000). "Functional recovery of paraplegic rats and motor axon regeneration in their spinal cords by olfactory ensheathing glia." Neuron **25**(2): 425-435.

Rao, J. S., C. Zhao, A. Zhang, H. Duan, P. Hao, R. H. Wei, J. Shang, W. Zhao, Z. Liu, J. Yu, K. S. Fan, Z. Tian, Q. He, W. Song, Z. Yang, Y. E. Sun and X. Li (2018). "NT3-chitosan enables de novo regeneration and functional recovery in monkeys after spinal cord injury." Proc Natl Acad Sci U S A **115**(24): E5595-E5604.

Raper, J. and C. Mason (2010). "Cellular strategies of axonal pathfinding." Cold Spring Harb Perspect Biol **2**(9): a001933.

Rauch, M. F., S. R. Hynes, J. Bertram, A. Redmond, R. Robinson, C. Williams, H. Xu, J. A. Madri and E. B. Lavik (2009). "Engineering angiogenesis following spinal cord injury: a coculture of neural progenitor and endothelial cells in a degradable polymer implant leads to an increase in vessel density and formation of the blood-spinal cord barrier." Eur J Neurosci **29**(1): 132-145.

Reichenbach, A., A. Derouiche and F. Kirchhoff (2010). "Morphology and dynamics of perisynaptic glia." Brain Res Rev **63**(1-2): 11-25.

Reier, P. J., B. S. Bregman and J. R. Wujek (1986). "Intraspinal transplantation of embryonic spinal cord tissue in neonatal and adult rats." J Comp Neurol **247**(3): 275-296.

Ren, J., P. Jin, M. Sabatino, A. Balakumaran, J. Feng, S. A. Kuznetsov, H. G. Klein, P. G. Robey and D. F. Stroncek (2011). "Global transcriptome analysis of human bone marrow stromal cells (BMSC) reveals proliferative, mobile and interactive cells that produce abundant extracellular matrix proteins, some of which may affect BMSC potency." Cytotherapy **13**(6): 661-674.

Retamal, M. A., N. Froger, N. Palacios-Prado, P. Ezan, P. J. Saez, J. C. Saez and C. Giaume (2007). "Cx43 hemichannels and gap junction channels in astrocytes are regulated oppositely by proinflammatory cytokines released from activated microglia." J Neurosci **27**(50): 13781-13792.

Richardson, P. M., U. M. McGuinness and A. J. Aguayo (1980). "Axons from CNS neurons regenerate into PNS grafts." Nature **284**(5753): 264-265.

Rigby, M. J., T. M. Gomez and L. Puglielli (2020). "Glial Cell-Axonal Growth Cone Interactions in Neurodevelopment and Regeneration." Front Neurosci **14**: 203.

Ritfeld, G. J., R. D. Nandoe Tewarie, K. Vajn, S. T. Rahiem, A. Hurtado, D. F. Wendell, R. A. Roos and M. Oudega (2012). "Bone marrow stromal cell-mediated tissue sparing enhances functional repair after spinal cord contusion in adult rats." Cell Transplant **21**(7): 1561-1575.

Ritfeld, G. J., A. Patel, A. Chou, T. L. Novosat, D. G. Castillo, R. A. Roos and M. Oudega (2015). "The role of brain-derived neurotrophic factor in bone marrow stromal cell-mediated spinal cord repair." Cell Transplant **24**(11): 2209-2220.

Roberts, T. T., G. R. Leonard and D. J. Cepela (2017). "Classifications In Brief: American Spinal Injury Association (ASIA) Impairment Scale." Clin Orthop Relat Res **475**(5): 1499-1504.

Rodriguez, J. J., C. Y. Yeh, S. Terzieva, M. Olabarria, M. Kulijewicz-Nawrot and A. Verkhratsky (2014). "Complex and region-specific changes in astroglial markers in the aging brain." Neurobiol Aging **35**(1): 15-23.

Romanyuk, N., T. Amemori, K. Turnovcova, P. Prochazka, B. Onteniente, E. Sykova and P. Jendelova (2015). "Beneficial Effect of Human Induced Pluripotent Stem Cell-Derived Neural Precursors in Spinal Cord Injury Repair." Cell Transplant **24**(9): 1781-1797.

Romero-Ramirez, L., S. Wu, J. de Munter, E. C. Wolters, B. W. Kramer and J. Mey (2020). "Treatment of rats with spinal cord injury using human bone marrow-derived stromal cells prepared by negative selection." J Biomed Sci **27**(1): 35.

Rosenzweig, E. S., G. Courtine, D. L. Jindrich, J. H. Brock, A. R. Ferguson, S. C. Strand, Y. S. Nout, R. R. Roy, D. M. Miller, M. S. Beattie, L. A. Havton, J. C. Bresnahan, V. R. Edgerton and M. H. Tuszynski (2010). "Extensive spontaneous plasticity of corticospinal projections after primate spinal cord injury." Nat Neurosci **13**(12): 1505-1510.

Rosenzweig, E. S., E. A. Salegio, J. J. Liang, J. L. Weber, C. A. Weinholtz, J. H. Brock, R. Moseanko, S. Hawbecker, R. Pender, C. L. Cruzen, J. F. Iaci, A. O. Caggiano, A. R. Blight, B. Haenzi, J. R. Huie, L. A. Havton, Y. S. Nout-Lomas, J. W. Fawcett, A. R. Ferguson, M. S. Beattie, J. C. Bresnahan and M. H. Tuszynski (2019). "Chondroitinase improves anatomical and functional outcomes after primate spinal cord injury." Nat Neurosci **22**(8): 1269-1275.

Rowitch, D. H. and A. R. Kriegstein (2010). "Developmental genetics of vertebrate glial-cell specification." Nature **468**(7321): 214-222.

Rowland, J. W., G. W. Hawryluk, B. Kwon and M. G. Fehlings (2008). "Current status of acute spinal cord injury pathophysiology and emerging therapies: promise on the horizon." Neurosurg Focus **25**(5): E2.

Ruitenberg, M. J., G. W. Plant, F. P. Hamers, J. Wortel, B. Blits, P. A. Dijkhuizen, W. H. Gispen, G. J. Boer and J. Verhaagen (2003). "Ex vivo adenoviral vector-mediated neurotrophin gene transfer to olfactory ensheathing glia: effects on rubrospinal tract regeneration, lesion size, and functional recovery after implantation in the injured rat spinal cord." J Neurosci **23**(18): 7045-7058.

Rupp, R. (2014). "Challenges in clinical applications of brain computer interfaces in individuals with spinal cord injury." Front Neuroeng **7**: 38.

Ruschel, J. and F. Bradke (2018). "Systemic administration of epothilone D improves functional recovery of walking after rat spinal cord contusion injury." Exp Neurol **306**: 243-249.

Ruschel, J., F. Hellal, K. C. Flynn, S. Dupraz, D. A. Elliott, A. Tedeschi, M. Bates, C. Sliwinski, G. Brook, K. Dobrindt, M. Peitz, O. Brustle, M. D. Norenberg, A. Blesch, N. Weidner, M. B. Bunge, J. L. Bixby and F. Bradke (2015). "Axonal regeneration. Systemic administration of epothilone B promotes axon regeneration after spinal cord injury." Science **348**(6232): 347-352.

Ruzicka, J., L. Machova-Urdzikova, J. Gillick, T. Amemori, N. Romanyuk, K. Karova, K. Zaviskova, J. Dubisova, S. Kubinova, R. Murali, E. Sykova, M. Jhanwar-Uniyal and P. Jendelova (2017). "A Comparative Study of Three Different Types of Stem Cells for Treatment of Rat Spinal Cord Injury." Cell Transplant **26**(4): 585-603.

Ruzicka, J., N. Romanyuk, A. Hejcl, M. Vetrik, M. Hruby, G. Cocks, J. Cihlar, M. Pradny, J. Price, E. Sykova and P. Jendelova (2013). "Treating spinal cord injury in rats with a combination of human fetal neural stem cells and hydrogels modified with serotonin." Acta Neurobiol Exp (Wars) **73**(1): 102-115.

Saha, R. N., X. Liu and K. Pahan (2006). "Up-regulation of BDNF in astrocytes by TNF-alpha: a case for the neuroprotective role of cytokine." J Neuroimmune Pharmacol **1**(3): 212-222.

Saijilafu, E. M. Hur, C. M. Liu, Z. Jiao, W. L. Xu and F. Q. Zhou (2013). "PI3K-GSK3 signalling regulates mammalian axon regeneration by inducing the expression of Smad1." Nat Commun **4**: 2690.

Salewski, R. P., R. A. Mitchell, L. Li, C. Shen, M. Milekovskaia, A. Nagy and M. G. Fehlings (2015). "Transplantation of Induced Pluripotent Stem Cell-Derived Neural Stem Cells Mediate Functional Recovery Following Thoracic Spinal Cord Injury Through Remyelination of Axons." Stem Cells Transl Med **4**(7): 743-754.

Sancho-Tello, M., S. Valles, C. Montoliu, J. Renau-Piqueras and C. Guerri (1995). "Developmental pattern of GFAP and vimentin gene expression in rat brain and in radial glial cultures." Glia **15**(2): 157-166.

Sandner, B., M. Ciatipis, M. Motsch, I. Soljanik, N. Weidner and A. Blesch (2016). "Limited Functional Effects of Subacute Syngeneic Bone Marrow Stromal Cell Transplantation After Rat Spinal Cord Contusion Injury." Cell Transplant **25**(1): 125-139.

Sandner, B., R. Puttagunta, M. Motsch, F. Bradke, J. Ruschel, A. Blesch and N. Weidner (2018). "Systemic epothilone D improves hindlimb function after spinal cord contusion injury in rats." Exp Neurol **306**: 250-259.

Santhosh, K. T., A. Alizadeh and S. Karimi-Abdolrezaee (2017). "Design and optimization of PLGA microparticles for controlled and local delivery of Neuregulin-1 in traumatic spinal cord injury." J Control Release **261**: 147-162.

Sarafian, T. A., C. Montes, T. Imura, J. Qi, G. Coppola, D. H. Geschwind and M. V. Sofroniew (2010). "Disruption of astrocyte STAT3 signaling decreases mitochondrial function and increases oxidative stress in vitro." PLoS One **5**(3): e9532.

Sasaki, M., B. C. Hains, K. L. Lankford, S. G. Waxman and J. D. Kocsis (2006). "Protection of corticospinal tract neurons after dorsal spinal cord transection and engraftment of olfactory ensheathing cells." Glia **53**(4): 352-359.

Sasaki, M., C. Radtke, A. M. Tan, P. Zhao, H. Hamada, K. Houkin, O. Honmou and J. D. Kocsis (2009). "BDNF-hypersecreting human mesenchymal stem cells promote functional recovery, axonal sprouting, and protection of corticospinal neurons after spinal cord injury." J Neurosci **29**(47): 14932-14941.

Satti, H. S., A. Waheed, P. Ahmed, K. Ahmed, Z. Akram, T. Aziz, T. M. Satti, N. Shahbaz, M. A. Khan and S. A. Malik (2016). "Autologous mesenchymal stromal cell transplantation for spinal cord injury: A Phase I pilot study." Cytotherapy **18**(4): 518-522.

Schackel, T., P. Kumar, M. Gunther, S. Liu, M. Brunner, B. Sandner, R. Puttagunta, R. Muller, N. Weidner and A. Blesch (2019). "Peptides and Astroglia Improve the Regenerative Capacity of Alginate Gels in the Injured Spinal Cord." Tissue Eng Part A **25**(7-8): 522-537.

Schmitt, A. B., S. Breuer, J. Liman, A. Buss, C. Schlangen, K. Pech, E. M. Hol, G. A. Brook, J. Noth and F. W. Schwaiger (2003). "Identification of regeneration-associated genes after central and peripheral nerve injury in the adult rat." BMC Neurosci **4**: 8.

Schreiner, A. E., S. Durry, T. Aida, M. C. Stock, U. Ruther, K. Tanaka, C. R. Rose and K. W. Kafitz (2014). "Laminar and subcellular heterogeneity of GLAST and GLT-1 immunoreactivity in the developing postnatal mouse hippocampus." J Comp Neurol **522**(1): 204-224.

Schwab, M. E. and S. M. Strittmatter (2014). "Nogo limits neural plasticity and recovery from injury." Curr Opin Neurobiol **27**: 53-60.

Schwartz, G. and M. G. Fehlings (2001). "Evaluation of the neuroprotective effects of sodium channel blockers after spinal cord injury: improved behavioral and neuroanatomical recovery with riluzole." J Neurosurg **94**(2 Suppl): 245-256.

Schwob, J. E., W. Jang, E. H. Holbrook, B. Lin, D. B. Herrick, J. N. Peterson and J. Hewitt Coleman (2017). "Stem and progenitor cells of the mammalian olfactory epithelium: Taking poietic license." J Comp Neurol **525**(4): 1034-1054.

Seabrook, T. J., L. Jiang, M. Maier and C. A. Lemere (2006). "Minocycline affects microglia activation, Abeta deposition, and behavior in APP-tg mice." Glia **53**(7): 776-782.

Seijffers, R., A. J. Allchorne and C. J. Woolf (2006). "The transcription factor ATF-3 promotes neurite outgrowth." Mol Cell Neurosci **32**(1-2): 143-154.

Seri, B., J. M. Garcia-Verdugo, L. Collado-Morente, B. S. McEwen and A. Alvarez-Buylla (2004). "Cell types, lineage, and architecture of the germinal zone in the adult dentate gyrus." J Comp Neurol **478**(4): 359-378.

Sezer, N., S. Akkus and F. G. Ugurlu (2015). "Chronic complications of spinal cord injury." World J Orthop **6**(1): 24-33.

Shih, A. Y., D. A. Johnson, G. Wong, A. D. Kraft, L. Jiang, H. Erb, J. A. Johnson and T. H. Murphy (2003). "Coordinate regulation of glutathione biosynthesis and release by Nrf2-expressing glia potently protects neurons from oxidative stress." J Neurosci **23**(8): 3394-3406.

Shih, C. H., M. Lacagnina, K. Leuer-Bisciotti and C. Proschel (2014). "Astroglial-derived periostin promotes axonal regeneration after spinal cord injury." J Neurosci **34**(7): 2438-2443.

Shinozaki, M., A. Iwanami, K. Fujiyoshi, S. Tashiro, K. Kitamura, S. Shibata, H. Fujita, M. Nakamura and H. Okano (2016). "Combined treatment with chondroitinase ABC and treadmill rehabilitation for chronic severe spinal cord injury in adult rats." Neurosci Res **113**: 37-47.

Shoichet, M. S., R. H. Li, M. L. White and S. R. Winn (1996). "Stability of hydrogels used in cell encapsulation: An in vitro comparison of alginate and agarose." Biotechnol Bioeng **50**(4): 374-381.

Shumsky, J. S., C. A. Tobias, M. Tumolo, W. D. Long, S. F. Giszter and M. Murray (2003). "Delayed transplantation of fibroblasts genetically modified to secrete BDNF and NT-3 into a spinal cord injury site is associated with limited recovery of function." Exp Neurol **184**(1): 114-130.

Silver, J. and J. H. Miller (2004). "Regeneration beyond the glial scar." Nat Rev Neurosci **5**(2): 146-156.

Silver, J., M. E. Schwab and P. G. Popovich (2014). "Central nervous system regenerative failure: role of oligodendrocytes, astrocytes, and microglia." Cold Spring Harb Perspect Biol **7**(3): a020602.

Silvestro, S., P. Bramanti, O. Trubiani and E. Mazzon (2020). "Stem Cells Therapy for Spinal Cord Injury: An Overview of Clinical Trials." Int J Mol Sci **21**(2).

Simard, J. M., O. Tsymbalyuk, K. Keledjian, A. Ivanov, S. Ivanova and V. Gerzanich (2012). "Comparative effects of glibenclamide and riluzole in a rat model of severe cervical spinal cord injury." Exp Neurol **233**(1): 566-574.

Singh, A., L. Tetreault, S. Kalsi-Ryan, A. Nouri and M. G. Fehlings (2014). "Global prevalence and incidence of traumatic spinal cord injury." Clin Epidemiol **6**: 309-331.

Sirko, S., G. Behrendt, P. A. Johansson, P. Tripathi, M. Costa, S. Bek, C. Heinrich, S. Tiedt, D. Colak, M. Dichgans, I. R. Fischer, N. Plesnila, M. Staufenbiel, C. Haass, M. Snapyan, A. Saghatelyan, L. H. Tsai, A. Fischer, K. Grobe, L. Dimou and M. Gotz (2013). "Reactive glia in the injured brain acquire stem cell properties in response to sonic hedgehog. [corrected]." Cell Stem Cell **12**(4): 426-439.

Sitoci-Ficici, K. H., M. Matyash, O. Uckermann, R. Galli, E. Leipnitz, R. Later, C. Ikonomidou, M. Gelinsky, G. Schackert and M. Kirsch (2018). "Non-functionalized soft alginate hydrogel promotes locomotor recovery after spinal cord injury in a rat hemimyelonectomy model." Acta Neurochir (Wien) **160**(3): 449-457.

Sloan, S. A., S. Darmanis, N. Huber, T. A. Khan, F. Birey, C. Caneda, R. Reimer, S. R. Quake, B. A. Barres and S. P. Pasca (2017). "Human Astrocyte Maturation Captured in 3D Cerebral Cortical Spheroids Derived from Pluripotent Stem Cells." Neuron **95**(4): 779-790 e776.

Soderblom, C., D. H. Lee, A. Dawood, M. Carballosa, A. Jimena Santamaria, F. D. Benavides, S. Jergova, R. M. Grumbles, C. K. Thomas, K. K. Park, J. D. Guest, V. P. Lemmon, J. K. Lee and P. Tsoulfas (2015). "3D Imaging of Axons in Transparent Spinal Cords from Rodents and Nonhuman Primates." eNeuro **2**(2).

Soderblom, C., X. Luo, E. Blumenthal, E. Bray, K. Lyapichev, J. Ramos, V. Krishnan, C. Lai-Hsu, K. K. Park, P. Tsoulfas and J. K. Lee (2013). "Perivascular fibroblasts form the fibrotic scar after contusive spinal cord injury." J Neurosci **33**(34): 13882-13887.

Sofroniew, M. V. (2009). "Molecular dissection of reactive astrogliosis and glial scar formation." Trends Neurosci **32**(12): 638-647.

Sofroniew, M. V. (2014). "Astrogliosis." Cold Spring Harb Perspect Biol **7**(2): a020420.

Sofroniew, M. V. (2014). "Multiple roles for astrocytes as effectors of cytokines and inflammatory mediators." Neuroscientist **20**(2): 160-172.

Sofroniew, M. V. (2015). "Astrocyte barriers to neurotoxic inflammation." Nat Rev Neurosci **16**(5): 249-263.

Sofroniew, M. V. (2018). "Dissecting spinal cord regeneration." Nature **557**(7705): 343-350.

Sofroniew, M. V. and H. V. Vinters (2010). "Astrocytes: biology and pathology." Acta Neuropathol **119**(1): 7-35.

Sorg, B. A., S. Berretta, J. M. Blacktop, J. W. Fawcett, H. Kitagawa, J. C. Kwok and M. Miquel (2016). "Casting a Wide Net: Role of Perineuronal Nets in Neural Plasticity." J Neurosci **36**(45): 11459-11468.

Spilker, M. H., I. V. Yannas, S. K. Kostyk, T. V. Norregaard, H. P. Hsu and M. Spector (2001). "The effects of tubulation on healing and scar formation after transection of the adult rat spinal cord." Restor Neurol Neurosci **18**(1): 23-38.

Spiller, K. L., S. Nassiri, C. E. Witherel, R. R. Anfang, J. Ng, K. R. Nakazawa, T. Yu and G. Vunjak-Novakovic (2015). "Sequential delivery of immunomodulatory cytokines to facilitate the M1-to-M2 transition of macrophages and enhance vascularization of bone scaffolds." Biomaterials **37**: 194-207.

Stevens, B., N. J. Allen, L. E. Vazquez, G. R. Howell, K. S. Christopherson, N. Nouri, K. D. Micheva, A. K. Mehalow, A. D. Huberman, B. Stafford, A. Sher, A. M. Litke, J. D. Lambris, S. J. Smith, S. W. John and B. A. Barres (2007). "The classical complement cascade mediates CNS synapse elimination." Cell **131**(6): 1164-1178.

Stokols, S. and M. H. Tuszynski (2006). "Freeze-dried agarose scaffolds with uniaxial channels stimulate and guide linear axonal growth following spinal cord injury." Biomaterials **27**(3): 443-451.

Stolt, C. C., P. Lommes, E. Sock, M. C. Chaboissier, A. Schedl and M. Wegner (2003). "The Sox9 transcription factor determines glial fate choice in the developing spinal cord." Genes Dev **17**(13): 1677-1689.

Stout, R. D. and J. Suttles (2004). "Functional plasticity of macrophages: reversible adaptation to changing microenvironments." J Leukoc Biol **76**(3): 509-513.

Strathmann, F. G., X. Wang and M. Mayer-Proschel (2007). "Identification of two novel glial-restricted cell populations in the embryonic telencephalon arising from unique origins." BMC Dev Biol **7**: 33.

Sun, F. and Z. He (2010). "Neuronal intrinsic barriers for axon regeneration in the adult CNS." Curr Opin Neurobiol **20**(4): 510-518.

Suzuki, A., S. A. Stern, O. Bozdagi, G. W. Huntley, R. H. Walker, P. J. Magistretti and C. M. Alberini (2011). "Astrocyte-neuron lactate transport is required for long-term memory formation." Cell **144**(5): 810-823.

Suzuki, H., C. S. Ahuja, R. P. Salewski, L. Li, K. Satkunendrarajah, N. Nagoshi, S. Shibata and M. G. Fehlings (2017). "Neural stem cell mediated recovery is enhanced by Chondroitinase ABC pretreatment in chronic cervical spinal cord injury." PLoS One **12**(8): e0182339.

Suzuki, H., T. Kanchiku, Y. Imajo, Y. Yoshida, N. Nishida, T. Gondo, S. Yoshii and T. Taguchi (2015). "Artificial collagen-filament scaffold promotes axon regeneration and long tract reconstruction in a rat model of spinal cord transection." Med Mol Morphol **48**(4): 214-224.

Suzuki, K., Y. Suzuki, K. Ohnishi, K. Endo, M. Tanihara and Y. Nishimura (1999). "Regeneration of transected spinal cord in young adult rats using freeze-dried alginate gel." Neuroreport **10**(14): 2891-2894.

Suzuki, Y., M. Kitaura, S. Wu, K. Kataoka, K. Suzuki, K. Endo, Y. Nishimura and C. Ide (2002). "Electrophysiological and horseradish peroxidase-tracing studies of nerve regeneration through alginate-filled gap in adult rat spinal cord." Neurosci Lett **318**(3): 121-124.

Sweeney, I. R., M. Miraftab and G. Collyer (2012). "A critical review of modern and emerging absorbent dressings used to treat exuding wounds." Int Wound J **9**(6): 601-612.

Tabata, H. (2015). "Diverse subtypes of astrocytes and their development during corticogenesis." Front Neurosci **9**: 114.

Takahashi, H., M. Yamazaki, A. Okawa, T. Sakuma, K. Kato, M. Hashimoto, K. Hayashi, T. Furuya, T. Fujiyoshi, J. Kawabe, T. Yamauchi, C. Mannoji, T. Miyashita, R. Kadota, M. Hashimoto, Y. Ito, K. Takahashi and M. Koda (2012). "Neuroprotective therapy using granulocyte colony-stimulating factor for acute spinal cord injury: a phase I/IIa clinical trial." Eur Spine J **21**(12): 2580-2587.

Takahashi, K. and S. Yamanaka (2006). "Induction of pluripotent stem cells from mouse embryonic and adult fibroblast cultures by defined factors." Cell **126**(4): 663-676.

Takami, T., M. Oudega, M. L. Bates, P. M. Wood, N. Kleitman and M. B. Bunge (2002). "Schwann cell but not olfactory ensheathing glia transplants improve hindlimb locomotor performance in the moderately contused adult rat thoracic spinal cord." J Neurosci **22**(15): 6670-6681.

Takano, T., G. F. Tian, W. Peng, N. Lou, W. Libionka, X. Han and M. Nedergaard (2006). "Astrocyte-mediated control of cerebral blood flow." Nat Neurosci **9**(2): 260-267.

Takeoka, A., I. Vollenweider, G. Courtine and S. Arber (2014). "Muscle spindle feedback directs locomotor recovery and circuit reorganization after spinal cord injury." Cell **159**(7): 1626-1639.

Tang, X., J. E. Davies and S. J. Davies (2003). "Changes in distribution, cell associations, and protein expression levels of NG2, neurocan, phosphacan, brevican, versican V2, and tenascin-C during acute to chronic maturation of spinal cord scar tissue." J Neurosci Res **71**(3): 427-444.

Tang, X. Q., D. L. Tanelian and G. M. Smith (2004). "Semaphorin3A inhibits nerve growth factor-induced sprouting of nociceptive afferents in adult rat spinal cord." J Neurosci **24**(4): 819-827.

Taylor, S. J., E. S. Rosenzweig, J. W. McDonald, 3rd and S. E. Sakiyama-Elbert (2006). "Delivery of neurotrophin-3 from fibrin enhances neuronal fiber sprouting after spinal cord injury." J Control Release **113**(3): 226-235.

Tcw, J., M. Wang, A. A. Pimenova, K. R. Bowles, B. J. Hartley, E. Lacin, S. I. Machlovi, R. Abdelaal, C. M. Karch, H. Phatnani, P. A. Slesinger, B. Zhang, A. M. Goate and K. J. Brennand (2017). "An Efficient Platform for Astrocyte Differentiation from Human Induced Pluripotent Stem Cells." Stem Cell Reports **9**(2): 600-614.

Teng, Y. D., E. B. Lavik, X. Qu, K. I. Park, J. Ourednik, D. Zurakowski, R. Langer and E. Y. Snyder (2002). "Functional recovery following traumatic spinal cord injury mediated by a unique polymer scaffold seeded with neural stem cells." Proc Natl Acad Sci U S A **99**(5): 3024-3029.

Teng, Y. D., I. Mocchetti, A. M. Taveira-DaSilva, R. A. Gillis and J. R. Wrathall (1999). "Basic fibroblast growth factor increases long-term survival of spinal motor neurons and improves respiratory function after experimental spinal cord injury." J Neurosci **19**(16): 7037-7047.

Testen, A., R. Kim and K. J. Reissner (2020). "High-Resolution Three-Dimensional Imaging of Individual Astrocytes Using Confocal Microscopy." Curr Protoc Neurosci **91**(1): e92.

Theodore, N., R. Hlubek, J. Danielson, K. Neff, L. Vaickus, T. R. Ulich and A. E. Ropper (2016). "First Human Implantation of a Bioresorbable Polymer Scaffold for Acute Traumatic Spinal Cord Injury: A Clinical Pilot Study for Safety and Feasibility." Neurosurgery **79**(2): E305-312.

Tien, A. C., H. H. Tsai, A. V. Molofsky, M. McMahon, L. C. Foo, A. Kaul, J. D. Dougherty, N. Heintz, D. H. Gutmann, B. A. Barres and D. H. Rowitch (2012). "Regulated temporal-spatial astrocyte precursor cell proliferation involves BRAF signalling in mammalian spinal cord." Development **139**(14): 2477-2487.

Tobias, C. A., S. S. Han, J. S. Shumsky, D. Kim, M. Tumolo, N. O. Dhoot, M. A. Wheatley, I. Fischer, A. Tessler and M. Murray (2005). "Alginate encapsulated BDNF-producing fibroblast grafts permit recovery of function after spinal cord injury in the absence of immune suppression." J Neurotrauma **22**(1): 138-156.

Toft-Hansen, H., L. Fuchtbauer and T. Owens (2011). "Inhibition of reactive astrocytosis in established experimental autoimmune encephalomyelitis favors infiltration by myeloid cells over T cells and enhances severity of disease." Glia **59**(1): 166-176.

Tom, V. J., C. M. Doller, A. T. Malouf and J. Silver (2004). "Astrocyte-associated fibronectin is critical for axonal regeneration in adult white matter." J Neurosci **24**(42): 9282-9290.

Tom, V. J., M. P. Steinmetz, J. H. Miller, C. M. Doller and J. Silver (2004). "Studies on the development and behavior of the dystrophic growth cone, the hallmark of regeneration failure, in an in vitro model of the glial scar and after spinal cord injury." J Neurosci **24**(29): 6531-6539.

Tonge, D. A., H. T. de Burgh, R. Docherty, M. J. Humphries, S. E. Craig and J. Pizzey (2012). "Fibronectin supports neurite outgrowth and axonal regeneration of adult brain neurons in vitro." Brain Res **1453**: 8-16.

Torres, C. R. G., M. C. Mailart, E. Crastechini, F. A. Feitosa, S. R. M. Esteves, R. Di Nicolo and A. B. Borges (2020). "A randomized clinical trial of class II composite restorations using direct and semidirect techniques." Clin Oral Investig **24**(2): 1053-1063.

Tsai, E. C., P. D. Dalton, M. S. Shoichet and C. H. Tator (2004). "Synthetic hydrogel guidance channels facilitate regeneration of adult rat brainstem motor axons after complete spinal cord transection." J Neurotrauma **21**(6): 789-804.

Tsai, E. C., P. D. Dalton, M. S. Shoichet and C. H. Tator (2006). "Matrix inclusion within synthetic hydrogel guidance channels improves specific supraspinal and local axonal regeneration after complete spinal cord transection." Biomaterials **27**(3): 519-533.

Tsai, M. C., L. F. Shen, H. S. Kuo, H. Cheng and K. F. Chak (2008). "Involvement of acidic fibroblast growth factor in spinal cord injury repair processes revealed by a proteomics approach." Mol Cell Proteomics **7**(9): 1668-1687.

Tsuji, O., K. Miura, Y. Okada, K. Fujiyoshi, M. Mukaino, N. Nagoshi, K. Kitamura, G. Kumagai, M. Nishino, S. Tomisato, H. Higashi, T. Nagai, H. Katoh, K. Kohda, Y. Matsuzaki, M. Yuzaki, E. Ikeda, Y. Toyama, M. Nakamura, S. Yamanaka and H. Okano (2010). "Therapeutic potential of appropriately evaluated safe-induced pluripotent stem cells for spinal cord injury." Proc Natl Acad Sci U S A **107**(28): 12704-12709.

Tsuji, O., K. Sugai, R. Yamaguchi, S. Tashiro, N. Nagoshi, J. Kohyama, T. Iida, T. Ohkubo, G. Itakura, M. Isoda, M. Shinozaki, K. Fujiyoshi, Y. Kanemura, S. Yamanaka, M. Nakamura and H. Okano (2019). "Concise Review: Laying the Groundwork for a First-In-Human Study of an Induced Pluripotent Stem Cell-Based Intervention for Spinal Cord Injury." Stem Cells **37**(1): 6-13.

Tuszynski, M. H., K. Gabriel, F. H. Gage, S. Suhr, S. Meyer and A. Rosetti (1996). "Nerve growth factor delivery by gene transfer induces differential outgrowth of sensory, motor, and noradrenergic neurites after adult spinal cord injury." Exp Neurol **137**(1): 157-173.

Tuszynski, M. H., D. A. Peterson, J. Ray, A. Baird, Y. Nakahara and F. H. Gage (1994). "Fibroblasts genetically modified to produce nerve growth factor induce robust neuritic ingrowth after grafting to the spinal cord." Exp Neurol **126**(1): 1-14.

Uemura, N., I. Oda, Y. Saito, H. Ono, J. Fujisaki, N. Matsuhashi, K. Ohata, N. Yahagi, T. Yada, M. Satoh, H. Tajiri, M. Inomata and S. Kitano (2019). "Efficacy and safety of 0.6% sodium alginate solution in endoscopic submucosal dissection for esophageal and gastric neoplastic lesion: A randomized controlled study." Dig Endosc **31**(4): 396-404.

Urdzikova, L., P. Jendelova, K. Glogarova, M. Burian, M. Hajek and E. Sykova (2006). "Transplantation of bone marrow stem cells as well as mobilization by granulocyte-colony stimulating factor promotes recovery after spinal cord injury in rats." J Neurotrauma **23**(9): 1379-1391.

van den Berg, M. E., J. M. Castellote, I. Mahillo-Fernandez and J. de Pedro-Cuesta (2010). "Incidence of spinal cord injury worldwide: a systematic review." Neuroepidemiology **34**(3): 184-192; discussion 192.

van Niekerk, E. A., M. H. Tuszynski, P. Lu and J. N. Dulin (2016). "Molecular and Cellular Mechanisms of Axonal Regeneration After Spinal Cord Injury." Mol Cell Proteomics **15**(2): 394-408.

Virchow, R. C. (1858). Die Cellularpathologie in ihrer Begründung auf physiologische und pathologische Gewebelehre. Hirschwald.

Volpato, F. Z., T. Fuhrmann, C. Migliaresi, D. W. Hutmacher and P. D. Dalton (2013). "Using extracellular matrix for regenerative medicine in the spinal cord." Biomaterials **34**(21): 4945-4955.

Volterra, A. and J. Meldolesi (2005). "Astrocytes, from brain glue to communication elements: the revolution continues." Nat Rev Neurosci **6**(8): 626-640.

Voskuhl, R. R., R. S. Peterson, B. Song, Y. Ao, L. B. Morales, S. Tiwari-Woodruff and M. V. Sofroniew (2009). "Reactive astrocytes form scar-like perivascular barriers to leukocytes during adaptive immune inflammation of the CNS." J Neurosci **29**(37): 11511-11522.

Vroemen, M., M. Caioni, U. Bogdahn and N. Weidner (2007). "Failure of Schwann cells as supporting cells for adult neural progenitor cell grafts in the acutely injured spinal cord." Cell Tissue Res **327**(1): 1-13.

Vue, T. Y., E. J. Kim, C. M. Parras, F. Guillemot and J. E. Johnson (2014). "Ascl1 controls the number and distribution of astrocytes and oligodendrocytes in the gray matter and white matter of the spinal cord." Development **141**(19): 3721-3731.

Walchli, T., J. M. Mateos, O. Weinman, D. Babic, L. Regli, S. P. Hoerstrup, H. Gerhardt, M. E. Schwab and J. Vogel (2015). "Quantitative assessment of angiogenesis, perfused blood vessels and endothelial tip cells in the postnatal mouse brain." Nat Protoc **10**(1): 53-74.

Walczak, P., A. H. All, N. Rumpal, M. Gorelik, H. Kim, A. Maybhate, G. Agrawal, J. T. Campanelli, A. A. Gilad, D. A. Kerr and J. W. Bulte (2011). "Human glial-restricted progenitors survive, proliferate, and preserve electrophysiological function in rats with focal inflammatory spinal cord demyelination." Glia **59**(3): 499-510.

Wallner, S., S. Peters, C. Pitzer, H. Resch, U. Bogdahn and A. Schneider (2015). "The Granulocyte-colony stimulating factor has a dual role in neuronal and vascular plasticity." Front Cell Dev Biol **3**: 48.

Wang, B., Y. Zhao, H. Lin, B. Chen, J. Zhang, J. Zhang, X. Wang, W. Zhao and J. Dai (2006). "Phenotypical analysis of adult rat olfactory ensheathing cells on 3-D collagen scaffolds." Neurosci Lett **401**(1-2): 65-70.

Wang, C., C. Sun, Z. Hu, X. Huo, Y. Yang, X. Liu, B. O. A. Botchway, H. Davies and M. Fang (2017). "Improved Neural Regeneration with Olfactory Ensheathing Cell Inoculated PLGA Scaffolds in Spinal Cord Injury Adult Rats." Neurosignals **25**(1): 1-14.

Wang, D. and J. Fawcett (2012). "The perineuronal net and the control of CNS plasticity." Cell Tissue Res **349**(1): 147-160.

Wang, D., R. M. Ichiyama, R. Zhao, M. R. Andrews and J. W. Fawcett (2011). "Chondroitinase combined with rehabilitation promotes recovery of forelimb function in rats with chronic spinal cord injury." J Neurosci **31**(25): 9332-9344.

Wang, J. J., M. I. Chuah, D. T. Yew, P. C. Leung and D. S. Tsang (1995). "Effects of astrocyte implantation into the hemisected adult rat spinal cord." Neuroscience **65**(4): 973-981.

Wang, J. M., Y. S. Zeng, J. L. Wu, Y. Li and Y. D. Teng (2011). "Cograft of neural stem cells and schwann cells overexpressing TrkC and neurotrophin-3 respectively after rat spinal cord transection." Biomaterials **32**(30): 7454-7468.

Wanner, I. B., M. A. Anderson, B. Song, J. Levine, A. Fernandez, Z. Gray-Thompson, Y. Ao and M. V. Sofroniew (2013). "Glial scar borders are formed by newly proliferated, elongated astrocytes that interact to corral inflammatory and fibrotic cells via STAT3-dependent mechanisms after spinal cord injury." J Neurosci **33**(31): 12870-12886.

Watkins, T. A., B. Emery, S. Mulinyawe and B. A. Barres (2008). "Distinct stages of myelination regulated by gamma-secretase and astrocytes in a rapidly myelinating CNS coculture system." Neuron **60**(4): 555-569.

Weidner, N., A. Blesch, R. J. Grill and M. H. Tuszynski (1999). "Nerve growth factor-hypersecreting Schwann cell grafts augment and guide spinal cord axonal growth and remyelinate central nervous system axons in a phenotypically appropriate manner that correlates with expression of L1." J Comp Neurol **413**(4): 495-506.

Weidner, N., A. Ner, N. Salimi and M. H. Tuszynski (2001). "Spontaneous corticospinal axonal plasticity and functional recovery after adult central nervous system injury." Proc Natl Acad Sci U S A **98**(6): 3513-3518.

Weidner, N., R. Rupp and K. E. Tansey (2017). Neurological aspects of spinal cord injury, Springer.

Wen, H., W. Xiao, S. Biswas, Z. Q. Cong, X. M. Liu, K. S. Lam, Y. H. Liao and W. Deng (2019). "Alginate Hydrogel Modified with a Ligand Interacting with alpha3beta1 Integrin Receptor Promotes the Differentiation of 3D Neural Spheroids toward Oligodendrocytes in Vitro." ACS Appl Mater Interfaces **11**(6): 5821-5833.

Wen, Y., S. Yu, Y. Wu, R. Ju, H. Wang, Y. Liu, Y. Wang and Q. Xu (2016). "Spinal cord injury repair by implantation of structured hyaluronic acid scaffold with PLGA microspheres in the rat." Cell Tissue Res **364**(1): 17-28.

Westergard, T. and J. D. Rothstein (2020). "Astrocyte Diversity: Current Insights and Future Directions." Neurochem Res.

Whetstone, W. D., J. Y. Hsu, M. Eisenberg, Z. Werb and L. J. Noble-Haeusslein (2003). "Blood-spinal cord barrier after spinal cord injury: relation to revascularization and wound healing." J Neurosci Res **74**(2): 227-239.

White, D. M. (1998). "Contribution of neurotrophin-3 to the neuropeptide Y-induced increase in neurite outgrowth of rat dorsal root ganglion cells." Neuroscience **86**(1): 257-263.

WHO (2013). "International Perspectives on Spinal Cord Injury." World Health Organization.

Wictorin, K., P. Brundin, B. Gustavii, O. Lindvall and A. Bjorklund (1990). "Reformation of long axon pathways in adult rat central nervous system by human forebrain neuroblasts." Nature **347**(6293): 556-558.

Wilhelmsson, U., E. A. Bushong, D. L. Price, B. L. Smarr, V. Phung, M. Terada, M. H. Ellisman and M. Pekny (2006). "Redefining the concept of reactive astrocytes as cells that remain within their unique domains upon reaction to injury." Proc Natl Acad Sci U S A **103**(46): 17513-17518.

Wilhelmsson, U., L. Li, M. Pekna, C. H. Berthold, S. Blom, C. Eliasson, O. Renner, E. Bushong, M. Ellisman, T. E. Morgan and M. Pekny (2004). "Absence of glial fibrillary acidic protein and vimentin prevents hypertrophy of astrocytic processes and improves post-traumatic regeneration." J Neurosci **24**(21): 5016-5021.

Williams, R. R., M. Henao, D. D. Pearse and M. B. Bunge (2015). "Permissive Schwann cell graft/spinal cord interfaces for axon regeneration." Cell Transplant **24**(1): 115-131.

Wilson, J. R., N. Forgione and M. G. Fehlings (2013). "Emerging therapies for acute traumatic spinal cord injury." CMAJ **185**(6): 485-492.

Winslow, C. and J. Rozovsky (2003). "Effect of spinal cord injury on the respiratory system." Am J Phys Med Rehabil **82**(10): 803-814.

Winter, C. C., K. S. Katiyar, N. S. Hernandez, Y. J. Song, L. A. Struzyna, J. P. Harris and D. K. Cullen (2016). "Transplantable living scaffolds comprised of micro-tissue engineered aligned astrocyte networks to facilitate central nervous system regeneration." Acta Biomater **38**: 44-58.

Winton, M. J., C. I. Dubreuil, D. Lasko, N. Leclerc and L. McKerracher (2002). "Characterization of new cell permeable C3-like proteins that inactivate Rho and stimulate neurite outgrowth on inhibitory substrates." J Biol Chem **277**(36): 32820-32829.

Wu, B., L. Sun, P. Li, M. Tian, Y. Luo and X. Ren (2012). "Transplantation of oligodendrocyte precursor cells improves myelination and promotes functional recovery after spinal cord injury." Injury **43**(6): 794-801.

Wu, J. C., W. C. Huang, Y. C. Chen, T. H. Tu, Y. A. Tsai, S. F. Huang, H. C. Huang and H. Cheng (2011). "Acidic fibroblast growth factor for repair of human spinal cord injury: a clinical trial." J Neurosurg Spine **15**(3): 216-227.

Wu, J. C., W. C. Huang, Y. A. Tsai, Y. C. Chen and H. Cheng (2008). "Nerve repair using acidic fibroblast growth factor in human cervical spinal cord injury: a preliminary Phase I clinical study." J Neurosurg Spine **8**(3): 208-214.

Wu, X. and X. M. Xu (2016). "RhoA/Rho kinase in spinal cord injury." Neural Regen Res **11**(1): 23-27.

Xiao, D., X. Liu, M. Zhang, M. Zou, Q. Deng, D. Sun, X. Bian, Y. Cai, Y. Guo, S. Liu, S. Li, E. Shiang, H. Zhong, L. Cheng, H. Xu, K. Jin and M. Xiang (2018). "Direct reprogramming of fibroblasts into neural stem cells by single non-neural progenitor transcription factor Ptf1a." Nat Commun **9**(1): 2865.

Xu, X. M., A. Chen, V. Guenard, N. Kleitman and M. B. Bunge (1997). "Bridging Schwann cell transplants promote axonal regeneration from both the rostral and caudal stumps of transected adult rat spinal cord." J Neurocytol **26**(1): 1-16.

Xu, X. M., V. Guenard, N. Kleitman, P. Aebischer and M. B. Bunge (1995). "A combination of BDNF and NT-3 promotes supraspinal axonal regeneration into Schwann cell grafts in adult rat thoracic spinal cord." Exp Neurol **134**(2): 261-272.

Xu, X. M., S. X. Zhang, H. Li, P. Aebischer and M. B. Bunge (1999). "Regrowth of axons into the distal spinal cord through a Schwann-cell-seeded mini-channel implanted into hemisected adult rat spinal cord." Eur J Neurosci **11**(5): 1723-1740.

Yang, Z., L. Zhu, F. Li, J. Wang, H. Wan and Y. Pan (2014). "Bone marrow stromal cells as a therapeutic treatment for ischemic stroke." Neurosci Bull **30**(3): 524-534.

Yao, L., W. Daly, B. Newland, S. Yao, W. Wang, B. K. Chen, N. Madigan, A. Windebank and A. Pandit (2013). "Improved axonal regeneration of transected spinal cord mediated by multichannel collagen conduits functionalized with neurotrophin-3 gene." Gene Ther **20**(12): 1149-1157.

Yiu, G. and Z. He (2006). "Glial inhibition of CNS axon regeneration." Nat Rev Neurosci **7**(8): 617-627.

Zador, Z., S. Stiver, V. Wang and G. T. Manley (2009). "Role of aquaporin-4 in cerebral edema and stroke." Handb Exp Pharmacol(190): 159-170.

Zai, L. J. and J. R. Wrathall (2005). "Cell proliferation and replacement following contusive spinal cord injury." Glia **50**(3): 247-257.

Zamanian, J. L., L. Xu, L. C. Foo, N. Nouri, L. Zhou, R. G. Giffard and B. A. Barres (2012). "Genomic analysis of reactive astrogliosis." J Neurosci **32**(18): 6391-6410.

Zeisel, A., H. Hochgerner, P. Lonnerberg, A. Johnsson, F. Memic, J. van der Zwan, M. Haring, E. Braun, L. E. Borm, G. La Manno, S. Codeluppi, A. Furlan, K. Lee, N. Skene, K. D. Harris, J. Hjerling-Leffler, E. Arenas, P. Ernfors, U. Marklund and S. Linnarsson (2018). "Molecular Architecture of the Mouse Nervous System." Cell **174**(4): 999-1014 e1022.

Zeng, X., X. C. Qiu, Y. H. Ma, J. J. Duan, Y. F. Chen, H. Y. Gu, J. M. Wang, E. A. Ling, J. L. Wu, W. Wu and Y. S. Zeng (2015). "Integration of donor mesenchymal stem cell-derived neuron-like cells into host neural network after rat spinal cord transection." Biomaterials **53**: 184-201.

Zhang, H., M. Chang, C. N. Hansen, D. M. Basso and L. J. Noble-Haeusslein (2011). "Role of matrix metalloproteinases and therapeutic benefits of their inhibition in spinal cord injury." Neurotherapeutics **8**(2): 206-220.

Zhang, Q., M. Raoof, Y. Chen, Y. Sumi, T. Sursal, W. Junger, K. Brohi, K. Itagaki and C. J. Hauser (2010). "Circulating mitochondrial DAMPs cause inflammatory responses to injury." Nature **464**(7285): 104-107.

Zhang, S., J. E. Burda, M. A. Anderson, Z. Zhao, Y. Ao, Y. Cheng, Y. Sun, T. J. Deming and M. V. Sofroniew (2015). "Thermoresponsive Copolypeptide Hydrogel Vehicles for Central Nervous System Cell Delivery." ACS Biomater Sci Eng **1**(8): 705-717.

Zhang, S. X., F. Huang, M. Gates and E. G. Holmberg (2013). "Role of endogenous Schwann cells in tissue repair after spinal cord injury." Neural Regen Res **8**(2): 177-185.

Zhang, X. and D. M. Mosser (2008). "Macrophage activation by endogenous danger signals." J Pathol **214**(2): 161-178.

Zhang, X., J. Wang, Q. Zhou, Y. Xu, S. Pu, J. Wu, Y. Xue, Y. Tian, J. Lu, W. Jiang and D. Du (2011). "Brain-derived neurotrophic factor-activated astrocytes produce mechanical allodynia in neuropathic pain." Neuroscience **199**: 452-460.

Zhang, Y., K. Chen, S. A. Sloan, M. L. Bennett, A. R. Scholze, S. O'Keeffe, H. P. Phatnani, P. Guarnieri, C. Caneda, N. Ruderisch, S. Deng, S. A. Liddelow, C. Zhang, R. Daneman, T. Maniatis, B. A. Barres and J. Q. Wu (2014). "An RNA-sequencing transcriptome and splicing database of glia, neurons, and vascular cells of the cerebral cortex." J Neurosci **34**(36): 11929-11947.

Zhao, X., Y. Chen, Q. Zhu, H. Huang, P. Teng, K. Zheng, X. Hu, B. Xie, Z. Zhang, M. Sander and M. Qiu (2014). "Control of astrocyte progenitor specification, migration and maturation by Nkx6.1 homeodomain transcription factor." PLoS One **9**(10): e109171.

Zheng, B., J. Atwal, C. Ho, L. Case, X. L. He, K. C. Garcia, O. Steward and M. Tessier-Lavigne (2005). "Genetic deletion of the Nogo receptor does not reduce neurite inhibition in vitro or promote corticospinal tract regeneration in vivo." Proc Natl Acad Sci U S A **102**(4): 1205-1210.

Zheng, B., C. Ho, S. Li, H. Keirstead, O. Steward and M. Tessier-Lavigne (2003). "Lack of enhanced spinal regeneration in Nogo-deficient mice." Neuron **38**(2): 213-224.

Zhou, L. and H. D. Shine (2003). "Neurotrophic factors expressed in both cortex and spinal cord induce axonal plasticity after spinal cord injury." J Neurosci Res **74**(2): 221-226.

Zhou, T., Y. Zheng, L. Sun, S. R. Badea, Y. Jin, Y. Liu, A. J. Rolfe, H. Sun, X. Wang, Z. Cheng, Z. Huang, N. Zhao, X. Sun, J. Li, J. Fan, C. Lee, T. L. Megraw, W. Wu, G. Wang and Y. Ren (2019). "Microvascular endothelial cells engulf myelin debris and promote macrophage recruitment and fibrosis after neural injury." Nat Neurosci **22**(3): 421-435.

Zhou, X. F., Y. S. Deng, C. J. Xian and J. H. Zhong (2000). "Neurotrophins from dorsal root ganglia trigger allodynia after spinal nerve injury in rats." Eur J Neurosci **12**(1): 100-105.

Zou, P., X. Yang, J. Wang, Y. Li, H. Yu, Y. Zhang and G. Liu (2016). "Advances in characterisation and biological activities of chitosan and chitosan oligosaccharides." Food Chem **190**: 1174-1181.

Zuidema, J. M., G. P. Desmond, C. J. Rivet, K. R. Kearns, D. M. Thompson and R. J. Gilbert (2015). "Nebulized solvent ablation of aligned PLLA fibers for the study of neurite response to anisotropic-to-isotropic fiber/film transition (AFFT) boundaries in astrocyte-neuron co-cultures." Biomaterials **46**: 82-94.

Zukor, K., S. Belin, C. Wang, N. Keelan, X. Wang and Z. He (2013). "Short hairpin RNA against PTEN enhances regenerative growth of corticospinal tract axons after spinal cord injury." J Neurosci **33**(39): 15350-15361.

7 Supplementary tables

7.1 Summary of animal experiments

Experiment	Group	Surgery	Treatment	Survival	Outcome measures	Group size	Animals excluded
non-coated vs. coated hydrogels	non-coated (**Control**)	unilateral hemisection at C5/6	hydrogel implant	4 weeks	CF, HAR/HMR, HC, βIII	n = 12 (3 died after SCI)	-
	coated **(+ PLO/lam**)	unilateral hemisection at C5/6	hydrogel implant	4 weeks	CF, HAR/HMR, HC, βIII	n = 12	n = 2 (contamination in hydrogel implant)
non-seeded vs. astrocyte-seeded hydrogels	non-seeded (+ PLO/lam, **Control**)	unilateral hemisection at C5/6	hydrogel implant	4 weeks	CF, Vas, βIII, 5-HT	n = 6	-
	astrocyte-seeded (**+ cortex-derived astrocytes**)	unilateral hemisection at C5/6	astrocyte-seeded hydrogel implant	4 weeks	CF, AF, AC, Vas, βIII, 5-HT	n = 10	-
astrocyte transplantation into intact spinal cord	**cortex-derived astrocytes P1**	bilateral cell injection at C5	-	2 weeks	MM	n = 3	-
				4 weeks	MM	n = 3	-
	spinal cord-derived astrocytes P3	bilateral cell injection at C5	-	2 weeks	MM	n = 3	-
				4 weeks	MM	n = 3	-
non-seeded vs astrocyte-seeded hydrogels with caudal astrocyte graft	non-seeded (+ PLO/lam, **Control**)	unilateral hemisection at C5/6	hydrogel implant	4 weeks	CF, Vas, βIII, 5-HT, BDA	n = 6	n = 1 (hydrogel destruction during tissue processing)
	+ cortex-derived astrocytes	unilateral hemisection at C5/6	astrocyte-seeded hydrogel implant + caudal cell graft	4 weeks	CF, AF, AC, CAM, Vas, βIII, 5-HT, BDA	n = 6	n = 1 (hydrogel destruction during tissue processing)
	+ spinal-derived astrocytes	unilateral hemisection at C5/6	astrocyte-seeded hydrogel implant + caudal cell graft	4 weeks	CF, AF, AC, CAM, Vas, βIII, 5-HT, BDA	n = 6	-
non-seeded vs astrocyte-seeded hydrogels with rostral and caudal astrocyte graft	non-seeded (+ PLO/lam, **Control**)	unilateral hemisection at C5/6	hydrogel implant	8 weeks	CF, Vas, βIII, 5-HT, BDA	n = 6	-
	+ cortex-derived astrocytes	unilateral hemisection at C5/6	astrocyte-seeded hydrogel implant + rostral/caudal cell graft	8 weeks	CF, AF, AC, CAM, Vas, βIII, 5-HT, BDA	n = 8 (2 died after SCI)	-
	+ spinal-derived astrocytes	unilateral hemisection at C5/6	astrocyte-seeded hydrogel implant + rostral/caudal cell graft	8 weeks	CF, AF, AC, CAM, Vas, βIII, 5-HT, BDA	n = 8 (2 died after SCI)	-

Supplementary table 1: Summary of animal experiments. CF: cell filling; HAR: host astroglial response; HMR: host microglial response; HC: host cell characterization; **β**III: **β**III-tubulin-labeled axons; 5-HT: 5-HT-labeled axons; Vas: vascularization; AF: astrocyte filling; AC: astrocyte colonization; MM: molecular marker expression; BDA: BDA-labeled axons; CAM: migration of caudally injection astrocytes

7.2 Impact of neonatal astrocytes as a cellular growth substrate within alginate-based hydrogel implants on axonal regeneration after traumatic spinal cord injury

Statistical test	Group	Distance	p value
Two-Way ANOVA for overall group differences p < 0.001, with Sidak's *post hoc*	PLO/laminin vs. + cortex-derived astrocytes	Rostral 500 µm	*p < 0.05
Two-Way ANOVA for distance p < 0.0001, with Sidak's *post hoc*	PLO/laminin	Rostral 100 µm vs. Rostral 500 µm	**p < 0.01
		Rostral 100 µm vs. Caudal 500 µm	*p < 0.05
		Rostral 500 µm vs. Caudal 100 µm	****p < 0.0001
		Caudal 500 µm vs. Caudal 100 µm	****p < 0.0001
	+ cortex-derived astrocytes	Rostral 100 µm vs. Rostral 500 µm	*p < 0.05
		Rostral 100 µm vs. Caudal 500 µm	**p < 0.01
		Rostral 500 µm vs. Caudal 100 µm	**p < 0.0001
		Caudal 500 µm vs. Caudal 100 µm	**p < 0.01
Interaction	Cell grafting x Distance		*p < 0.05

Supplementary table 2: Statistical analysis of cell filling within hydrogel implants (FIG 13C).

Statistical test	Group	Distance	p value
Two-Way ANOVA for overall group differences p = 0.09	PLO/laminin vs. + cortex-derived astrocytes	-	ns
Two-Way ANOVA for distance p < 0.0001, with Sidak's *post hoc*	PLO/laminin	Rostral 100 µm vs. Rostral 500 µm	*p < 0.05
		Rostral 100 µm vs. Caudal 500 µm	*p < 0.05
	+ cortex-derived astrocytes	Rostral 100 µm vs. Rostral 500 µm	***p < 0.001
		Rostral 100 µm vs. Caudal 500 µm	**p < 0.01

Supplementary table 3: Statistical analysis of axonal growth within hydrogel channels (FIG 15C).

Statistical test	Group	Distance	p value
Two-Way ANOVA for overall group differences p < 0.001, with Sidak's *post hoc*	PLO/laminin vs. + cortex-derived astrocytes	Rostral 100 µm	*p < 0.05
Two-Way ANOVA for distance p < 0.0001, with Sidak's *post hoc*	PLO/laminin	Rostral 100 µm vs. Rostral 500 µm	*p < 0.05
		Rostral 100 µm vs. Caudal 500 µm	**p < 0.01
		Rostral 500 µm vs. Caudal 100 µm	*p < 0.05
		Caudal 500 µm vs. Caudal 100 µm	*p < 0.05
	+ cortex-derived astrocytes	Rostral 100 µm vs. Rostral 500 µm	****p < 0.0001
		Rostral 100 µm vs. Caudal 500 µm	****p < 0.0001
		Rostral 500 µm vs. Caudal 100 µm	**p < 0.01
		Caudal 500 µm vs. Caudal 100 µm	**p < 0.01

Supplementary table 4: Statistical analysis of axonal growth within hydrogel implants (FIG 15D).

Statistical test	Group	Distance	p value
Two-Way ANOVA for overall group differences p = 0.27	PLO/laminin vs. + cortex-derived astrocytes	-	ns
Two-Way ANOVA for distance p < 0.0001, with Sidak's *post hoc*	PLO/laminin	-	ns
	+ cortex-derived astrocytes	Rostral 100 µm vs. Rostral 500 µm	***p < 0.001
		Rostral 100 µm vs. Caudal 500 µm	***p < 0.001
		Rostral 100 µm vs. Caudal 100 µm	***p < 0.001

Supplementary table 5: Statistical analysis of growth of serotonergic axons within hydrogel channels (FIG 16C).

Statistical test	Group	Distance	p value
Two-Way ANOVA for overall group differences p = 0.14	PLO/laminin vs. + cortex-derived astrocytes	-	ns
Two-Way ANOVA for distance differences p < 0.0001, with Sidak's *post hoc*	PLO/laminin	-	ns
	+ cortex-derived astrocytes	Rostral 100 µm vs. Rostral 500 µm	****p < 0.0001
		Rostral 100 µm vs. Caudal 500 µm	****p < 0.0001
		Rostral 100 µm vs. Caudal 100 µm	****p < 0.0001

Supplementary table 6: Statistical analysis of growth of serotonergic axons within hydrogel implants (FIG 16D).

7.3 Impact of neonatal spinal cord-derived astrocytes as a cellular growth substrate within alginate-based hydrogel implants and in the surrounding host spinal cord on axonal regeneration after traumatic spinal cord injury

Statistical test	Group	Distance	p value
Two-Way ANOVA for overall group differences p = 0.51	PLO/laminin vs. + cortex-derived astrocytes vs. + spinal cord-derived astrocytes	-	ns
Two-Way ANOVA for distance p < 0.0001, with Tukey's *post hoc*	PLO/laminin	-	ns
	+ cortex-derived astrocytes	Rostral 100 µm vs. Center 1000 µm	**p < 0.01
		Center 1000 µm vs. Caudal 100 µm	**p < 0.01
	+ spinal cord-derived astrocytes	-	ns

Supplementary table 7: Statistical analysis of cell filling within hydrogel implants (FIG 17D).

Statistical test	Group	Distance	p value
Two-Way ANOVA for cell type p < 0.001, with Sidak's *post hoc*	+ cortex-derived astrocytes vs. +spinal cord-derived astrocytes	Caudal 0 – 500 µm	**p < 0.01
		Caudal 500 – 1000 µm	*p < 0.05
Two-Way ANOVA for distance p < 0.0001, with Sidak's *post hoc*	+ cortex-derived astrocytes	Caudal 0 – 500 µm vs. Caudal 1000 – 1500 µm	***p < 0.001
		Caudal 0 – 500 µm vs. Caudal 1500 – 2000 µm	****p < 0.0001
		Caudal 500 – 1000 µm vs. Caudal 1500 – 2000 µm	*p < 0.05
	+ spinal cord-derived astrocytes	-	ns

Supplementary table 8: Statistical analysis of graft cell migration caudal to the hydrogel implants (FIG 28I).

Statistical test	Group	Distance	p value
Two-Way ANOVA for overall group differences p < 0.05, with Tukey's *post hoc*	PLO/laminin vs. + cortex-derived astrocytes	-	ns
	PLO/laminin vs. + spinal cord-derived astrocytes	Rostral 100 µm	**p < 0.01
	+ cortex-derived astrocytes vs. + spinal cord-derived astrocytes	Rostral 100 µm	**p < 0.01
Two-Way ANOVA for distance p = 0.21	PLO/laminin	-	ns
	+ cortex-derived astrocytes	-	ns
	+ spinal cord-derived astrocytes	-	ns

Supplementary table 9: Statistical analysis of axonal growth within hydrogel channels (FIG 31D).

Statistical test	Group	Distance	p value
Two-Way ANOVA for overall group differences $p < 0.05$, with Tukey's *post hoc*	PLO/laminin vs. + cortex-derived astrocytes	-	ns
	PLO/laminin vs. + spinal cord-derived astrocytes	Rostral 100 µm	*p < 0.05
	+ cortex-derived astrocytes vs. + spinal cord-derived astrocytes	-	ns
Two-Way ANOVA for distance $p = 0.07$	PLO/laminin	-	ns
	+ cortex-derived astrocytes	-	ns
	+ spinal cord-derived astrocytes	-	ns

Supplementary table 10: Statistical analysis of axonal growth within hydrogel implants (FIG 31E).

Statistical test	Group	Distance	p value
Two-Way ANOVA for overall group differences $p < 0.05$, with Tukey's *post hoc*	PLO/laminin vs. cortex-derived astrocytes	Rostral 100 µm	*p < 0.05
	PLO/laminin vs. + spinal cord-derived astrocytes	Rostral 100 µm	**p < 0.01
	+ cortex-derived astroctytes vs. + cortex-derived astroctes	-	ns
Two-Way ANOVA for distance $p < 0.0001$, with Tukey's *post hoc*	PLO/laminin	-	ns
	+ cortex-derived astrocytes	Rostral 100 µm vs. Rostral 500 µm	*p < 0.05
		Rostral 100 µm vs. Center 1000 µm	***p < 0.001
		Rostral 100 µm vs. Caudal 500 µm	**p < 0.01
		Rostral 100 µm vs. Caudal 100 µm	**p < 0.01
	+ spinal cord-derived astrocytes	Rostral 100 µm vs. Rostral 500 µm	*p < 0.05
		Rostral 100 µm vs. Center 1000 µm	***p < 0.001
		Rostral 100 µm vs. Caudal 500 µm	***p < 0.01
		Rostrall 100 µm vs. Caudal 100 µm	***p < 0.01

Supplementary table 11: Statistical analysis of growth of serotonergic axons within hydrogel channels (FIG 32D).

Statistical test	Group	Distance	p value
Two-Way ANOVA for overall group differences $p < 0.05$, with Tukey's *post hoc*	PLO/laminin vs. + cortex-derived astrocytes	Rostral 100 µm	****p < 0.0001
	PLO/laminin vs. + spinal cord-derived astrocytes	Rostral 100 µm	*p < 0.05
	+ cortex-derived astrocytes vs. + spinal cord-derived astrocytes	-	ns
Two-Way ANOVA for distance $p < 0.0001$, with Tukey's *post hoc*	PLO/laminin	-	ns
	+ cortex-derived astrocytes	Rostral 100 µm vs. Rostral 500 µm	****p < 0.0001
		Rostral 100 µm vs. Center 1000 µm	****p < 0.0001
		Rostral 100 µm vs. Caudal 500 µm	****p < 0.0001
		Rostral 100 µm vs. Caudal 100 µm	****p < 0.0001
	+ spinal cord-derived astrocytes	Rostral 100 µm vs. Rostral 500 µm	*p < 0.05
		Rostral 100 µm vs. Center 1000 µm	***p < 0.001
		Rostral 100 µm vs. Caudal 500 µm	***p < 0.01
		Rostral 100 µm vs. Caudal 100 µm	***p < 0.01
Interaction	Cell grafting x Distance		*p < 0.05

Supplementary table 12: Statistical analysis of growth of serotonergic axons within hydrogel implants (FIG 32E).

Statistical test	Group	Distance	p value
Two-Way ANOVA for overall group differences $p < 0.05$, with Tukey's *post hoc*	PLO/laminin vs. + cortex-derived astrocytes	-	ns
	PLO/laminin vs. + spinal cord-derived astrocytes	Rostral 100 µm	*p < 0.05
	+ cortex-derived astrocytes vs. + spinal cord-derived astrocytes	-	ns
Two-Way ANOVA for distance $p = 0.12$	PLO/laminin	-	ns
	+ cortex-derived astrocytes	-	ns
	+ spinal cord-derived astrocytes	-	ns

Supplementary table 13: Statistical analysis of growth of descending axons within hydrogel channels (FIG 33D).

Statistical test	Group	Distance	p value
Two-Way ANOVA for overall group differences p = 0.28	PLO/laminin vs. + cortex-derived astrocytes	-	ns
	PLO/laminin vs. + spinal cord-derived astrocytes	-	ns
	+ cortex-derived astrocytes vs. + spinal cord-derived astrocytes	-	ns
Two-Way ANOVA for distance p < 0.05, with Tukey's *post hoc*	PLO/laminin	-	ns
	+ cortex-derived astrocytes	-	ns
	+ spinal cord-derived astrocytes	Rostral 100 µm vs. Caudal 500 µm	*p < 0.05
		Rostrall 100 µm vs. Caudal 100 µm	*p < 0.05

Supplementary table 14: Statistical analysis of growth of descending axons within hydrogel implants (FIG 33E).

7.4 Implantation of astrocyte-seeded alginate-based hydrogel implants together with additional astrocytic grafts into the rostral and caudal host spinal cord after traumatic spinal cord injury

Statistical test	Group	Distance	p value
Two-Way ANOVA for overall group differences p < 0.0001, with Tukey's *post hoc*	PLO/laminin vs. + cortex-derived astrocytes	Rostral 100 µm	*p < 0.05
		Center 1000 µm	****p < 0.0001
		Caudal 500 µm	*p < 0.05
		Caudal 100 µm	***p < 0.001
	PLO/laminin vs. + spinal cord-derived astrocytes	Center 1000 µm	****p < 0.0001
		Caudal 500 µm	*p < 0.05
		Caudal 100 µm	***p < 0.001
	+ cortex-derived astrocytes vs. + spinal cord-derived astrocytes	-	ns
Two-Way ANOVA for distance p < 0.001, with Tukey's *post hoc*	PLO/laminin	Rostral 100 µm vs. Center 1000 µm	***p < 0.001
		Rostral 500 µm vs. Center 1000 µm	*p < 0.05
	+ cortex-derived astrocytes	-	ns
	+ spinal cord-derived astrocytes	-	ns

Supplementary table 15: Statistical analysis of cell filling within hydrogel implants (FIG 35D).

Statistical test	Group	Distance	p value
Two-Way ANOVA for overall group differences p < 0.05, with Tukey's *post hoc*	PLO/laminin vs. + cortex-derived astrocytes	Rostral 100 µm	**p < 0.01
		Rostral 500 µm	*p < 0.05
		Caudal 100 µm	**p < 0.01
	PLO/laminin vs. + spinal cord-derived astrocytes	Rostral 100 µm	**p < 0.01
		Caudal 100 µm	*p < 0.05
	+ cortex-derived astrocytes vs. + spinal cord-derived astrocytes	-	ns
Two-Way ANOVA for distance p < 0.0001, with Tukey's *post hoc*	PLO/laminin	-	ns
	+ cortex-derived astrocytes	Rostral 100 µm vs. Center 1000 µm	***p < 0.001
		Rostral 100 µm vs. Caudal 500 µm	***p < 0.001
		Rostral 500 µm vs. Center 1000 µm	**p < 0.01
		Rostral 500 µm vs. Caudal 500 µm	*p < 0.05
		Center 1000 µm vs. Caudal 100 µm	***p < 0.001
		Caudal 500 µm vs. Caudal 100 µm	**p < 0.01
	+ spinal cord-derived astrocytes	Rostral 100 µm vs. Rostral 500 µm	**p < 0.01
		Rostral 100 µm vs. Center 1000 µm	****p < 0.0001
		Rostral 500 µm vs. Caudal 100 µm	*p < 0.05
		Center 1000 µm vs. Caudal 500 µm	*p < 0.05
		Center 1000 µm vs. Caudal 100 µm	***p < 0.001
Interaction	Cell grafting x Distance		*p < 0.05

Supplementary table 16: Statistical analysis of axonal growth within hydrogel channels (FIG 38D).

Statistical test	Group	Distance	p value
Two-Way ANOVA for overall group differences p < 0.01, with Tukey's *post hoc*	PLO/laminin vs. + cortex-derived astrocytes	Rostral 100 µm	***p < 0.001
		Rostral 500 µm	**p < 0.01
		Caudal 100 µm	****p < 0.0001
	PLO/laminin vs. + spinal cord-derived astrocytes	Rostral 100 µm	**p < 0.01
		Caudal 500 µm	*p < 0.05
		Caudal 100 µm	**p < 0.01
	+ cortex-derived astrocytes vs. + spinal cord-derived astrocytes	-	ns
Two-Way ANOVA for distance p < 0.0001, with Tukey's *post hoc*	PLO/laminin	-	ns
	+ cortex-derived astrocytes	Rostral 100 µm vs. Center 1000 µm	**p < 0.01
		Rostral 500 µm vs. Caudal 100 µm	**p < 0.01
		Center 1000 µm vs. Caudal 100 µm	****p < 0.0001
		Caudal 500 µm vs. Caudal 100 µm	****p < 0.0001
	+ spinal cord-derived astrocytes	Rostral 100 µm vs. Rostral 500 µm	*p < 0.05
		Rostral 100 µm vs. Center 1000 µm	**p < 0.01
		Rostral 500 µm vs. Caudal 100 µm	**p < 0.01
		Center 1000 µm vs. Caudal 100 µm	***p < 0.001

Supplementary table 17: Statistical analysis of axonal growth within hydrogel implants (FIG 38E).

Statistical test	Group	Distance	p value
Two-Way ANOVA for overall group differences $p < 0.05$, with Tukey's *post hoc*	PLO/laminin vs. + cortex-derived astrocytes	Rostral 100 µm	**p < 0.01
	PLO/laminin vs. + spinal cord-derived astrocytes	Rostral 100 µm	****p < 0.0001
		Rostral 500 µm	*p < 0.05
	+ cortex-derived astrocytes vs. + spinal cord-derived astrocytes	-	ns
Two-Way ANOVA for distance $p < 0.0001$, with Tukey's *post hoc*	PLO/laminin	-	ns
	+ cortex-derived astrocytes	Rostral 100 µm vs. Rostral 500 µm	*p < 0.05
		Rostral 100 µm vs. Center 1000 µm	****p < 0.0001
		Rostral 100 µm vs. Caudal 500 µm	****p < 0.0001
		Rostral 100 µm vs. Caudal 100 µm	****p < 0.0001
	+ spinal cord-derived astrocytes	Rostral 100 µm vs. Rostral 500 µm	****p < 0.0001
		Rostral 100 µm vs. Center 1000 µm	****p < 0.0001
		Rostral 100 µm vs. Caudal 500 µm	****p < 0.0001
		Rostral 100 µm vs. Caudal 100 µm	****p < 0.0001
		Rostral 500 µm vs. Center 1000 µm	**p < 0.01
		Rostral 500 µm vs. Caudal 500 µm	*p < 0.05
Interaction	Cell grafting x Distance		**p < 0.01

Supplementary table 18: Statistical analysis of growth of serotonergic axons within hydrogel channels (FIG 39D).

Statistical test	Group	Distance	p value
Two-Way ANOVA for overall group differences $p < 0.05$, with Tukey's *post hoc*	PLO/laminin vs. + cortex-derived astrocytes	Rostral 100 µm	****p < 0.0001
		Rostral 500 µm	*p < 0.05
		Caudal 100 µm	*p < 0.05
	PLO/laminin vs. + spinal cord-derived astrocytes	Rostral 100 µm	****p < 0.0001
		Rostral 500 µm	**p < 0.01
		Caudal 100 µm	**p < 0.01
	+ cortex-derived astrocytes vs. + spinal cord-derived astrocytes	-	ns
Two-Way ANOVA for distance $p < 0.0001$, with Tukey's *post hoc*	PLO/laminin	Rostral 100 µm vs. Rostral 500 µm	*p < 0.05
		Rostral 100 µm vs. Center 1000 µm	***p < 0.001
		Rostral 100 µm vs. Caudal 500 µm	**p < 0.01
		Rostral 100 µm vs. Caudal 100 µm	**p < 0. 01
	+ cortex-derived astrocytes	Rostral 100 µm vs. Rostral 500 µm	****p < 0.0001
		Rostral 100 µm vs. Center 1000 µm	****p < 0.0001
		Rostral 100 µm vs. Caudal 500 µm	****p < 0.0001
		Rostral 100 µm vs. Caudal 100 µm	****p < 0.0001
		Rostral 500 µm vs. Center 1000 µm	*p < 0.05
		Center 1000 µm vs. Caudal 100 µm	*p < 0.05
	+ spinal cord-derived astrocytes	Rostral 100 µm vs. Rostral 500 µm	****p < 0.0001
		Rostral 100 µm vs. Center 1000 µm	****p < 0.0001
		Rostral 100 µm vs. Caudal 500 µm	****p < 0.0001
		Rostral 100 µm vs. Caudal 100 µm	****p < 0.0001
		Rostral 500 µm vs. Center 1000 µm	****p < 0.0001
		Rostral 500 µm vs. Caudal 500 µm	***p < 0.001
		Center 1000 µm vs. Caudal 100 µm	****p < 0.0001
		Caudal 500 µm vs. Caudal 100 µm	**p < 0.01
Interaction	Cell grafting x Distance		****p < 0.0001

Supplementary table 19: Statistical analysis of growth of serotonergic axons within hydrogel implants (FIG 39E).

Statistical test	Group	Distance	p value
Two-Way ANOVA for overall group differences p < 0.01, with Tukey's *post hoc*	PLO/laminin vs. + cortex-derived astrocytes	Rostral 100 µm	****p < 0.0001
		Rostral 500 µm	****p < 0.0001
		Caudal 500 µm	*p < 0.05
		Caudal 100 µm	**p < 0.01
	PLO/laminin vs. + spinal cord-derived astrocytes	Rostral 100 µm	*p < 0.05
		Rostral 500 µm	*p < 0.05
	+ cortex-derived astrocytes vs. + spinal cord-derived astrocytes	Rostral 100 µm	**p < 0.01
		Caudal 100 µm	**p < 0.01
Two-Way ANOVA for distance p < 0.0001, with Tukey's *post hoc*	PLO/laminin	-	ns
	+ cortex-derived astrocytes	Rostral 100 µm vs. Center 1000 µm	****p < 0.0001
		Rostral 100 µm vs. Caudal 500 µm	****p < 0.0001
		Rostral 100 µm vs. Caudal 100 µm	****p < 0.0001
		Rostral 500 µm vs. Center 1000 µm	****p < 0.0001
		Rostral 500 µm vs. Caudal 500 µm	****p < 0.0001
		Rostral 500 µm vs. Caudal 100 µm	****p < 0.0001
	+ spinal cord-derived astrocytes	Rostral 100 µm vs. Center 1000 µm	**p < 0.01
		Rostral 100 µm vs. Caudal 500 µm	**p < 0.01
		Rostral 100 µm vs. Caudal 100 µm	**p < 0.01
Interaction	Cell grafting x Distance		**p < 0.01

Supplementary table 20: Statistical analysis of growth of descending axons within hydrogel channels (FIG 40D).

Statistical test	Group	Distance	p value
Two-Way ANOVA for overall group differences p < 0.01, with Tukey's *post hoc*	PLO/laminin vs. + cortex-derived astrocytes	Rostral 100 µm	****p < 0.0001
		Rostral 500 µm	****p < 0.0001
		Center 1000 µm	*p < 0.05
		Caudal 500 µm	**p < 0.01
		Caudal 100 µm	***p < 0.001
	PLO/laminin vs. + spinal cord-derived astrocytes	-	ns
	+ cortex-derived astrocytes vs. + spinal cord-derived astrocytes	Rostral 100 µm	***p < 0.001
Two-Way ANOVA for distance p < 0.0001, with Tukey's *post hoc*	PLO/laminin	-	ns
	+ cortex-derived astrocytes	Rostral 100 µm vs. Rostral 500 µm	***p < 0.001
		Rostral 100 µm vs. Center 1000 µm	****p < 0.0001
		Rostral 100 µm vs. Caudal 500 µm	****p < 0.0001
		Rostral 100 µm vs. Caudal 100 µm	****p < 0.0001
		Rostral 500 µm vs. Center 1000 µm	**p < 0.01
	+ spinal cord-derived astrocytes	-	ns
Interaction	Cell grafting x Distance		**p < 0.01

Supplementary table 21: Statistical analysis of growth of descending axons within hydrogel implants (FIG 40E).